Characterisation of vacua of the String Theory Landscape

Mikel Álvarez Urquiola

eman ta zabal zazu

Universidad del País Vasco

Euskal Herriko Unibertsitatea

PhD Thesis

Department of Physics - Theory Division

Leioa, September 2021

A Elena y Adrián

Contents

Agradecimientos ix

Summary (in Basque) xi

List of publications xvii

I Introduction 1

1 The String Theory Landscape 3
- 1.1 A bird's eye view of String Theory . . . 3
- 1.2 Compactification with Calabi-Yau geometries . . . 5
- 1.3 Effective theory and flux compactifications . . . 10
- 1.4 The String Theory Landscape . . . 17
- 1.5 Non-perturbative stability of vacua . . . 19

II Moduli stabilization 29

2 Towards a complete mass spectrum 31
- 2.1 Introduction . . . 31
- 2.2 Flux vacua at Large Complex Structure . . . 34
- 2.3 Flux vacua with enhanced symmetries . . . 37
- 2.4 Complete tree-level mass spectrum . . . 40
- 2.5 One-parameter example: the $\mathbb{WP}^4_{[1,1,1,1,4]}$ model . . . 48
- 2.6 Statistics of vacua . . . 52
- 2.7 Conclusions . . . 62

3 A universal mass spectrum for any compactification around the LCS point 67
- 3.1 Introduction . . . 67
- 3.2 A universal mass spectrum at Large Complex Structure . . . 68
- 3.3 Example: the hypersurface $\mathbb{WP}^4_{[1,1,1,6,9]}$ . . . 72
- 3.4 Discussion . . . 80

4 Racetrack potentials and the de Sitter swampland conjecture 81
- 4.1 Introduction . . . 81
- 4.2 Explicit Examples for Type IIB compactification scenarios . . . 83

4.3 Validity of the solutions . . . 89
4.4 de Sitter saddle points and the Refined de Sitter Conjecture . . . 91
4.5 Discussion . . . 92

III Cosmological aspects of the Landscape 95

5 Slepian models for Gaussian Random Landscapes 97
5.1 Introduction . . . 97
5.2 Preliminaries for Gaussian Random Fields . . . 100
5.3 Slepian Models for constrained Gaussian random fields . . . 101
5.4 Tunneling in a Gaussian random landscape . . . 106
5.5 Inflation in a Slepian Random Landscape . . . 114
5.6 Summary and conclusions . . . 119

6 Brane nucleation in supersymmetric models 123
6.1 Introduction . . . 123
6.2 Global Supersymmetric Field Theories . . . 125
6.3 Tunneling from a supersymmetry-breaking vacuum . . . 134
6.4 Flat membranes and domain walls in Supergravity . . . 139
6.5 Membrane nucleation in Supergravity . . . 143
6.6 Conclusions . . . 150

IV Final remarks 153

7 General conclusions and outlook 155

V Appendices 159

A Hodge decomposition of the flux vector 161

B Numerical search of no-scale solutions in the octic 163
B.1 Polynomial homotopy continuation and Paramotopy . . . 163
B.2 Search for no-scale solutions in one-parameter models . . . 164
B.3 Redundancies of the EFT and solution duplicates . . . 165

C Density distribution of no-scale flux vacua 167
C.1 Derivation of the Denef-Douglas distribution . . . 167
C.2 Constrained flux distribution . . . 169
C.3 Density of generic no-scale vacua . . . 170
C.4 Density of constrained vacua . . . 172

D Bounds on the LCS parameter 173
D.1 No-scale equations near the LCS point . . . 173
D.2 Lower bound on the LCS parameter . . . 175
D.3 Maximum value consistent with small instanton corrections . . . 176
D.4 Accuracy of the statistical description . . . 178

E Construction of Slepian models **181**
E.1 Introductory remarks and some properties of Gaussian random variables . . . 181
E.2 Conditioned Gaussian random vectors . . . 182
E.3 Gaussian random fields . . . 183
E.4 Useful correlations . . . 184
E.5 The Kac-Rice formula and conditioned Gaussian random fields . . . 185
E.6 Conditioned Gaussian random field for a critical point . . . 186
E.7 Conditioned Gaussian random field for an inflection point . . . 191

F Numerical implementation of Slepian models **195**
F.1 Generation of Gaussian random fields: Karhunen-Loève expansion . . . 195
F.2 Numerical evaluations of Critical points . . . 196
F.3 Numerical evaluations of Inflection points . . . 197

G Inflection point inflation **199**

H Single three-form multiplets **203**
H.1 Three-form multiplets in supersymmetry . . . 203
H.2 Three-form multiplets in supergravity . . . 207

Bibliography **213**

Agradecimientos

Sin duda, esta tesis no hubiera sido posible sin la paciencia y dedicación de mi director, José Juan Blanco Pillado, al que le debo, entre muchas cosas, haber podido acabar este trabajo con motivación y curiosidad para seguir por este camino. Durante este tiempo he podido colaborar con buenos investigadores y aun mejores personas. Es por ello que debo darles las gracias también a Kepa Sousa, Jeremy Wachter e Igor Bandos por este tiempo que hemos podido trabajar juntos.

Quiero agradecerle a mi familia todo el cariño que me han dado estos últimos años. Han creído en mí desde el principio y han estado ahí para consolarme en los momentos no tan buenos que conlleva un trabajo de este calibre. Un abrazo enorme, sobre todo, a mis abuelos, por hacerme sentir tan especial y por recibirme siempre con los brazos abiertos. Desde luego, son los responsables de que haya llegado tan lejos.

He tenido la suerte de poder entablar amistad con muchísima gente gracias a este doctorado. Quiero darles las gracias a todos ellos, y especialmente a Dani, Fran, María, Asier, Aitor, Ander y Sara, mis compañeros de viaje durante esta época. Ha sido todo un placer poder crecer y compartir experiencias todos juntos.

Por último, quiero dedicarle estas últimas lineas a Adrián, por haber estado siempre ahí cuando más lo he necesitado. En muchos aspectos, hemos podido crecer juntos y no podría imaginarme a nadie más adecuado para tener a mi lado este tiempo.

Muchas gracias a todos vosotros por estos cuatro años, han sido inolvidables.

Summary

(in Basque)

Grabitate kuantikoaren teoria bateratzailea da Soka-Teoria. Aitzitik, teoriaren tinkotasuna bermatzeko 10 espazio-denborako dimentsiotan deskribatu behar dugu. Jakina, Soka-Teoria fenomenologikoki onargarria izan dadin, energia baxuko eremu-teoria eraginkorra 4 dimentsiotan deskribatu beharko dugu. Horretarako, espazio-denboraren gehiegizko dimentsio horiek nolabait trinkotu behar ditugu; adibidez, IIB motako Soka-Teoriaren gehiegizko 6 dimentsioen geometria *Calabi-Yau espazioen* bidez deskribatu ohi dira. Trinkoketa horien inguruko zenbait aspektu fenomenologiko aztertzea da tesi honen helburu nagusia.

Barne-geometriaren oinarrizko ezaugarriak erabiliz, zuzenean froga daiteke trinkoketa horiek hainbat eratara deformatu daitezkeela energia-kosturik gabe. Horrenbestez, barne-geometria deskribatzen dituzten ehunka parametroak (*moduluak*) masarik gabeko eremu bezala joko dira lau dimentsioko ikuspuntu behagarriarengandik, eta hori bateraezina da gaur egungo behaketekin. Hori dela eta, nahitaezkoa zaigu modulu horiei masa ematea eta nolabait egonkortzea. Hartara, 1. kapituluan deskribatutakoaren arabera, teorian bertan ageri diren fluxuak erabili daitezke moduluen potentzial eskalar bat osatzeko. Ehunka dimentsioko potentzial eskalar horri *Paisaia* deritzo, horren egitura konplexua dela eta. Paisaiaren minimoek Soka-Teoriaren barne-geometriaren egoera egonkorrak adierazten dituzte; hortaz, horien inguruko ezagutza tinkoa izatea ezinbestekoa zaigu Soka-Teoriaren eredu fenomenologikoki zuzenak eraikitzeko.

Tesiaren I. atalean IIB motako Soka-Teoriaren eta horren energia baxuko eremu-teoria eraginkorra den IIB Supergrabitatearen oinarriak bildu ditugu. Horiekin, geometria konplexuaren oinarrizko zenbait nozio erabiliz, Paisaia nola eraiki daitekeen laburbildu dugu. Paisaia bi modulu motez osatuta dago, hots, egitura konplexuaren moduluez eta Kähler moduluez. Lehenengoek barne-geometriaren *itxura* adierazten dute intuitiboki; bigarrenek, aldiz, trinkoketaren *tamainarekin* dute zerikusia. Guzti horiek egonkortzea ez da batere erraza, eta sektore bakoitzaren inguruko xehetasunak eman ditugu, tesian zehar behin eta berriro aplikatu ditugunak.

Arestian esan bezala, Pasaiaren fenomenologia ikertzea ezinbestekoa da teoriaren ondorio behagarriak ondo ulertzeko. Tesi honetan Paisaiaren zenbait aspektu kosmologikoetan jarri dugu arreta, *inflazioan* eta *sasihutsaren iraungitzean*, hain zuzen ere, eta horien inguruko sarrera eman dugu kapitulu horren bukaeran.

Tesiaren II. zatia barne-geometriaren moduluen egonkortze-prozeduren inguruan datza, 1. kapituluko osagaiak erabiliz. Zehatzago esanda, 2. eta 3. kapituluetan axiodilatoiaren eta egitura konplexuaren modulu *guztien* egonkortzea aztertzera jo dugu. Bestalde, 4. kapituluan Kähler sektorearen inguruko eztabaida egingo dugu. Hauxe da zati horretako kapitulu bakoitzean landu dugunaren laburpena:

2. kapitulua

Arestian esan bezala, Calabi-Yau geometrien modulu kopurua, orokorrean, $\mathcal{O}(100)$ da. Jakina, guztiz kalkulaezina zaigu dimentsio horretako funtzioen minimoak (edota bestelako puntu berezien ezaugarriak) aztertzea. Hori dela eta, Paisaiaren hutsen deskribapen analitikoa lortzeko potentzial hori nolabait sinplifikatu beharra dugu. Ondorengo kapituluetan, sinplifikazio hori *trunkamendu supersimetriko tinkoen* bidez egin dugu. Horietan, trinkoketen simetria-taldeak erabiliz modulu-espektroaren zati bat ekintza eraginkorretik baztertu dezakegu. Eredu horietan, simetriarekiko inbarianteak diren fluxuak bakarrik pizten baldin badira, egitura konplexuaren modulu-kopuru handi bat *hoztu* ahal izango dugu fluxuek sortutako potentzial eskalarraren hutsetan. Beraz, Eremu-Teoria Eraginkorra (ETEa) murriztu ahal izango dugu, hots, eremu gutxi batzuen bidez deskribatu ahal izango da fisika guztia.

Trunkatze hori literaturan zeharo aztertu den arren, operazio horretan hozten diren eremuen ezaugarriak nekez ikertu dira inon. Lan honen helburua da trunkatutako modulusektorearen ezaugarriak hobeto ulertzea, simetria handiko ereduetan. Garrantzitsua da nabarmentzea trunkatutako moduluak ez direla teoria eranginkorretik integratzen; hain zuzen ere, horrela lortu dezakegun ETEa energia baxuko teoria osoaren *trunkamendu supersimetriko tinkoa* da, zuhaitz mailan behintzat.

IIB motako supersoken Calabi-Yau trinkoketen zuhaitz mailako hutsak aztertu ditugu oraingo honetan, Egitura Konplexu Handiko (EKH) eskualdean. Bestalde, geometria sinpleenak erabili ditugu hemen, hots, murriztutako egitura konplexuaren sektorea modulu bakarrez osatuta dutenak. Horrela, EKH eskualdean zuhaitz mailako masa-espektroa kalkulatu dugu axiodilatoiarentzat eta egitura konplexuaren modulu-eremu guztientzat, *trunkatutakoak barne*. Horrez gain, hutsen zenbait ezaugarrien estatistikak lortu ahal izan ditugu Denef-Douglas hurbilketa, alegia, fluxu jarraituen hurbilketa, erabiliz.

Lan honetan proposatu ditugun aurreikuspen analitiko guztiak berresteko $\mathbb{WP}^4_{[1,1,1,1,4]}$ Calabi-Yau orientatea (*orientifold*) erabili dugu trinkoketa gisa, eta horren zenbakizko fluxuhutsen ekorketa egin dugu, bertatik lortutako datuen estatistikak kalkulatu ahal izateko. Hipergainazal-familia horren egitura konplexuaren modulu-espazioa $h^{2,1} = 149$ dimentsiokoa da; aitzitik, EKH eskualdeko geometriaren simetria-maila handia dela eta, moduluen inguruko fisika osoa eremu bakarrera murriztu dezakegu era tinkoan. Eredu horren teoria eraginkor murriztua erabiliz, fluxu-huts multzo handia lortu ahal izan dugu, eta horren bitartez ondorengo kapituluan ere erabiliko ditugun masa-espektroak egiaztatu ahal izan ditugu. Azpimarratzekoa da horrela aurkitu dugun huts bakoitzaren trunkatutako 148 eremuen masak lor ditzakegula gure emaitzak erabiliz, *ETE osora jo beharrik gabe*.

Kapitulu hau ondorengo artikuluan oinarritzen da:

J.J. Blanco-Pillado, K. Sousa, M.A. Urkiola & J.M. Wachter
Towards a complete mass spectrum of type-IIB flux vacua at large complex structure
J. High Energ. Phys. **04** (2021) 149
arXiv: 2007.10381 [hep-th]

3. kapitulua

Kapitulu honetan aurreko eztabaida edonolako Calabi-Yau geometrietara zabaldu dugu, arestiko analisian egitura konplexuaren modulu bakarra (trunkaketa supersimetrikoa bideratu ostean) duten Calabi-Yau orientateen inguruko emaitzak erabiliz.

Kapitulu honetan zera frogatu dugu: EKH eskualdean, fluxu egokiak erabiliz, era tinkoan trunkatu dezakegula *Calabi-Yau trinkoketa orokorren* ETEa, egitura konplexuaren modulu bakar batera. Aurreko kapituluan ez bezala, ez dugu isometria taldeen beharrik izango, EKH puntuaren inguruko monodromia transformazioak baitira gure emaitzen oinarria.

Bestalde, trunkamendua bizirauten duen eremua monodromia-norabidearen araberakoa da. Hartara, aldaezintasun-ezaugarri horiek erabiliz, huts-sorta handia eraiki dugu, axiodilatoiaren eta egitura konplexuaren moduluen masa-espektroaren gaineko kontrol analitiko paregabea mantenduz.

Aurreko kapituluko adierazpen analitikoak erabiliz, zuzenean frogatu ahal izango ditugu kapitulu honetako emaitza nagusiak. Hori ez ezik, guzti horiek $\mathbb{WP}^4_{[1,1,1,6,9]}$ Calabi-Yau orientatearen fluxu-hutsen zenbakizko ekorketa baten bidez berretsi ahal izan ditugu.

Kapitulu honen oinarria ondorengo artikulua da:

J.J. Blanco-Pillado, K. Sousa, M.A. Urkiola & J.M. Wachter
Universal Class of Type-IIB Flux Vacua with Analytic Mass Spectrum
Phys. Rev. D **103** (2021) 106006
arXiv: 2011.13953 [hep-th]

4. kapitulua

Kapitulu honetan Kähler sektorearen egonkortzea ikertzera jo dugu, *de Sitter Zingira-aieruaren* ikuspuntutik. Hain zuzen ere, duela pare bat urte formulatutako Zingira-aieru horren arabera, grabitate kuantikoarekiko tinkoa den edozein potentzial eskalarretan ezin daiteke existitu de Sitter motako huts metaegonkorrik. Hori ez ezik, aieruak edonolako de Sitter puntu kritikoren existentzia ere debekatzen du, zela-puntuak barne.

Gauzak horrela, soka-trinkoketen de Sitter zela-puntuen existentzia aztertu dugu, de Sitter aierua murriztaileegia den ala ez frogatzeko. Horretarako, Kähler modulu bakarra duen trinkoketa-eredua erabili dugu. Eremu hori, axiodilatoia eta egitura konplexuaren moduluak egonkortu ahal izan ditugu aurreko kapituluetako fluxuak erabiliz, eta ekarpen ez-perturbatiboen eragina ere kontuan hartuz superpotentzialean. Osagai horiekin guztiekin *Racetrack* motako potentziala sortu dugu eredu horren moduluak egonkortzeko.

Eredu horren zenbait soluzio jakin abiapuntutzat hartuz, ekarpen ez-perturbatiboak eta fluxuak doitu ditugu anti-deSitter huts supersimetrikoak eta de Sitter zela-puntuak dituzten ereduak sortzeko. Hori ez ezik, huts horiek zenbait tinkotasun baldintza betetzen dituztela frogatu dugu; hortaz, horrela lortutako soluzioak fenomenologikoki tinkoak dira eta eredu konplexuagoetako hutsak bilatzeko baliagarriak izan daitezke.

Azkenik, gure soluzioak de Sitter zingira-aieruaren bertsio ahulagoarekin aldaratu ditugu eta aieru berri horrekin bat datozela nabaritu dugu.

Kapitulu honen emaitzak ondorengo artikulu zientifikoan jaso ditugu:

J.J. Blanco-Pillado, M.A. Urkiola & J.M. Wachter
Racetrack potentials and the de Sitter swampland conjectures
J. High Energ. Phys. **01** (2019) 187
arXiv: 1811.05463 [hep-th]

Tesiaren III. zatia Paisaiaren aspektu kosmologikoei buruz datza. Lehen esan bezala, Paisaiak sasihutsen iraungitzea ahalbidetzen du, eta baita prozesu inflazionarioak gertatzea ere. Ondorengo bi kapituluetan prozesu fisiko horiek zeharo aztertu ditugu Paisaiaren zenbait eredu erabiliz.

5. kapitulua

Lehen aipatu dugun bezala, Paisaiaren ohiko eremu-kopurua $\mathcal{O}(100)$ da. Horren ondorioz, potentzialaren azterketa zehatza erabat ezinezkoa da eta horrek eremu-espazioa nolabait trunkatzera behartzen gaitu. Bestalde, eredu horiek aztertzeko alternatiba interesgarria metodo estatistikoak erabiltzean datza, non potentzial eskalarra ausazko eremutzat hartzen den.

Kapitulu honetan, Ausazko Eremu Gausstarren (AEGen) bidez deskribatutako potentzialak izango ditugu aztergai. Horiek erabiltzeko motibazio nagusia da hainbat terminoren gehiketa bezala jo dezakegula 4 dimentsioko potentziala. Termino horiek jatorri klasikoa edo kuantikoa izan dezakete trinkoketa-mekanismoan, eta horiek guztiak aintzat hartzerakoan sortuko den potentzial konplexua ausazko eremu gausstartzat jo dezakegu.

Soka-Teoriaren Paisaiaren fenomenologia aztertzea, Kosmologiaren ikuspuntutik, ezinbestekoa da. Izan ere, Unibertso Goiztiarreko energia altuko fisikak Soka-Teoriaren ondorio behagarrietan izugarrizko eragina izan dezake. Horren inguruko Paisaiaren ikerketek potentzialaren puntu jakin batzuen ezaugarriak ezagutzean oinarritzen dira, adibidez, konstante kosmologiko jakin bateko minimoetan, edo deribatu jakin batzuk dituen inflexio-puntuetan, horietan inflazioa gerta litekeelako. Aitzitik, puntu horietan inposatzen ditugun murrizketen arabera, oso zaila izan daiteke ezaugarri horiek dituen potentziala aurkitzea, ausazko funtzio horren hainbat iterazio eginda ere. Hain zuzen ere, de Sitter huts metaegonkorrak edota behaketa fenomenologikoekin bat datozen inflexio-puntu inflazionarioak oso arraroak dira Paisai orokorretan. Kapitulu honetan potentzial horiek sortzeko estrategia berri bat aurkeztuko dugu; horren bitartez, potentzialak forma jakin bat izatera baldintzatuko ditugu lokalki, ausazko Paisaiaren ezaugarri globalak guztiz errespetatuz. Horiexek dira *Slepian ereduak*.

Hemen aurkeztu ditugun teknika matematikoak erakusteko, guk doitutako puntu kritikoak (maximo, minimo edo zela-puntuak) edota inflexio-puntuak dituzten baldintzatutako AEGak eraikiko ditugu eta horien inguruko informazio estatistiko garrantzitsua lortuko dugu.

Alde batetik, baldintzatutako minimoak dituzten potentzialak erabiliz, horien sasihutsen iraungitzea aztertu ahal izan dugu AnyBubble Mathematicako paketea erabiliz. Horrekin, prozesu horien estatistikak kalkulatu ahal izan ditugu bi dimentsioko ausazko potentzialetan.

Gainera, tuneleatze horiek kalkulatzeko zenbait hurbilketa baieztatu ditugu, iraungitzeen gertatze-tasa dimentsio altuagoko potentzialetan kalkulatu ahal izateko.

Potentzialen baldintzatze-metodoen bigarren aplikazioa inflexio-puntuen doikuntzan datza, horien inguruko prozesu inflazioak ikertzeko. Zehatzago esanda, parametro inflazionario behagarrien menpekotasuna ikertu dugu eremu eskalarren hasierako baldintzekiko eta inflexio-puntuaren egitura lokalarekiko. Hartara, eremuen hasierako baldintza horiek inguruko sasihuts baten iraungitzearen irteera-puntuen bidez definitu ditugu. Kontuan izan horrelako analisia bideratzeko ezinbestekoa zaigula inflexio-puntuaren inguruko potentziala ezagutzea eta baita hortik gertu egon daitezkeen minimoen informazioa jakitea. Horri esker, gure metodoa oso baliagarria izango da ikerketa horretarako, potentzialaren ezaugarri estatistiko globalen eta lokalen informazio osoa ezagutzea ahalbidetzen baitu. Azpimarragarria da hauxe dela literaturan lehen aldiz ageri den inflexio-puntuentzako Slepian eredua.

Kapitulu hau ondorengo artikuluan oinarritzen da:

J.J. Blanco-Pillado, K. Sousa & M.A. Urkiola
Slepian models for Gaussian random landscapes
J. High Energ. Phys. **05** (2020) 142
arXiv: 1911.07618 [hep-th]

6. kapitulua

Aurreko kapituluetan, sasihutsen iraungitzea ohiko eremu eskalarren potentzialen testuinguruan landu dugu, Coleman-deLuccia iraungitzeak deritzenak. Nahiz eta prozesu horiek zeharo aztertu diren literaturan, Paisaiaren oinarrizko osagaiak bateratzen dituzten bestelako iraungitze-mekanismoak aztertzea garrantzitsua da.

Horren harira, Coleman-deLuccia iraungitzeen antzeko prozesuak ditugu Brownek eta Teitelboimek aztertutakoak. Azken horietan fluxuak eta mintzak dira ekintzaren osagai nagusiak. Hortaz, energetikoki posiblea izan daiteke espazioaren eskualderen bat 3-formek sortutako fluxu-huts batetik beste batera tuneleatzea, fluxu horri akoplatutako mintz baten nukleazioaren bidez.

Aurreko osagai guztiak bateratzen dituzte Soka-Teoriaren trinkoketek, non 3-formen fluxuak erabiltzen diren teoriaren gehiegizko dimentsioak barietate trinko batean egonkortzeko. Lehenengo kapituluan aipatu dugunaren arabera, fluxuak naturalki akoplatzen dira, adibidez, IIB Soka-Teorian ageri diren D-branetara. Bestalde, badakigu trinkoketa-prozesuan ehunka modulu ageri direla, barne-barietatearen geometria parametrizatzen dutenak. Hortaz, oso esanguratsua izan daiteke osagai guzti horiek barneratzen dituzten iraungitzeak aztertzea eremu-teoria eraginkorraren ikuspuntutik, $\mathcal{N} = 1$ supergrabitatearen ikuspuntutik, hain justu, $D = 4$ dimentsiotan.

Lan honetan, 3-formak eta mintzak teoria supersimetriko batean nola barneratu daitezkeen pausoz-pauso azaldu dugu lehenbizi (bai grabitatea arbuiatuz, bai grabitatea kontuan hartuta). Ondoren, fluxuek osatutako hutsen arteko egonkortasun ez-perturbatiboa aztertu dugu; horretarako, Coleman-deLuccia eta Brown-Teitelboim prozeduren konbinazio jakin

bat erabiliz. Noski, lehen esan bezala, huts supersimetrikoak guztiz egonkorrak izan behar dira sasihutsaren iraungitzeekiko. Hortaz, gure lagrangearretan supersimetria samurki hausten dituzten terminoak barneratu ditugu. Azken horiek nahi bezain txikiak egin daitezke, eta sasihutsen iraungitzea horien arabera aztertu dugu. Horrelako teoria emanda, sasihutsa eremu eskalar isotropo eta eskalar batez eta baita 3-forma baten balio jakin batez osatuta dagoela suposatu dugu. Bestalde, instantoi soluzioa forma-eremuari akoplatutako mintz esferiko batez osatuta dagoela suposatu dugu, non mintzaren barnealdea eta kanpoaldea fluxu-balio ezberdinez osatuta dauden (Brown-Teitelboim instantoian bezala). Ondorioz, mintzaren alde bakoitza potentzial *ezberdin* batek deskribatzen du. Horrelako prozesuak energetikoki bideragarriak direla baieztatuko dugu, eta zenbait adibide eman ditugu, bai grabitatea kontutan hartuz, bai grabitatea arbuiatuz. Bestalde, supersimetria hausten duten parametroak txikiagotu ahala, mintz-erradioa handiagotzen dela ikusi dugu, limite supersimetrikoaren erradio infinituko soluzioarekin (alegia, domeinu-pareta lauarekin) bat datorrena.

Kapitulu horretako emaitzak ondorengo artikuluan oinarritzen dira:

I. Bandos, J.J. Blanco-Pillado, K. Sousa & M.A. Urkiola
Brane nucleation in supersymmetric models
Prestatzen

Azkenik, tesiaren IV. zatian lan guzti horien zenbait ondorio orokor bildu ditugu.

List of publications

Published papers

J.J. Blanco-Pillado, M.A. Urkiola & J.M. Wachter
Racetrack potentials and the de Sitter swampland conjectures
J. High Energ. Phys. **01** (2019) 187
arXiv: 1811.05463 [hep-th]

J.J. Blanco-Pillado, K. Sousa & M.A. Urkiola
Slepian models for Gaussian random landscapes
J. High Energ. Phys. **05** (2020) 142
arXiv: 1911.07618 [hep-th]

J.J. Blanco-Pillado, K. Sousa, M.A. Urkiola & J.M. Wachter
Towards a complete mass spectrum of type-IIB flux vacua at large complex structure
J. High Energ. Phys. **04** (2021) 149
arXiv: 2007.10381 [hep-th]

J.J. Blanco-Pillado, K. Sousa, M.A. Urkiola & J.M. Wachter
Universal Class of Type-IIB Flux Vacua with Analytic Mass Spectrum
Phys. Rev. D **103** (2021) 106006
arXiv: 2011.13953 [hep-th]

In preparation

I. Bandos, J.J. Blanco-Pillado, K. Sousa & M.A. Urkiola
Brane nucleation in supersymmetric models
In preparation

Part I

Introduction

Chapter 1

The String Theory Landscape

In this opening chapter, we will briefly review the most notable features of string theory and its low energy description, supergravity. After describing the components of type IIB supergravity, which we will mainly focus on, we will give some details about how it can be compactified to four spacetime dimensions. The most direct consequence of this last procedure is the appearance of hundreds of massless scalar fields, the moduli. We will explore the scheme of flux compactifications, through which we can generate a scalar potential with which the moduli can be stabilized. The vastness of this potential (both from the number of fields involved and all the possible minima it involves) has granted it its most celebrated name: the Landscape. We will explore some physical consequences of this Landscape, which will be relevant in the following chapters, mostly focusing on its relation to an early-Universe inflationary epoch and the possibility of semi-classical decaying processes from local minima of this potential.

1.1 A bird's eye view of String Theory

String theory[1], which started as a theory of the strong interaction in the 60s, [5], is nowadays one of the leading candidates to a unifying theory of quantum gravity. It describes the dynamics of a plethora of fields in a completely self-consistent manner, and only in terms of a single free parameter, the string tension. For future reference, let us denote it by $T = (2\pi\alpha')^{-1}$, where α' is known as the Regge slope. This also sets a mass scale for massive excitations of the string, namely $M_s = 1/\sqrt{\alpha'}$ and a characteristic length scale $\ell_s = 2\pi\sqrt{\alpha'}$.

Quantizing the string vibrational modes leads to bosonic fields, and among the massless spectrum a graviton is found. However, the bosonic string comes with several problems. First and foremost, the quantization of the bosonic string only includes bosonic fields and tachyons are present within the spectrum. Moreover, the theory appears to be anomaly-free only when the spacetime dimension is $D = 26$ [6].

All the above issues are solved (or, at least alleviated) by introducing supersymmetry into the theory. These remove the tachyon and, of course, introduce fermions into the spectrum, all the while reducing the number of spacetime dimensions to $D = 10$. There are several ways to consistently introduce supersymmetry in String Theory, which lead to

[1] Some standard references which cover a wide range of topics in String Theory are [1–4].

different Superstring theories, namely: type I, heterotic $SO(32)$ and $E_8 \times E_8$, type IIA and type IIB. All of these are related by dualities and are perturbative limits of an 11-dimensional M-theory [7, 8]. Most interestingly, at low energies (or equivalently, at first order in α'), i.e. when only the massless spectrum is considered, each Superstring theory is described by a Supegravity limit in $D = 10$ or 11 spacetime dimensions.

Of course, if we are ultimately interested in making contact with our four-dimensional real-world experience, it is vital to deal with the extra dimensions present in the theory. The most common way to do so is through the *compactification* of these 6 (or 7) dimensions, and has become central in the study of phenomenological aspects of string theory.

In this thesis we will be particularly interested in type IIB string theory and its supergravity limit. We will be dealing with flux compactifications in this setup, introduced in the pioneering works of [9–11]. There are, of course, many other schemes to compactify the extra dimensions present in all Superstring theories, for a broader perspective on the topic see, e.g., [12–14].

As we mentioned above, the low energy limit of IIB String Theory is described by type IIB supergravity, whose bosonic action reads, in the conventions of [4] and in Einstein frame,

$$S_{\text{IIB}} = \frac{1}{2\kappa_{10}^2}\int d^{10}x\sqrt{-G}\left[R - \frac{\partial_M\tau\partial^M\bar{\tau}}{2\,(\text{Im}\,\tau)^2} - \frac{|G_3|^2}{2(\text{Im}\,\tau)} - \frac{|F_5|^2}{4}\right] + \frac{1}{8i\kappa_{10}^2}\int \frac{C_4\wedge G_3\wedge \overline{G}_3}{\text{Im}\,\tau} + S_{\text{loc}} \tag{1.1}$$

where $2\kappa_{10}^2 = (2\pi)^7(\alpha')^4$, S_{loc} denotes the contribution(s) from localalised sources which we will explain below, and the field content of the theory is the following:

- First of all, we have the 10-dimensional metric G_{MN}, along with its corresponding Ricci scalar R. Splitting our spacetime (as we will shortly do) as $M_4 \times X_6$ where M_4 represents our four-dimensional spacetime and X_6 is a compact (and Ricci-flat) manifold will relate κ_{10} with the usual four-dimensional Planck mass. More concretely, it can easily be checked that $M_{\text{Pl}}^2 = \mathcal{V}/(g_s\kappa_{10})^2$, where $\mathcal{V}$ is the volume of the compact manifold and g_s represents the string coupling in the string frame.

- τ is known as the *axiodilaton* and it is a complex combination of the 0-form C_0 present in type IIB supergravity and the *dilaton* Φ, which controls the string coupling; assuming this field is constant, the coupling can be described as $g_s = e^{\Phi}$. We thus define $\tau = C_0 + ie^{-\Phi}$. We will generically work in the perturbative limit where $g_s \ll 1$, which will in turn imply $\text{Im}\,\tau \gg 1$.

- Apart from C_0, type IIB supergravity also includes other form fields, namely the Neveu-Schwarz-Neveu-Schwarz (NS-NS) two-form B_2 (which appears already within the bosonic string spectrum), and the Ramond-Ramond (RR) 2- and 4-forms, C_2 and C_4 respectively. These last ones are usually referred to as Ramond-Ramond p-forms, as they arise from a specific choice of periodicity conditions in the fermionic sector of the superstring. All of these forms appear in the action (1.1) as combinations of

themselves with their field strengths:

$$F_3 = dC_2, \qquad H_3 = dB_2, \qquad G_3 = F_3 - \tau H_3, \qquad F_5 = dC_4 - \frac{1}{2} C_2 \wedge H_3 + \frac{1}{2} B_2 \wedge F_3 \tag{1.2}$$

As we will analyze below, these combinations allow the symmetries of the action to be reflected more clearly both at the level of the action (1.1) and on the resulting four-dimensional theory.

Finally, among the localized sources present in type IIB supergravity, D3-branes will play an important role in our following discussion. These are 3-dimensional extended objects, on which open strings can end. They are particularly interesting from a phenomenological point of view, as they can be considered to fill the 3 spatial, non-compact directions of our spacetime and, since branes carry gauge degrees of freedom on their worldvolume [15,16], localised stacks of N of these objects may generate an $SU(N)$ gauge theory on the non-compact spacetime.

The action of a D3-brane, at lowest order in α', reads [4]

$$S_{\text{D3}} = \mu_3 \int_{\mathcal{W}_4} C_4 - T_3 \int_{\mathcal{W}_4} d^4x \sqrt{-g} \tag{1.3}$$

where $\mathcal{W}_4$ is the 4-dimensional worldvolume (which, as we said above, will in general coincide with M_4), μ_3 represents the brane's (electric) coupling with the 4-form, while T_3 is the brane's tension. These last two quantites are related via $\mu_3 = g_s T_3 = 2\pi \ell_s^{-4}$.

1.2 Compactification with Calabi-Yau geometries

In order to make contact with our four-dimensional universe, we must *compactify* the 10 dimensions present in the type IIB supergravity theory to 4. The most straightforward choice seems to be the direct product $M_4 \times X_6$ where M_4 is a maximally symmetric, 4-D spacetime and X_6 is a *compact* and six-dimensional manifold[2].

Ultimately, we will be interested in arriving to a $D = 4$, $\mathcal{N} = 1$ supegravity theory in the non-compact space, as it allows for an unmatched perturbative control over the resulting field theory and allows for huge simplifications from a mathematical perspective. Of course, supersymmetry will have to be broken at a later stage in order to make contact with observations.

1.2.1 Calabi-Yau manifolds

By far, the most studied models of string compactifications involve *Calabi-Yau manifolds*, which due to their symmetries preserve a quarter of the ten-dimensional supersymmetry in the reduced, 4-D spacetime. These geometries were first proposed in [17] in the context of

[2]This simple ansatz is found to be inconsistent with the backreaction of the fluxes and branes on the background [11]. Generically the 10-dimensional metric is given as a warp product of the form $ds^2_{10} = e^{2A(y)} g_{\mu\nu} dx^\mu dx^\nu + e^{-2A(y)} g_{mn} dy^m dy^n$ where $A(y)$ is a function of the compact dimensions and Greek and Latin indices denote the coordinates on the non-compact and compact manifold, respectively.

compactification of Heterotic Superstring theories, where it was noted that they possessed just the right properties to leave a fraction of the 10-dimensional supercharges in the non-compact 4-D theory. These constructions gained popularity ever since and have been thoroughly explored as compactification manifolds in the rest of the Superstring theories.

First of all, Calabi-Yau spaces are *complex* manifolds[3], meaning that the coordinate charts map open sets of the manifold $U_\alpha \in X$ to $\mathbb{C}^n$, where n is the dimension of the manifold.[4] In general, not every real $2n$-dimensional manifold can be mapped to an n-dimensional complex manifold. This depends on the existence of a so-called *complex structure*. An *almost complex structure* is a map $\mathcal{J} : TX \to TX$, where TX is the tangent bundle of a real manifold X, such that $\mathcal{J}^2 = -1$. If every patch U_α of M admits a choice of complex coordinates $z^{\mu_1}, \ldots, z^{\mu_n}$ and their conjugates $\bar{z}^{\bar{\mu}_1}, \ldots, \bar{z}^{\bar{\mu}_n}$ such that, in component form, $\mathcal{J}^\mu_\nu = i\delta^\mu_\nu$ and $\mathcal{J}^{\bar{\mu}}_{\bar{\nu}} = -i\delta^{\bar{\mu}}_{\bar{\nu}}$ then $\mathcal{J}$ is known as a *complex structure* and M is a complex manifold.

From the definitions above, we can now see that when working with complex manifolds all structures involving vectors and forms will depend on two different variables: those with holomorphic indices and those with antiholomorphic ones. Of particular importance for the discussion that will follow are *(p,q)-forms*, which we define as

$$\omega = \frac{1}{p!q!}\omega_{\mu_1\ldots\mu_p\bar{\nu}_1\ldots\bar{\nu}_q} dz^{\mu_1} \wedge \ldots \wedge dz^{\mu_p} \wedge d\bar{z}^{\bar{\nu}_1} \wedge \ldots \wedge d\bar{z}^{\bar{\nu}_q} \in A^{p,q} \tag{1.4}$$

where $A^{p,q}$ denotes the space of (p,q)-forms. The usual exterior derivative d on real forms can be extended to complex forms, via the maps $\partial : A^{p,q} \to A^{p+1,q}$ and $\bar{\partial} : A^{p,q} \to A^{p,q+1}$ which satisfy $\partial^2 = \bar{\partial}^2 = 0$, in analogy with the real case. The real and complex exterior derivatives are related via

$$d = \partial + \bar{\partial} \tag{1.5}$$

It is then clear to see that, in particular, any $\bar{\partial}$-*exact form* $F_{p,q} = \bar{\partial} C_{p,q-1}$ will be $\bar{\partial}$-*closed*, i.e., $\bar{\partial} F_{p,q} = 0$. This leads to the definition of the so-called *Dolbeaut cohomology group* of a complex manifold M as the following equivalence class:

$$H^{p,q}_{\bar{\partial}}(M,\mathbb{C}) = \frac{Z^{p,q}(M)}{\bar{\partial} A^{p,q-1}(M)} \tag{1.6}$$

where $Z^{p,q}(M)$ denotes the space of all $\bar{\partial}$-closed (p,q)-forms, while $\bar{\partial} A^{p,q-1}(M)$ denotes the space of $\bar{\partial}$-exact (p,q)-forms. Basically, two closed forms are considered equivalent if they differ by an exact form, in analogy with real cohomologies. The dimension of each Dolbeaut cohomology group is given by the *Hodge numbers*:

$$h^{p,q} = \dim H^{p,q}_{\bar{\partial}}(M,\mathbb{C}) \tag{1.7}$$

These numbers will be closely related to the discussion on the String Theory Landscape below. Indeed, they will denote the number of massless fields in the low-energy theory arising from the deformations of the internal geometry.

[3] See, e.g., [4,18] for thorough introductions to complex geometry and, particulary, Calabi-Yau manifolds.

[4] We will be mostly working with $n = 3$, as it corresponds to the case of 6 real dimensions.

Having established the basics of complex manifolds and forms, we now turn to discuss the metric of such spaces. Of special interest will be the concept of a *Hermitian metric*, that is, a metric which in local coordinates satisfies

$$g = g_{\mu\bar{\nu}} dz^{\mu} \otimes d\bar{z}^{\bar{\nu}} + g_{\bar{\mu}\nu} d\bar{z}^{\bar{\mu}} \otimes dz^{\nu} \tag{1.8}$$

with $g_{\mu\bar{\nu}} = \overline{g_{\nu\bar{\mu}}}$. A complex manifold with such a metric is said to be Hermitean. This metric allows us to construct a special (1,1)-form, namely the *Kähler form* associated to the Hermitian metric:

$$\omega = i g_{\mu\bar{\nu}} dz^{\mu} \wedge d\bar{z}^{\bar{\nu}} \tag{1.9}$$

which is central to this discussion.

Indeed, a *Kähler manifold* is a Hermitean manifold whose Kähler form is closed:

$$d\omega = 0. \tag{1.10}$$

A direct consequence of this definition is that the metric $g_{\mu\bar{\nu}}$ of the manifold can be locally expressed in terms of a *Kähler potential* K, such that

$$g_{\mu\bar{\nu}} = \partial_{\mu}\partial_{\bar{\nu}} K. \tag{1.11}$$

We will encounter this potential quite a number of times in what follows, specially in the discussion of $\mathcal{N} = 1$, $D = 4$ supegravity, since the field space metric of that theory is actually Kählerian.

With the metric in hand, we can now construct the Ricci curvature tensor and scalar, as in the real case. The Ricci tensor is given by

$$R_{\mu\bar{\nu}} = -\partial_{\mu}\partial_{\bar{\nu}} (\log \det g) \tag{1.12}$$

Particularly, a *Ricci-flat* manifold is one which satisfies $R_{\mu\bar{\nu}} = 0$ for every coordinate patch. In the same fashion as we constructed the Kähler form, we now introduce the *Ricci form*

$$\mathscr{R} = i R_{\mu\bar{\nu}}\, dz^{\mu} \wedge dz^{\bar{\nu}} = -i\partial\bar{\partial} (\log \det g). \tag{1.13}$$

This object is actually a closed form with respect to the ordinary exterior derivative $d = \partial + \bar{\partial}$, which can be readily checked from its definition. However, it is not necessarily an exact form, since $\det g$ transforms non-trivially under coordinate transformations. This motivates the construction of the following equivalence class

$$c_1 = -\frac{i}{2\pi} [\mathscr{R}] \in H^2(X, \mathbb{R}) \tag{1.14}$$

known as the *first Chern class*.

We are now prepared to give a definition for a Calabi-Yau manifold. Calabi-Yau spaces are compact Kähler manifolds with vanishing first Chern class. We will not delve into the details regarding these interesting spaces, however, let us describe some of the most useful

properties of these manifolds.

First and foremost, the vanishing first Chern class indicates that this manifold is Ricci-flat (and thus satisfies the vacuum Einstein equations). Furthermore, as Yau proved [19], there exists a unique Ricci-flat metric associated to the Kähler form; however, no explicit metric has been found to date. Thus, while many different Calabi-Yau constructions are known [20], they are identified through their topological data. In any case, as we will shortly see, we will be more interested in finding the *deformations* of this metric, rather than the metric itself.

A Calabi-Yau manifold admits a *single* (cohomologically unique) and nowhere vanishing (3,0)-form, which we will denote as Ω. Furthermore, using all the dualities and symmetries between complex forms (such as Hodge and Poincaré duality), we find that the only non-vanishing Hodge numbers for any Calabi-Yau 3-form are $h^{0,0} = h^{3,3} = h^{3,0} = h^{0,3} = 1$, $h^{1,1} = h^{2,2}$ and $h^{1,2} = h^{2,1}$. Therefore, the whole complex cohomology of the manifold is specified only via two numbers: $h^{1,1}$ and $h^{2,1}$.

Calabi-Yau manifolds have SU(3) as holonomy group. This implies the existence of a covariantly constant spinor in the compact space [9], such that only one quarter of the 10-dimensional supersymmetry is preserved in the non-compact 4-dimensional space. Therefore, $\mathcal{N} = 1$ supersymmetry in 10 dimensions (which has 16 supercharges) reduces to $\mathcal{N} = 1$, $D = 4$ supersymmetry. On the other hand, type IIB supergravity actually has $\mathcal{N} = 2$ supersymmetry in 10 dimensions (i.e., 32 supercharges), so after compactification we will be left with $\mathcal{N} = 2$, $D = 4$ supersymmetry. As we will see below, in order to further reduce supercharges, we will need to use orientifold projections in order to reach the desired $\mathcal{N} = 1$, $D = 4$ supergravity theory.

1.2.2 *Moduli space of Calabi-Yau manifolds*

As we have seen in the previous section, Ricci-flatness is basically the defining feature of Calabi-Yau spaces. However, metrics satisfying such conditions are far from unique. Note that, for example, given any Ricci-flat metric $g_{\bar{\mu}\nu}$, the rescaling $g_{\bar{\mu}\nu} \to \lambda g_{\bar{\mu}\nu}$ defines another Ricci-flat metric. We could ask ourselves whether, given a Hermitean metric defined with respect to a certain complex structure, we can deform this metric in such a way that Ricci-flatness is preserved, i.e.

$$R_{\mu\bar{\nu}}(g) = 0 \;\to\; R_{\mu\bar{\nu}}(g + \delta g) = 0 \tag{1.15}$$

where δg represents a linear deformation of the metric:

$$\delta g = \delta g_{\mu\bar{\nu}} dz^{\mu} d\bar{z}^{\bar{\nu}} + \delta g_{\mu\bar{\nu}} dz^{\mu} dz^{\nu} + \text{c.c.} \tag{1.16}$$

which does not change the topological properties of the complex manifold. The space of all possible deformations of the metric compatible with the Ricci-flatness condition is called the *moduli space* of a Calabi-Yau manifold [21].

It can be shown that the deformations corresponding to $\delta g_{\mu\bar{\nu}}$ and $\delta g_{\mu\nu}$ are actually decoupled, and thus they correspond to independent classes of deformations. The former

are readily found to arise from deformations of the Kähler form

$$\delta\omega = i\delta g_{\mu\bar{\nu}}\, dz^{\mu} \wedge d\bar{z}^{\bar{\nu}}. \tag{1.17}$$

From Yau's theorem we know that any deformed Kähler form $\omega + \delta\omega$ still corresponds to a Ricci-flat Kähler manifold. Therefore, we can expand these deformations in terms of a basis of $(1,1)$-forms t^I, $I = 1, \ldots, h^{1,1}$, so that

$$\delta g_{\mu\bar{\nu}} = b_I(x)\, t^I_{\mu\bar{\nu}} \tag{1.18}$$

leading to $h^{1,1}$ scalar fields ($b_I(x)$) in the four-dimensional spacetime.

On the other hand, we might be tempted to neglect the moduli arising from $\delta g_{\mu\nu}$, as they seem incompatible a Hermitian metric. However, recall that the object that allowed us to write the local complex coordinates in the very first place is the complex structure. Thus, deformations of the metric with only (anti)holomorphic indices, indicate that the coordinates we are using do not correspond to our original complex structure. It is then inferred that $\delta g_{\mu\nu}$ and $\delta g_{\bar{\mu}\bar{\nu}}$ are related to deformations of the complex structure. These are parametrized with complex scalar fields z^a as

$$\delta g_{\mu\nu} = \frac{i}{||\Omega||^2}\bar{z}^a (\chi_a)_{\mu\bar{\mu}\bar{\nu}} \Omega^{\bar{\mu}\bar{\nu}}{}_{\nu} \tag{1.19}$$

where Ω is the unique (3,0)-form of the Calabi-Yau, $||\Omega||^2 = \frac{1}{3!}\Omega_{\mu\nu\rho}\overline{\Omega}^{\mu\nu\rho}$, and the forms χ_a constitute a basis for $H^{1,2}_{\bar{\partial}}(X, \mathbb{C})$. Therefore, deformations of the complex structure lead to $h^{2,1}$ complex scalar fields.

1.2.3 Calabi-Yau orientifolds

Following our previous discussion, Calabi-Yau compactifications preserve a quarter of the 10-dimensional supercharges, which in the case of type IIB supergravity means that the effective 4-D theory will be described by $\mathcal{N} = 2$ supergravity. For this end, all of the Kaluza-Klein modes of the bosonic and fermionic fields, plus the Kähler and complex structure moduli above will need to be arranged into supersymmetric multiplets (see [22] for a detailed description of the action and its components).

We will ultimately be interested in an effective $\mathcal{N} = 1$ supersymmetric Lagrangian in 4 dimensions. In order to achieve this, it is customary to accompany the dimensional reduction with an additional operation known as *orientifolding* (see [23] for a review). In type IIB supergravity, orientifold actions involve the reversal of the string world-sheet orientation and a geometric involution which reverses the sign of the (3,0)-form Ω of the compact space, leaving the Kähler form and complex structure invariant. The subsets of the 10-dimensional spacetime invariant under this symmetry give rise to p-dimensional *orientifold planes*, or Op-planes for short. These are non-dinamical objects, negatively charged with respect to the Ramond-Ramond p-forms, and they will be crucial in the following discussion. More concretely, in the cases we will be interested in, the orientifold action only acts on the compact manifold, with its fixed points being either four-cycles or points in X_6,

thus yielding O3/O7-planes.[5]

As anticipated, compactifications with Calabi-Yau manifolds accompanied by an orientifold symmetry (also known as *Calabi-Yau orientifolds*) project out half of the $D = 4$ supercharges, leading to $\mathcal{N} = 1$ supergravity in 4 dimensions. Naturally, some of the scalar fields present in the theory will be projected out due to this symmetry, and the remaining ones will need to be assembled into chiral supermultiplets. It can be shown that the bosonic spectrum surviving the orientifolding is composed of the following fields:

- $h^{1,1}$ complex scalar fields T^ρ, $\rho = 1, \ldots, h^{1,1}$ parametrizing, among other quantities, the volume of the compactified space, $\mathcal{V}(T^\rho)$. These are the Kähler moduli we described above. A fraction of these present axionic properties, with rich phenomenological applications [24, 25].

- $h^{2,1}$ complex scalar fields[6] z^i, $i = 1, \ldots, h^{2,1}$, related to the complex structure moduli. These will actually be central to the discussion on flux compactifications.

- The axiodilaton τ, introduced in (1.1).

All in all, Calabi-Yau orientifolds will give rise to $h^{1,1} + h^{2,1} + 1$ massless complex scalar fields. Tipically, this sum may be of the order of the hundreds (see, e.g., [26, 27]). Of course, current phenomenological constraints (coming from Big Bang Nucleosynthesis, for example) rule out the possibility of such light vacua [28]. Thus, these fields must acquire mass somehow; as we will see below, one of the most researched methods to induce a potential on these moduli is through *flux compactifications* [11, 29].

1.3 Effective theory and flux compactifications

In this subsection we will summarize the relevant formulae for compactifications of type IIB superstrings on the orientifold $\tilde{X}_6$ of a Calabi-Yau manifold X_6 (see [22, 30] for a review). We will work in units of the reduced Planck mass, $M_p^{-2} = 8\pi G = 1$.

As we described above, the low-energy spectrum of type IIB string theory compactified on a Calabi-Yau orientifold $\tilde{X}_6$ includes[7] the axio-dilaton τ, $h^{2,1}$ the complex structure moduli z^i, and $h^{1,1}$ Kähler moduli T^ρ, which are assembled into scalar multiplets in $\mathcal{N} = 1$, $D = 4$ supergravity. The bosonic sector of such a theory is built using two ingredients: the Kähler potential, introduced in eq. (1.11), and the *superpotential*. The former gives a metric for the field space, which arises in the kinetic part of the Lagrangian as

$$\mathcal{L}_{\text{bos,4D}} = -K_{i\bar{j}}\partial^\mu \phi^i \partial_\mu \bar{\phi}^{\bar{j}} - V(\phi, \bar{\phi}), \qquad K_{i\bar{j}} = \frac{\partial^2 K}{\partial \phi^i \partial \bar{\phi}^{\bar{j}}} \tag{1.20}$$

[5] Type IIB string theory may also include O5/O9-planes [22, 23]. These are not relevant for the scheme of flux compactifications we will develop below

[6] The cohomology group $H^{2,1}(M, \mathbb{C})$ decomposes into odd and even subgroups under the orientifold action. In this case, the complex structure moduli actually arise from the odd part, i.e., $H^{2,1}_-$ with dimension $h^{2,1}_-$. We will omit the subscript in favor of a clearer notation.

[7] We will ignore further degrees of freedom, such as possible $h^{1,1}_-$ axion multiplets, $D3$- and $D7$-brane moduli, or matter fields.

On the other hand, the scalar potential is a function of both the Kähler potential and the superpotential. In the absence of interactions with the gauge sector, it reads[8]

$$V(\phi,\bar{\phi}) = e^{K}\left[K^{i\bar{j}}D_i W D_{\bar{j}}\overline{W} - 3|W|^2\right] \tag{1.21}$$

where $D_i = \partial_i + K_i$ are Kähler covariant derivatives and the indices run over all bosonic scalar fields, i.e., the axiodilaton and the Kähler and complex structure sectors.

To leading order in α' and g_s, the Kähler potential K of the corresponding 4-dimensional supergravity theory can be read from the effective action once the extra dimensions have been compactified [21, 22]. In this case, the Kähler potential is given by

$$K = -2\log\mathcal{V} - \log(-\mathrm{i}(\tau-\bar{\tau})) - \log\left(\mathrm{i}\int_{X_6}\Omega\wedge\overline{\Omega}\right). \tag{1.22}$$

Here $\mathcal{V}(T^\rho,\overline{T}^\rho)$ denotes the Kähler moduli-dependent volume of $\tilde{X}_6$, measured in the Einstein frame and in units of the string length ℓ_s. In the concrete case of a single Kähler modulus, i.e., $h^{1,1}=1$, it reads [4]

$$\mathcal{V} = (T+\overline{T})^{3/2}. \tag{1.23}$$

On the other hand, the last term of (1.22) is written it terms of the unique holomorphic form Ω of the Calabi-Yau which, in turn, depends implicitly on the complex structure moduli, c.f. equation (1.19). For this Kähler potential to provide a good description of the moduli space geometry, and in particular for the α' corrections to remain under control, we will restrict ourselves to the large volume regime[9], $\mathcal{V}\to\infty$, see [31] for more detail.

The couplings of the theory are conveniently expressed by specifying a symplectic basis[10] of 3-cycles of the Calabi-Yau $\{A^I, B_I\}$, with $I = 0,\ldots,h^{2,1}$, and a dual basis of three-forms α^I and β_I such that

$$\int_{A^I}\alpha_J = \delta^I_J \qquad \int_{B_I}\beta^J = -\delta^J_I, \qquad \int_{M_3}\alpha_I\wedge\beta^J = \delta^J_I, \qquad \int_{A^I}\beta^J = \int_{B_I}\alpha_J = 0\,. \tag{1.24}$$

When Ω is expressed in this basis, it reads

$$\Omega = X^I\alpha_I - \mathscr{F}_I\beta^I, \qquad \text{with} \qquad X^I = \int_{A^I}\Omega, \qquad \mathscr{F}_I = \int_{B_I}\Omega\,. \tag{1.25}$$

The X^I are projective coordinates in the complex structure moduli space, and the corresponding moduli fields can be defined to be $z^i \equiv -\mathrm{i}X^i/X^0$, $i=1,\ldots,h^{2,1}$. In order to find a more convenient expression for the Kähler potential, the quantities X^I and $\mathscr{F}_I$ are grouped in a symplectic *period vector* $\Pi^T = (X^I,\mathscr{F}_I)$. Then, it is possible to write the Kähler potential

[8] We denote by $K^{\rho\bar{\sigma}} = (K_{\rho\bar{\sigma}})^{-1}$, $K^{\tau\bar{\tau}} = (K_{\tau\bar{\tau}})^{-1}$ and $K^{i\bar{j}} = (K_{i\bar{j}})^{-1}$ the inverses of the field space metrics on the Kähler, axio-dilaton and complex structure sectors respectively.

[9] Note that the Kaluza-Klein mass scale arising from the scalar fields in the compact directions will need to be clearly separated from the mass these fields acquire through fluxes or other mechanisms. As shown in [31], this separation of scales is under control in the large volume limit.

[10] The number of n-cycles of a manifold is given by the n-th *Betti number* b_n. For Calabi-Yau manifolds in particular, the number of 3-cycles is $b_3 = \sum_{p+q=3} h^{p,q} = 2h^{2,1}+2$.

of the complex structure moduli space K_{cs} as

$$e^{-K_{cs}} = i\int_{M_3} \Omega\wedge\overline{\Omega} = -i(X^I\overline{\mathscr{F}}_I - \overline{X}^I\mathscr{F}_I) = i\Pi^\dagger\cdot\Sigma\cdot\Pi, \tag{1.26}$$

where Σ is the symplectic matrix

$$\Sigma = \begin{pmatrix} 0 & \mathbb{1} \\ -\mathbb{1} & 0 \end{pmatrix}. \tag{1.27}$$

The previous expression is invariant under transformations $\mathrm{Sp}(2h^{2,1}+2,\mathbb{Z})$ associated with different choices for the symplectic basis (1.24). These symplectic transformations act on the period vector as follows

$$\Pi \longrightarrow S\cdot\Pi \qquad \text{where} \qquad S^T\cdot\Sigma\cdot S = \Sigma. \tag{1.28}$$

The quantities $\mathscr{F}_I$ can be expressed as the derivatives of a holomorphic function of the X^I, *the prepotential*, so that

$$\mathscr{F}_I(X) = \partial_I\mathscr{F}(X). \tag{1.29}$$

The prepotential is a homogeneous function of degree 2, i.e., $\mathscr{F}(\lambda X) = \lambda^2\mathscr{F}(X)$, and therefore it satisfies

$$X^I\mathscr{F}_I = 2\mathscr{F}(X). \tag{1.30}$$

Setting the gauge $X^0 = 1$, and using the homogeneity of the prepotential, the period vector can be written as

$$\Pi(z^i) = \begin{pmatrix} 1 \\ iz^i \\ 2\mathscr{F} - z^j\mathscr{F}_j \\ -i\mathscr{F}_i \end{pmatrix}. \tag{1.31}$$

Thus, the complex structure term of the Kähler potential in $\mathcal{N}=1$, $D=4$ supergravity can be easily expressed only in terms of the prepotential, which depends on the geometry of the compact space.

1.3.1 *No-scale flux vacua*

We now turn to study how the scalar potential can be generated for the moduli, which in turn means we need to look for a suitable superpotential. It can be shown that the kinetic term for the composite 3-form G_3 in (1.1), when fluxes are turned on only in the compact space, generates a scalar potential for the moduli. This scheme is known as *flux compactification*, introduced in [9]. The scalar potential arising from the fluxes is described in terms of the

Gukov-Vafa-Witten superpotential [29]:

$$W = \frac{1}{\ell_s^2\sqrt{4\pi}}\int_{M_3} G_{(3)}\wedge\Omega\,, \tag{1.32}$$

where $G_{(3)} = F_{(3)} - \tau H_{(3)}$, denoting by $F_{(3)}$ and $H_{(3)}$ the RR and NS-NS 3-form field strengths respectively. Note that the presence of the holomorphic 3-form Ω indicates the implicit dependence on the complex structure moduli of this superpotential.

This potential can be described in terms of flux quanta threading the internal manifold's 3-cycles. Fluxes are required to satisfy the following quantization conditions[11]

$$\begin{aligned}
&\frac{1}{\ell_s^2}\int_{A^I} F_{(3)} = -f_A^I \in \mathbb{Z}\,, \qquad \frac{1}{\ell_s^2}\int_{B_I} F_{(3)} = -f_I^B \in \mathbb{Z}\,,\\
&\frac{1}{\ell_s^2}\int_{A^I} H_{(3)} = -h_A^I \in \mathbb{Z}\,, \qquad \frac{1}{\ell_s^2}\int_{B_I} H_{(3)} = -h_I^B \in \mathbb{Z}\,.
\end{aligned} \tag{1.33}$$

Here minus signs have been introduced in all expressions for convenience. These fluxes can be decomposed in the symplectic basis as

$$F_{(3)} = -\ell_s^2\,(f_A^I\alpha_I - f_I^B\beta^I), \qquad H_{(3)} = -\ell_s^2\,(h_A^I\alpha_I - h_I^B\beta^I). \tag{1.34}$$

If we define the symplectic flux vectors $f^T = (f_A^I, f_I^B)$, $h^T = (h_A^I, h_I^B)$, and $N = f - \tau\, h$, we can write the flux superpotential in a compact way as

$$W = \frac{1}{\sqrt{4\pi}}\left[(f_A^I - \tau h_A^I)\mathcal{F}_I - (f_I^B - \tau h_I^B)X^I\right] = \frac{1}{\sqrt{4\pi}}\,N^T\cdot\Sigma\cdot\Pi\,. \tag{1.35}$$

Note that the superpotential depends only on the complex structure moduli (through the period vector Π) and on the axiodilaton (through the flux vector N).

At tree-level, the Kähler sector satisfies the no-scale property [22] $K^{\rho\bar\sigma}K_\rho K_{\bar\sigma} = 3$, and therefore the scalar potential of the effective supergravity action reads

$$V_{\text{tree}} = \mathrm{e}^K\left[K^{i\bar j}D_i W D_{\bar j}\overline{W} + K^{\tau\bar\tau}D_\tau W D_{\bar\tau}\overline{W}\right] \geq 0 \tag{1.36}$$

which does not involve the Kähler moduli. Thus, at tree-level, only the axio-dilaton and complex structure sector may be stabilized. In order to constrain the Kähler moduli, the superpotential and the Kähler potential need to take into account α' perturbative corrections [32, 33] and non-perturbative effects [34, 35]. It is important to emphasize that the no-scale structure leading to the potential (1.36) is broken by these corrections. However, provided these terms remain under control, they will only induce subleading contributions to the mass spectra on the axio-dilaton/complex structure sector, which may be computed from

[11] The following are generalizations of the Dirac quantization condition of electromagnetic charges. In this case, they required to have a consistent description of the wave function of the D-brane that couples to these fluxes; see [12], [3, ch.6] and [4, ch.18] for more detail and the correspondence of this quantization with instantons in string theory.

the tree-level potential.[12].

In part II of this thesis we will mostly consider critical points of the no-scale potential, denoted by $\{\tau_c, z_c^i\}$, where the axio-dilaton/complex structure sector configuration preserves supersymmetry, namely points satisfying

$$D_\tau W|_{\tau_c, z_c^i} = 0, \qquad \text{and} \qquad D_i W|_{\tau_c, z_c^i} = 0 \quad \text{for all} \quad i = 1\ldots, h^{2,1}\,. \tag{1.37}$$

Note, however, that in general supersymmetry is still broken by the Kähler sector, since $D_\rho W = K_\rho W \neq 0$ unless the expectation value of the flux superpotential vanishes, $W|_{\tau_c, z_c^i} = 0$. In what follows, field configurations satisfying (1.37) will be referred to as *no-scale vacua*.

We comment in passing that the expressions for the flux superpotential (1.35) and the previous one for the $D3$-charge are both manifestly invariant under the action of the symplectic group $\mathrm{Sp}(2h^{2,1}+2, \mathbb{Z})$, provided the flux vector also transforms as

$$N \longrightarrow S \cdot N, \qquad S \in \mathrm{Sp}(2h^{2,1}+2, \mathbb{Z}). \tag{1.38}$$

Actually, the combined actions (1.28) and (1.38) represent redundancies of the effective supergravity description, and therefore no-scale solutions related by these transformations should be regarded as equivalent. In addition, the previous characterisation of flux vacua is also invariant under $\mathrm{SL}(2, \mathbb{Z})$ transformations acting simultaneously on the axio-dilaton τ and the fluxes as

$$\tau \to \frac{a\tau + b}{c\tau + d}, \qquad \begin{pmatrix} F_3 \\ H_3 \end{pmatrix} \to \begin{pmatrix} a & b \\ c & d \end{pmatrix} \cdot \begin{pmatrix} F_3 \\ H_3 \end{pmatrix}, \tag{1.39}$$

with $a, b, c, d \in \mathbb{Z}$ and $ad - bc = 1$. As in the case of symplectic transformations, these actions should also be regarded as redundancies, thus, different no-scale vacua connected by them represent the same physical state.

1.3.2 *Tadpole cancellation*

Before closing our discussion on the complex structure moduli, let us comment on a subtlety regarding the fluxes and the values they may take. From the type IIB supergravity action (1.1) the equation of motion of the R-R 4-form C_4 is found to be a generalization of Gauss' law. Integrating this over the compact manifold yields the crucial condition that all sources for C_4 must cancel each other [4, 13]. Intuitively, this is simply the general statement that all electric field lines in a compact manifold must start and end on some charge, lest they cross each other. From (1.1) we can see that the Chern-Simons term provides a source for C_4 if the fluxes G_3 only thread the compact dimensions. D3-branes are also sources of C_4, see the first term of (1.3), as well as O3-planes, whose coupling to the R-R form is opposite to and half of the one of the D3-brane. Taking all of these into account, we find the following

[12] Here, following [31, 34–36] we assume that no-scale configurations (1.37) represent a good classical background for the computation of quantum corrections in string theory, including the case when $W|_{\tau_c, z_c^i} \neq 0$. For a criticism of this approach see [37] (see also [38]).

constraint on the fluxes:

$$N_{\text{flux}} + N_{D3} - \frac{1}{2} N_{O3} = 0 \tag{1.40}$$

where N_{D3} and N_{O3} are the number of D3-branes and O3-planes respectively present in our setup, and N_{flux} is defined as

$$N_{\text{flux}} \equiv \frac{1}{8i\kappa_{10}^2} \int_{X_6} \frac{G_3 \wedge \overline{G}_3}{\text{Im}\,\tau} = \frac{1}{\ell_s^4} \int_{M_3} F_{(3)} \wedge H_{(3)} = \left(f_I^B h_A^I - h_I^B f_A^I\right) = h^T \cdot \Sigma \cdot f = \frac{N^\dagger \cdot \Sigma \cdot N}{\tau - \bar{\tau}}. \tag{1.41}$$

Equation (1.40) is usually also expressed in the following convenient way

$$N_{\text{flux}} \leq N_{\text{flux}} + N_{D3} = L, \tag{1.42}$$

where L denotes the contribution from the orientifold planes. As we will see later on, this allows us to define the numerical problem of finding proper fluxes for no-scale vacua in a more convenient way. This expression can also be connected with extremely interesting properties of *F-theory*, a particularly useful geometrical generalization of type IIB String Theory [39].

The requirement of zero net charge is generically known as *tadpole cancellation* in the literature [13] since, in an open string language, failure to do so translates into anomalies in the scattering amplitudes.

1.3.3 *Stabilization of Kähler moduli*

We saw in subsection 1.3.1 that in the effective theory, fluxes only act on the dilaton and complex structure sector, thus leaving the Kähler sector massless at this stage. Therefore, further ingredients are required in order to have complete control over these geometric moduli. The most prominent approaches to deal with this issue are known as the KKLT scenario [35] and the Large Volume Scenario (LVS) [34] (see [40, 41] for comprehensive reviews).

The KKLT approach

In order to generate a contribution for the Kähler moduli, in this scenario one introduces non-perturbative contributions to the superpotential due to *gaugino condensation* [42]. Schematically, we can introduce into our compactification setup a number of $D7$-branes wrapping up some 4-cycle Σ_4 of the Calabi-Yau. The worldvolume theory of such a stack of branes is a Yang-Mills action and, provided the compact directions are integrated out, we are left with an $\mathcal{N} = 1$ super-Yang-Mills (SYM) in four dimensions. This theory is shown to generate a non-zero vacuum expectation value for gaugino bilinears [42] which, in the language of our effective field theory, translates into a contribution to the superpotential given by

$$W_{\text{np}} = A e^{-aT} \tag{1.43}$$

where we have only considered one Kähler modulus T and A and a are numerical constants.[13] The appearance of the Kähler modulus in this terms is related to the fact that the effective gauge coupling of the four-dimensional theory is proportional to the volume of the 4-cycle the branes are wrapping, which in turn is proportional to the overall volume of the Calabi-Yau.

With these comments in mind, the full superpotential reads

$$W = W_0 + W_{\text{np}} \tag{1.44}$$

where W_0 is the Gukov-Vafa-Witten superpotential (1.32) and thus, together with the Kähler potential (1.22), this theory is now capable of stabiling all moduli. Once again, neglecting corrections to the Kähler potential requires that the solution has a large volume, i.e., $\text{Re}(T) \gg 1$, which in this scheme implies $W_0 \ll 1$ at critical points of the scalar potential.

In practice, in order to be able to generate an extremely small flux superpotential, one usually first works with the dilaton and axiodilaton sector and tunes the fluxes in order to have $W_0 \ll 1$. These fields receive a mass term due to the fluxes and are then fixed to those values. Finally, Kähler moduli are stabilized through the inclusion of (1.43). Note that in general, in order to be able to freeze the axio-dilaton and complex structure sector, we will need to require that the masses of these fields are sufficiently large so the inclusion of non-perturbative terms does not significantly change their values.

Large Volume Scenario

Let us briefly describe the most prominent alternative to the KKLT approach for Kähler moduli stabilization, the Large Volume Scenario (LVS), first introduced in [31, 34]. The most relevant feature of this scheme is that it will allow us to stabilize the moduli at *exponentially* large volume (thus allowing us to neglect corrections to the theory which might be subleading in $\mathcal{V}$), without imposing any restriction on the value of W_0, thus allowing for consistent compactifications with $W_0 \sim \mathcal{O}(1-10)$.

In order to achieve stabilization, not only are non-perturbative corrections included in the superpotential, as in (1.43), but also *perturbative* corrections to the Kähler potential of the Kähler moduli, which read

$$K_K = -2\,\ln\left(\mathcal{V} + \frac{\xi}{2g_s^{3/2}}\right), \quad \xi \equiv -\frac{\chi(X_6)\zeta(3)}{2(2\pi)^3} \tag{1.45}$$

In the last expression, ξ is a constant parameter defined in terms of $\chi(X_6)$, the Euler number of the compact spaces, and ζ, the Riemann Zeta function. Of course, these corrections will break the no-scale structure condition of the Kähler potential.

For the purposes of LVS stabilization, the models we are interested in feature, at least, 2 Kähler moduli. Furthermore, in order to generate a competition in the resulting scalar potential between the non-perturbative terms (1.43) and the perturbative term in (1.45), a hierarchy between the Kähler moduli is required. One of the most simple examples to study

[13] This non-perturbative superpotential may be generalized to include many such terms, i.e, $W_{\text{np}} = \sum_i A_i e^{-a_i T}$. As we will see in chapter 4, this leads to *racetrack potentials* and are actively researched as candidates for Kähler moduli stabilization.

this scenario is the $\mathbb{WP}^4_{[1,1,1,6,9]}$ hypersurface (see chapters 3 and 4), which has $h_{1,1} = 2$ Kähler moduli. The volume of this compactification is given by $\mathcal{V} \propto \tau_b^{3/2} - \tau_s^{3/2}$, with $\tau_i = Re(T_i)$, and the subscripts stand for "big" and "small", respectively. Working through the algebra of the scalar potential and its critical points, it can be checked (see, e.g., [31] for all details and derivations) that requiring $\tau_b \gg \tau_s \gg 1$ will allow us to stabilize the volume at

$$\mathcal{V} \sim |W_0| e^{a\tau_s}, \tag{1.46}$$

where a is the exponential factor of (1.43) and no requirements have been imposed, a priori, on W_0. Thus, exponentially large volumes may be consistently reached in such compactification schemes.

1.4 The String Theory Landscape

Using the mechanisms described above, we are able (in principle, at least) to stabilize *all* moduli for a given compactification. However, the vacua found this way will always be either Minkowski or anti-de Sitter minima, since supersymmetry remains unbroken at this stage. In order to make contact with observations, we require some mechanism to *uplift* a fraction of these vacua to de Sitter. While we will not discuss them in detail (see, e.g. [35, 43]), it is important to stress that several uplifting mechanisms have been found in String Theory which are able to generate minima with a positive cosmological constant.

Taking into account all these ingredients, we are thus left with an ensemble of vacua (with any sign of cosmological constant), arising from the stabilization of moduli from the compact manifold threaded with fluxes and with corrections taken into account. The collection of all of these four-dimensional vacua with all moduli stabilized is known as the *String Theory Landscape* [44]. One may wonder what is the expected amount of vacua that may be found within this Landscape. From our previous analysis alone, it is clear that ranging from the amount of possible Calabi-Yau geometries to the fluxes they may be threaded with (in accordance with the tadpole constraint), we should expect an enormous number of possible vacua, a small fraction of which may be compatible with current constraints on observable quantities of our Universe (such as the Higgs mass, the cosmological constant etc.). An estimate may be obtained from the tadpole condition and Hodge numbers of the Calabi-Yau we want to examine [13, 45, 46], which typically yields[14] a number of vacua of the order of 10^{500}.

In order to characterise vacua in the Landscape, two main approaches may be followed. On the one hand, a completely analytical treatment of the effective field theory allows us to pinpoint exact solutions in the moduli space, along with the properties of such solutions such as their meta-stability against non-perturbative decays (to be further explored above) or the couplings that arise between different sectors of the field content of the vacuum solution. On the other hand, the huge amount of vacua estimated in the Landscape motivates a *statistical* study of the ensemble of solutions, initiated by [48]. This approach allows us, assuming some simplifying assumptions (such as taking the flux variables as continuum parameters), to obtain approximate distributions of many observables for these vacua, which grants a further

[14] However, recent studies of the estimate of vacua in F-theory have placed it around $10^{272,000}$ [47]

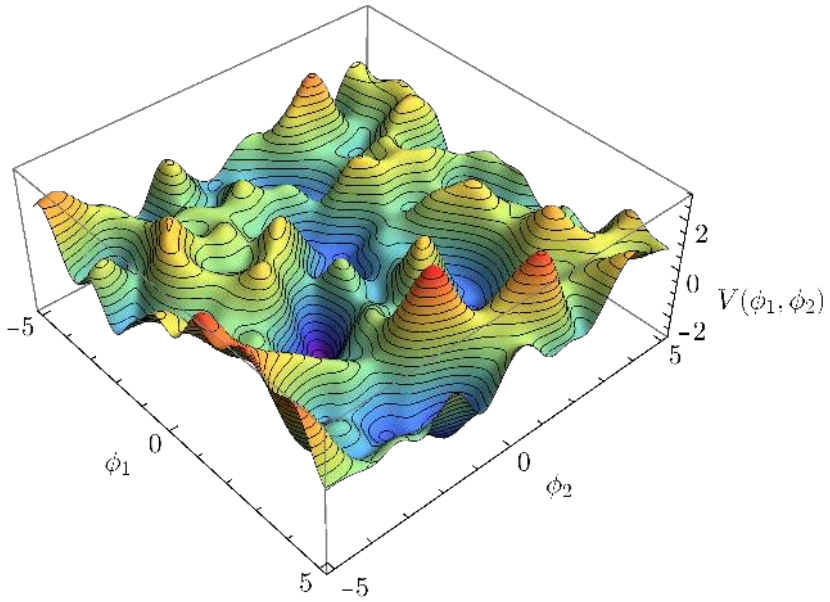

Figure 1.1: A pictorial (and simplified) version of the String Theory flux Landscape, consisting of two scalar fields.

understanding of the characteristics of realistic solutions in String Theory. Throughout this thesis, we will tackle both of these directions in our work, and show the interplay among them, by finding explicit solutions to compactification examples and comparing the distributions of these vacua with their expected statistical behaviour.

With such a great number of (in principle) attainable vacua in the Landscape, one might be tempted to think that any possible EFT coupled to gravity may be found as a low energy limit of some vacuum in the Landscape. However, this might not be possible from what we know about our particular Universe and, actually, one might be able to discern if such an EFT can actually be embedded within a high energy theory. In this sense, all the consistent 4D EFTs which cannot be found in the Landscape are said to lie in the *Swampland* [49–51].

In order to discern which vacua may lie in the Landscape and which may belong to the Swampland, over the past decades many *Swampland conjectures* have been formulated. These generically state properties which may need to be satisfied in order for a certain EFT to have a UV completion in String Theory. These conjectures arise from observations about extreme phenomena within our Universe; for example, from the properties of extremal black holes, one is lead to the *Weak Gravity Conjecture* [52], stating that gravity should always be the weakest force present in the EFT, or to the requirement that no global symmetries may exist in the theory [53]. More recently, the very existence of de Sitter critical points (either minima, maxima or saddle points) in a scalar potential of the EFT has been put into question within String Theory in [54]. This conjecture sparkled quite a lot of studies upon its release (see e.g. [55–65] and chapter 4) and it is still a matter of debate both from a foundational [66] and phenomenological [59] perspective.

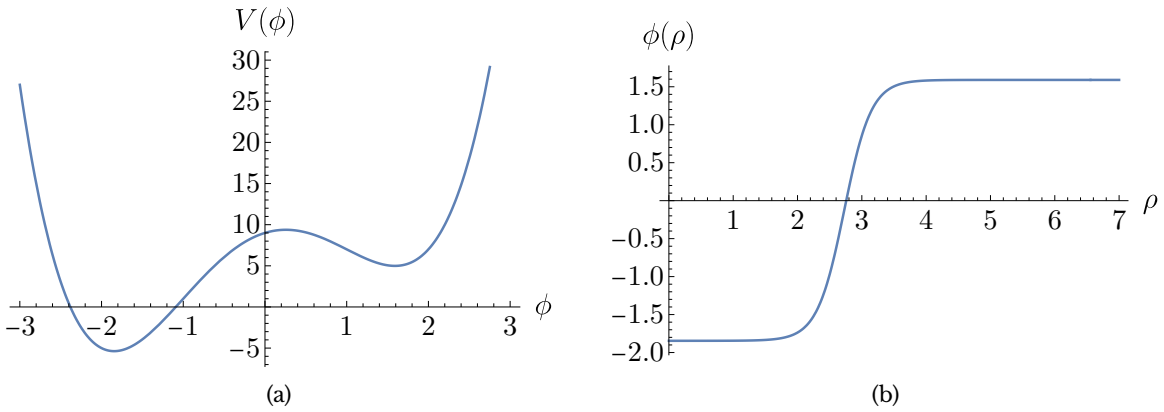

Figure 1.2: (a) Canonical double well scalar potential with non-degenerate vacua. (b) Euclidean spherical solution to the previous potential, for a background of false vacuum.

1.5 Non-perturbative stability of vacua

We have seen that the String Theory Landscape is composed of all kinds of vacua, arising from the compactification geometry, the fluxes we thread it with and all sorts of configurations involving branes and orientifold planes. In order to get a intuitive idea of the potentials such configurations generate, one may think of the Landscape as a collection of vacua like the one shown in figure 1.1. Note that while these potentials are clearly simplified versions of actual EFTs arising from compactifications, they serve as a good case study to tackle more complicated schemes later on.

Given this huge collection of (generically) non-degenerate vacua, one may wonder about their stability against quantum non-perturbative effects. Indeed, as noted by Coleman and collaborators in [67–69], quantum tunneling may be consistently generalized to field theories, leading to the concept of *False Vacuum Decay*.

In this section, we will closely follow the seminal papers [69, 70]; for more detail and examples see [71, 72].

1.5.1 False Vacuum Decay

The study of quantum tunneling in the context of field theory can be stated most simply in terms of a single scalar field ϕ, with a potential like the one shown in figure 1.2(a). While this picture may be expanded to include more fields with involved interactions, this simple example will give us an intuitive idea of what to expect in this kind of decays.

Thus, the problem we are trying to solve can be simply described as follows: given a configuration where the field rests at the highest local minimum (the *false vacuum*) of the potential everywhere in space, what is the probability per unit volume and time that this field may tunnel through the barrier to reach the lower minimum, i.e., the *true vacuum*? Of course, we will also be interested in obtaining the profile of the field in spacetime once the tunnelling occurs. In order to answer this question, we may proceed by generalizing the semiclassical, WKB approximation in quantum mechanics to field theory.

The WKB approximation and the Euclidean approach

Given a system with several generalized degrees of freedom assembled into a vector $\boldsymbol{q}$ and described by a Lagrangian

$$L = \frac{1}{2}\left(\frac{\partial \boldsymbol{q}}{\partial t}\right)^2 - V(\boldsymbol{q}), \tag{1.47}$$

in can be shown [73] that the tunneling amplitude from a certain initial (and classically stable) point $\boldsymbol{q}_0 = \boldsymbol{q}(0)$ to another configuration $\boldsymbol{q}_f = \boldsymbol{q}(s_f)$ is given by

$$|T| = A\, e^{-B/2} \tag{1.48}$$

at first order in $\hbar$. In this expression A is a theory-dependent, $\mathcal{O}(1)$ numerical factor and B is given by

$$B[P] = \int_0^{s_f} ds \sqrt{2(V(\boldsymbol{q}(s)) - E)} \tag{1.49}$$

where s parametrizes the trajectory in configuration space in terms of $(ds)^2 = (d\boldsymbol{q})^2$ and $E = V(\boldsymbol{q}_0)$. If the emergence point of this tunnelling is not specified in advance, then the most probable escape path (MPEP) can be obtained by minimizing (1.49).

This problem is most easily understood from the perspective of Lagrangian mechanics. We know that given a system described by (1.47), its equations of motion are

$$\frac{d^2 q_i}{dt^2} = -\frac{\partial V}{\partial q_i}. \tag{1.50}$$

Furthermore, from the Jacobi-Maupertuis principle [74], we know that the trajectory followed in configuration space can also be obtained by minimising the following integral:

$$I = \int_0^{s_f} ds \sqrt{2(E - V(\boldsymbol{q}(s)))}. \tag{1.51}$$

Thus, it seems we might be able to find a minimum of (1.49) working in a similar fashion. Indeed, noting that (1.49) can be obtained from (1.51) by taking $V \to -V$, the trajectory corresponding to the from this integral will correspond to the one followed by the equations of motion

$$\frac{d^2 q_i}{d\tau^2} = \frac{\partial V}{\partial q_i}. \tag{1.52}$$

where we have introduced Euclidean time $\tau = i\,t$, which effectively incorporates the reversal of the potential from the original equations of motion (1.50). These e.o.m.'s can be obtained by extremizing the *Euclidean action*

$$S_E = \int d\tau \left[\frac{1}{2}\left(\frac{d\boldsymbol{q}}{d\tau}\right)^2 + V(\boldsymbol{q})\right]. \tag{1.53}$$

For later application, we will be most interested in paths which, in terms of Euclidean time,

start off from $\boldsymbol{q}_0$ at $\tau = -\infty$, reach $\boldsymbol{q}_f$ at some finite Euclidean time and then return to $\boldsymbol{q}_0$ at $\tau = +\infty$. These are known as *bounces*. It can be shown that for these trajectories

$$B = S_E[\bar{\boldsymbol{q}}] - S_E[\boldsymbol{q}_0] \tag{1.54}$$

where the first term corresponds to the evaluation of the Euclidean action (1.53) for a path satisfying the Euclidean equations of motion (1.52), while the second one simply integrates the action with $\boldsymbol{q} = \boldsymbol{q}_0$.

In summary, we have found that the MPEP may be found by extremizing the Euclidean action associated to the theory under study. The solution to the equations of motion arising from it follows this tunneling path and can actually be used to obtain the exponential factor in the tunneling amplitude (1.48).

Generalizing to field theory

The key idea of Coleman is to generalize the above results to a scalar field theory with equations of motion given by

$$\left(-\frac{\partial^2}{\partial t^2} + \nabla^2\right)\phi = -\frac{\partial V}{\partial \phi} \tag{1.55}$$

where $V(\phi)$ is shown in figure 1.2(a) and the field is initially assumed to sit in the false vacuum everywhere in space. According to our previous analysis, we may be able to find a bounce of the Euclidean equations provided we extremize the Euclidean action, which is given by

$$S_E = \int d\tau d^3\boldsymbol{x}\left[\frac{1}{2}(\partial_\tau\phi)^2 + \frac{1}{2}(\nabla\phi)^2 + V(\phi)\right]. \tag{1.56}$$

Thus, the Euclidean equation of motion to be solved and its boundary conditions are

$$\Box_e\phi \equiv \left(\frac{\partial^2}{\partial\tau^2} + \nabla^2\right)\phi = \frac{\partial V}{\partial\phi}, \quad \lim_{\tau\to\pm\infty}\phi(\tau,\boldsymbol{x}) = \phi_{\text{fv}}, \quad \left.\frac{\partial\phi}{\partial\tau}\right|_{\tau=0} = 0, \quad \lim_{\boldsymbol{x}\to\pm\infty}\phi(\tau,\boldsymbol{x}) = \phi_{\text{fv}}. \tag{1.57}$$

where ϕ_{fv} stands for the value of ϕ at the false vacuum of $V(\phi)$. The first two conditions arise from requiring that the Euclidean solution is a bounce, while the third one simply arises from the fact that crossing the potential barrier separating the false and true vacua requires some amount of energy, and thus only a compact region of space may undergo this tunnelling.

The equation of motion and boundary conditions hint at a possible O(4) symmetry of the Euclidean solution. Actually, it can be shown that such a solution minimizes the Euclidean action for the case of a single field [70], and it may be generalized to multifield scalar theories [75]. Thus, in terms of a radial coordinate $\rho^2 = \tau^2 + \boldsymbol{x}^2$, we can rewrite the Euclidean action as

$$S_E = 2\pi^2\int_0^\infty d\rho\ \rho^3\left[\frac{1}{2}\left(\frac{d\phi}{d\rho}\right)^2 + V(\phi)\right] \tag{1.58}$$

where we have integrated over the angular variables. This means that the tunneling probability per unit volume and time is given by

$$\Gamma/V \approx Ae^{-B}, \qquad B = 2\pi^2 \int_0^\infty d\rho\, \rho^3 \left[\frac{1}{2} \left(\frac{d\bar{\phi}}{d\rho} \right)^2 + V(\bar{\phi}) - V_{\text{fv}} \right] \tag{1.59}$$

for a field configuration $\bar{\phi}$ which extremizes (1.58) and where $V_{\text{fv}} = V(\phi_{\text{fv}})$. Note that while (1.58) is divergent, the integral (1.59) is actually finite.[15] The equation of motion and the boundary conditions are now given by

$$\frac{d^2\phi}{d\rho^2} + \frac{3}{\rho}\frac{d\phi}{d\rho} = \frac{dV}{d\phi}, \quad \lim_{\rho\to\infty} \phi(\rho) = \phi_{\text{fv}}, \quad \left.\frac{d\phi}{d\rho}\right|_{\rho=0} = 0. \tag{1.60}$$

This equation may be interpreted as the 1+1 dimensional equation of motion of a particle with time coordinate ρ and spatial coordinate $\phi(\rho)$ moving under the effect of a potential $-V(\phi)$, and subject to a time-dependent friction term. The boundary conditions then simply state that this "particle" starts moving from rest (from an unknown initial position), only to end up at rest after an infinite time in the local maximum located at ϕ_{fv} of $-V(\phi)$. It can be shown that, at least in the single-field case, this problem always has a solution due to an *undershoot/overshoot* argument. Essentially, we can always find two starting points in this upside-down potential where the particle either crosses the maximum at ϕ_{fv} with non-zero velocity (overshoot) or it does not have enough energy to reach it (undershoot); therefore, there exists a point between these where the particle exactly reaches the maximum at infinite time.

Figure 1.2(b) shows the solution $\phi(\rho)$ associated to the tunneling from the false vacuum to the true one of $V(\phi)$ in fig. 1.2(a). Note that while this solution may be easily obtained in 1-D by, for example, iteratively reducing the undershoot/overshoot field range, this problem may be extremely difficult to solve for 2 or more scalar fields. The biggest difficulty in these cases stems from both the lack of knowledge about the initial starting point and the many possible paths in field space that the Euclidean solution might follow. One usually resorts to sophisticated numerical software to solve these bounces; in this thesis we have extensively used `AnyBubble` [76], though many other diverse programs exist such as `CosmoTransitions` [77] or `SimpleBounce` [78].

On the other hand, there exist many schemes one can take to get an approximate Euclidean action. Among these, the *thin-wall approximation* [67, 79] is one of the most widely used. It assumes a small separation of energies between the false and true vacuum, i.e., $\epsilon \equiv V(\phi_{\text{fv}}) - V(\phi_{\text{tv}}) \ll 1$, so that the barrier separating both vacua (c.f. figure 1.2(b)) is extremely thin and may be assumed to be infinitesimal in the perpendicular direction. Other more sophisticated approaches have also been proposed, such as [80], which provide quite accurate values even when the thin-wall scheme fails. We will consider these approximations in detail in chapter 5.

[15] The preexponential factor A will not be relevant for our discussion. For details on its precise value, see [68].

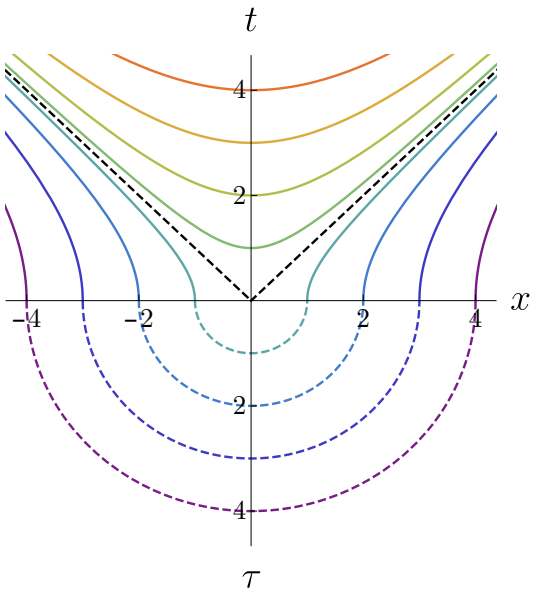

Figure 1.3: Schematic view of a solution to the Euclidean equations of motion (1.60) and its Lorentzian continuation. Constant field surfaces are shown as dashed lines in Euclidean space, while their continuation to the Lorentzian regime is shown with solid curves. The interior of the lightcone emanating from the origin of the bubble cannot be reached from the Euclidean solution, so it must be obtained by analytic continuation from the outside.

Properties of the Lorentzian solution

In order to obtain the solution after tunneling, one only needs to Wick-rotate back to real time, so the initial conditions on the field can be written as

$$\phi(t=0,\boldsymbol{x}) = \phi(\tau=0,\boldsymbol{x}), \qquad \partial_t\phi(t=0,\boldsymbol{x}) = 0 \tag{1.61}$$

and the evolution follows according to the classical equation of motion (1.55).

The solution we have found in Euclidean space makes all the following analysis quite simpler. Equation (1.55) is the Lorentzian counterpart of (1.57), so the solution we found earlier will still hold once we turn to real time, i.e.

$$\phi(t,\boldsymbol{x}) = \phi(\rho = \sqrt{\boldsymbol{x}^2 - t^2}). \tag{1.62}$$

and thus the $O(4)$ symmetry of Euclidean space is translated into $O(3,1)$ invariance in Lorentzian coordinates. From (1.61) we see that the initial profile of the field after its emergence will be

$$\phi(t=0,\boldsymbol{x}) = \phi(\rho_0 = (0^2 + \boldsymbol{x}^2)^{1/2}) \tag{1.63}$$

so the actual profile we show in fig. 1.2(b) will correspond to the initial radial profile of a true vacuum bubble.

As a final remark, it is easy to check that for any constant-ϕ hypersurface expanding in

Minkowski space (see figure 1.3), this wall will follow a hyperbolic curve given by

$$R(t) = \sqrt{R_0^2 + t^2} \tag{1.64}$$

which follows from the spherical ansatz in Euclidean space.

Note that these solutions only make sense out of the light-cone located at the origin of the nucleated bubble. In order to solve the equations of motion for the field inside this light-cone we can either analytically continue our solution to this region or, equivalently, solve

$$\frac{d^2\phi}{du^2} + \frac{3}{u}\frac{d\phi}{du} = -\frac{dV}{d\phi}, \quad u = \sqrt{t^2 - \boldsymbol{x}^2} \tag{1.65}$$

with appropriate boundary conditions. Note that in the $\boldsymbol{x} - t$ plane the surfaces of constant ϕ are hyperboloids with timelike normals. We will see that this fact has important consequences when false vacuum decay is analysed from a cosmological perspective.

1.5.2 *Cosmological consequences: inflation and the multiverse*

Up to this moment we have only discussed the tunneling from two non-degenerate vacua in a field theory setting, without considering the effect of gravity in this process. Of course, we are interested in the application of this process in a cosmological setup, gravity is a fundamental ingredient to take into account. Following [69,72], we will give a brief overview of this process, known as *Coleman-deLuccia instantons*.

Coleman-deLuccia instantons

Let us consider a scalar field theory minimally coupled to gravity with action

$$S = \int d^4x\sqrt{-g}\left[-\frac{1}{2\kappa}R + \frac{1}{2}g^{\mu\nu}\partial_\mu\phi\partial_\nu\phi - V(\phi)\right]. \tag{1.66}$$

where $\kappa = 8\pi G$. In complete analogy with the non-gravitational case, we will obtain the tunneling ratio in terms of Euclidean coordinates and assume[16] an $O(4)$ symmetry on the system. This implies that the metric is of the form

$$ds^2 = d\xi^2 + \rho(\xi)^2 d\Omega_3^2 \tag{1.67}$$

where $d\Omega_3^2$ is the surface element of a 3-sphere. The equations of motion derived from this action are

$$\phi'' + \frac{3\rho'}{\rho}\phi' = \frac{dV}{d\phi} \tag{1.68}$$

[16] Note that this assumption is inherited from the non-gravitational analogue of this process. However, there is no actual proof stating that bounces with $O(4)$ symmetry maximize their tunneling probability per unit volume and time.

$$\left(\frac{\rho'}{\rho}\right)^2 = \frac{1}{\rho^2} + \frac{\kappa}{3}\left(\frac{\phi'^2}{2} - V(\phi)\right) \tag{1.69}$$

where primes denote derivatives with respect to ξ.

A couple of comments about these equations are in order. First of all, note that the first equation corresponds to the non-gravitational case (1.60) when $\rho(\xi) = \xi$, which would correspond to an Euclidean flat Universe in (1.67). Furthermore, for a general case, we will not be able to assume the second term in (1.68) represents a dampening term, since ρ' could very well be negative. Thus, solutions to this problem cannot be justified to exist following an undershoot/overshoot reasoning.

On the other hand, note that the topology of the Euclidean spacetime will play an important role in the possible transitions allowed in this system. Particularly interesting are the de Sitter to de Sitter transitions; since both the true and false vacua in those cases have the topology of a 4-sphere (in Euclidean coordinates), up-tunnelings from the true to the false vacuum are allowed [81, 82]. More concretely, the closed Euclidean geometry of both the bubble and its background implies that the integral over the false vacuum background is finite, even if the true vacuum potential is higher than the false one (and thus the probability of generating such a bubble is non-zero either way). Quite interestingly, from the viewpoint of the String Theory Landscape, this "recycling" mechanism may help in populating this huge potential with bubbles of any kind of vacua, as it allows the exploration of minima which may not be reachable without the inclusion of gravity.

Properties of the Lorentzian solution

Once a solution to the Euclidean equations has been found, we must Wick-rotate back to real time to find the evolution of the bubble just formed. The scalar field both inside and outside the light-cone behaves exactly as in the non-gravitational case, i.e., the constant field surfaces are hyperboloids with timelike and spacelike normals, respectively, with the lightcone at the origin as their asymptote (see figure 1.3). This is just a consequence from the requirement of $O(4)$ symmetry on the Euclidean solution, which must transform into $O(3,1)$ once we turn to real time.

Let us analyze the physics of the bubble interior in more detail. The symmetries of the problem generate hyperbolic constant field surfaces; therefore, a very useful foliation of this space-time can be obtained by respecting this very symmetry. Indeed, once we Wick-rotate the Euclidean solution to real time and analytically continue to the interior of the light-cone, the metric is given by [69, 72]

$$ds^2 = dt^2 - a(t)^2 dH_3^2 \tag{1.70}$$

where dH_3^2 represents the surface element of a hyperboloid with timelike normal vector. The equations of motion are given by

$$\ddot{\phi} + \frac{3\dot{a}}{a}\dot{\phi} = -\frac{dV}{d\phi} \tag{1.71}$$

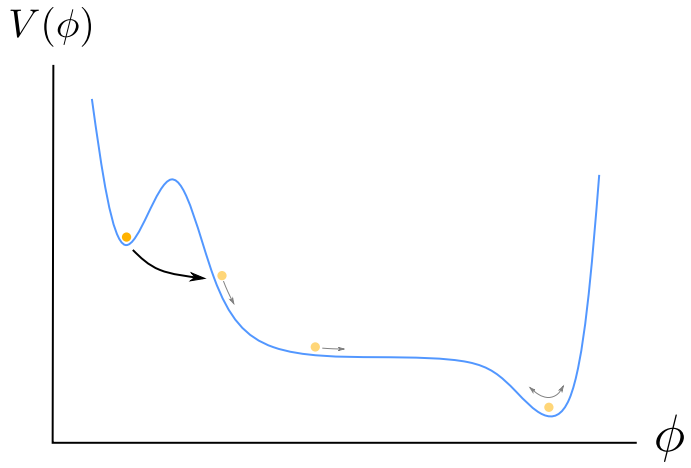

Figure 1.4: An example of a scalar potential where a scalar field initially with value ϕ_{fv} everywhere in space may tunnel through the barrier, form a true-vacuum bubble, and undergo a slow-roll inflationary epoch inside it. Such a potential may be found within the Landscape.

$$\left(\frac{\dot{a}}{a}\right)^2 = \frac{1}{a^2} + \frac{\kappa}{3}\left(\frac{\dot{\phi}^2}{2} + V(\phi)\right) \tag{1.72}$$

where dots represent derivatives with respect to t. We see that (1.70) is an open FRW metric and, furthermore, (1.72) is the Friedmann equation for a scalar field with $k = -1$. If we are to believe that our Universe is the interior of such a bubble, then homogeneity and isotropy require that constant field surfaces correspond to constant-time surfaces as well. Thus, the FRW metric of an observer within this bubble corresponds to an open one. This statement is a generic prediction of any Coleman-deLuccia tunneling event.

Inflation and the Multiverse

Equation (1.72) hints at a possible application of False Vacuum Decay for cosmological purposes. Indeed, this tunneling process has played a central role in the study of cosmological models, starting with Alan Guth's proposal [83] for an inflationary epoch in the early universe. In short, Guth proposed an exponentially expanding stage of our early universe could be the key to explain why the Universe is found flat (locally, at least) and to give a reason for its homogeneity. Such an expanding phase may be obtained assuming the existence of a homogeneous scalar field, sitting in a false vacuum of a potential where $V(\phi_{\text{fv}})$. This inflationary phase may then be cut off due to the percolation of true vacuum bubbles whose scalar potential in the interior corresponds to our actual cosmological constant. However, such a simple model was found to be inconsistent [83, 84] since, among other problems, the tunneling rate too low for percolation of the bubbles to their new phase. Moreover, even if our universe were to be the inside of such a bubble, the domination of the curvature term of the Friedmann equations which is completely inconsistent with observations (at least when potentials similar to the ones in figure 1.2(a) are considered).

The search for inflationary mechanisms continued to expand over the years (see [40, 85, 86] introductions to inflation and extensive reviews on inflationary models). In the last few decades, the increasing interest on the String Theory Landscape has rekindled the search for

inflationary universes and possible quantum transitions between vacua from a cosmological viewpoint [87]. An interesting inflationary potential which combines false vacuum decay along with a slow-roll inflationary epoch [82] is shown in figure 1.4. A potential such as this one may be considered to be found within the Landscape, alluding to its vastness. In such a case, our Universe may again be initially considered to be the product of a vacuum decay, a true vacuum bubble created due to a quantum tunneling process. In this setup, we could easily tackle the homogeneity and flatness problems with a slow-roll inflationary potential lasting for several e-folds occurring *after* the nucleation of the bubble. In chapter 5, we will construct many such potentials in two-field models which are capable of inflating in such a way as to be compatible with current inflationary parameters. Of course, our Universe may only be the one of a huge fractal-like structure of bubbles within bubbles of different vacua [82]. Such a structure is known in the literature as the *multiverse* [88, 89].

As we said above, universes generated through false vacuum decay are to be described by an open FRW geometry, due to the $O(3,1)$ symmetry of the scalar field inside the bubble. Such a universe has been considered from a phenomenological point of view in the literature [90–92] leading to interesting prospects of a possible verification[17] of the open foliation of our spacetime through the low ℓ multipoles of the CMB spectrum.

In this chapter we have seen how compatibility of String Theory with our observed Universe leads to the concept of geometric moduli arising from the compactification of 6 (or 7) dimensions. In order to stabilize these moduli, we have reviewed how the inclusion of different ingredients of the theory such as fluxes and branes, generates a potential for these moduli, known as the Landscape. In the first part of this thesis we will describe our recent progress on the problem of moduli stabilization. More concretely, we will first show novel analyses to stabilize all the complex structure moduli present in some compactifications and the consequences of the mass spectra generated following such mechanisms. We will follow this discussion with a study of the Kähler moduli in a well-studied example (a hypersurface of the complex projective space $\mathbb{WP}^4_{[1,1,1,6,9]}$) and compare our results with the de Sitter swampland conjecture and several phenomenological constraints. In the second part of the thesis, we will focus on the Landscape from a cosmological perspective, focusing on the study of False Vacuum Decay and inflation on Gaussian Random Landscapes. While these may be considered as extremely simplified versions of the original problem, they provide good working examples to analyze the complexity of higher dimensional potentials. Finally, we will end up with a discussion on a vacuum decay mechanism involving branes and fluxes, which offers a new way of undergoing quantum tunneling in a more realistic Landscape, built from the foundational ingredients described in this chapter.

[17] If closed spatial curvature were observed through this method (or by any other means), this may offer a window towards disproving a single-bubble universe originated through Coleman-de Luccia tunneling in the Landscape. On the other hand, a recent review [93] of the application of WKB methods to field theory has suggested that, contrary to the results of Coleman and de Luccia [69], the assumption of open universes inside the bubbles may have to be dropped in favor of closed universes. While this idea is still under development, it questions the general consensus that the Landscape leads to a open universe.

Part II

Moduli stabilization

Chapter 2

A complete mass spectrum in one-parameter models

After discussing the main properties and consequences of the String Theory Landscape, we now turn to study a particular strategy to compute the low energy effective field theory which greatly simplifies the task of stabilizing the hundreds of moduli present in the theory. We will consider Calabi-Yau manifolds with discrete symmetries, which effectively reduce the number of moduli and make the computation of the truncated effective field theory possible. In this approach, however, the couplings and masses of the truncated fields are left undetermined. In this chapter, we will discuss the tree-level mass spectrum of type IIB flux compactifications at Large Complex Structure, focusing on models with a reduced one-dimensional complex structure sector. We will compute the tree-level spectrum for the dilaton and complex structure moduli, *including the truncated fields*, which can be expressed entirely in terms of the known couplings of the reduced theory. This will allow us to show that the masses of this set of fields are naturally heavy at vacua consistent with the KKLT construction, and we will discuss other phenomenologically interesting scenarios where the spectrum involves fields much lighter than the gravitino. We will also derive the probability distribution for the masses on the ensemble of flux vacua, and show that it exhibits universal features independent of the details of the compactification. Finally, we will check our results on a large sample of flux vacua constructed in a concrete, one-dimensional example. This chapter is based on [94].

2.1 Introduction

As we discussed in chapter 1, the need to compactify the 6 or 7 extra dimensions of supersymmetric string theories leads to significant technical problems, which make the study of the phenomenological and cosmological implications of the Landscape of $4d$ Effective Field Theories (EFTs) exceedingly difficult. One of these problems is the huge number of moduli describing the geometry of the compact space. This makes the computation of the complete EFT prohibitively complex, and as a consequence it has only been obtained for simple compactifications. Another difficulty is the vast number of possible ways to compactify the extra dimensions, which makes it unfeasible to characterise every possible four dimensional

vacuum of the theory.

In the last few decades, several complementary strategies have been followed to overcome these technical problems. On the one hand, many efforts have been dedicated to studying explicit models where most of the moduli can be truncated or integrated out, leaving only a few fields (up to ten) for which the EFT can be computed [31, 34–36, 45, 95–101]. In such models the observational implications can be studied in detail, and these explicit computations have been used as lampposts to guide the analysis of more complex scenarios. Another possible approach, which we will exhaustively study in chapter 5, is to take a statistical perspective on the ensemble of vacua and characterize their properties through particular statistics (for example, via Gaussian Random Fields). This, in the end, alleviates the need to compute the underlying effective field theories and makes the overall problem more tractable. For references on this topic, see [102–118].

In this part of the thesis we will take a conservative approach and discuss one of the best studied domains of the Landscape: the tree-level flux vacua on Calabi-Yau compactifications of type IIB superstrings at Large Complex Structure (LCS). The construction of the EFTs describing this corner of the Landscape, and the applicability of these theories, has been widely discussed in the literature [11, 21, 119, 120]. Among this class of models, phenomenologically interesting compactifications generally involve a large number of complex structure moduli and only a few Kähler moduli (see, e.g., [101]). However, as we mentioned above, the detailed construction of the complete Effective Field Theory is prohibitive in general. Consequently, explicit constructions of flux vacua are often based on Calabi-Yau manifolds invariant under large groups of discrete symmetries which allow a consistent supersymmetric truncation of a large fraction of the complex structure moduli [45, 96–99, 101]. Provided only fluxes invariant under these symmetries are turned on, it is possible to *freeze* a large set of complex structure moduli at a critical point of the resulting flux scalar potential, leaving a reduced theory for a few surviving fields [45, 96–98]. The phenomenological and cosmological predictions of these models are then computed after including the relevant quantum corrections and supersymmetry breaking effects *in the reduced theory*. However, the fate of the truncated fields is rarely discussed in detail [99, 101].

The main objective of the following work is to take a first step towards a more precise understanding of the truncated moduli sector in this class of models. Note that, in the approach we just described, the truncated moduli are not *integrated out*; instead, the resulting EFT is a *consistent supersymmetric truncation* of the complete low energy theory at tree-level, and thus there is not necessarily a mass gap between the frozen moduli and those in the reduced theory [121–123]. Actually, although the truncated sector is guaranteed to be at a stable configuration at tree-level, the spectrum might contain arbitrarily light fields. Thus, in principle the quantum corrections and the breaking of supersymmetry could render some of these light fields tachyonic. Alternatively, the fixed point of the discrete symmetry group could cease to be a critical point of the corrected scalar potential.

Here we will focus on the simplest possible class of these models, those where the reduced theory contains a single complex structure modulus. Although this is a rather restrictive type of compactification, it contains plenty of examples (see, e.g., [124–128]). Furthermore, the moduli space geometry is well characterised for many of them [129–132], including the well known family of quintic hypersurfaces $\mathbb{WP}^4_{[1,1,1,1,1]}$ and its generalisations [119, 124, 125, 133].

We will prove, using only symmetry arguments and properties of the effective theory on type IIB compactifications at LCS, that it is possible to compute the tree-level mass spectrum for the axio-dilaton and the complete set of $h^{2,1}$ complex structure moduli fields, *including the truncated ones*.

In order to illustrate our results, we have compared our analytic formulae with a numerical scan of flux vacua of type IIB compactified on an orientifold of $\mathbb{WP}^4_{[1,1,1,1,4]}$ [124, 133]. This family of hypersurfaces has a $h^{2,1} = 149$ dimensional complex structure moduli space, which can be consistently reduced to a single field at the fixed locus of a $\mathbb{Z}_8^2 \times \mathbb{Z}_2$ symmetry. Using the known reduced effective theory, we construct a large ensemble of flux vacua and verify the validity of the formulae we derived for masses of the axio-dilaton and the complex structure field on the reduced theory. It is important to stress that, at each of these vacua, our results allowed us to infer the masses of all of the truncated 148 complex structure fields, *without the need to compute the complete EFT*.

For generic vacua, the mass spectrum has a dependence on the fluxes and thus, to have a characterisation of the perturbative stability independent of the flux choice, we resorted to statistical methods. More specifically, we used the techniques derived in the seminal papers [46, 134], whose only assumption is the continuous flux approximation.[1] With this at hand, we were able to analytically compute the probability distribution for the complete set of masses in the ensemble of flux vacua, and showed that the statistical properties of the spectrum are independent of the compactification. Then, we compared the "empirical" mass distributions from the ensemble of vacua in the $\mathbb{WP}^4_{[1,1,1,1,4]}$ model with the predicted probability distributions, and showed they are in good agreement within the regime of validity of both the EFT and the continuous flux approximation.

The chapter is organized as follows. In section 2.2 we review the effective theory for the axio-dilaton and complex structure sector on type IIB compactifications, and collect the relevant formulae for the computation of the tree-level mass spectrum. In section 2.3 we revisit the effective reduction of the complex structure moduli space on a Calabi-Yau admitting a discrete group of symmetries. We also derive the restrictions that these symmetries impose on the structure of the Hessian and the fermion mass matrix. Section 2.4 contains the main results of this chapter where we analytically derive the tree-level mass spectrum for the class of models we consider. In section 2.5 we present the EFT for the compactification of type IIB in the $\mathbb{WP}^4_{[1,1,1,1,4]}$ Calabi-Yau manifold. In section 2.6 we analyze the statistical properties of the computed spectra in the ensemble of flux vacua, and verify our conclusions by performing a numerical scan on the $\mathbb{WP}^4_{[1,1,1,1,4]}$ model. We present our conclusions in section 2.7.

[1] As the name suggests, this simply means that the fluxes defined in (1.33) are assumed to take continuous values. We will further develop on this topic in section 2.4 and appendix C.

2.2 Flux vacua at Large Complex Structure

2.2.1 *Effective theory*

As we mentioned in the introduction, in this chapter we will be focusing on compactifications in the Large Complex Structure regime [30], whose effective theory can be obtained from the following prepotential:

$$\mathscr{F} = \frac{\mathrm{i}}{6}\kappa_{ijk}z^i z^j z^k + \frac{1}{2}\kappa_{ij}z^i z^j + \mathrm{i}\kappa_i z^i + \frac{1}{2}\kappa_0 + \mathscr{F}_{\text{inst}}\,. \tag{2.1}$$

where z^i represent complex structure moduli, defined in sections 1.2.2 and 1.3. On the other hand, the terms κ_{ijk}, κ_{ij} and κ_i are numerical constants which can be computed from the topological data of the mirror manifold to M_3. In particular, for historical reasons the coefficients κ_{ijk} are often referred to as the classical *Yukawa couplings*. The constant contribution κ_0 is determined by the Euler number $\chi(M_3) = 2(h^{1,1} - h^{2,1})$ of the Calabi-Yau:

$$\kappa_0 = \mathrm{i}\frac{\zeta(3)}{(2\pi)^3}\chi(M_3)\,, \tag{2.2}$$

where ζ is the Riemann zeta function. Finally, $\mathscr{F}_{\text{inst}}$ denotes exponentially suppressed string worldsheet instanton contributions, which can be expressed as [101]

$$\mathscr{F}_{\text{inst}} = -\frac{\mathrm{i}}{(2\pi)^3}\sum_{\boldsymbol{d}} n_{\boldsymbol{d}}\,\mathrm{Li}_3[\mathrm{e}^{-2\pi d_i z^i}]\,. \tag{2.3}$$

Here the integers $n_{\boldsymbol{d}}$ are the genus zero Gopakumar-Vafa invariants, which are labeled by the vector $d^i \in \mathbb{Z}^+$, and the function $\mathrm{Li}_3(q)$ is the polylogarithm $\mathrm{Li}_p(q) = \sum_{k>0}\frac{q^k}{k^p}$. In the LCS regime, the contribution to $\mathscr{F}$ from instantons is subleading, and in the following calculations we will neglect it entirely.[2]

As we saw in chapter 1, the prepotential defines all the necessary ingredients to build the effective theory, namely the Kähler potential and the superpotential. Using the results developed in section 1.3 and provided we discard the instanton contribution, the Kähler potential reads

$$K_{cs} = -\log\left(\frac{1}{6}\kappa_{ijk}(z+\bar{z})^i(z+\bar{z})^j(z+\bar{z})^k - 2\mathrm{Im}(\kappa_0)\right). \tag{2.4}$$

It is straightforward to check that the field space metric derived from the Kähler potential K in (1.22) is real and block-diagonal in the axio-dilaton and complex structure sectors, namely,

$$\begin{aligned} K_{\tau\bar{\tau}} &= \frac{1}{2(\mathrm{Im}\,\tau)^2}\,,\\ K_{i\bar{j}} &= -\mathring{\kappa}_{ijk}(z+\bar{z})^k + \frac{1}{4}\mathring{\kappa}_{ilm}\mathring{\kappa}_{jnp}(z+\bar{z})^l(z+\bar{z})^m(z+\bar{z})^n(z+\bar{z})^p\,, \end{aligned} \tag{2.5}$$

[2] Note, however, that these corrections will be considered when comparing numerical results with the expressions that will follow from this prepotential. In general, numerical results will be required to have small instantonic corrections.

where subscripts denote the derivatives of the Kähler functions, i.e., $K_{\tau\bar{\tau}} \equiv \partial_\tau \partial_{\bar{\tau}} K$ and $K_{i\bar{j}} \equiv \partial_i \partial_{\bar{j}} K$, and the quantities $\mathring{\kappa}_{ijk} \equiv \mathrm{e}^{K_{cs}} \kappa_{ijk}$ are usually called the *rescaled Yukawa couplings* [119].

2.2.2 *Mass spectrum at tree-level vacua*

The main focus of this chapter is the study of the mass spectrum at no-scale supersymmetric vacua, $\{\tau_c, z^i_c\}$, satisfying (1.37). In this subsection we will enumerate the relevant properties of the Hessian of the potential (1.36) at these points and its spectrum of eigenvalues. This information will in turn determine the tree-level masses of the moduli fields.

At no-scale vacua the scalar potential vanishes identically, regardless of the configuration of the Kähler moduli, as a consequence, the Kähler moduli remain flat directions of V_{tree}. This means that to study the spectrum of excitations of these configurations, it is sufficient to focus on the axio-dilaton/complex structure sector, since all the Kähler moduli are massless.[3] Additionally, in order to simplify the computations, we will make use of the freedom to perform a field redefinition to bring the field space metric to a canonical form at the vacuum $\{\tau_c, z^i_c\}$. To be more specific, since the Kähler metric (2.5) is real and block-diagonal in the axio-dilaton and complex structure sectors, we can redefine the complex structure fields as $z^a = e^a_i z^i$ with $e^a_i \in \mathrm{GL}(h^{2,1}, \mathbb{R})$, so that

$$(e^{-1})^i_a \, (e^{-1})^j_b \, K_{i\bar{j}}\Big|_{\tau_c z^i_c} = \delta_{ab} \tag{2.6}$$

with $a, b = 1, \ldots, h^{2,1}$. Then, the matrices $e^i_a \equiv (e^{-1})^i_a$ can be identified with a *real* vielbein basis for the metric $K_{i\bar{j}}$ at the point $\{\tau_c, z^i_c\}$. Note that this does not completely fix the freedom to choose a matrix e^i_a, as we are still allowed to make field redefinitions $z^a \to \Lambda^a_b z^b$ (equivalently $e^a_i \to \Lambda^a_b e^b_i$) preserving the canonical form of the metric, that is with $\Lambda \in \mathrm{SO}(h^{2,1})$. Similarly, we can use the real vielbein $e^\tau_0 = \mathrm{i}(\tau - \bar{\tau})$ to obtain the canonical normalisation of the axio-dilaton at the vacuum $\{\tau_c, z^i_c\}$. For convenience we will also use the index $A = 0, \ldots, h^{2,1}$ to collectively label the canonically normalized axio-dilaton ($A = 0$) and the complex structure fields ($A \geq 1$), so that the full Kähler metric in the axio-dilaton/complex structure sector takes the form $K_{A\bar{B}} = \delta_{A\bar{B}}$ at the no-scale vacuum.

After bringing the field-space metric to a canonical form, it is straightforward to check that the Hessian of the scalar potential (1.36) at no-scale vacua $\{\tau_c, z^i_c\}$ has the following structure[4]

$$\mathscr{H} \equiv \begin{pmatrix} \nabla_A \nabla_{\bar{B}} V & \nabla_A \nabla_B V \\ \nabla_{\bar{A}} \nabla_{\bar{B}} V & \nabla_{\bar{A}} \nabla_B V \end{pmatrix} = \begin{pmatrix} Z_{AC} \overline{Z}^C{}_{\bar{B}} + \delta_{A\bar{B}} \, m^2_{3/2} & 2 m_{3/2} \, Z_{AB} \, \mathrm{e}^{-\mathrm{i}\alpha_W} \\ 2 m_{3/2} \, \overline{Z}_{\bar{A}\bar{B}} \, \mathrm{e}^{\mathrm{i}\alpha_W} & \overline{Z}_{\bar{A}\bar{C}} Z^{\bar{C}}{}_B + \delta_{\bar{A}B} \, m^2_{3/2} \end{pmatrix}, \tag{2.7}$$

where $m_{3/2} \equiv \mathrm{e}^{K/2}|W|$ is the gravitino mass, $\alpha_W = \arg(W)$ is the phase of the flux superpotential and $Z_{AB} \equiv \mathrm{e}^{K/2} D_A D_B W$. Equivalently, we can rewrite the Hessian as

$$\mathscr{H} = \left(m_{3/2} \, \mathbb{1} + \mathscr{M} \right)^2 \qquad \text{with} \qquad \mathscr{M} \equiv \begin{pmatrix} 0 & Z_{AB} \, \mathrm{e}^{-\mathrm{i}\alpha_W} \\ \overline{Z}_{\bar{A}\bar{B}} \, \mathrm{e}^{\mathrm{i}\alpha_W} & 0 \end{pmatrix}. \tag{2.8}$$

[3] Of course, while this does not constitute a phenomenologically well founded model, we will leave the details on Kähler moduli stabilization to chapter 4. See also [31, 35] and references therein.

[4] Indices are here raised and lowered with the canonical form of the metric $\delta^{A\bar{B}}$ and $\delta_{A\bar{B}}$.

Since the field space metric is already in a canonical form, the eigenvalues of the matrix $\mathscr{H}$ can be identified with the squared masses of the $2(h^{2,1}+1)$ real scalar fields in the axio-dilaton/complex structure sector at $\{\tau_c, z^i_c\}$. Therefore to find the spectrum of $\mathscr{H}$ it suffices to diagonalize the matrix $\mathscr{M}$, which can be identified with the fermion mass matrix (see, e.g., [135]). Moreover, note that the eigenvalues of $\mathscr{M}$ come in pairs of opposite signs $\pm m_\lambda$, and therefore the mass spectrum of the scalar sector at tree-level is simply [123]

$$\mu^2_{\pm\lambda} = (m_{3/2} \pm m_\lambda)^2 \geq 0\,, \tag{2.9}$$

where $\lambda = 0, \ldots, h^{2,1}$. The positivity of the masses squared $\mu^2_{\pm\lambda}$ ensures that all no-scale vacua are perturbatively stable, which could have been anticipated by noting that the tree-level potential (1.36) is always non-negative, and vanishes at no-scale vacua.

In practice, the simplest way to find the fermion masses m_λ, and thus also the scalar mass spectrum, is to consider the $(h^{2,1}+1)\times(h^{2,1}+1)$ hermitian matrix $(ZZ^\dagger)_{AB} \equiv Z_{AC}\overline{Z}^C{}_{\overline{B}}$, whose $h^{2,1}+1$ eigenvalues m^2_λ coincide with those of

$$\mathscr{M}^2 = \begin{pmatrix} Z_{AC}\overline{Z}^C{}_{\overline{B}} & 0 \\ 0 & \overline{Z}_{\overline{A}}{}^C Z_{CB} \end{pmatrix}. \tag{2.10}$$

Regarding the structure of the matrix Z_{AB}, it is straightforward to prove that, at no-scale vacua, we always have $Z_{00} = \mathrm{e}^{K/2}(e^\tau_0)^2\, D_\tau D_\tau W = 0$. Moreover, when our model is defined in terms of a prepotential as in (2.1), we can simplify the computations with the identity [21,46]

$$Z_{ij} = -(\tau-\bar\tau)\mathrm{e}^{K_{cs}}\kappa_{ijk}K^{k\bar l}\overline{Z}_{\bar\tau\bar l}, \tag{2.11}$$

which we have written in a form invariant under redefinitions of the z^i fields to ease comparison with previous works. If we instead use canonically normalised fields, plus the definition of the rescaled Yukawa couplings $\mathring\kappa_{abc} = \mathrm{e}^{K_{cs}}\kappa_{abc}$, the previous identity takes the simpler form

$$Z_{ab} = \mathrm{i}\mathring\kappa_{abc}\overline{Z}_{0c}\,. \tag{2.12}$$

For later reference we will also collect here the following form of the tadpole constraint (1.42) which, at no-scale vacua, can be expressed in terms of the expectation value of the gravitino mass and the quantities Z_{0a} as (see appendix A)

$$0 \leq 4\pi\mathcal{V}^2\left(m^2_{3/2} + |Z_{0a}|^2\right) = N_{\text{flux}} \leq L. \tag{2.13}$$

To summarise, the scalar mass spectrum $\mu^2_{\pm\lambda}$ at no-scale vacua (2.9) can be computed from the gravitino mass $m_{3/2}$, the quantities Z_{0a}, and the canonically normalised and rescaled Yukawas $\mathring\kappa_{abc}$, using the formulae (2.12) and diagonalising the matrix $ZZ^\dagger$. In the next section we will discuss compactifications on Calabi-Yau manifolds invariant under a group of discrete symmetries. As we shall see, at no-scale vacua preserving those symmetries, the structure of both the Yukawa couplings and Z_{0a} is severely constrained.

2.3 Flux vacua with enhanced symmetries

In this section we will consider the special case where the Calabi-Yau geometry is invariant under a global group of discrete isometries. As discussed in [96], provided that only fluxes which are invariant under these symmetries are turned on, the low energy action is consistent with the *supersymmetric truncation* of a subset of the complex structure fields. Indeed, in this setting the spacetime isometries act non-trivially on the complex structure fields, while leaving the low energy supergravity action invariant. Then, the consistent truncation of the theory is defined by restricting the complex structure moduli space to the fixed locus of this symmetry, in other words, a subset of the fields is *frozen* at the fixed locus. The consistency of the truncation ensures that any solution of the reduced theory obtained after freezing a subset of the fields is also a solution of the complete theory. In particular, critical points of the reduced scalar potential are also critical points in the full effective theory. Moreover, if the fields surviving the truncation are stabilized at a supersymmetric critical point, the full complex structure sector also preserves supersymmetry [96] (see also discussion in [99]).

In the next paragraphs we will review how the presence of discrete symmetries in the Calabi-Yau geometry can be used to truncate a sector of the complex structure fields. We will also discuss the restrictions that these symmetries impose on the couplings of the resulting reduced theory.

2.3.1 *Invariant fluxes and low energy symmetries*

As we mentioned in the introduction, in many interesting compactifications the Calabi-Yau geometry is invariant under the action of a discrete group of transformations, $\mathcal{G}$. These transformations act on the complex structure fields, $z^i \to \hat{z}^i$, and thus also induce a change on the period vector $\Pi(z^i)$, defined in (1.31). Since the Calabi-Yau geometry is left invariant under these symmetries, these transformations must also leave the geometry on its moduli space invariant. Therefore, the action of a transformation $g \in \mathcal{G}$ on the period vector must be of the form

$$\Pi(z^i) \longrightarrow \Pi(\hat{z}^i) = \mathrm{e}^{\Lambda_g(z)}\, S_g \cdot \Pi(z^i)\,, \tag{2.14}$$

with $\Lambda_g(z^a)$ a holomorphic function of the complex structure fields and S_g a constant symplectic matrix in $\mathrm{Sp}(2h^{2,1}+2,\mathbb{Z})$, both determined by the group element g. In addition, when the three-form fluxes are turned on, the invariance of the effective action under the group $\mathcal{G}$ requires that the flux vector $N = f - \tau h$ transforms as in (1.38). Then, it is easy to check that under a transformation $g \in \mathcal{G}$, the Kähler potential K_{cs} and the superpotential W experience a g-dependent Kähler transformation

$$K_{cs}(\hat{z}^i, \hat{\bar{z}}^i) = K_{cs}(z^i, \bar{z}^i) + \Lambda_g(z^i) + \overline{\Lambda}_g(\bar{z}^i)\,, \qquad W_{\hat{f},\hat{h}}(\hat{z}^i) = \mathrm{e}^{-\Lambda_g(z)}\, W_{f,h}(z^i)\,. \tag{2.15}$$

Here we have explicitly indicated for clarity the dependence of the superpotential on the flux vectors (f,h) and their transformed values $(\hat{f},\hat{h})$ under (1.38). However, the symmetry groups $\mathcal{G}$ that we are considering are discrete and of finite order, and thus it is always possible

to choose a Kähler gauge so that K_{cs} and W transform as scalars under[5] $\mathcal{G}$ (see [136]), that is,

$$K_{cs}(\hat{z}^i, \hat{\bar{z}}^i) = K_{cs}(z^i, \bar{z}^i), \quad W_{\hat{f},\hat{h}}(\hat{z}^i) = W_{f,h}(z^i). \tag{2.16}$$

It is important to note that despite of the behaviour (2.16) of the Kähler potential and the flux superpotential under the group of transformations $\mathcal{G}$, generically they do not constitute a proper symmetry of the low energy effective theory for the moduli fields [98]. Indeed, each choice of fluxes defines an effective theory for the moduli, where the flux integers (f,h) appear as coupling constants (see [137]). Therefore, since the group $\mathcal{G}$ generally acts non-trivially on the fluxes, i.e., the couplings of the EFT, in general it will not correspond to a low energy symmetry for the moduli effective action. On the contrary, if we restrict the flux configuration $N = f - \tau h$ to be invariant under the transformations (1.38), then $\mathcal{G}$ will be a symmetry of the low-energy action defined by this choice of fluxes. Indeed, from (2.16) we have that for an invariant set of fluxes

$$K_{cs}(\hat{z}^i, \hat{\bar{z}}^i) = K_{cs}(z^i, \bar{z}^i), \quad W_{f,h}(\hat{z}^i) = W_{f,h}(z^i), \tag{2.17}$$

so the low energy supergravity theory of the moduli is properly invariant under the action of $\mathcal{G}$.

In the following we will assume that the fluxes are invariant under the action of $\mathcal{G}$, and we will again omit the subscripts (f,h) in the superpotential in order to simplify the notation.

2.3.2 *Consistent truncation of the moduli space*

We will now discuss how the symmetry group $\mathcal{G}$ aids in the task of finding solutions to the no-scale equations (1.37). In general, for a given group $\mathcal{G}$ we can always split the complex structure fields into two sets, $z^i = \{z^\alpha, w^{\alpha'}\}$: those invariant under the action of the symmetry group, z^α with $\alpha = 1, \dots, h^{2,1}_{\text{red}}$, and those fields which transform non trivially, $w^{\alpha'} \to \hat{w}^{\alpha'}$, where $\alpha' = h^{2,1}_{\text{red}} + 1, \dots, h^{2,1}$.

Then, if the symmetry group $\mathcal{G}$ admits a fixed locus *on the moduli space*, i.e., a configuration of the fields $w^{\alpha'}_*$ satisfying $\hat{w}^{\alpha'}_* = w^{\alpha'}_*$, the derivatives of the scalar potential V and the Kähler potential along the non-invariant fields $w^{\alpha'}$ must vanish there

$$\partial_{w^{\alpha'}} V = 0, \quad K_{w^{\alpha'}} = 0 \quad \text{at} \quad z^i = (z^\alpha, w^{\alpha'}_*) \quad \text{for all} \quad \tau, z^\alpha. \tag{2.18}$$

To prove this it is sufficient to note that, for an invariant choice of fluxes, both the no-scale potential V and the Kähler potential transform as scalar fields under the action of $\mathcal{G}$, and thus $\partial_{z^i} V$ and K_i will transform as tensors. Then, in the case of the scalar potential, we have that a generic point of the moduli space satisfies

$$\partial_{w^{\alpha'}} V(z^\alpha, w^{\alpha'}) = \frac{\partial \hat{w}^{\beta'}}{\partial w^{\alpha'}} \partial_{\hat{w}^{\beta'}} V(z^\alpha, \hat{w}^{\beta'}). \tag{2.19}$$

[5] The invariant Kähler gauge $K^{\text{inv}}_{cs} = K_{cs} + \Lambda^{\text{inv}}(z) + \overline{\Lambda}^{\text{inv}}(\bar{z})$ can be found noting that under a transformation $g : z^i \to \hat{z}^i$ we must have $\Lambda^{\text{inv}}(\hat{z}) = \Lambda^{\text{inv}}(z) - \Lambda_g(z)$. It is easy to check that this condition is solved by $\Lambda^{\text{inv}}(z) = \frac{1}{[\mathcal{G}]} \sum_{g \in \mathcal{G}} \Lambda_g(z)$, where $[\mathcal{G}]$ is the order of the group $\mathcal{G}$.

At the fixed locus, where $\hat{w}^{\alpha'}_* = w^{\alpha'}_*$, the previous expression can be seen as a system of equations for $\partial_{w^{\alpha'}} V(z^\alpha, w^{\alpha'}_*)$. But this system only admits the trivial solution (2.18) because, by assumption, all the fields $w^{\alpha'}$ transform non-trivially away from the fixed point implying that all equations are independent. Moreover, in the previous discussion the expectation values of the dilaton or the $\mathcal{G}$-invariant fields are irrelevant, and therefore the fixed point will always be a stationary point of the superpotential regardless of the field configuration (τ, z^α). Although our argument has been derived in the particular Kähler gauge where K_{cs} and W transform as scalars (2.16), our conclusion is a Kähler invariant statement. Different derivations can be found in [96, 99, 101].

The first condition in (2.18) implies that the fixed locus of the symmetry group $\mathcal{G}$ is always a critical point of the scalar potential, while the second one leads to a consistency condition on the geometry of the moduli space. In particular, this geometric condition implies that the moduli space metric on the fixed locus is block-diagonal in the truncated and surviving sectors $K_{z^\alpha \overline{w}^{\beta'}} = 0$. Moreover, the reduced moduli space defined by the fixed locus $w^{\alpha'} = w^{\alpha'}_*$ must be a *totally geodesic submanifold* of the full moduli space (see [123]). In other words, any geodesic on the moduli space manifold with at least one point located at the fixed locus of $\mathcal{G}$, and which is locally tangent to it, should be entirely contained in the reduced moduli space.

These are very strong requirements which ensure the consistency of freezing the moduli $w^{\alpha'}$ at the level of the EFT Lagrangian $\mathscr{L}_{EFT}(\tau, z^i)$, thus defining a reduced theory involving the surviving fields alone:

$$\mathscr{L}^{\text{red}}_{EFT}(\tau, z^\alpha) \equiv \mathscr{L}_{EFT}(\tau, z^\alpha, w^{\alpha'} = w^{\alpha'}_*)\,. \tag{2.20}$$

Indeed, the conditions (2.18) guarantee that any solution of the reduced theory given by $\mathscr{L}^{\text{red}}_{EFT}$ is also a solution of the complete EFT. Moreover, using (2.17) and a similar argument to the one given above, it is possible to prove that the flux potential is also extremized at the fixed locus of $\mathcal{G}$

$$D_{w^{\alpha'}} W|_{w=w_*} = \partial_{w^{\alpha'}} W|_{w=w_*} = 0 \qquad \text{for all} \qquad \tau, z^\alpha\,, \tag{2.21}$$

which means that the truncated fields $w^{\alpha'}$ preserve supersymmetry there. If supersymmetry is preserved in the reduced theory, it is also unbroken in the original EFT. Then, the process of freezing the non-invariant fields $w^{\alpha'}$ constitutes a consistent supersymmetric truncation of the theory (see [122, 123, 138]).

From (2.21) it follows that compactifications admitting a discrete symmetry group are particularly convenient for the search of no-scale vacua since at the fixed locus of $\mathcal{G}$, the non-invariant fields automatically satisfy the no-scale equations (1.37). No-scale vacua located at the fixed locus of the symmetry group $\mathcal{G}$ are often called *enhanced symmetry vacua*. Moreover, provided we are interested only in this class of vacua, the consistency of the truncation ensures that it is sufficient to calculate the couplings, i.e., the period vector, of the reduced action (see, e.g., [101, 119, 139–142]), which renders the computation of the EFT tractable.

2.3.3 *Mass matrix structure at enhanced symmetry vacua*

The high degree of symmetry present in low energy theories with $\mathcal{G}$-invariant fluxes provides valuable information regarding the structure of the fermion mass matrix and the Hessian at enhanced symmetry vacua. First, as we saw above, at the fixed locus of $\mathcal{G}$ the moduli space metric is block diagonal in the truncated and surviving sectors, and from (2.18) and (2.21) it also follows that

$$D_\tau D_{w^{\alpha'}} W|_{w_*} = D_{z^\alpha} D_{w^{\beta'}} W|_{w_*} = 0\,, \qquad \nabla_{z^\alpha} \nabla_{w^{\beta'}} V|_{w_*} = \nabla_{z^\alpha} \nabla_{\overline{w}^{\beta'}} V|_{w_*} = 0\,, \tag{2.22}$$

regardless of the configuration of the reduced moduli (τ, z^α). This, in turn, implies that the fermion mass matrix $\mathscr{M} = \mathscr{M}_{\{\tau,z^\alpha\}} \otimes \mathscr{M}_{\{w^{\alpha'}\}}$ and the Hessian of the potential $\mathscr{H} = \mathscr{H}_{\{\tau,z^\alpha\}} \otimes \mathscr{H}_{\{w^{\alpha'}\}}$ are block-diagonal in the two sectors at no-scale vacua, which means that it is consistent to study the perturbative stability of the fields (τ, z^α) and $w^{\alpha'}$ separately. Moreover, the particular structure of the fermion mass matrix on the EFTs we are considering, i.e., the identity (2.11), leads to an additional simplification. From (2.22) it is easy to see that the only non-vanishing quantities $Z_{\tau z^i}$ are those with components on the surviving sector, $Z_{\tau z^\alpha}$.

Collecting all the previous results, and using (2.12), we can see that the components of the canonically normalised matrix Z_{AB} which appears in $\mathscr{M}$ satisfy the relations

$$Z_{0w^{a'}} = Z_{z^{\tilde{a}} w^{b'}} = 0\,, \qquad Z_{z^{\tilde{a}} z^{\tilde{b}}} = \mathrm{i}\kappa_{\tilde{a}\tilde{b}\tilde{c}}\, \overline{Z}_{\bar{0}\bar{z}^{\tilde{c}}}\,, \qquad Z_{w^{a'} w^{b'}} = \mathrm{i}\kappa_{a'b'\tilde{c}}\, \overline{Z}_{\bar{0}\bar{z}^{\tilde{c}}}\,, \tag{2.23}$$

where fields $z^{\tilde{a}}$ correspond to the canonically normalised fields of the reduced theory, $\tilde{a}, \tilde{b} = 1, \ldots, h^{2,1}_{\text{red}}$ (see eq. (2.6)), and $w^{a'}$ to those of the truncated sector, $a', b' = h^{2,1}_{\text{red}} + 1, \ldots, h^{2,1}$.

Thus, the main result of this section can be summarized as follows: at enhanced symmetry vacua the canonically normalized Hessian of the no-scale potential can be entirely expressed in terms of the derivatives of the flux superpotential *of the reduced theory*, $Z_{0z^{\tilde{a}}}$, plus $\mathring{k}_{\tilde{a}\tilde{b}\tilde{c}}$ and $\mathring{k}_{a'b'\tilde{c}}$ of the canonically normalized invariant Yukawa couplings. Furthermore, in the class of models we are interested in, the sector surviving the truncation is one dimensional, and thus the indices $\tilde{a}$, $\tilde{b}$ and $\tilde{c}$ in (2.23) can only take one value, which we choose to be "1" without loss of generality. The non-vanishing components of the matrix Z_{AB} then read

$$Z_{11} = \mathrm{i}\mathring{\kappa}_{111}\, \overline{Z}_{\bar{0}\bar{1}}, \qquad Z_{a'b'} = \mathrm{i}\mathring{\kappa}_{a'b'1}\, \overline{Z}_{\bar{0}\bar{1}}. \tag{2.24}$$

As we shall see in section 2.4, for the class of models we discuss here, the quantities $\mathring{\kappa}_{111}$ and $\mathring{\kappa}_{a'b'1}$ appearing in these expressions can also be completely expressed in terms of the field expectation values and the known couplings of the reduced theory.

2.4 Complete tree-level mass spectrum

We begin the present section by deriving certain universal properties of the type IIB couplings which are valid in a generic Calabi-Yau compactification at LCS. We will then restrict ourselves to Calabi-Yau manifolds admitting a symmetry group which enables a consistent reduction

of the complex structure moduli space to a single surviving field. Using these results together with the ones in the previous sections we will show how to compute the tree-level spectrum for the complete axio-dilaton/complex structure sector at no-scale vacua.

2.4.1 *Universal features of the type IIB effective field theory*

In this subsection we will obtain general properties satisfied by the canonically normalised Yukawa couplings in the large complex structure regime. More specifically, we will show that a subset of the rescaled Yukawas $\mathring{\kappa}_{abc}$ can be expressed in terms of a single parameter $\xi \in [0, 1/2]$, which can be defined in terms of known quantities appearing in the reduced theory as

$$\xi \equiv \frac{-2e^{K_{cs}}\,\mathrm{Im}\,\kappa_0}{1+2e^{K_{cs}}\,\mathrm{Im}\,\kappa_0}\,. \tag{2.25}$$

This quantity can be understood as a coordinate parametrising the complex structure moduli space, with the LCS point located at $\xi = 0$. For the models we are interested in, with a few Kähler moduli and a large complex structure sector $h^{1,1} \ll h^{2,1}$, we have from (2.2) that $\mathrm{Im}\,\kappa_0 < 0$. Combined with the definition (2.25), the latter condition also implies that physical configurations satisfy $\xi \geq 0$. Then, it is easy to check that field configurations with $\xi = 1/2$ are those at the boundary of the moduli space, that is, for $\xi > 1/2$ the Kähler metric has a negative eigenvalue, leading to unphysical solutions.

The argument below will proceed along the lines of [143–145], where analogous properties for the Yukawas where found strictly at the LCS point ($\xi = 0$). But here we will only assume that the exponentially suppressed instanton contributions to the prepotential (2.1) can be entirely neglected. Therefore, the results presented below generalize those of [143–145], as the regime of validity of our analysis can be extended to the entire region of the moduli space where the polynomial approximation of the prepotential (2.1) is under control.

The starting point of the derivation is the Kähler metric (2.5) on the complex structure moduli space. Following [145] we introduce the following real vector of unit norm

$$e_1^i \equiv \frac{1}{x}(z+\bar{z})^i\,, \qquad K_{i\bar{j}}\, e_1^i \bar{e}_1^j = 1, \tag{2.26}$$

where the parameter x is a normalisation constant which has yet to be determined. Without loss of generality, and making use of the residual $\mathrm{SO}(h^{2,1})$ freedom to define the canonically normalised fields, we rotate the vielbein basis e_a^i so that the first vector coincides with e_1^i. Since the Kähler metric (2.5) has the canonical form δ_{ab} when expressed in the basis e_a^i, we find that the rescaled and canonically normalised Yukawa couplings should satisfy

$$\delta_{ab} = -\mathring{\kappa}_{ab1}\, x + \frac{1}{4}\mathring{\kappa}_{a11}\mathring{\kappa}_{b11}\, x^4\,. \tag{2.27}$$

Note also that from the definition of the Yukawa couplings, $\mathring{\kappa}_{abc} = e^{K_{cs}}\kappa_{abc}$, and the expression for the Kälher potential (2.4), we have

$$e^{-K_{cs}} = \frac{1}{6}\kappa_{111}x^3(1+\xi) \qquad \Longrightarrow \qquad \frac{1}{6}\mathring{\kappa}_{111}x^3(1+\xi) = 1\,. \tag{2.28}$$

Solving the two previous conditions for the Yukawas of the form $\mathring{\kappa}_{ab1}$, it is straightforward to obtain

$$\mathring{\kappa}_{111} = \frac{2(1+\xi)^2}{\sqrt{3(1-2\xi)^3}}, \qquad \mathring{\kappa}_{a'11} = 0 \quad \text{and} \quad \mathring{\kappa}_{a'b'1} = -\frac{1+\xi}{\sqrt{3(1-2\xi)}}\delta_{a'b'}\,. \tag{2.29}$$

with $a', b' = 2, \dots h^{2,1}$. The rest of the rescaled Yukawa couplings $\kappa_{a'b'c'}$ are not constrained by the conditions above, and therefore a priori they can be generic. The normalisation constant x of the vielbein e_1^i is found to be

$$x^2 = \frac{3(1-2\xi)}{(1+\xi)^2}\,. \tag{2.30}$$

To the best of our knowledge these relations have never been presented before in the literature.

The direction specified by the vielbein e_1^i has a concrete geometrical significance. It corresponds to *the no-scale direction* of the complex structure moduli space [146,147]

$$K_a = -\frac{1}{2}\mathring{\kappa}_{a11}x^2 = -\sqrt{3/(1-2\xi)}\delta_a^1\,. \tag{2.31}$$

The previous relation also implies the following generalised no-scale property

$$K_i K_{\bar{j}} K^{i\bar{j}} = 3/(1-2\xi) \geq 3\,, \tag{2.32}$$

which is satisfied by any type IIB compactification with $h^{1,1} \leq h^{2,1}$ at LCS (see appendix A in [146]).

Note that in the models we are interested in, where only one field survives the truncation, the v.e.v. of the complex structure field z^a is necessarily aligned with the vector Z_{0a}, since both of them point along the unique direction of the reduced complex structure moduli space. Therefore, the Yukawa couplings $\mathring{\kappa}_{a'b'1}$ computed above are precisely those also appearing in the expression (2.24), and thus we already have all the necessary ingredients to compute the tree-level spectrum at a generic no-scale vacuum.

2.4.2 *Fermion and scalar mass spectra at no-scale vacua*

We begin by computing the fermion mass spectrum as described in section 2.2.2, that is, diagonalising the hermitian matrix $ZZ^\dagger$, and using the formula (2.9) to obtain the masses of the scalar fields. First, the vector

$$Z_{0a} = \delta_{a1} Z_{01} \tag{2.33}$$

is necessarily aligned with the no scale direction (recall that in these models a can only take one value, as $h^{2,1}_{\text{red}} = 1$). From the expressions (2.29) for the rescaled Yukawa couplings, and

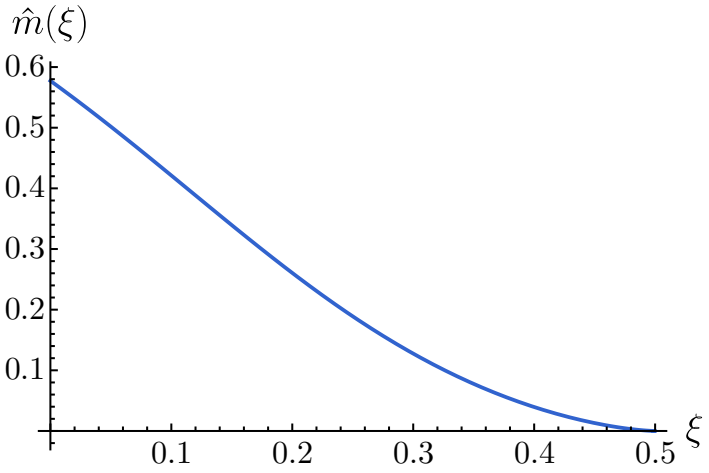

Figure 2.1: Plot of $\hat{m}(\xi)$, as defined in (2.36).

the relations (2.24), we find that matrix Z_{AB} has the following structure

$$Z_{AB} = \begin{pmatrix} 0 & Z_{01} & 0 \\ Z_{01} & \mathrm{i}\mathring{\kappa}(\xi)\overline{Z}_{01} & 0 \\ 0 & 0 & -\frac{1+\xi}{\sqrt{3(1-2\xi)}}\delta_{a'b'}\overline{Z}_{01} \end{pmatrix}, \tag{2.34}$$

where we used the shorthand $\mathring{\kappa}(\xi) \equiv \mathring{\kappa}_{111}(\xi)$. Then, after factorising an overall scale $m_{\text{susy}} \equiv |Z_{01}| = |e^{K/2} D_0 D_1 W|$, and computing the spectrum of eigenvalues m_λ^2 of $ZZ^\dagger$, we obtain

$$m_\lambda / m_{\text{susy}} = \begin{cases} \hat{m}(\xi) & \lambda = 0 \\ 1/\hat{m}(\xi) & \lambda = 1 \\ \dfrac{1+\xi}{\sqrt{3(1-2\xi)}} & \lambda = 2, \ldots, h^{2,1} \end{cases}, \tag{2.35}$$

where we defined

$$\hat{m}(\xi) \equiv \frac{1}{\sqrt{2}} \left(2 + \mathring{\kappa}(\xi)^2 - \mathring{\kappa}(\xi) \sqrt{4 + \mathring{\kappa}(\xi)^2} \right)^{1/2}, \tag{2.36}$$

which is shown in figure 2.1.

Interestingly, it can be seen that all the fermions on the truncated sector have the same mass. In particular, at the LCS point ($\xi = 0$) the fermion mass spectrum reads simply

$$m_0 / m_{\text{susy}} = \frac{1}{\sqrt{3}}, \qquad m_1 / m_{\text{susy}} = \sqrt{3}, \qquad \text{and} \qquad m_{\lambda'} / m_{\text{susy}} = \frac{1}{\sqrt{3}}. \tag{2.37}$$

with $\lambda' = 2, \ldots, h^{2,1}$.

The mass spectrum of the scalar fields can be immediately obtained from equation (2.9). To write it down, it is convenient to introduce the angular parameter θ_W (dependent on the

choice of flux) as

$$\cos\theta_W \equiv \frac{\mathcal{V}\, m_{3/2}}{\sqrt{N_{\rm flux}/4\pi}}\,, \qquad \text{with} \qquad \theta_W \in [0,\pi/2]\,, \tag{2.38}$$

where the range of values of θ_W follows from the tadpole constraint (2.13). Despite appearances, the parameter θ_W has no dependence on the Calabi-Yau volume or the Käher moduli, since the combination $\mathcal{V}\, m_{3/2} = \frac{1}{\sqrt{2}} e^{K_{cs}/2} {\rm Im}(\tau)^{-1/2} |W|$, often denoted by W_0 in the literature, depends solely on the axio-dilaton and complex structure fields. Furthermore, recalling that $Z_{0a'} = 0$, we find from (2.13) that the total $D3$-charge induced by fluxes is simply

$$N_{\rm flux} = 4\pi \mathcal{V}^2 \left(m_{3/2}^2 + m_{\rm susy}^2 \right) \qquad \Longrightarrow \qquad \tan\theta_W = m_{\rm susy}/m_{3/2}\,, \tag{2.39}$$

and then it is straightforward to check that the complete set of scalar masses at tree-level in the axio-dilaton/complex structure sector is given by

$$\boxed{\mu_{\pm\lambda}^2/m_{3/2}^2 = \begin{cases} (1 \pm \tan\theta_W\, \hat{m}(\xi))^2 & \lambda = 0 \\ \left(1 \pm \dfrac{\tan\theta_W}{\hat{m}(\xi)}\right)^2 & \lambda = 1 \\ \left(1 \pm \dfrac{(1+\xi)\tan\theta_W}{\sqrt{3(1-2\xi)}}\right)^2 & \lambda = 2,\ldots,h^{2,1} \end{cases}}\,. \tag{2.40}$$

This mass spectrum is the main result of this chapter. All the parameters appearing in the previous expression can easily be computed in the reduced theory, as ξ is determined by the configuration of the complex structure fields surviving the truncation, and θ_W depends only on the expectation value of the flux superpotential W_0 and the total $D3$-charge $N_{\rm flux}$, induced by the fluxes.

It is worth noticing that this result is independent of both the specific details of the compactification and the number of moduli fields. Moreover, these masses only depend on the choice of fluxes via an overall scale given by the gravitino mass $m_{3/2} = W_0/\mathcal{V}$ and the angular parameter θ_W. We have chosen to present the masses normalised by the gravitino mass in order to eliminate their dependence on the Calabi-Yau volume $\mathcal{V}$, which appears as an overall multiplicative factor.

An interesting case to mention is that of the KKLT scenario [35], where the consistency of the EFT requires that the value of $W_0 \ll 1$ is very close to zero, or equivalently $\theta_W \sim \pi/2$. In this limit the scalar spectrum simplifies to

$$\textbf{KKLT scenario:} \qquad \mu_{\pm\lambda}^2/m_{3/2}^2 \approx \begin{cases} \tan^2\theta_W\, \hat{m}(\xi)^2 & \lambda = 0 \\ \dfrac{\tan^2\theta_W}{\hat{m}(\xi)^2} & \lambda = 1 \\ \dfrac{(1+\xi)^2\tan^2\theta_W}{3(1-2\xi)} & \lambda = 2,\ldots,h^{2,1} \end{cases}\,. \tag{2.41}$$

implying that all the masses in the spectrum are very large compared to the gravitino mass,

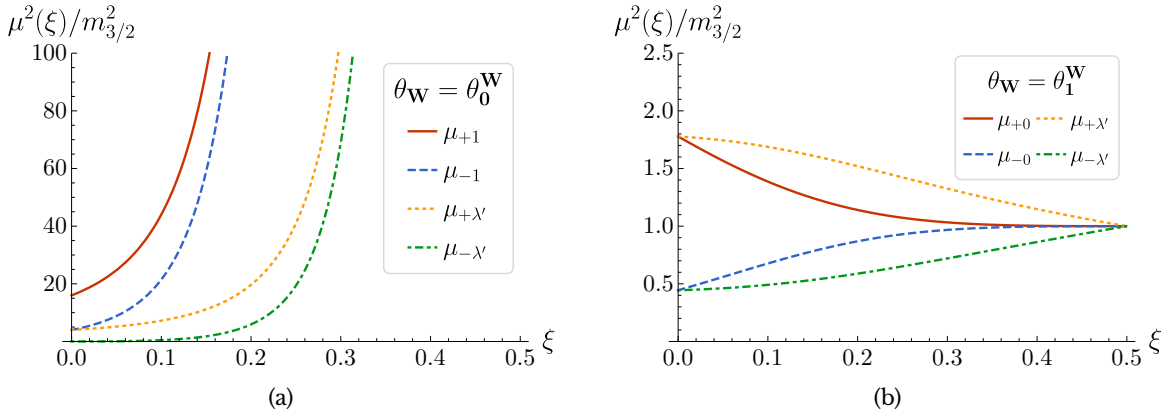

Figure 2.2: Scalar mass spectra associated with the critical values for θ_W (2.42) where the mass spectrum contains at least a zero mode. (a) Spectrum for $\theta_W = \theta_0^W$ where $\mu_{-0}^2 = 0$ and $\mu_{+0}^2 = 4m_{3/2}^2$. (b) Spectrum for $\theta_W = \theta_1^W$ where $\mu_{-1}^2 = 0$ and $\mu_{+1}^2 = 4m_{3/2}^2$.

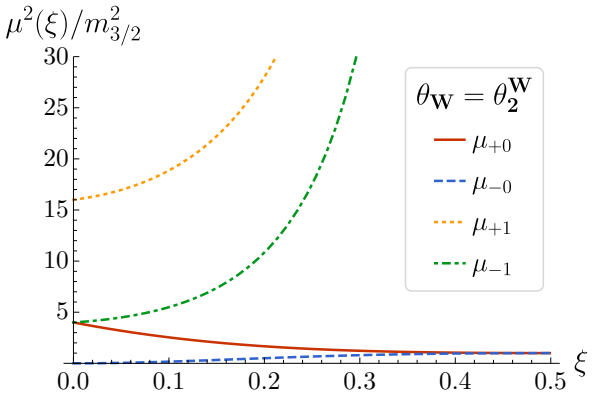

Figure 2.3: Scalar mass spectrum for $\theta_W = \theta_2^W$ where there are $h^{2,1} - 1$ massless modes in the truncated sector $\mu_{-\lambda'}^2 = 0$ and $\mu_{+\lambda'}^2 = 4m_{3/2}^2$.

$\mu_{\pm\lambda}^2 \gg m_{3/2}^2$. As discussed in detail in [148–150], in generic situations this guarantees the consistency of neglecting the complete axio-dilaton/complex structure sector in KKLT constructions, even after including quantum corrections and supersymmetry breaking effects in the theory. However, very light modes might still appear in the spectrum when considering no-scale solutions at special points of the moduli space [151, 152].

In the following two subsections we will discuss another two special cases where the value of the parameter θ_W is fixed, and thus we can write the entire (normalised) mass spectrum as a function of the parameter ξ alone.

2.4.3 *Flux vacua with massless scalars*

An important consequence of (2.40) is that at no-scale vacua we might encounter spectra with very light or even massless scalar fields, since $\tan\theta_W \in [0, \infty)$. In general the presence of those light fields is not convenient for phenomenological applications, as such vacua might become tachyonic after including quantum corrections or due to supersymmetry breaking effects. However, no-scale solutions with light (or massless) modes are still of interest for certain constructions of dS vacua [153, 154], and for implementing inflation. Thus, we will

now briefly discuss the properties of their mass spectra.

Note that, for any given value of the parameter ξ, there are three values of θ_W such that the spectrum contains one, or several massless modes. They are given by

$$\tan\theta_0^W = \hat{m}(\xi)^{-1}\,, \qquad \tan\theta_1^W = \hat{m}(\xi)\,, \qquad \text{and} \qquad \tan\theta_2^W = \frac{\sqrt{3(1-2\xi)}}{1+\xi}\,, \tag{2.42}$$

and for each of these values the massless field(s) correspond(s) to μ^2_{-0}, μ^2_{-1}, and $\mu^2_{-\lambda'}$, respectively. The corresponding spectra associated to these branches of vacua are displayed in figures 2.2 and 2.3. In the case of the critical values $\theta_W = \theta_0^W$ and $\theta_W = \theta_1^W$, away from the LCS point ($\xi > 0$) the spectrum contains exactly one vanishing mass, corresponding to fields in the reduced theory: $\mu^2_{-0} = 0$ and $\mu^2_{-1} = 0$, respectively. In those two cases all the other fields have masses of at least the order of the gravitino mass. These classes of vacua might be particulary interesting to realise the construction of dS vacua of [153,154], which required a massless field in the complex structure sector at tree-level. Regarding the last branch, $\theta_W = \theta_2^W$, away from the LCS point the spectrum contains $h^{2,1} - 1$ massless modes $\mu^2_{-\lambda'} = 0$, that is *half of the scalar modes* in the truncated sector.

In section 2.6 we will discuss the statistics of this mass spectrum in the ensemble of no-scale flux vacua. This will help us to estimate how generic these classes of vacua are in the Landscape.

2.4.4 *No-scale vacua with* $N_A^0 = 0$

In the present subsection we consider the second class of no-scale vacua for which the parameter θ_W is fixed in terms of ξ, namely flux vacua where the flux vector satisfies the constraint $N_A^0 = 0$. The flux N_A^0 is associated to the period (1.31) that grows without bound in the LCS limit. The main consequence of setting this flux to zero is that the terms of the superpotential which are cubic in z^i are also identically zero.

The main motivation to study this class vacua is the analyses done in [145,155]. On the one hand, in [155] it was argued (via a numerical analysis) that for generic choices of the fluxes, and at points of the moduli space near the LCS point the cubic terms of the superpotential typically become dominant.[6] On the other hand, as proven in [145,155], when the cubic terms of W dominate no vacua can exist in the region of the moduli space where $\xi \approx 0$. As a consequence, no-scale vacua with $N_A^0 \neq 0$ are expected to be very scarce, or even non-existent, in a small neighbourhood of the LCS point. On the contrary, the conclusions in [145,155] cannot be applied to the class of vacua where the flux N_A^0 is set to zero, since the cubic terms of the superpotential are identically zero, and therefore can never become dominant. Thus, it is expected that the constrained class of vacua with $N_A^0 = 0$ may still be present, and even become the dominant type of vacua in a small neighbourhood of the LCS point.

To give further support to this conclusion, in appendix D we have estimated the minimal values of ξ for which it is possible to find no-scale solutions with both non-vanishing N_A^0

[6] Actually this is true even for points in field space not associated with a vacuum.

and when subject to the constraint $N_A^0 = 0$. We find

$$\xi_{\min}|_{N_A^0 \neq 0} \gtrsim \frac{|\mathrm{Im}\kappa_0|}{4\sqrt{N_{\rm flux}}} \tag{2.43}$$

for $N_A^0 \neq 0$, while in the case $N_A^0 = 0$ the parameter ξ remains unbounded below. In agreement with the analyses in [145,155], we can see that vacua with $N_A^0 = 0$ are expected to be dominant in a small neighbourhood of the LCS point. As we shall show in section 2.6, the numerical scan of no-scale vacua in the $\mathbb{WP}^4_{[1,1,1,1,4]}$ model confirms this expectation, and matches perfectly with the conclusions of [145,155].

To prove that in this type of vacua the angular parameter θ_W is determined by the value of ξ, it is convenient to make use of the Hodge decomposition of the flux vector N [46]. As we review in appendix A, at any given no-scale vacuum $\{\tau_c, z_c^i\}$ the flux vector can be written in terms of the period vector Π and its Kähler covariant derivatives $D_a\Pi = (\partial_a + K_a)\Pi$ as

$$N = \sqrt{4\pi} e^{K_{cs}} \left(i W \overline{\Pi} + D_{\bar{0}} D_{\bar{a}} \overline{W}\, D_a \Pi \right). \tag{2.44}$$

Setting $N_A^0 = 0$ in this expression, we find

$$W = i D_{\bar{0}} D_{\bar{a}} \overline{W}\, K_a\,, \tag{2.45}$$

where we have used that in the gauge (1.31) the period vector satisfies $\Pi_A^0 = 1$. Finally, taking into account the result (2.31) and the definition of the angular parameter θ_W (2.38) together with (2.13), we arrive at the constraint

$$\tan\theta_W = \sqrt{(1-2\xi)/3} \qquad \Longrightarrow \qquad \theta_W \in \left[0, \frac{\pi}{6}\right]. \tag{2.46}$$

Alternatively, this relation can be expressed in the following useful way.

$$W_0^2 = \mathcal{V}^2 m_{3/2}^2 = \frac{3N_{\rm flux}}{8\pi(2-\xi)} \geq \frac{N_{\rm flux}}{8\pi} \sim \mathcal{O}(10 - 10^3), \tag{2.47}$$

which relates the flux parameter W_0 and the total $D3$-charge $N_{\rm flux}$. From here we can see immediately that these solutions are not compatible with the KKLT construction of dS vacua, since that scenario requires $W_0 \ll 1$. On the contrary, this class of no-scale vacua is suitable for the construction of LVS vacua, where $W_0 \sim \mathcal{O}(1-10)$.

In order to find the scalar spectrum at these no-scale solutions, we just need to substitute the relation (2.46) into our main result (2.40), which leads to

$$\mathbf{N_A^0 = 0}: \qquad \mu_{\pm\lambda}^2 / m_{3/2}^2 = \begin{cases} \left(1 \pm \sqrt{(1-2\xi)/3}\, \hat{m}(\xi)\right)^2 & \lambda = 0 \\ \left(1 \pm \dfrac{\sqrt{(1-2\xi)}}{\sqrt{3}\hat{m}(\xi)}\right)^2 & \lambda = 1 \\ \left(1 \pm \dfrac{1+\xi}{3}\right)^2 & \lambda = 2, \ldots, h^{2,1} \end{cases}. \tag{2.48}$$

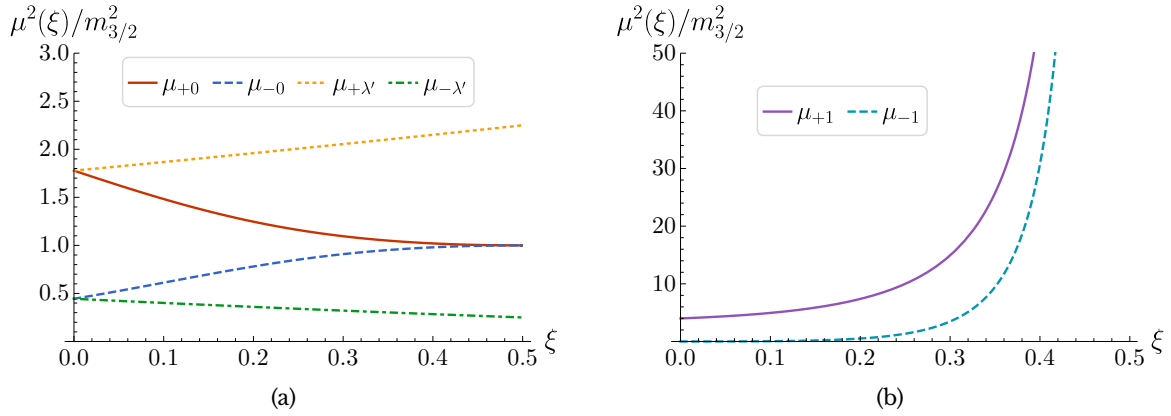

Figure 2.4: Spectrum of scalar masses for vacua with the restriction $N^0_A = 0$ on the flux configuration. The masses are plotted as a function of the LCS parameter $\xi \in [0, 1/2]$ and are normalised by the gravitino mass $m_{3/2}$. (a) Branches corresponding to the masses $\{\mu^2_{\pm 0}, \mu^2_{\pm\lambda'}\}$, where $\mu^2_{\pm\lambda'}$ are the $2(h^{2,1}-1)$ masses in the truncated sector. (b) Scalar mass branches $\{\mu^2_{+1}, \mu^2_{-1}\}$. We can see that in these branches of vacua there are no light truncated fields $\mu^2_{\pm 1} \ll m^2_{3/2}$ in the entire LCS regime.

We have displayed the dependence of these masses on the parameter ξ in figure 2.4. Note that the previous spectrum is independent of the details of the Calabi-Yau compactification. With the aid of (2.47), it can be computed entirely from the total $D3$-charge N_{flux}, the LCS parameter ξ, and the Calabi-Yau volume $\mathcal{V}$.

Finally, as we approach the LCS point $\xi \to 0$, the mass spectrum (2.48) takes the universal form

$$\mathbf{N^0_A = 0},\ \ \xi = \mathbf{0}: \qquad \mu^2_{\pm\lambda}/m^2_{3/2} = \begin{cases} \left(1 \pm \frac{1}{3}\right)^2 & \lambda = 0, 2, \ldots, h^{2,1} \\ (1 \pm 1)^2 & \lambda = 1 \end{cases} . \tag{2.49}$$

This result is reminiscent of the deterministic spectra found in [145, 155] at generic moduli configurations (not necessarily vacua) near the LCS point.

2.5 One-parameter example: the $\mathbb{WP}^4_{[1,1,1,1,4]}$ model

In order to illustrate our results we have analysed a large sample of no-scale vacua of an orientifold of the Calabi-Yau hypersurface $\mathbb{WP}^4_{[1,1,1,1,4]}$ (the *octic*). We will now briefly review the effective field theory for the compactification of type IIB superstrings in this Calabi-Yau, and we will discuss the statistical properties of the resulting ensemble in section 2.6. For a more detailed description of this compactification see [97, 124].

2.5.1 *Effective theory*

The Calabi-Yau geometries that we will consider can be defined in terms of the following family of hypersurfaces

$$4x_0^2 + x_1^8 + x_2^8 + x_3^8 + x_4^8 - 8\psi x_0 x_1 x_2 x_3 x_4 = 0 \tag{2.50}$$

in the complex projective space $x^i \in \mathbb{WP}^4_{[1,1,1,1,4]}$.

This family of hypersurfaces is characterised by a single complex deformation parameter ψ, with $\arg\psi \in [0, \frac{\pi}{4}]$. However, this Calabi-Yau three-fold has $h^{1,1} = 1$ Kähler moduli and $h^{2,1} = 149$ complex structure fields, and thus there are many other deformations that one could consider. The Calabi-Yau geometries described by (2.50) are all invariant under a large group of discrete symmetries, namely $\mathcal{G} = \mathbb{Z}_8^2 \times \mathbb{Z}_2$ with order $[\mathcal{G}] = 128$, and all the deformations that we have not included in (2.50) are those transforming non-trivially under this group [96, 97]. Thus, by retaining only the deformation parametrised by ψ, we are realizing a consistent truncation of the complex structure moduli space, just as we discussed in section 2.3.

In the neighbourhood of the large complex structure point, $\psi \to \infty$, the truncated action is characterised by the prepotential [124, 133]

$$\mathcal{F}(z) = \frac{\mathrm{i}}{3}z^3 + \frac{3}{2}z^2 + \mathrm{i}\frac{11}{6}z - \mathrm{i}\frac{37}{2\pi^3}\zeta(3) + \mathcal{F}_{\text{inst}}\,, \tag{2.51}$$

where $z \approx \frac{4}{\pi}\log(4\psi)$ and $\mathrm{Im}z \in [-1/2, 1/2)$. Here, $\mathcal{F}_{\text{inst}}$ represents exponentially suppressed instanton corrections to the prepotential. Its leading term is of the form

$$\mathcal{F}_{\text{inst}} \approx -\frac{\mathrm{i}n_1}{(2\pi)^3}\mathrm{e}^{-2\pi z} + \ldots, \qquad \text{with} \qquad n_1 = 29504\,. \tag{2.52}$$

The expansion for the prepotential (2.51) around the LCS point is valid in the region $|\psi| > 1$, or equivalently $\xi \lesssim \xi_{\text{cnf}} \equiv 0.39$, away from the conifold singularity at $\psi = 1$ [124, 133]. However, here we will require in addition that the instanton corrections cause small variations on the moduli space geometry and the relevant physical quantities (e.g., the Yukawa couplings $\mathring{\kappa}_{abc}$, the vielbeins e_i^a, and $m_{3/2}$). As we discuss in appendix D.3, the most restrictive bound is found when imposing that the relative corrections to the moduli space vielbein are small. Although this is checked for each particular vacuum, a simple estimate shows that the corrections remain moderately small ($< 20\%$) as long as the LCS parameter satisfies

$$\xi \lesssim \xi_{\text{max}} = 0.185 < \xi_{\text{cnf}}\,, \tag{2.53}$$

which is a more conservative bound than just requiring the convergence of (2.51).

Following [46, 96, 97], we will regard this compactification as an orientifold limit of a compactification of F-theory on the fourfold $M_4 = \mathbb{WP}^5_{[1,1,1,1,8,12]}$, where the orientifold action is defined by the transformations[7] $x_0 \to -x_0$ and $\psi \to -\psi$ [156, 157]. The advantage of considering the embedding in F-theory is that compactifications on a fourfold allow a great deal of freedom in the choice of fluxes, which is particularly appropriate for performing a statistical analysis [46]. Indeed, the tadpole constraint L is

$$L = \frac{\chi(M_4)}{24}\,, \tag{2.54}$$

where $\chi(M_4)$ is the Euler number of the fourfold, which typically greatly exceeds the one

[7] As shown in [96], it is possible to turn on the three-forms $F_{(3)}$ and $H_{(3)}$ on the four periods of the reduced theory consistently with the orientifold action.

of the associated Calabi-Yau orientifold $\tilde{M}_3$. In the case at hand, the Euler number of the fourfold $\mathbb{WP}^5_{[1,1,1,1,1,8,12]}$ is $\chi(M_4) = 23328$, and thus the upper bound on the $D3$-brane charge induced by the fluxes is $N_{\text{flux}} \leq L = 972$.

As a final remark, note that the F-theory embedding also requires including in the theory additional $D7$-brane moduli (see [14]). The problem of the stabilisation of those moduli is however beyond the scope of this thesis, and we refer the reader to [158–162] and the references therein for works on the subject.

2.5.2 *Numerical search for flux vacua*

In order to perform a numerical exploration of the flux landscape of the octic, we used `Paramotopy` [163]. This software uses a numerical technique known as the *Polynomial Homotopy Continuation* (PHC) method [164,165], which efficiently finds all roots of non-linear polynomial systems, such as the no-scale equations (1.37) (see appendix B). Therefore, given a flux ensemble satisfying the tadpole condition (1.42), the PHC method allows for an exhaustive search of all the solutions to the no-scale equations (1.37) [166,167].

As described in detail in appendix B, we have constructed two separate ensembles of no-scale vacua: one with generic fluxes satisfying the tadpole constraint, and one where fluxes additionally satisfy the condition $N^0_A = 0$, as considered in section 2.4.4. We shall refer to them as the *generic* and *constrained* ensembles, respectively. The starting point for the construction of each of the ensembles is a collection of fluxes f and h randomly selected from a uniform distribution with support $[-50, 50]$. This starting set consists of 10^7 choices of flux for the generic ensemble, and 10^6 choices for the constrained one.

For each choice of flux, the corresponding set of no-scale vacua were found using the PHC method. We then selected all solutions which have a small string coupling constant $g_s = (\text{Im}\tau)^{-1} < 1$ and small instanton corrections, i.e., which satisfy (2.53). In addition, when constructing the ensemble we checked that there was no double-counting of vacua related by either an $\text{SL}(2,\mathbb{Z})$ action (1.39), or the symplectic transformations (1.28) and (1.38). Regarding the symplectic transformations, as proposed in [98], all no-scale solutions have been mapped to the fundamental domain of the axio-dilaton, where the redundant copies have been identified and discarded.[8] As for symplectic transformations, there is the monodromy around the LCS point [124,133] which we have treated similarly, by mapping all solutions to a fundamental domain of the complex structure modulus z and eliminating duplicate solutions.

The ensemble of vacua with unconstrained fluxes that we obtained with this method contains 119,139 solutions, while the constrained ensemble has 57,487. The results of this procedure for the generic ensemble are displayed in figure 2.5, where we show the distribution of no-scale vacua in the fundamental domain of the axio-dilaton τ, in the complex structure field z, and in the $(\text{Re}z, \text{Im}\tau)$. For completeness, let us mention that more conservative constraints could be imposed on the vacua, e.g., $g_s < 0.1$ and instanton corrections

[8] We avoided imposing conditions on the fluxes to eliminate the redundancies, as done, e.g., in [166,167]. In particular, our analysis showed that the constraints on the fluxes proposed in [166] to deal with the $\text{SL}(2,\mathbb{Z})$ symmetry lead to spurious correlations arising in the statistical analysis, and which are incompatible with the predictions derived from the continuous flux approximation [46].

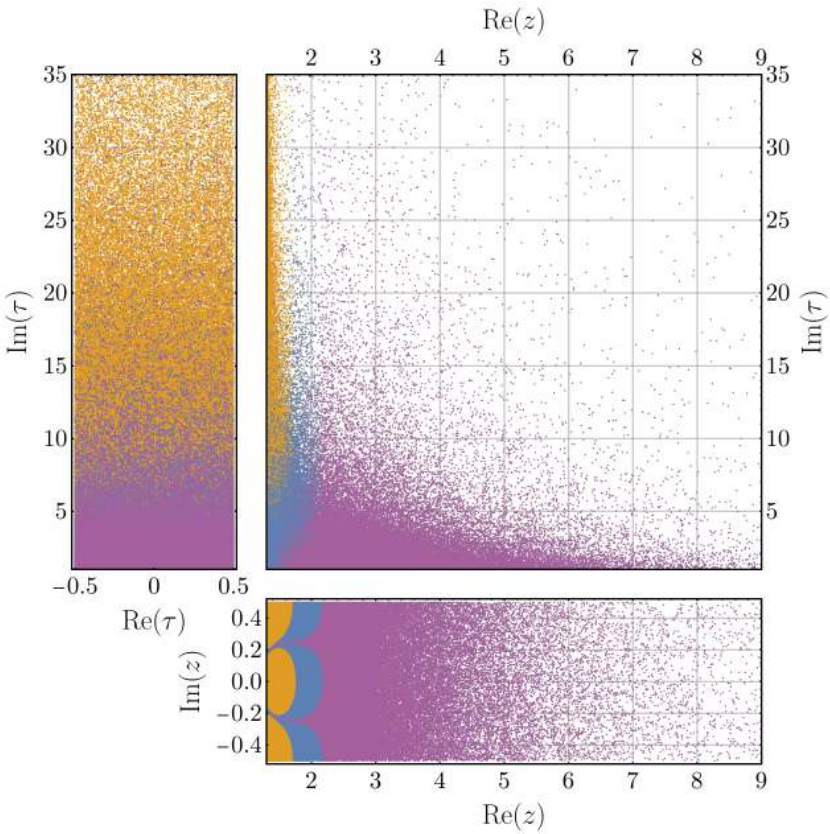

Figure 2.5: Distribution of the numerically generated set of generic no-scale solutions on the (τ, z) field space. We have represented in orange vacua with large instanton corrections $> 20\%$ *(leading term in (2.52)), in blue when corrections are in the range* $1 - 20\%$*, and in purple when corrections are* $< 1\%$*. The $(Re z, Im\tau)$ plane exhibits nicely delineated regions, which are nevertheless likely to be blurred by higher order contributions to (2.52). The generic ensemble of vacua analysed in the text is comprised of those solutions with small instanton corrections* $< 20\%$*, and small string coupling $g_s = (Im\tau)^{-1} < 1$ (blue and purple, 119,139 solutions).*

below $< 1\%$, leading to a considerably smaller ensemble with 427 vacua. However, in order to have a sufficiently large sample to perform the statistical analysis, in the following we will consider all vacua in the weak coupling regime $g_s < 1$ and with moderately small instantons corrections $< 20\%$.

In order to check the validity of our main result, (2.35), at each of the no-scale solutions, we computed the eigenvalues of the fermion mass matrix (2.8) for the reduced theory (involving only τ and z) using two different methods: first via the direct diagonalisation of the mass matrices obtained numerically, and then using the analytic formula (2.35). We display the outcome of these computations in figure 2.6, which demonstrates the perfect the agreement of both methods. Regarding the 148 truncated complex structure moduli, although the EFT given above has no specific information about them, the expressions (2.35) allowed us to determine the fermionic masses corresponding to this sector at each no-scale solution. Finally, the scalar mass spectra in the whole axio-dilaton/complex structure sector for the ensemble of no-scale solutions were computed via (2.9). We checked that these masses coincide with those obtained by diagonalizing the Hessian (2.7) at each no-scale

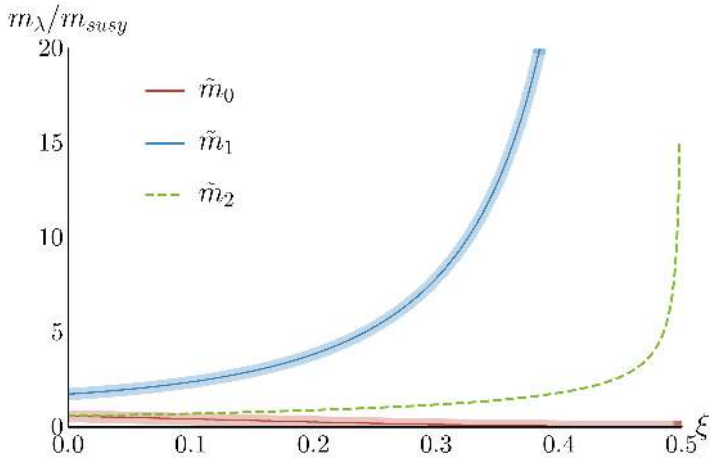

Figure 2.6: Fermion masses in the $\mathbb{WP}^4_{[1,1,1,1,4]}$ compactification versus the LCS parameter ξ at no-scale vacua. The fermion masses are normalised by the supersymmetric mass scale, $\tilde{m}_\lambda \equiv m_\lambda / m_{susy}$. The uppermost and lowermost thick curves represent the analytic result in (2.35) for the two fermions in the reduced theory. The thin solid curves, composed of (indistinguishable) data points, show masses obtained diagonalising numerically the fermion mass matrix (2.10) at each vacuum of the ensemble. The middle dashed curve represents the mass of the 148 fermions in the truncated sector (with a priori unknown EFT couplings), which was computed via the third equation in (2.35).

vacuum. The statistical properties of these spectra will be analysed in the next section.

2.6 Statistics of vacua

As we discussed in section 2.4, the no-scale mass spectrum will depend in general on the flux configuration. To determine the properties of the spectra that may arise in the ensemble of flux vacua, we will adopt the statistical approach of [46], and derive the probability distributions for the masses and other quantities of interest. We begin by presenting the relevant formulae for general compactifications before using them to study the particular models we consider.

Our starting point for this analysis will be the formula for the density of flux vacua derived in [46] using the continuous flux approximation. This approximation is based on the assumption that for large tadpoles, $L \gg 1$, flux quantisation can be neglected, and thus it is possible to replace the sums over flux configurations by integrals.

$$\sum_{N_A^I, N_I^B} \longrightarrow \int d^{2n} N_A d^{2n} N^B \,, \tag{2.55}$$

where $n = h^{2,1} + 1$ and each component of $N = f - \tau h$ is a complex number parametrized by the two tuples of integers f and h. Furthermore, as was proven in [46] and reviewed in appendix A, by using the Hodge decomposition of the flux vector it is possible to establish a one-to-one correspondence between the $2n$ *continuous* flux complex variables $\{N_A^I, N_I^B\}$ and the $2n$ complex quantities $\{Z_A, F_A\}$ $(A = 0, \ldots, h^{2,1})$ given by

$$Z_0 \equiv \mathcal{V} e^{K/2} W \,, \qquad Z_a \equiv \mathcal{V} Z_{0a} \,, \qquad F_0 \equiv \mathcal{V} e^{K/2} D_0 W \,, \qquad F_a \equiv \mathcal{V} e^{K/2} D_a W \,. \tag{2.56}$$

These variables are particularly convenient choices for describing the flux ensemble, as no-scale vacua can be equivalently characterised as flux configurations satisfying the conditions $F_A = 0$. Thus, assuming a flat probability distribution on the fluxes, and using a generalisation of the Kac-Rice formula[9] [168,169] (see [170] for a review), the *density function* for no-scale vacua follows as [46]

$$d\mu_{vac}(Z_A, u^A) = \mathcal{N} \cdot |\det \mathscr{H}|^{1/2} |\det g| e^{-|Z|^2} \cdot d^{2n}Z \cdot d^{2n}u\,, \tag{2.57}$$

where we denote the fields collectively by $u^A = \{\tau, z^a\}$, g is the moduli space metric, and $\mathscr{H}$ is the canonically normalised Hessian of the no-scale potential given by (2.7) and (2.12) (see appendix C). Here, and throughout the text, $\mathcal{N}$ indicates some normalization constant which must be computed for each particular distribution.

In the class of models we are interested in, the number of complex structure moduli can be arbitrarily high but only one survives the truncation. In addition, as explained in section 2.3, the truncation requires that only the components $I = 0, 1$ of the flux vector $N = \{N^I_A, N^B_I\}$ are turned on (8 flux integers). Therefore, the statistics of these models can be described by (2.57), setting $h^{2,1} = 1$ ($n = 2$). In this case, the determinant of the Hessian $\mathscr{H}$ takes the particularly simple form

$$|\det \mathscr{H}|^{1/2} = ||Z_0|^4 + |Z_1|^4 - (2 + \mathring{\kappa}^2)|Z_0|^2|Z_1|^2|\,, \tag{2.58}$$

which will considerably simplify the computation of the mass distributions.

2.6.1 *Moduli space distribution of generic no-scale vacua.*

Integrating (2.57) over the flux parameters Z_A (with $h^{2,1} = 1$) one obtains the following density distribution of no-scale vacua [46]:

$$d\mu(z,\tau) = \mathcal{N} \cdot |\det g| \cdot \left(2 - \mathring{\kappa}^2 + \frac{2\mathring{\kappa}^3}{\sqrt{4+\mathring{\kappa}^2}}\right) d^2\tau\, d^2 z\,, \tag{2.59}$$

where

$$|\det g| = \frac{3}{16}\left(\frac{2\kappa_{zzz}}{3|\mathrm{Im}\kappa_0|}\right)^{2/3} \frac{(r^3-2)r}{(r^3+1)^2\, s^2} \tag{2.60}$$

is the determinant of the moduli space metric, with κ_{zzz} denoting Yukawa coupling for the (non-canonically normalised) field z. We have also introduced the shorthands

$$s \equiv \mathrm{Im}\tau \qquad \text{and} \qquad r \equiv 1/\xi^{1/3} = \left(\frac{2\kappa_{zzz}}{3|\mathrm{Im}\kappa_0|}\right)^{1/3} \mathrm{Re}\, z\,. \tag{2.61}$$

Thus the quantity $\mathring{\kappa}$, defined in (2.29) in terms of ξ, should be understood as a function of Rez in the expression (2.59) for the no-scale vacua density function. The corresponding

[9] Essentially, the Kac-Rice formula counts the roots of continuous functions in a certain domain using the properties of the Dirac delta function. As we will thoroughly see in chapter 5 and appendices C and E, it can be applied to random functions with known distributions to compute, among many other quantities, their expected number of vacua in a given volume.

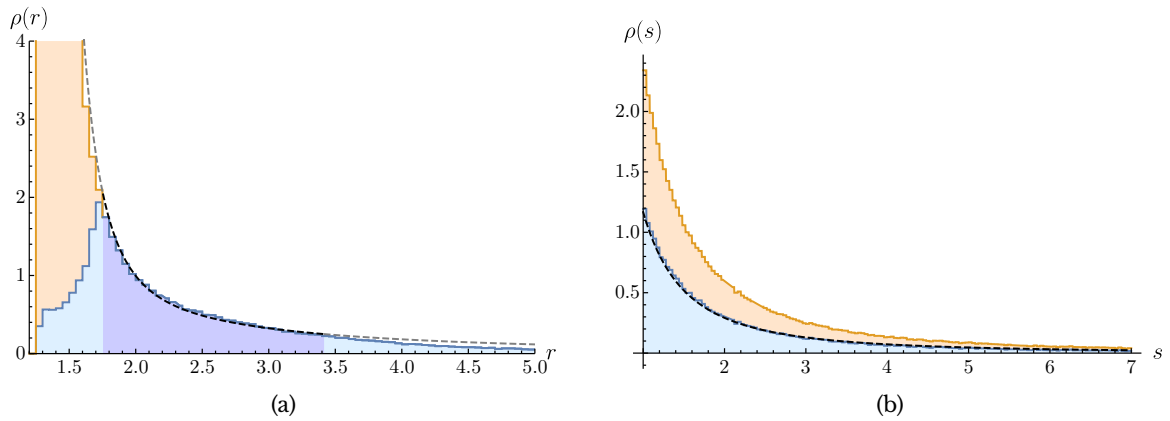

Figure 2.7: (a) Marginalised density of no-scale vacua on the complex structure sector (2.59) (dashed line), and numerically obtained histogram of generic no-scale solutions in the $\mathbb{WP}^4_{[1,1,1,1,4]}$ flux ensemble. The quantity $r \equiv (2\kappa_{zzz}/3|Im\kappa_0|)^{1/3} Re z$ represents the complex structure field at the vacua, with the boundaries of the moduli space located at $r = 2^{1/3}$ and $r \to \infty$ (the LCS point). The orange area represents excluded solutions with large instanton corrections ($> 20\%$). In dark blue we indicate the subset of the remaining vacua well described by (2.59) (normalised in $r \in [1.75, 3.42]$). (b) Marginalised distribution (2.59) for the imaginary part of the axio-dilaton, $s \equiv Im\tau$ (dashed line), and histogram of solutions in the generic ensemble of no-scale vacua.

marginal probability distributions for Re z and Im τ are displayed in figure 2.7. The plots show a remarkable agreement with the histograms obtained from the numerical scan of the octic model. Combining (2.59) and (2.61) it is also straightforward to find the probability distribution function for the LCS parameter ξ,

$$d\mu(\xi) = \mathcal{N} \cdot \frac{(1-2\xi)}{(1+\xi)^2\,\xi^{2/3}} \left(2 - \mathring{\kappa}(\xi)^2 + \frac{2\mathring{\kappa}(\xi)^3}{\sqrt{4+\mathring{\kappa}(\xi)^2}} \right) d\xi \,, \tag{2.62}$$

which we have displayed in figure 2.8, together with the histogram obtained from the direct computation from the octic flux ensemble data.

It is interesting to note that the density of vacua grows without bound as we move towards small values of r (i.e., $\xi \to 1/2$), where the conifold point is located, $r_{\rm cnf} \approx 1.37$ ($\xi_{\rm cnf} = 0.39$). This is consistent with the expectation that the density of vacua is enhanced in regions of large moduli space curvature [97, 171, 172]. Actually, the marginalised density functions for Re z obtained from (2.59) are not normalisable when we define its support to be the entire range[10] $r \in [2^{1/3}, \infty)$. This property of the ensemble has an observable effect: as the underlying distribution from which we are extracting the vacua is not normalisable, regardless of the size of the sample, the histograms will always exhibit a deficit of vacua with respect to the probability distribution (see region $\xi \gtrsim 0.3$ in figure 2.8). Nevertheless, in practice, we have to acknowledge that this distribution cannot be trusted outside the regime of validity of the EFT. Recall that the EFT for the octic can only be considered in the region where the instanton corrections can be safely neglected, that is, in the region given by the bound (2.53), or equivalently with $r \in [1.75, \infty)$. Thus, as long as the support of (2.59) is

[10] Recall that we obtained the condition $\xi < 1/2$, satisfied away from the moduli space boundaries, neglecting completely the instanton contributions, and thus it gives no information about the position of the conifold point at $\xi_{\rm cnf} = 0.39$.

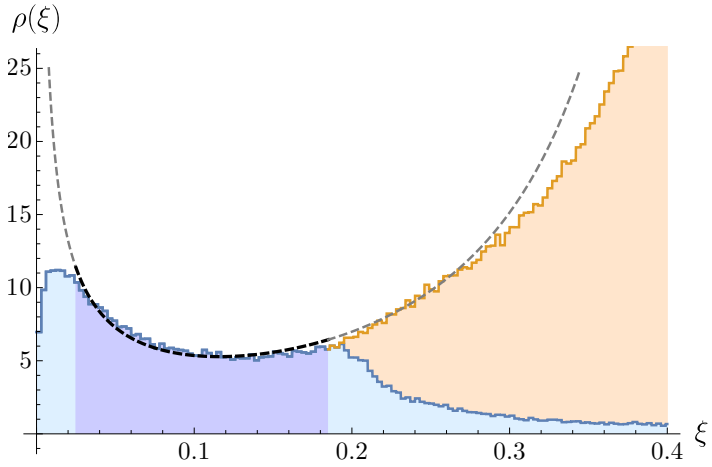

Figure 2.8: Distribution for the LCS parameter ξ (2.62) in the flux ensemble with unconstrained N_A^0 (dashed line), and histogram of solutions obtained from the numerical scan in the $\mathbb{WP}^4_{[1,1,1,1,4]}$ model. The colours are the same as in figure 2.7.

taken to be the region of validity of the EFT, the probability distribution we will work with will be finite and normalizable, and thus well defined.

In figure 2.8, it can also be seen that the density of generic no-scale vacua near the LCS point ($\xi \approx 0$) is considerably lower that the statistical prediction based on the continuous flux approximation (dashed line). This to be expected from the analyses in [145, 155], where it was shown that the statistics of generic no-scale vacua (with unconstrained N_A^0) cannot be described with the continuous flux approximation in the strict LCS limit, and that actually in a small neighborhood of the LCS point there are no no-scale solutions with $N_A^0 \neq 0$. Such behavior was also anticipated in [134], where the authors argued that the techniques presented there could fail to describe vacua statistics restricted to small regions of the moduli space. In appendix D.2 we derive an estimate for the region of validity of the continuous flux approximation (eq. (2.43)) which, in the present ensemble, leads to the additional constraint on the LCS parameter

$$\xi \geq \xi_{\text{min}} = 0.025\,. \tag{2.63}$$

In the following section we will discuss the statistics of the mass spectrum in the regime where the EFT is under control and, in addition, where the continuous flux approximation is a good characterisation of the flux ensemble. That is, in the moduli region determined by the bounds (2.53) and (2.63).

Before we end this subsection let us comment briefly on the distribution of the string coupling constant g_s. Both the analytical result in eq. (2.59), and the numerical histogram displayed in figure 2.7(b), indicate that the probability density for $\text{Im}(\tau)$ has the form $\rho(\text{Im}\tau) \propto 1/(\text{Im}\tau)^2$. Therefore, it is straightforward to check that the string coupling $g_s = (\text{Im}\tau)^{-1}$ is uniformly distributed. This conclusion is relevant in the computation in [173] of the distribution of the supersymmetry breaking scale in the Landscape which relies on g_s having a uniform distribution.

2.6.2 *Mass distributions at generic no-scale vacua*

With the joint probability distribution (2.57) at hand it is now straightforward to compute probability distributions for the masses, both the fermions and the scalar modes, at the no-scale vacua in our flux ensemble.

In particular, at a given vacuum with LCS parameter ξ and angular parameter θ_W, the fermion mass spectrum normalised by the gravitino mass $m_\lambda/m_{3/2}$ is given by

$$x_\lambda \equiv m_\lambda/m_{3/2} = \begin{cases} \zeta\,\hat{m}(\xi) & \lambda = 0 \\ \zeta\,\hat{m}(\xi)^{-1} & \lambda = 1 \\ \dfrac{\zeta(1+\xi)}{\sqrt{3(1-2\xi)}} & \lambda = 2,\ldots,h^{2,1} \end{cases}, \tag{2.64}$$

where we have used (2.35) in combination with (2.39), with $\zeta \equiv \tan^2\theta_W \in [0,\infty]$. Then, in order to find the distribution for these masses, we need the joint distribution for $\{\xi,\zeta\}$. This distribution can be obtained from (2.57) and (2.58) by integrating over the phases $\arg(Z_0)$ and $\arg(Z_1)$, the total $D3$-charge induced by fluxes $|Z_A|^2 = N_{\rm flux}$, and the field space directions τ and Im z. Using the ζ and ξ variables, this yields

$$d\mu(\zeta,\xi) = \mathcal{N}\cdot\frac{(1-2\xi)}{\xi^{2/3}(1+\xi)^2(1+\zeta)^4}\left|\zeta-\hat{m}(\xi)^2\right|\left|\zeta-\hat{m}(\xi)^{-2}\right|\cdot d\zeta\,d\xi\,. \tag{2.65}$$

From (2.64) we can see that given a fixed value of ξ, we can establish a one-to-one correspondence between ζ and each of the rescaled fermion masses x_λ. Therefore, by performing a change of random variables $\{\zeta,\xi\}\to\{x_\lambda,\xi\}$ in (2.65), we can derive three separate distribution functions, each involving a different scaled mass x_λ. After integrating over the LCS parameter on the interval $\xi\in[\xi_{\rm min},\xi_{\rm max}]$ given by (2.53) and (2.63), the resulting marginal distributions for the fermion masses in the reduced theory read

$$\rho_0^f(x_0) = \mathcal{N}\left|x_0^2-1\right|x_0\int_{\xi_{\rm min}}^{\xi_{\rm max}} d\xi\,\frac{(1-2\xi)\,\hat{m}(\xi)^2}{\xi^{2/3}(1+\xi)^2(\hat{m}(\xi)^2+x_0^2)^4}\left|x_0^2-\hat{m}(\xi)^4\right|, \tag{2.66}$$

and

$$\rho_1^f(x_1) = \mathcal{N}\left|x_1^2-1\right|x_1\int_{\xi_{\rm min}}^{\xi_{\rm max}} d\xi\,\frac{(1-2\xi)\,\hat{m}(\xi)^2}{\xi^{2/3}(1+\xi)^2(1+x_1^2\,\hat{m}(\xi)^2)^4}\left|x_1^2\,\hat{m}(\xi)^4-1\right|. \tag{2.67}$$

Without further computations, we can already see that the probability of finding vacua with $m_{\lambda=0,1}=m_{3/2}$ (equivalently $x_{\lambda=0,1}=1$) is suppressed, i.e., $\rho^f_{\lambda=0,1}(1)=0$. This is a direct consequence of the generalized Kac-Rice formula (2.57). To see this, note that density of vacua is proportional to the square root of the Hessian determinant $|\det\mathscr{H}|^{1/2}$. This means that the probability of finding no-scale solutions with massless scalar modes in the flux ensemble should vanish. Since according to (2.9) massless scalar modes occur precisely whenever one fermion mass equals that of the gravitino, we conclude that no-scale vacua with $m_\lambda = m_{3/2}$ are quite rare in the Landscape. It is important to emphasize that this does not preclude vacua with $m_{\lambda=0,1}=m_{3/2}$ from existing, it just means they represent a very small fraction of the total number of vacua. Actually, the suppression of critical points

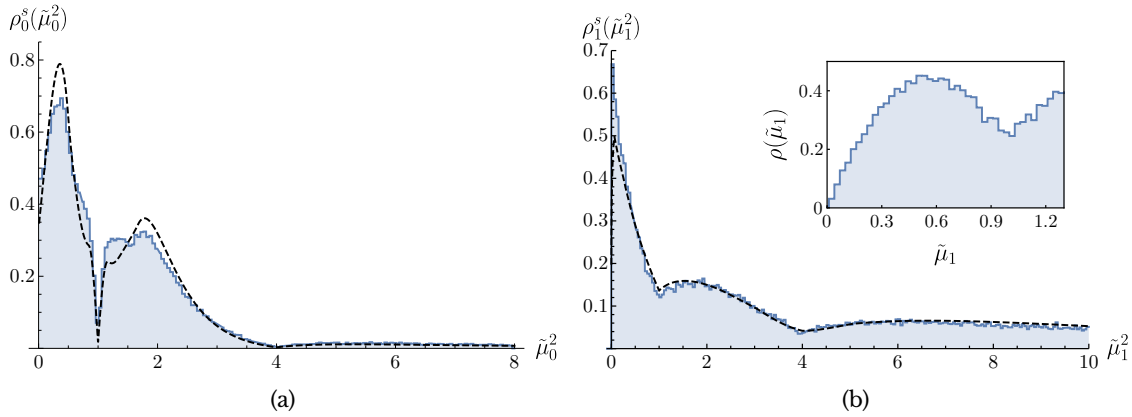

(a) (b)

Figure 2.9: Distribution of the squared scalar masses normalised by the gravitino mass, $\tilde{\mu}_\lambda^2 \equiv \mu_\lambda^2 / m_{3/2}^2$, in the ensemble with unconstrained fluxes. The dashed lines in (a) and (b) correspond to the probability distribution (2.69) (evaluated with (2.66) and (2.67), resp.) for the masses of the scalars in the reduced theory. We also show the mass histograms obtained numerically from the flux ensemble of the $\mathbb{WP}^4_{[1,1,1,1,4]}$ model (blue). The inset in (b) shows the obtained distribution $\rho(\tilde{\mu}_1)d\tilde{\mu}_1$ near the origin, which presents a suppression for the massless mode.

with of zero eigenvalues on the Hessian, which also leads to an apparent repulsion between critical points, is a generic feature of random functions (see, e.g., [170]), and has already been observed in other characerisations of the Landscape [174, 175].

Regarding the rescaled mass of the truncated fermions $x_{\lambda'} = m_{\lambda'}/m_{3/2}$, we find the distribution

$$\rho^f_{\lambda'}(x_{\lambda'}) = \mathcal{N} x_{\lambda'} \int_{\xi_{\min}}^{\xi_{\max}} d\xi \frac{(1-2\xi) f(\xi)^{-2} \left| x_{\lambda'}^2 f(\xi)^{-2} - \hat{m}(\xi)^2 \right| \left| x_{\lambda'}^2 f(\xi)^{-2} - \hat{m}(\xi)^{-2} \right|}{\xi^{2/3}(1+\xi)^2 (1 + x_{\lambda'}^2 f(\xi)^{-2})^4}, \tag{2.68}$$

where $f(\xi) \equiv \frac{1+\xi}{\sqrt{3(1-2\xi)}}$. Note that for generic values of ξ there appears to be no suppression on the probability of finding $x_{\lambda'} = 1$ in the truncated sector; in other words, $\rho^f_{\lambda'}(1) \neq 0$. This in turn shows that massless scalar modes on the truncated sector are *not suppressed*. This is a surprising result that is at odds with what would be expected from the analysis of generic random functions. This reflects the important role that symmetries of the EFT play in shaping the flux Landscape. In particular, this observation is of importance for the construction of dS vacua proposed in [153, 154], which relies on the existence of no-scale solutions with massless modes at tree-level.

A common feature to the three distributions (2.66), (2.67) and (2.68), is that they all vanish for $m_\lambda = 0$ (equivalently $x_\lambda = 0$). That is, the probability of finding no-scale solutions with massless fermions also appears to be suppressed in the ensemble of flux vacua. This result can be traced back to the structure of the fermion mass matrix $\mathscr{M}$ given in (2.7), whose eigenvalues come in pairs $\pm m_\lambda$, and the well known *eigenvalue repulsion* effect [176], which is characteristic of random matrix ensembles[11] (see [180] for a review).

[11] The collection of mass matrices $\mathscr{M}$ associated with the ensemble no-scale vacua can be regarded as an statistical ensemble of matrices with random entries [123, 134, 177–179].

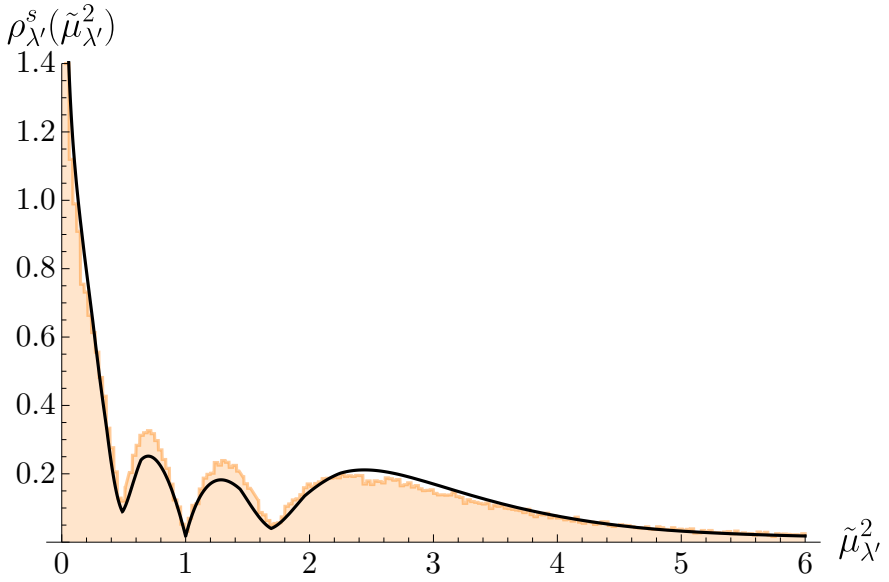

Figure 2.10: The theoretical prediction for the probability distribution of the normalised squared masses $\tilde{\mu}^2_{\lambda'} = \mu^2_{\lambda'}/m^2_{3/2}$ of the truncated scalar fields (solid line), eqs. (2.69) and (2.68). For comparison we also show in orange a histogram of scalar masses generated with (2.40).

With the above distributions for $m_\lambda/m_{3/2}$ at hand, the probability density functions for the scalar masses can be easily obtained with a simple change of variables. Indeed, for each λ the probability distribution for the combined two branches of scalar masses $\mu^2_{\pm\lambda}$ reads

$$\rho^s_\lambda(\tilde{\mu}^2_\lambda)d\tilde{\mu}^2_\lambda = \mathcal{N}\cdot\tilde{\mu}_\lambda^{-1}\left[\rho^f_\lambda(1+\tilde{\mu}_\lambda)+\rho^f_\lambda(|1-\tilde{\mu}_\lambda|)\right]d\tilde{\mu}^2_\lambda, \tag{2.69}$$

where $\tilde{\mu}^2_\lambda \equiv \mu^2_\lambda/m^2_{3/2}$. These theoretical distributions are plotted in figures 2.9 and 2.10, along with the scalar mass histograms obtained from the numerical scan. As described in section 2.5, the masses of the scalar modes in the sector surviving the truncation, $\mu^2_{\lambda=0,1}$ are obtained via the diagonalisation of the fermion mass matrix (2.10) at each vacuum together with the formula (2.9), while those associated to the truncated modes $\mu^2_{\lambda'}$ are computed from the formula (2.40). The plots show a remarkable agreement of the numerical results and analytical predictions in the regime where both the low energy EFT and the continuous flux approximation are expected to provide a good description of the theory.[12]

It is interesting to note that the spectra in the surviving sector of figure 2.9 show a suppressed probability of no-scale solutions with scalar masses[13] $\mu^2_\lambda/m^2_{3/2} = 0,1,4$. This is consistent with our discussion above, as the first and third cases correspond to vacua with one or more fermion masses equal to $m_{3/2}$ (see relation (2.9)), and the second case to vacua with massless fermions. Therefore, making contact with our discussion in section 2.4.3, we can see that the branches of solutions corresponding to $\theta_W = \{\theta^W_0, \theta^W_1\}$ have a low probability to

[12] The histograms in figs. 2.9 and 2.10 show slight deviations with respect to the theoretical distributions. As argued in [46], the discrepancies might be due to restricting the vacua to lie in a bounded region of moduli space, i.e., within the limits (2.53) and (2.63).

[13] Note that the $\mu^2_1/m^2_{3/2} = 0$ suppression is not evident in the main plot of figure 2.9(b). This is due to the factor $1/\tilde{\mu}_1$ in (2.69), which makes it difficult to resolve the suppression in the numerical histogram. The inset of this figure shows the histogram for $\tilde{\mu}_1$, which does present clearly the suppressed probability of the massless modes.

occur, since they are respectively the vacua where the masses μ_{-0} and μ_{-1} vanish.

By contrast, in the spectra for the truncated sector (figure 2.10) we see a suppression of vacua with masses $\mu_\lambda^2/m_{3/2}^2 = 1$ (i.e., with massless fermions), while the distribution function *diverges* in the limit $\mu_\lambda^2/m_{3/2}^2 \to 0$, that is, for the branch of solutions with $\theta_W = \theta_2^W$ discussed in section 2.4.3. In other words, for a large fraction of no-scale solutions, half of the scalar modes in the truncated sector have masses much lower than the gravitino. It is precisely these vacua which are in danger of developing tachyonic instabilities upon including quantum effects (α' corrections or instanton effects). In particular we observe that approximately 11% of the vacua contain modes with masses satisfying $\mu_{\lambda'}^2 \lesssim 10^{-2}\, m_{3/2}^2$, and about 3% with masses $\mu_{\lambda'}^2 \lesssim 10^{-3}\, m_{3/2}^2$. Moreover, a closer examination of the mass spectra in the ensemble reveals the presence of vacua with large mass hierarchies, with modes as light as $\mu_{\lambda'}^2 \sim 10^{-10}\, m_{3/2}^2$.

Note also that the suppressions seen in figure 2.10 around $\mu_{\lambda'}^2 \approx 0.5\, m_{3/2}^2$ and $\mu_{\lambda'}^2 \approx 1.7\, m_{3/2}^2$ are due to modes of the reduced theory becoming massless, i.e., the branches of vacua with $\theta_W = \{\theta_0^W, \theta_1^W\}$. Indeed, recall that due to the form of the spectrum (2.40) the mass distributions for all the modes arise from the same probability density function (2.65), and thus the suppression of any particular branch of vacua can also be observed in the statistics of all the other masses.

As a final remark, let us point out that equation (2.57) and (2.58) imply that the masses (2.40) and g_s are statistically independent from each other. As a consequence, although the ensemble discussed here involves vacua with a marginally small string coupling $g_s \leq 1$, the statistical properties of the spectrum would not be affected by restricting the analysis to vacua with very small string coupling $g_s \ll 1$. As a consistency check, we also computed the numerical histograms represented in figures 2.9 and 2.10 for the subset of vacua in our ensemble with $g_s \leq 0.1$ (~ 5000 vacua), but no significant changes where observed, and thus, we will not present them here.

2.6.3 *Statistical properties of the constrained ensemble*

We will now turn to the statistics of the constrained ensemble of vacua, where $N_A^0 = 0$. As we show in appendix C, the statistical methods in [46] can easily be adapted to describe this ensemble. In particular, the density of flux vacua with $N_A^0 = 0$ is found to be

$$d\mu_{\rm vac}(z,\tau)\big|_{N_A^0=0} = \mathcal{N}\cdot\frac{(1+\xi)\xi^{2/3}}{(2-\xi)^2(\mathrm{Im}\tau)^2}d^2z d^2\tau\,, \tag{2.70}$$

where ξ should be understood here as a function of $\mathrm{Re}z$. It is worth noting that, provided we consider only the weak coupling regime $\mathrm{Im}\tau > 1$, the density of no-scale vacua is normalisable within the whole moduli space, even near the conifold point $\xi \to \xi_{\rm cnf}$ where the EFT is known to become inaccurate. Indeed, contrary to the generic case, the density (2.70) is not enhanced (and remains finite) as we approach the conifold point, and as a result the distribution is well defined in the whole range of z (i.e., in $\xi \in [0, 1/2]$). Furthermore, as we show in appendix C, for this sub-ensemble, flux quantisation and a finite tadpole do not

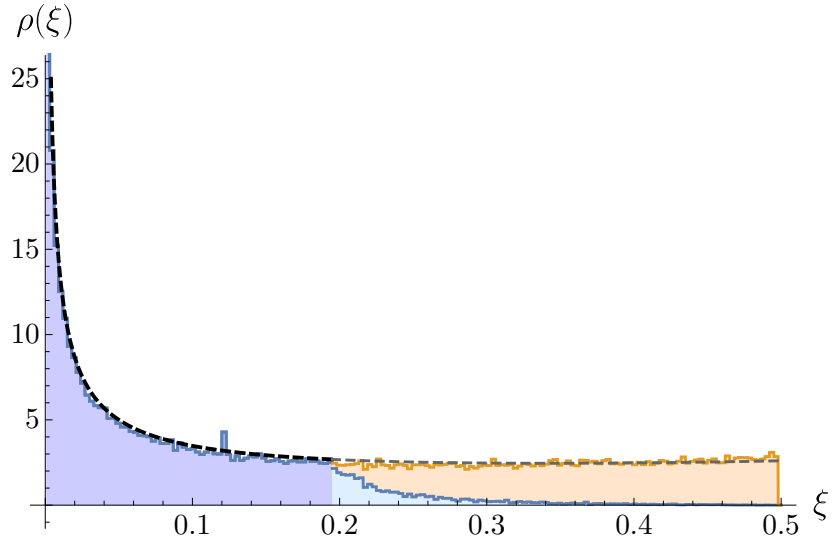

Figure 2.11: Distribution for the LCS parameter for the constrained flux ensemble. The dashed line represents the theoretical distribution (2.11) *normalized for data in the range* $5.10^{-5} \leq \xi \leq 0.185$ *(see footnote 14). We also show the histogram of* ξ *at no-scale vacua, with colours the same as in figure 2.7.*

lead to the breakdown of the statistical description near the LCS point.[14] As a consequence, in contrast with the case of generic no-scale solutions, the continuous flux approximation provides an excellent characterisation of the ensemble in the strict LCS regime. As we shall see next, these features of the model will lead to an almost perfect agreement between the statistical description and the results of the numerical scan in the octic model.

As in the previous section, we begin by computing the probability distribution for the LCS parameter ξ, which takes the simple form

$$\rho(\xi)d\xi = \frac{2^{1/3}(1+\xi)}{(2-\xi)^2\xi^{2/3}}d\xi\,. \tag{2.71}$$

This distribution, together with the histogram obtained from the numerical scan, is plotted in figure 2.11. As is evident, the analytic formula perfectly matches the histogram over the whole range of ξ. The histogram includes all of the no-scale solutions at points where the moduli space metric is well defined, $\xi \in [0, 1/2]$, however only those shaded in light and dark blue correspond to vacua with small instanton corrections. Excluding solutions with sizeable corrections (orange) leads to the fall-off (light blue) observed around $\xi \approx 0.2$. The statistical description does not incorporate the effects of truncating the ensemble, and therefore it can only provide a good description in the region of ξ where few vacua (or none) are excluded from the ensemble. This region of ξ, which we shaded in dark blue, represents the set of vacua we will use next to characterise the statistics of the mass spectra, both numerically and using the continuous flux approximation.

As a curiosity, it is worth mentioning the small enhancement[15] on the number of vacua

[14] This observation relies on the fact that when $N_A^0 = 0$, the flux N_B^0 is not bounded by the flux tadpole. However, in practice the flux integers are extracted from a uniform distribution in $[-50, 50]$, which results in deviations from the continuous flux approximation in the range $\xi \lesssim \xi_{\text{min}} = 5 \cdot 10^{-5}$.

[15] This spike in the histogram of ξ induces similar enhancements in the mass distributions displayed in figures 2.12 and 2.13, as they all depend on the former.

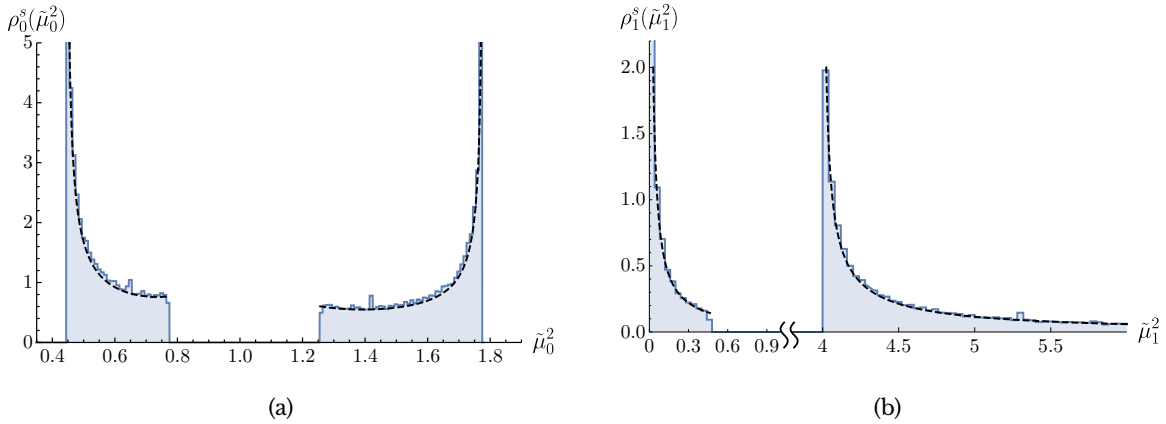

(a) (b)

Figure 2.12: Distribution for the squared scalar masses with constrained fluxes $N_A^0 = 0$ normalised by the gravitino mass $\tilde{\mu}_\lambda^2 = \mu_\lambda^2 / m_{3/2}^2$, with $\lambda = 0, 1$ in (a) and (b), respectively. The dashed lines correspond to the theoretical mass distributions of fields in the reduced theory, (2.69) evaluated with (2.72). We compare with the histograms obtained numerically from the flux ensemble of the $\mathbb{WP}^4_{[1,1,1,1,4]}$ model.

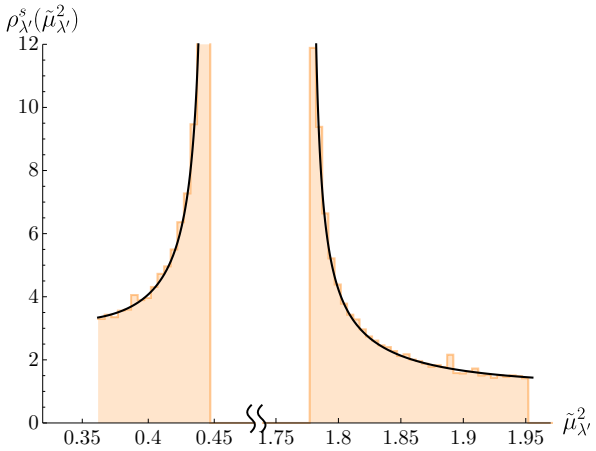

Figure 2.13: Theoretical prediction (solid line) for the probability distribution of the normalised squared masses of the truncated scalar fields $\tilde{\mu}_{\lambda'}^2 = \mu_{\lambda'}^2 / m_{3/2}^2$, eqs. (2.69) and (2.72), in the constrained ensemble. For comparison we display the histogram of values obtained by applying (2.40) to the vacua ensemble.

with $\xi \approx 0.12$. An examination of these solutions reveals that they all correspond to flux configurations satisfying the relation $N_A^1 = N_B^0$ and $\mathrm{Im} z = 0$. Although we have not made further inquiries regarding the origin of the enhancement, it seems plausible that this particular choice of fluxes leads to a new symmetry in the EFT (exact or approximate), which is known to produce accumulations of no-scale solutions at special points of the moduli space [98].

In complete analogy with the previous section, the density function (2.71) can be used to derive the distributions for the rescaled fermion masses $m_\lambda / m_{3/2}$. Performing a change of variables from ξ to each of the normalised masses, and using (2.64) with $\tan\theta_W = \sqrt{(1-2\xi)/3}$ (see section 2.4.4), we obtain

$$\rho_\lambda^f(x_\lambda)\, dx_\lambda = \frac{2^{1/3}(1+\xi)}{(2-\xi)^2 \xi^{2/3}\, (dx_\lambda(\xi)/d\xi)}\Big|_{\xi(x_\lambda)} dx_\lambda\,, \tag{2.72}$$

where we use the shorthand $x_\lambda = m_\lambda / m_{3/2}$ which was introduced above. The distributions for the squared scalar masses can then be found using (2.69), which are displayed along with the histograms derived from the numerical scan in figures 2.12 and 2.13. As in the case of the generic ensemble, the mass histograms of the scalar modes in the reduced theory, $\mu^2_{\pm 0}$ and $\mu^2_{\pm 1}$, have been obtained first by computing the eigenvalues of the fermion mass matrix (2.10), and then via (2.9). The histogram for the masses in the truncated modes $\mu^2_{\pm\lambda'}$ were found using (2.48) instead. Here again we can observe the excellent agreement between the analytical predictions and the direct numerical computation of the masses in the octic. It is important to mention that, as in the case of the generic ensemble described above, it can be checked that the string coupling g_s is statistically independent from the masses in (2.48). Thus, while the numerical histograms presented here correspond to an ensemble of marginally weakly coupled vacua $g_s \leq 1$, our conclusions remain valid also for very weakly coupled vacua with[16] $g_s \ll 1$.

The most important feature of these distributions is the divergence of the probability density for the masses $\mu^2_{\pm 1} \ll m^2_{3/2}$ (see figure 2.12(b)). This implies that in this ensemble the branch of solutions with $\theta_W = \theta^W_1$, defined in (2.42), occurs with relatively high frequency. This contrasts with the results obtained for the generic ensemble, where the same branch was shown to have a suppressed probability to appear.

Finally, for completeness we have also studied the dependence of the mass spectrum on the distance of vacua from the LCS point. For this purpose, we obtained the mass histograms for subsets of no-scale solutions restricted to be in neighbourhoods of the LCS point of varying sizes. The results are displayed in figure 2.14, where we have plotted the histograms for four sets of vacua with $\xi \leq \xi_{\text{max}}$, where $\xi_{\text{max}} = \{0.15, 0.1, 0.05, 0.01\}$. As it can be seen in the plots, the closer the solutions are to the LCS point, the more deterministic the mass distributions become. Note also that in the case $\xi \leq 0.01$ the spectrum is already very peaked at the values given in (2.49), which correspond to the strict limit $\xi \to 0$. Interestingly, in this regime the spectrum always contains a (nearly) massless field, $\mu^2_{-1} \approx 0$, which belongs to the reduced moduli space (i.e., $\theta_W \approx \theta^W_1$).

2.7 Conclusions

No-scale vacua of type IIB flux compactifications are an essential stepping stone in the construction of dS vacua and inflationary models in KKLT and Large Volume Scenarios. Guaranteeing the validity of these constructions requires a good understanding of the perturbative spectrum of the no-scale solutions. Indeed, while the no-scale property ensures the absence of tachyons in the axio-dilaton/complex structure sector at tree-level, this does not prevent the existence of arbitrarily light fields, which may turn tachyonic upon including quantum corrections, uplifting terms, or the effect of matter fields [179, 181]. These light modes might also lead to difficulties when implementing viable inflationary models in these scenarios, as the backreaction effects caused by the inflaton might also result in their destabilisation.

[16] We checked explicitly that this is indeed the case by computing the numerical mass histograms for the subset of solutions in the constrained ensemble with $g_s \leq 0.1$ (~ 2500 vacua).

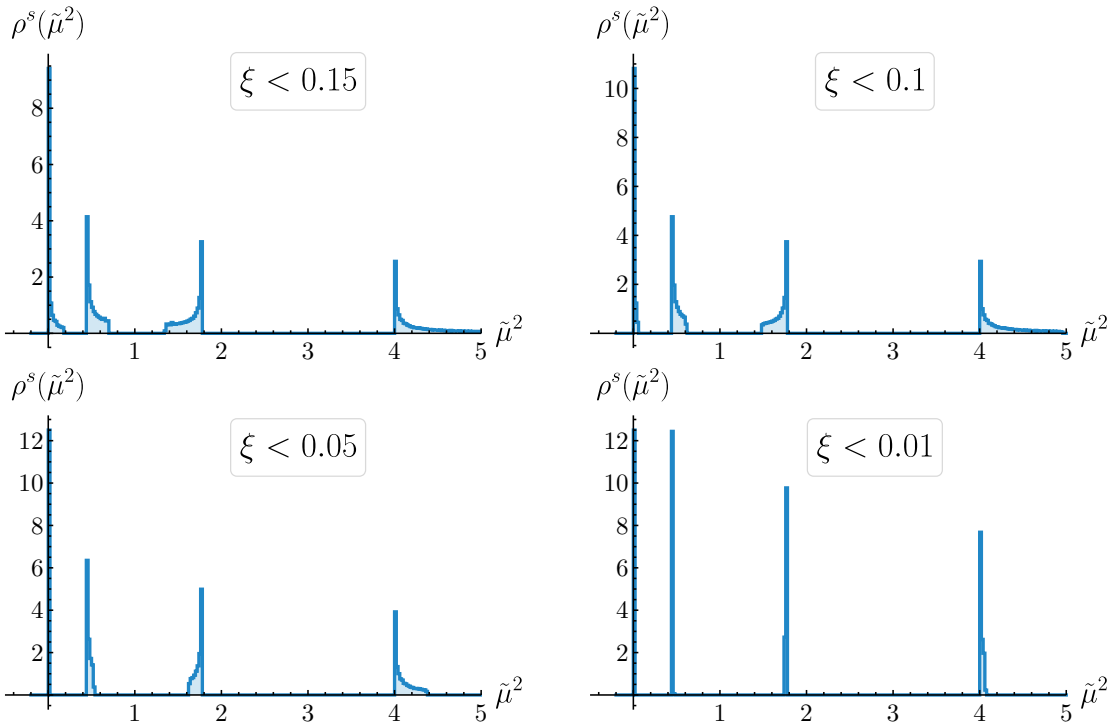

Figure 2.14: Histograms for the normalized squared masses $\tilde{\mu}^2_{\lambda=0,1} = \mu^2_{\lambda=0,1}/m^2_{3/2}$ of the scalars in the reduced theory. The plots represent vacua in the constrained ensemble, with varying upper bounds on the LCS parameter ξ. Note that as the upper bound on ξ decreases the distributions become increasingly deterministic, peaking at the limiting $\xi \to 0$ values given in (2.49). The plots also show the presence of a light mode $\mu_{-1} \ll m_{3/2}$ in all vacua, whose mass becomes zero $\mu_{-1} \to 0$ in the limit $\xi \to 0$.

Despite its importance, a complete analytic understanding of the perturbative spectrum at no-scale vacua has remained elusive, primarily due to the complexity of the corresponding EFTs and the large number of fields involved. In this chapter we have considered a particular class of Calabi-Yau compactifications with an arbitrary number of moduli fields, and computed *analytically* the complete mass spectrum of the axio-dilaton/complex-structure sector at no-scale vacua in the LCS regime (see (2.40)). The Calabi-Yau geometries we considered here are invariant under large discrete isometry groups, which allows for a consistent reduction of the complex structure sector to a single field. An important feature of this class of models is that the Calabi-Yau symmetries make the computation of an EFT for the unique complex structure modulus surviving the truncation feasible [21, 119, 124, 133]. Then, using only symmetry arguments, together with certain universal properties satisfied by the EFT couplings at LCS, we derived the mass spectrum of the full axio-dilaton/complex structure sector, including the truncated fields. Remarkably, the full spectrum can be expressed solely in terms of the couplings of the reduced EFT theory, which can be determined. This result applies to plenty of interesting compactifications such as: the family of quintic hypersurfaces in $\mathbb{WP}_{[1,1,1,1,1]}$ [119] admitting the discrete symmetry groups discussed in [125]; the close relatives to the quintic (i.e., the sextic, octic and dectic) with analogous symmetric configurations [124, 133]; and many more, see [94] and references therein. Moreover, we can also use these results to describe the LCS regime of the hundreds of one-parameter models listed in [128]. We should remark that these discrete global symmetries are nevertheless

expected to be broken upon including all sub-leading α' and quantum effects [53,182,183], what will induce small corrections in the spectrum (2.40), lifting, in particular, the large degeneracy of the truncated sector.

In the class of models that we consider here, the strict LCS/weak-coupling limit is of particular interest, as it is the region of moduli space where one has the best perturbative control of the EFT. However, as shown in [145,155], generic flux configurations will not yield any vacua in this region of the moduli space. These conclusions can nevertheless be avoided by setting to zero the flux associated with the period which grows without bound in this limit ($N_A^0 \equiv f_A^0 - \tau h_A^0 = 0$ in (1.35)). Indeed, in this case the higher order terms in the flux superpotential are identically zero, and thus the above no-go theorem does not apply. In section 2.4.4 we computed the mass spectrum at this class of no-scale vacua for the models described above, and proved it to have a universal form in the strict LCS limit. In particular it can be observed that the spectrum always contains exactly one massless field, while the rest of the moduli have masses of the order of the gravitino mass $m_{3/2}$. It is also worth mentioning that closely related classes of vacua surviving in the strict LCS limit were also discussed in [184,185], and in particular those of [152] also present a massless field in the no-scale spectrum, which is nevertheless lifted by instanton corrections.

The previous results are consistent with [186,187], where it was argued that obtaining vacua parametrically close to the LCS point requires turning on *unbounded fluxes*, that is, fluxes not contributing to the total $D3$-charge and therefore unconstrained by the tadpole condition. Furthermore, as discussed in [187], the contribution to the flux potential due to the unbounded fluxes must also be asymptotically vanishing in the strict LCS limit. Interestingly, the class of no-scale solutions (and thus Minkowski vacua) described above satisfies both of these conditions, and is therefore consistent with the no-go theorems derived in [187] (see section 2.4.4). On the one hand, setting to zero the flux $N_A^0 \equiv f_A^0 - \tau h_A^0$ on the diverging period implies that the flux on the dual B-cycle, i.e., $N_0^B \equiv f_0^B - \tau h_0^B$, does not contribute to the tadpole. On the other hand, as the term in the flux superpotential associated to N_0^B is just a constant, it also follows that its contribution to the no-scale potential is asymptotically vanishing at the LCS point. Note that the analyses in [186,187] only refer to the strict LCS limit, while the results presented here also allow one to characterise the properties of the no-scale potential away from the LCS point, i.e., over a region of moduli space not captured in those works.

For generic flux vacua, not necessarily close to the LCS point, the mass spectrum will not have the deterministic form of (2.49), and thus will in general be dependent on the choice of fluxes. Therefore, in order to obtain a characterisation of the spectrum independent of the choice of flux we have studied the statistical properties of the moduli masses in the ensemble of flux vacua. More specifically, using the continuous flux approximation, we computed analytically the probability distributions for the density of vacua and the masses, both for the generic ensemble of vacua and for the constrained ensemble with vanishing flux N_A^0. Moreover, we verified the validity of the obtained distributions by comparing them with the result of a numerical scan on the octic model $\mathbb{WP}^4_{[1,1,1,4]}$. As can be seen in figures 2.7–2.13, the analytical and empirical distributions show an excellent agreement in the expected regime of applicability of the continuous flux approximation.

Regarding the density of vacua, for the generic ensemble the result of the numerical

scan in the octic model shows a suppression on the density of vacua close to the LCS point with respect to the statistical predictions (see figure 2.8). This discrepancy with the theoretical distributions was nevertheless already anticipated in [145, 155] (see also [46]), due to a breakdown of the continuous flux approximation. In the generic ensemble, vacua with $N_A^0 = 0$ represent only 0.08% of total vacua and, as we mentioned above, the results of [145, 155] show that only vacua with vanishing flux N_A^0 may be found parametrically close to the LCS point. By contrast, as can be seen in figure 2.11, the constrained ensemble exhibits no suppression near the LCS point, indicating that this subclass of solutions will dominate in this region of the moduli space.

Concerning the statistics of vacua in the constrained ensemble, our results show that the mass spectra change significantly due to the condition imposed on the fluxes. In particular, contrary to the generic ensemble, in this class of vacua the lightest field is always in the reduced moduli space (see figure 2.12). In order to understand the dependence of the spectra on the distance to the LCS point, we considered subsets of vacua constrained to be in neighbourhoods of this point with varying sizes. This analysis showed that the smaller the neighbourhood around the LCS point, the more deterministic the mass spectrum becomes, recovering the limiting form (2.49) in the strict LCS limit. In other words, for the dominant class of vacua near the LCS point, the spectrum was always observed to contain a very light (and asymptotically massless) field in the reduced moduli space (see figure 2.14).

Chapter 3

A universal mass spectrum for any compactification around the LCS point

After our in-depth study of effectively one-parameter models in chapter 2, we are now ready to generalize our results to more general models in the Large Complex Structure regime. More concretely, we will find that a particular choice of fluxes, along with an ansatz for the complex structure moduli allows us, to leading order in α' and g_s, to compute the complete scalar mass spectrum independently of the choice of Calabi-Yau. This will be given by the scalar mass formula obtained above for one-parameter models (c.f. (2.48)), and thus our study of this spectrum in chapter 2 will apply to this case as well. We will check our results by constructing an ensemble of thousands of solutions for the Calabi-Yau hypersurface $\mathbb{WP}^4_{[1,1,1,6,9]}$, where the masses of the axio-dilaton and the 272 complex structure fields can be explicitly computed.

This chapter is based on [188].

3.1 Introduction

The main goal of this chapter is to expand our previous discussion on the stabilization of the complex structure and axiodilaton sector to more general geometries. Our previous analysis was carried out for compactifications on the orientifold of Calabi-Yau manifolds which allow the consistent truncation of all the complex structure fields except one. This study assumed a Calabi-Yau geometry admitting a large discrete isometry group which, provided the flux configuration is also invariant under these symmetries, allows the effective reduction of the complex structure sector. In this setting it was shown that *the complete mass spectrum* of the axio-dilaton and complex structure sector (including the truncated fields) can be explicitly computed in the Large Complex Structure (LCS)/weak string coupling regime. For the class of vacua which can be found parametrically close to the LCS point and up to exponentially small corrections, the scalar moduli masses was found to be the one in equation (2.48).

In the present chapter we will prove that, in the LCS regime and provided the fluxes

are conveniently constrained, the EFT of *generic Calabi-Yau compactifications* always admits a consistent truncation of all complex structure fields but one. Here, in contrast with the previous chapter, we do not require the presence of a discrete isometry group, and our results rely instead on the existence of monodromy transformations around the LCS point. That is, we will require only the invariance of the EFT under discrete shifts of the complex structure fields z^i

$$z^i \to z^i - \mathrm{i} v^i, \qquad v^i \in \mathbb{Z}^{h^{2,1}}, \tag{3.1}$$

combined with an appropriate transformation of the fluxes of the form fields. This invariance is a common feature of all Calabi-Yau compactifications in the LCS regime. Moreover, the choice of field surviving the truncation is highly non-unique, with each possibility associated to a different monodromy direction v^i. This simple, and yet powerful, observation allows us to extend our previous results to generic Calabi-Yau compactifications and, as a consequence, opens the door to generating a large landscape of vacua with an unprecedented analytic control over the mass spectrum of the axio-dilaton and complex structure moduli.

This chapter is organized as follows. In section 3.2, we will work out an ansatz for the fluxes and the moduli in order to yield any compactification in the LCS regime effectively one-dimensional, so its mass spectrum is given by (2.48). In section 3.3 we will apply and verify our results in a particular model, namely the $\mathbb{WP}^4_{[1,1,1,6,9]}$ hypersurface, all the while detailing the vacuum scanning process. Finally, we end up with some comments and conclusions in section 3.4.

3.2 A universal mass spectrum at Large Complex Structure

3.2.1 Effective Field Theory and monodromies

In this chapter we will once again consider the regime of the Large Complex Structure (LCS), described by the prepotential

$$\mathscr{F} = \frac{\mathrm{i}}{3!}\kappa_{ijk} z^i z^j z^k + \frac{1}{2}\kappa_{ij} z^i z^j + \mathrm{i}\,\kappa_i z^i + \frac{1}{2}\kappa_0. \tag{3.2}$$

The terms κ_{ijk}, κ_{ij} and κ_i are numerical constants which can be computed from the topological data of the mirror manifold to M_3 (see [120]). In particular, it will be important to note that the quantities κ_{ijk} are integers, and the coefficients κ_{ij} and κ_i are rational. As we did above, at the level of the analytical calculation we will neglect the instanton corrections that the prepotential receives, though they will be considered in the numerical results.

The present description of the EFT has an inherent redundancy associated to the choice of homology basis. More specifically, a change of basis induces a transformation of the period and flux vectors,

$$\Pi \to S\cdot\Pi, \qquad N \to S\cdot N, \tag{3.3}$$

with $S \in \mathrm{Sp}(2h^{2,1}_- + 2, \mathbb{Z})$, leading to different descriptions of the same theory. Finally, the

requirement that the period vector transforms by symplectic transformations under the monodromies (3.1) leads to the following condition on the couplings [139,189]

$$\kappa_{ij}v^j + \frac{1}{2}\kappa_{ijk}v^j v^k \in \mathbb{Z}. \tag{3.4}$$

3.2.2 *Consistent supersymmetric truncation to one-parameter models*

As we mentioned in the introduction, we will be interested in generalizing the mass spectrum (2.48) to models with an arbitrary number of complex structure, without relying on any symmetry group underlying in the solution. From our discussion in chapter 2, this spectrum relies on two assumptions:

- First and foremost, the matrix Z_{AB} satisfies

  $$Z_{0a} = \delta_{a1} Z_{01}. \tag{3.5}$$

  This was trivial in the cases studied in the previous chapter (as the index a could only take a single value). However, in more general compactifications, this property does not necessarily hold when more than 1 complex structure modulus is present and we will need to impose it on our solutions. Vacua satisfying (3.5) will be referred to as *no-scale aligned vacua*, due to the $a = 1$ direction being parallel to K_a (c.f. equation (2.31)).

- The fluxes are required to satisfy $N^0_A = 0$. From our analysis in the previous chapter, we know this choice of fluxes allows for vacua extremely close to the LCS point (where we have complete parametric control over the corrections to the prepotential).

In order to see how (3.5) can be enforced, let us first describe the superpotential and its covariant derivatives in full detail. Plugging the prepotential (3.2) into the period vector, we can easily obtain the Gukov-Vafa-Witten superpotential, the Kähler potential and the covariant derivatives, as explained in chapter 1. Imposing $N^0_A = 0$ and the no-scale vacuum conditions, we find

$$W = \frac{1}{2}\kappa_{ijk}N^i_A z^j z^k - \mathrm{i}\left(\kappa_{ij}N^j_A + N^B_i\right) z^i - N^B_0 + \kappa_i N^i_A \tag{3.6}$$

$$D_0 W = -\frac{\mathrm{i}}{2}\kappa_{ijk}\overline{N}^i_A z^j z^k - \left(\kappa_{ij}\overline{N}^j_A + \overline{N}^B_i\right) z^i + \mathrm{i}\overline{N}^B_0 - \mathrm{i}\kappa_i \overline{N}^i_A = 0 \tag{3.7}$$

$$D_i W = \kappa_{ijk}N^j_A z^k - \mathrm{i}\left(\kappa_{ij}N^j_A + N^B_i\right) + K_i W = 0 \tag{3.8}$$

$$D_0 D_i W = -\mathrm{i}\kappa_{ijk}\overline{N}^j_A z^k - \left(\kappa_{ij}\overline{N}^j_A + \overline{N}^B_i\right) \tag{3.9}$$

where we have used the frame vector $e^0_\tau = \mathrm{i}(\tau - \bar{\tau})$ and the direction i is not canonically normalised. Note that (3.5) is tantamount to imposing $D_0 D_i W$ is parallel to K_i, by virtue of the definition of the no-scale direction.

Using (3.8), we can rewrite (3.9) as

$$D_0 D_i W = -2\mathrm{i}\kappa_{ijk}\overline{N}^j_A \mathrm{Re}(z^k) - \mathrm{i}K_i \overline{W}. \tag{3.10}$$

Using the canonically normalised basis (2.26), this reads

$$D_0 D_a W = -\mathrm{i}\kappa_{ab1}\overline{N}^b_A x - iK_a \overline{W}. \tag{3.11}$$

Now, since $K_a \propto \delta^1_a$ (c.f. (2.31)) and applying the properties of the normalised Yukawa couplings (2.29), we find that satisfying (3.5) requires $N^{a'}_A = 0$ (where $a' = 2,\dots,h^{2,1}$ runs over the canonically normalised directions). This implies that, in non-canonical coordinates, N^i_A must be parallel to the no-scale direction, which in turn is given by $\mathrm{Re}(z^i)$. In other words,

$$N^i_A = v^i \hat{N}_A, \qquad \mathrm{Re}(z^i) = r\, v^i \tag{3.12}$$

where $r \in \mathbb{R}$ and $\hat{N}_A \equiv \hat{f}_A - \tau \hat{h}_A$, with $\hat{f}_A, \hat{h}_A \in \mathbb{Z}$. Furthermore, flux quantization imposes v^i to have integer (and coprime) components.

This last result suggests the ansatz

$$z^i = \hat{z} v^i, \qquad \hat{z} \in \mathbb{C}, \tag{3.13}$$

for no-scale aligned equations. Indeed, note that the first term in (3.9) is then parallel to K_i, since

$$\kappa_{ijk}\overline{N}^j_A z^k \propto \kappa_{ijk} v^j v^k \propto \kappa_{i11} = e^a_i \kappa_{a11} = e^{-K_{cs}}\, e^a_i\, \mathring{\kappa}_{a11} \propto K_i, \tag{3.14}$$

where, in the last step, we have used (2.31). In order to render the second term in (3.9) parallel to K_i as well, we will impose the following condition on the fluxes:

$$N^B_i = q\kappa_{ijk} v^j v^k \hat{N}^B - \left(\kappa_{ij} + \frac{1}{2}\kappa_{ijk} v^k\right) N^j_A \tag{3.15}$$

where $q^{-1} \equiv \gcd(\kappa_{ijk} v^j v^k)$ and $\hat{N}^B \equiv \hat{f}^B - \tau \hat{h}^B$, with $\hat{f}^B, \hat{h}^B \in \mathbb{Z}$. Note that flux quantization is automatically satisfied in this ansatz by virtue of κ_{ijk} being integers and the constraint (3.4). With this choice of flux, we find

$$\kappa_{ij} N^j_A + N^B_i = \kappa_{ijk} v^j v^k \left(q\hat{N}^B - \frac{1}{2}\hat{N}_A\right) \tag{3.16}$$

which is parallel to K_i, as shown in (3.14).

With all of these results in mind, let us collect them into the main result of this chapter:

Let us consider a $h^{2,1}$-dimensional vector v^i of coprime integers, which lies in the Kähler cone of the mirror Calabi-Yau. Then, the ansatz $z^i = \hat{z} v^i$ with $\hat{z} \in \mathbb{C}$ defines a consistent supersymmetric truncation of the EFT (3.2), when the flux configuration is of the form

$$N^0_A = 0, \qquad N^i_A = v^i \hat{N}_A, \qquad N^B_i = q\kappa_{ijk} v^j v^k \hat{N}^B - \left(\kappa_{ij} + \frac{1}{2}\kappa_{ijk} v^k\right) N^j_A, \tag{3.17}$$

and N_0^B arbitrary. Here $\hat{N}_A \equiv \hat{f}_A - \tau \hat{h}_A$, $\hat{N}^B \equiv \hat{f}^B - \tau \hat{h}^B$ with $\{\hat{f}_A, \hat{h}_A, \hat{f}^B, \hat{h}^B\} \in \mathbb{Z}$ and $q^{-1} \equiv gcd(\kappa_{ijk} v^j v^k)$. *Proof.* First, note that the constraint (3.4) ensures that the vectors f and h defined in (1.33) have integer components, as required by the flux quantization condition. To prove that the ansatz $z^i = \hat{z} v^i$ with $\hat{z} \in \mathbb{C}$ defines a consistent supersymmetric truncation of the EFT with the fluxes (3.17), we need to check that the F-flatness condition, $w^i(\partial_{z^i} + \partial_{z^i} K) W|_{\hat{z} v^i} = 0$, is satisfied along all directions w^i orthogonal to the reduced field space defined by the truncation ansatz, i.e., orthogonal to v^i, regardless of the value of $\hat{z}$ and τ [122, 123, 138, 190]. Substituting the flux configuration (3.17) into (3.8) we find that the F-flatness condition reads

$$\kappa_{ijk} w^i v^j v^k \left[\left(\hat{z} + \frac{\mathrm{i}}{2} \right) \hat{N}_A - \mathrm{i} q \hat{N}^B \right] + w^i \left[\partial_{z^i} K W \right]_{\hat{z} v^i} = 0. \tag{3.18}$$

Actually the two terms in this expression vanish independently, as they are both proportional to $\kappa_{ijk} w^i \mathrm{Re}(z^j) \mathrm{Re}(z^k) \propto \kappa_{i11} w^i = 0$, where we have noted that w^i is orthogonal to the no-scale direction (c.f. equation (2.29)) in the last step. ■

In the language of the canonically normalised basis, the above statements amount to showing that $D_{a'} W = 0|_{z^i = \hat{z} v^i}$. Indeed, as we showed above, the ansatze $z^i = \hat{z} v^i$ along with (3.17) yield all the terms in (3.8) parallel to K_i. Therefore, since $K_i = e_i^a K_a$ and $K_a \propto \delta_a^1$ (c.f. (2.31)), we will automatically satisfy $D_{a'} W = 0$.

The previous result guarantees that the ansatz $z^i = \hat{z} v^i$ can be consistently substituted into the action, obtaining a reduced theory with an effectively 1-dimensional complex structure moduli space parametrised by $\hat{z}$. The couplings of the reduced action are still characterised by the Kähler potential and superpotential which arise from (3.2), but they me also be obtained from an effective prepotential given by

$$\hat{\mathscr{F}} \equiv \frac{\mathrm{i}}{3!} \kappa_{vvv} \hat{z}^3 + \frac{1}{2!} \kappa_{vv} \hat{z}^2 + \mathrm{i}\, \kappa_v \hat{z} + \frac{1}{2} \kappa_0 \tag{3.19}$$

and an effective 4-dimensional flux vector

$$\hat{N} \equiv \left(0, \hat{N}_A, N_0^B, q \kappa_{vvv} \hat{N}_B\right)^T, \tag{3.20}$$

where we introduced the shorthands $\kappa_{vvv} \equiv \kappa_{ijk} v^i v^j v^k$ and $\kappa_v \equiv \kappa_i v^i$. Any solution of this reduced theory is also a solution of the full action in the LCS regime and to leading order in α' and g_s. Furthermore, if the fields surviving the truncation satisfy the F-flatness conditions

$$D_\tau W = \partial_\tau W + K_\tau W = 0, \qquad D_{z^i} W = \partial_{z^i} W + K_{z^i} W = 0 \tag{3.21}$$

the axio-dilaton/complex structure sector of the complete theory will satisfy them as well (c.f. subsection 2.3.2 and [123, 191]).

Therefore, given an EFT for some Calabi-Yau compactification, we can immediately generate large families of flux vacua in the LCS regime (one family for each choice of v^i) where we can compute the mass spectrum of the complete axio-dilaton/complex structure sector. Indeed, we just need solve the F-flatness conditions (3.21) for the reduced model

defined by (3.19) and (3.20). Then, the mass spectrum at the resulting vacua can be obtained using the results in chapter 2, which apply whenever the complex structure sector can be consistently truncated to a single field. More specifically, the formula (2.48) gives the squared masses of all the $2h^{2,1}+2$ scalar modes in the axio-dilaton/complex structure sector, including the truncated ones, in terms of a single parameter $\xi \equiv \frac{-3\text{Im}\kappa_0}{2\kappa_{vvv}\text{Im}(\hat{z})^3}$, and normalised by the gravitino mass,

$$m_{3/2}^2 \equiv e^K |W|^2 = \frac{3}{\pi}\frac{N_{\text{flux}}}{(2-\xi)\mathcal{V}^2}, \tag{3.22}$$

where $Q_{D3} \equiv h^T \cdot \Sigma \cdot f \geq 1$ is the flux induced $D3-$charge. In equation (2.48), the masses with $\lambda = 0,1$ are those associated to the fields surviving the truncation, $\{\tau, \hat{z}\}$, while those with $\lambda = 2,\ldots,h^{2,1}$ are the masses of the remaining fields in the truncated sector. It is also worth mentioning that solutions to (3.21) with $N_A^0 = 0$ are of particular interest, as they are the dominant class of vacua near the LCS point, as we showed in chapter 2, which is where we have the best perturbative control of the EFT.

3.3 Example: the hypersurface $\mathbb{WP}^4_{[1,1,1,6,9]}$

We will now illustrate our results by constructing an ensemble of the class of vacua presented above. For this purpose we will consider the compactification of type IIB string theory in an orientifold of the Calabi-Yau hypersurface $\mathbb{WP}^4_{[1,1,1,6,9]}$, which has $h^{1,1}=2$ Kähler moduli and and $h^{2,1}=272$ complex structure fields. For geometries admitting a $\mathcal{G}=\mathbb{Z}_{18}\times\mathbb{Z}_6$ isometry group, and provided only $\mathcal{G}$-invariant fluxes are turned on, the complex structure sector can be consistently truncated, leaving only two surviving complex structure fields which also transform trivially under $\mathcal{G}$. In the LCS regime, the couplings for the two $\mathcal{G}$-invariant complex structure fields are determined by a prepotential with coefficients [141]

$$\kappa_{111}=9,\quad \kappa_{112}=3,\quad \kappa_{122}=1,\quad \kappa_{11}=-\frac{9}{2},\quad \kappa_{22}=0,\quad \kappa_{12}=-\frac{3}{2},\quad \kappa_1=\frac{17}{4},\quad \kappa_2=\frac{3}{2} \tag{3.23}$$

and $\kappa_0 = -540\zeta(3)/(2\pi\text{i})^3$. Recall that the presence of the group $\mathcal{G}$ is not necessary for our results to apply, however such isometries are often required to make the computation of the EFT couplings tractable (see [101]). On the other hand, in order to relax the tadpole constraint on the fluxes, we considered the setting adopted in [45], where the type IIB compactification on $\mathbb{WP}^4_{[1,1,1,6,9]}$ was regarded as the orientifold limit of F-theory on an elliptically fibered Calabi-Yau fourfold, M_4. In the F-theory framework, the maximum allowed $D3$ charge induced by the fluxes is determined by the Euler number of the fourfold, leading in the present case to[1] $Q_{D3} \leq \chi(M_4)/24 = 273$ [45].

[1]The caveat on this approach is that it introduces additional $D7$-brane moduli fields. For simplicity, here we will ignore those additional moduli, and we refer the reader to [158–162,192,193] for discussions on their stabilisation.

3.3.1 *Vacua scan*

The procedure described in the previous section allows us to further reduce the complex structure sector to a single field. Consider for definiteness the truncation ansatz defined by the monodromy direction $v^i = (1,1)$. The resulting effective prepotential (3.19) is given by the couplings $\kappa_{vvv} = 21$ and $\kappa_v = \frac{23}{4}$.

In order to construct the vacua ensemble, we first generated 10^7 tuples $\{f_0^B, h_0^B, \hat{f}_{A,B}, \hat{h}_{A,B}\}$ with entries in the interval $[-25,25]$ satisfying the tadpole constraint. For each of these, we numerically solved the F-flatness conditions (3.21) of the reduced model given by (3.19) and (3.20), employing the software `Paramotopy` (see [163–165] and Appendix B.1). The resulting set of 37,156 solutions is displayed in figure 3.1 (blue dots), which shows the distribution of vacua on a fundamental domain of $\{\tau, \hat{z}\}$. This ensemble includes only solutions at the weak string coupling/LCS regime, i.e., where $g_s = (\mathrm{Im}\tau)^{-1} < 1$ and with small instanton corrections to the prepotential (using similar criteria as in the previous chapter).

As we detailed before, the truncation ansatz $z^i = \hat{z}v^i$ together with (3.17) allows us to lift each of these solutions to a vacuum of the complete $\mathbb{WP}^4_{[1,1,1,6,9]}$ model. After the lift, we computed the scalar mass spectrum at each vacuum for the axio-dilaton and the $\mathcal{G}$-invariant z^i modes ($\lambda = 0,1,2$) by direct diagonalisation of the Hessian of the flux potential of the $\mathbb{WP}^4_{[1,1,1,6,9]}$ model. The result perfectly matched the formula (2.48) in all cases. It is important to emphasise that, at each of the obtained solutions, equation (2.48) also gives the masses of the 270 truncated complex fields which transform non-trivially under $\mathcal{G}$, i.e., the modes with $\lambda = 3,\ldots,272$. This is a remarkable result, given that we only used the EFT couplings for the $\mathcal{G}$-invariant moduli computed in [141].

In order to have a sufficiently large sample of vacua to perform a statistical analysis we considered the effective reduction of the complex structure sector along the monodromy directions $v^i = \{(1,1),(1,2),(1,3)\}$, and we combined in a single ensemble the solutions to the F-flatness conditions (3.21) found for each of the three cases. Other families could also have been considered; however, the study of any of them is very computationally demanding and, due to the universal features of these vacua, we do not expect to gain any new information from studying a different family.

The resulting ensemble contains 206,479 vacua in the weak string-coupling regime, i.e., with $(\mathrm{Im}\tau)^{-1} = g_s < 1$, out of which 95,626 are in the LCS regime. Here we defined the LCS regime by the condition that the leading instanton contributions to the prepotential (3.2), given by (see [141])

$$\mathcal{F}_{\text{inst}} = -\frac{135}{2\pi^3}\mathrm{i}e^{-2\pi z^1} - \frac{3}{8\pi^3}\mathrm{i}e^{-2\pi z^2} + \ldots, \tag{3.24}$$

induce small relative corrections ($< 5\%$) to the moduli space geometry (i.e., to the field space metric and the canonically normalised couplings κ_{ijk}) and to the gravitino mass $m_{3/2}$. It is important to mention that our definition of the LCS regime is more restrictive than just requiring $\mathcal{F}_{\text{inst}}$ to be small (in absolute value) with respect to the perturbative part of the prepotential (3.2) (see, e.g., [166]). Indeed, the moduli space metric becomes degenerate far from the LCS point ($\xi \to -1$ for $\chi(M_3) > 0$ and $\xi \to 1/2$ for $\chi(M_3) < 0$) and thus, in that regime, the metric eigenvalues are small and very sensitive to the instanton corrections,

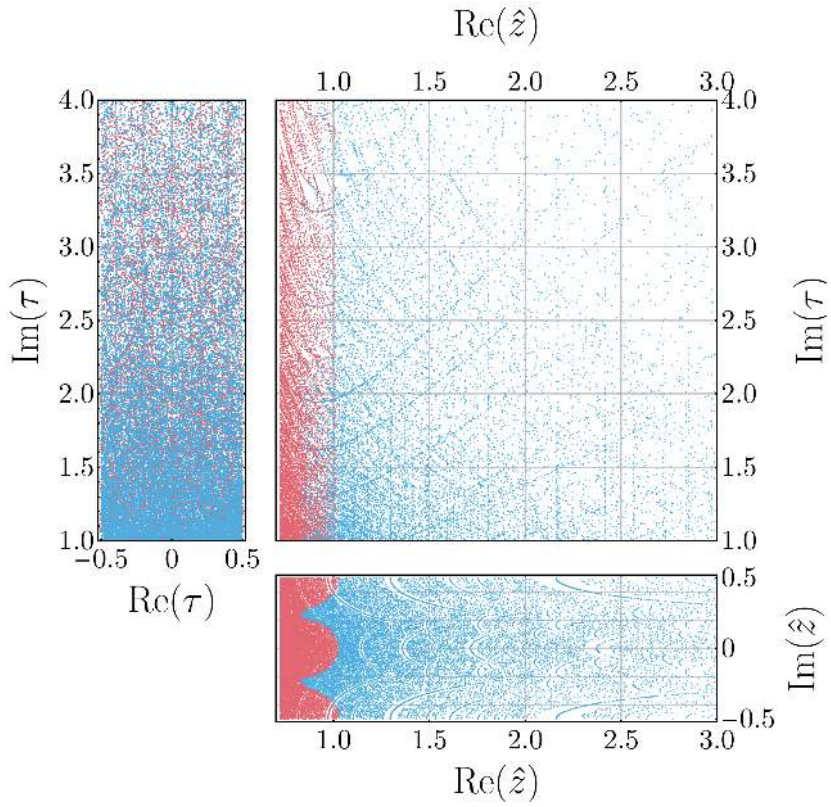

Figure 3.1: Numerically generated distribution of flux vacua on the fundamental domain of the reduced field space, with Re$\tau \in [-1/2, 1/2)$, Im$\tau > 1$ and Re$\hat{z} \in [-1/2, 1/2)$, for the $\mathbb{WP}^4_{[1,1,1,6,9]}$ model. The plot represents a total of 69,567 vacua obtained by reducing the EFT along the monodromy direction $v^i = (1, 1)$. We indicated in red vacua with large (> 5%) instanton corrections to the Kähler metric and $m_{3/2}$, and in blue (37,156 solutions) those with corrections < 5%.

even for small ratios $|\mathscr{F}_{\text{inst}}/\mathscr{F}| \sim 0.01$.

The method used here for avoiding duplicities in the counting of vacua is essentially the same as the one used in chapter 2 (see also [98]). However, the case at hand requires certain specific considerations related to the truncation of the moduli space so, for completeness, we will briefly summarise this method in the next section.

3.3.2 *Redundancies and solution duplicates*

The description of the EFT presented above has two inherent redundancies, namely those associated to the choice of holonomy basis (3.3), and the well known SL$(2, \mathbb{Z})$ modular transformations acting on τ. Those vacua which can be related to each other by these gauge transformations should be regarded as physically equivalent, and thus when constructing the ensemble one must ensure that each distinct solution is only counted once.

Regarding the choice of holonomy basis, the coefficients κ_{ij}, κ_i and κ_0 are only defined modulo integers, with different representatives associated to different choices of this basis. Therefore, by selecting a particular expression for the prepotential the symplectic gauge is partially fixed, with the residual gauge given by the monodromy transformations around the LCS point, i.e., $z^i \to z^i - \mathrm{i}\,\delta^i_p$ with $p \in 1, \ldots, h^{2,1}$. As a result of imposing the truncation ansatz $z^i = \hat{z} v^i$, the gauge freedom is further reduced, leaving as the only source of gauge

redundancy the monodromy transformations $z^i \to z^i - \mathrm{i}v^i$, which amounts to the shift

$$\hat{z} \to \hat{z} - \mathrm{i} \tag{3.25}$$

on the field surviving the truncation. The corresponding symplectic transformation $\mathscr{S}_{(v)} \in \mathrm{Sp}(2h^{2,1}+2,\mathbb{Z})$, acts on the period vector as (see [139])

$$\Pi(z^i - \mathrm{i}v^i) = \mathscr{S}_{(v)} \cdot \Pi(z^i), \quad \text{with} \quad \mathscr{S}_{(v)} \equiv \begin{pmatrix} A & 0 \\ B & \left(A^T\right)^{-1} \end{pmatrix}. \tag{3.26}$$

The matrices A and B are given by

$$A = \begin{pmatrix} 1 & 0 \\ v^i & \mathbb{1} \end{pmatrix}, \quad B = \begin{pmatrix} 2\kappa_v + \frac{1}{6}\kappa_{vvv} & -\kappa_{jv} + \frac{1}{2}\kappa_{jvv} \\ -\kappa_{iv} - \frac{1}{2}\kappa_{ivv} & -\kappa_{ijv} \end{pmatrix}. \tag{3.27}$$

Note that the condition (3.4) is necessary for $\mathscr{S}_{(v)}$ to have integer entries, which also requires the additional constraint $2\kappa_v + \frac{1}{6}\kappa_{vvv} \in \mathbb{Z}$ [189].

Finally, to obtain the action of the residual monodromy transformation (3.26) on the fluxes of the reduced theory, we just need to impose the ansatz (3.17) together with (3.3). We find the transformation rules

$$\begin{aligned} &\hat{N}_A \to N_A, \\ &\hat{N}^B \to \hat{N}^B - q^{-1}\hat{N}_A, \\ &N_0^B \to N_0^B - \hat{N}_A\left(\kappa_{vv} - \frac{1}{2}\kappa_{vvv}\right) - q\kappa_{vvv}\hat{N}^B \end{aligned} \tag{3.28}$$

The condition $N_A^0 = 0$ is preserved.

In addition to these transformations, one must also take into account the modular transformations $SL(2,\mathbb{Z})$, which act on the axio-dilaton and the fluxes as

$$\tau \to \frac{a\tau + b}{c\tau + d}, \qquad \begin{pmatrix} f \\ h \end{pmatrix} \to \begin{pmatrix} a & b \\ c & d \end{pmatrix} \cdot \begin{pmatrix} f \\ h \end{pmatrix}, \tag{3.29}$$

with $a,b,c,d \in \mathbb{Z}$ and $ad - bc = 1$.

In order to eliminate equivalent solutions related by the transformations (3.26) and (3.29), all the vacua in the ensemble were transported to a fundamental domain defined by $\mathrm{Re}(\tau) \in [-1/2, 1/2)$, $|\tau| > 1$, and $\mathrm{Im}(\hat{z}) \in [-1/2, 1/2)$ using (3.25), (3.28) and (3.29). Once in the fundamental domain duplicate solutions are easily identified and discarded, as they correspond to those with the same configuration for the fields and the fluxes. The result of this procedure for the ensemble of vacua discussed above is displayed in figure 3.1.

3.3.3 *Analytic formulae and numerical results*

We now turn to the analysis of the statistical properties of the ensemble. As we saw in section 2.6, for compactifications with an effectively one-dimensional complex structure sector and

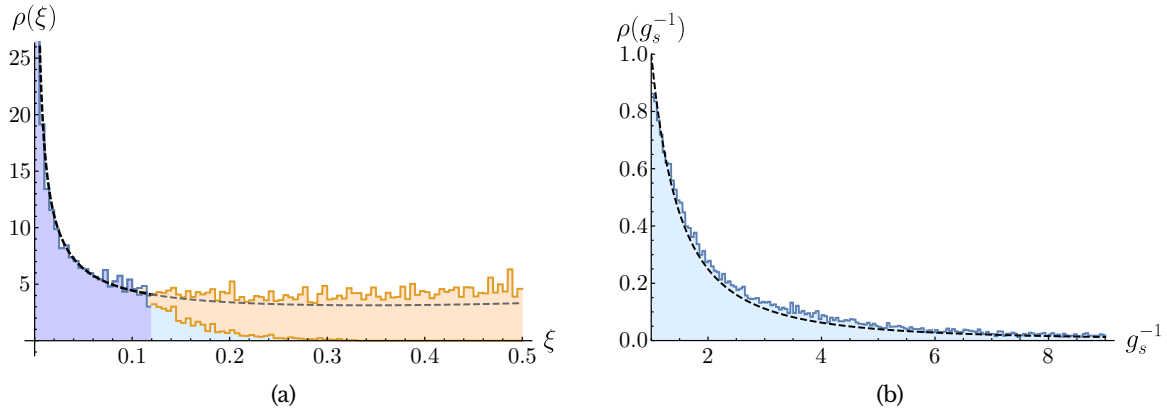

Figure 3.2: (a) Density of flux vacua in the reduced complex structure space in terms of the parameter ξ. The plot shows the numerical distribution obtained directly form the ensemble of 206,479 flux vacua. We have indicated in (dark and light) blue the 95,626 vacua with small ($< 5\%$) instanton corrections, and in orange those where the instanton contribution is large ($> 5\%$). The dashed line represents the analytic distribution (3.30) normalised in the range $\xi \in [0.001, 0.12]$ where most vacua are in the LCS regime and the continuous flux approximation holds (dark blue). (b) Distribution of the string coupling g_s, in terms of $g_s^{-1} = Im\tau$. The histogram represents the normalised distribution of the data points lying in the interval $\xi \in [0.001, 0.12]$, while the dashed curve is the expected result from the continuous flux approximation.

a large $D3$-charge tadpole, $N_{\text{flux}}|_{\text{max}} \gg 1$, the statistics of the flux ensemble can be accurately described using the continuous flux approximation of [46]. This approximation consists in neglecting the quantization of the fluxes, which are then treated as continuous random variables with a uniform distribution, only subject to the tadpole constraint $h^T \cdot \Sigma \cdot f \leq N_{\text{flux}}|_{\text{max}}$. Using this simplification as the starting point, we found in chapter 2 that the distribution of vacua in the reduced, one-dimenstional complex structure is given by (c.f. eq. (2.70))

$$\rho(\xi)d\xi = \mathcal{N} \cdot \frac{(1+\xi)}{(2-\xi)^2\xi^{2/3}}d\xi\,, \quad \xi \equiv \frac{-3\text{Im}(\kappa_0)}{2\kappa_{vvv}\text{Re}(\hat{z})^3}, \tag{3.30}$$

where, for convenience, we have given the distribution of $\text{Re}(\hat{z})$ in terms of the parameter ξ. In the previous expression and the following ones, $\mathcal{N}$ represents a normalisation constant which should be determined for each particular distribution. It is remarkable that this distribution is independent of the details of the Calabi-Yau orientifold, or the choice of the surviving field in the reduced theory, i.e., of v^i. As a consequence, this expression can be used to describe mixed ensembles containing vacua from different compactifications and/or obtained from different truncation ansatze.

The distribution of values for the parameter ξ obtained numerically for our ensemble of vacua, combining the cases $v^i = \{(1,1),(1,2),(1,3)\}$, is displayed in figure 3.2(a). The figure shows a stacked histogram with the 95,626 vacua at the LCS regime indicated in (light and dark) blue, and in orange those solutions with a large contribution from instantons ($> 5\%$). Since the formula (3.30) was obtained while completely ignoring the contribution from instantons, it is expected to work only in the regime of ξ space where few vacua, or none, are discarded due to having large corrections (that is, for $\xi \lesssim 0.12$). Furthermore, due to the

limitations of our numerical method, the flux integers in the ensemble range only in the interval $[-25,25]$, leading to an artificial bound to how close the vacua in the ensemble can be to the LCS point, $\xi \gtrsim 0.001$ (see Appendix D.4). As a consequence, the distribution (3.30) is expected to describe correctly the statistics of vacua in the range $\xi \in [0.001, 0.12]$, which we have indicated in figure 3.2(a) in dark blue.

The distribution (3.30), normalised in its range of validity, is also indicated in the figure with a dashed line and, as it can be observed, it provides a very good description for the density of flux vacua. It is also interesting to note that, despite the divergence of the distribution (3.30) at $\xi = 0$, this function is normalizable in $\xi \in [0, 1/2)$, and thus it predicts a finite number of vacua in any neigbourhood of the LCS point.

Regarding the axio-dilaton, it can also be shown that, according to the continuous flux approximation, the string coupling constant $g_s = (\text{Im}\tau)^{-1}$ has a uniform probability distribution in this class of vacua or, equivalently, the probability density function for the imaginary part of τ is of the form $\rho(\text{Im}\tau) \propto (\text{Im}\tau)^{-2}$. This is also consistent with the distribution which we obtained numerically, as it can be seen in figure 3.2(b).

Our analysis of the distribution of scalar masses will closely follow the one we did in the previous chapter (see subsection 2.6.3). Indeed, we found that the fermion masses at no-scale vacua, m_λ, normalised by the gravitino mass $\tilde{m}_\lambda \equiv m_\lambda / m_{3/2}$, are given by

$$\tilde{m}_\lambda(\xi) = \begin{cases} \sqrt{(1-2\xi)/3}\,\hat{m}(\xi) & \lambda = 0, \\ \frac{\sqrt{(1-2\xi)}}{\sqrt{3}\hat{m}(\xi)} & \lambda = 1, \\ \frac{1+\xi}{3} & \lambda = 2,\dots,h^{2,1}. \end{cases} \tag{3.31}$$

Then, combining the previous expressions with (3.30) and using that the functions $\tilde{m}_\lambda(\xi)$ are monotonic, it is immediate to obtain $h^{2,1}+1$ separate probability distributions, one for each of the rescaled fermion masses

$$\rho^f_\lambda(\tilde{m}_\lambda)\, d\tilde{m}_\lambda = \mathcal{N} \cdot \frac{(1+\xi)}{(2-\xi)^2 \xi^{2/3}\, (d\tilde{m}_\lambda(\xi)/d\xi)}\Big|_{\xi(\tilde{m}_\lambda)} d\tilde{m}_\lambda\,, \tag{3.32}$$

where $\lambda = 0,\dots,h^{2,1}$. Finally, from the relation

$$\mu^2_{\pm\lambda} = (m^2_{3/2} \pm m_\lambda)^2 \tag{3.33}$$

between the scalar and fermion masses, we can obtain $h^{2,1}+1$ separate probability distributions, one for each pair of normalised scalar masses $\tilde{\mu}^2_{\pm\lambda} \equiv \mu^2_{\pm\lambda}/m^2_{3/2}$

$$\rho^s_\lambda(\tilde{\mu}^2_\lambda)\, d\tilde{\mu}^2_\lambda = \mathcal{N} \cdot \tilde{\mu}_\lambda^{-1} \left[\rho^f_\lambda(1+\tilde{\mu}_\lambda) + \rho^f_\lambda(|1-\tilde{\mu}_\lambda|)\right] d\tilde{\mu}^2_\lambda. \tag{3.34}$$

In order to generate the numerical mass distributions for our ensemble of vacua, at each solution to (3.21) we diagonalised the Hessian of the scalar potential induced by the fluxes, i.e., the potential in the theory defined by (3.2) with the couplings (3.23), which describe the $\mathcal{G}$-invariant sector of the moduli space in the $\mathbb{WP}^4_{[1,1,1,6,9]}$ model. In all cases, the resulting masses for the three $\mathcal{G}$-invariant modes (including the axio-dilaton) were in agreement with equation (2.48) with $\lambda = 0,1,2$. The numerical distributions for the scalar $\mu^2_{\pm 0}$, $\mu^2_{\pm 1}$ and

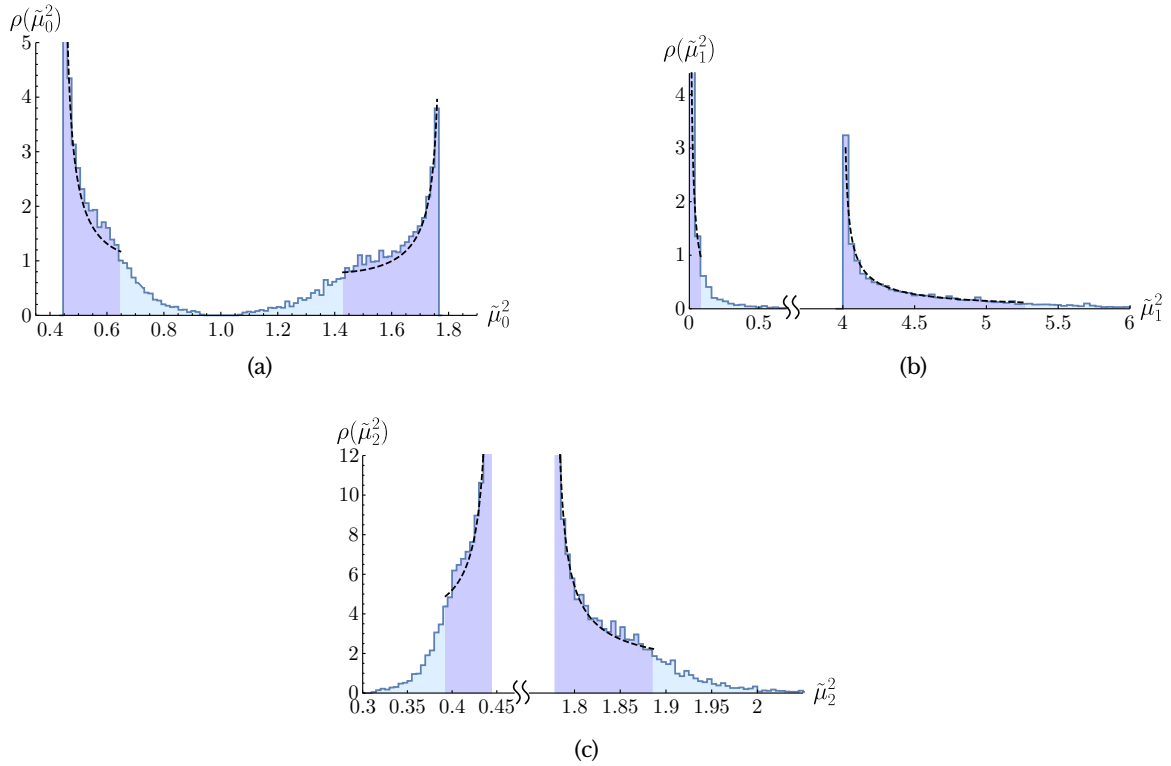

Figure 3.3: Numerical distributions for the normalised scalar masses $\tilde{\mu}^2_{\pm\lambda} = \mu^2_{\pm\lambda}/m^2_{3/2}$ of the $\mathscr{G}-$invariant modes, $\lambda = \{0,1,2\}$ in the ensemble of 95,626 vacua at LCS. In each figure, the dashed line represents the analytic formula (2.48) for each value of λ, normalised in the same range $\xi \in [0.001, 0.12]$. The darker regions represent the solutions for which the continuous flux approximation applies.

$\mu^2_{\pm 2}$ are displayed in figure 3.3, along with the theoretical distribution (3.34) normalised in the range $\xi \in [0.001, 0.12]$. As expected from the analysis of the distribution $\rho(\xi)$ (3.30), in figure 3.3 we can see that the theoretical probability densities for the masses are in good agreement with the obtained numerical results. The most significant feature of these plots is that the density distribution for $\mu^2_{\pm 1}$ is peaked around zero, indicating that a large fraction of vacua involve a light field in the spectrum. This can be understood recalling that, on the one hand, vacua with $N^0_A = 0$ (as those discussed here) can be found parametrically close to the LCS point [145,186,187], and thus a large fraction is expected to be found near $\xi = 0$ (see figure 3.2(a)). On the other hand, from (2.48) it follows that the spectrum of these vacua contains an asymptotically massless mode in the limit $\xi \to 0$, which explains the peak of $\rho^s_1(\mu^2_1)$ at $\mu^2_1 = 0$ observed in figure 3.3(b). This feature is expected to be generic for the class of vacua discussed here, regardless of the choice of Calabi-Yau compactification or the truncation ansatz, as both the mass spectrum (2.48) and the probability distributions (3.33) and (3.34) are completely universal. Note also that half of the masses in the spectrum are smaller than the gravitino mass $m^2_{3/2}$.

The sharp edges of the mass sectra shown in figure 3.3 correspond to the cutoffs we have set on the parameter $\xi \in [0.001, 0.12]$, with the peaks of the probability distributions corresponding to the minimum value of ξ. The effect of changing the bounds of ξ can be seen in figure 3.4. The plot in figure 3.4(a) represents the combined distribution for the masses of the three $\mathscr{G}-$invariant modes, with $\xi \in [0.001, 0.02]$. We see that the distribution

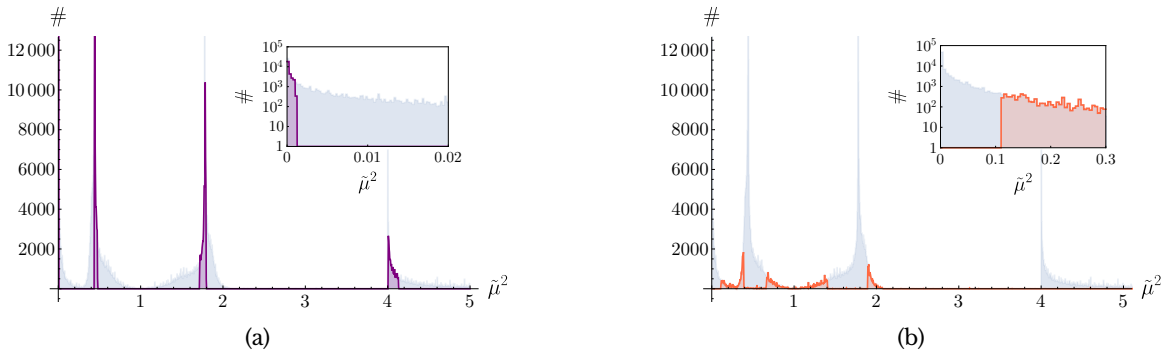

(a) (b)

Figure 3.4: Complete distribution of scalar masses $\tilde{\mu}^2_\lambda$, $\lambda = \{0,1,2\}$, in the ensemble of 95,626 vacua at LCS. In each histogram, solutions with (a) $\xi \in [0.001, 0.02]$ and (b) $\xi \in [0.13, 0.5)$ have been highlighted. The insets in these plots show the mass distribution near $\tilde{\mu}^2 \approx 0$, illustrating the presence of an asymptotically massless mode at vacua near the LCS point (a), and the absence of light modes in the spectrum when solutions near the LCS point are excluded (b).

becomes very peaked, with the maxima at the values

$$\mu^2_{\pm\lambda}/m^2_{3/2} = \left\{0, \frac{4}{9}, \frac{16}{9}, 4\right\}, \tag{3.35}$$

which is precisely the strict LCS limit ($\xi \to 0$) of the spectrum (2.48). This result illustrates the appearance of an asymptotically massless mode at vacua located in a small neigbourhood of the LCS point. Figure 3.4(b) shows the combined the mass distribution for the $\mathscr{G}-$invariant modes, with the parameter ξ restricted to $\xi \in [0.13, 0.5)$, that is, for vacua with small instanton corrections but well separated from the LCS point. In the inset of figure 3.4(b) we can see that for all these vacua the mass of the lightest mode is now bounded below $\mu^2_{-1} \gtrsim 0.11\, m^2_{3/2}$. Then, as we mentioned above, it can be seen that by excluding solutions from a neighbourhood of the LCS point we can construct an ensemble of vacua whose spectrum does not contain light modes, and thus, which are good candidates for considering the stabilisation of the Kähler moduli.

We note that the peaks shown in fig. 3.4 are in contrast with the general predictions based on the statistical modelling of a landscape where this distribution is found using Random Matrix Theory [123, 134, 177, 179] and random Landscapes (see chapter 5 for more detail). The origin of this difference comes from the lack of sufficient complexity in our ensemble of effective field theories. The reason for this is that the structure of the couplings in our ensemble of vacua is quite rigid and does not display the sufficient random nature for the scalar potential induced by the fluxes to be described by a multidimensional Gaussian random field.

Finally, the 270 truncated complex structure fields transforming non-trivially under the symmetry group $\mathscr{G}$ have the same masses as the $\mathscr{G}$-invariant modes with $\lambda = 2$, namely $\mu^2_{\pm\lambda} = \left(1 \pm \frac{1}{3}(1+\xi)\right)^2$ for all $\lambda = 2, \dots h^{2,1}$, and thus their probability distributions coincide with the one displayed in the lower plot of figure 3.3. Let us emphasize again that this is a rather exceptional result, as the EFT couplings for these fields are not determined by (3.23), and thus they were unknown a priori.

3.4 Discussion

In this chapter, we presented a method to construct ensembles of flux vacua for generic Calabi-Yau compactifications at LCS, where the masses of the axio-dilaton and complex structure moduli are given by the universal formula (2.48). This result provides full analytic control, to leading order in α' and g_s, over the masses of those fields, and therefore the vacua we consider are an excellent stepping-stone towards the complete stabilisation of the compactification, i.e., including the Kähler moduli. Interestingly, up to an overall scale, the masses given in (2.48) are completely determined by the vacuum values of the complex structure fields. As a consequence, knowing the magnitude of the α' and nonperturbative corrections which generate the Kähler moduli potential, it is possible to guarantee the stability of the axio-dilaton and all the complex structure fields by restricting the search of vacua to appropriate regions of moduli space. In particular, the spectrum (2.48) involves a single asymptotically massless mode in the neighbourhood of the LCS point, $\mu^2_{-1}|_{\xi\to 0} = 0$, with all the remaining masses being at least of the order of the gravitino mass $m_{3/2}$. In other words, in the LCS limit there is only one potentially dangerous mode which might threaten the stability of the compactification. On the contrary, away from the LCS point the mass of the lightest mode in (2.48) becomes of the order of $m_{3/2}$, and thus as long as the perturbative and nonperturbative contributions to the EFT are under control, the final vacuum with the Kähler moduli fixed will not develop an instability. Nevertheless, it is expected that such contributions will induce small corrections in the spectrum (2.48) which, in particular, will lift the degeneracy of the modes $\lambda = 2, \dots, h^{2,1}$.

Note that the class of vacua we discussed is only appropriate for the construction of LVS solutions, but not for the KKLT scenario. For the solutions presented here, the flux superpotential satisfies $W_0 \equiv \mathcal{V}\, m_{3/2} \geq 1/\sqrt{\pi}$ (see eq. (3.22)), while the KKLT vacua require W_0 to be exponentially small. Therefore, a logical future direction would be to consider the stabilisation of the Kälher moduli at the class of vacua presented here within the LVS framework. Another interesting continuation of this work would be to study other truncation schemes compatible with the more general vacua discussed in the previous chapter, where the spectrum can also be explicitly computed, and W_0 could be arbitrarily small.

To conclude we will briefly comment on the possible extension of our results to other regimes away from the LCS limit. In general, such an analysis would require a specific treatment which is beyond the reach of the present analysis, as our derivations depend crucially on the universal properties satisfied by the couplings of the EFT at LCS. However, in the specific case of conifold limits of the moduli space, it might be possible to make some progress following an analogous procedure to the one described in [194,195] (see also [196]). In those works, it was explicitly demonstrated that one can stabilise a subset of the complex structure moduli near a conifold point, while fixing the rest near the LCS point, i.e., at a *conifold-LCS regime*. As shown in [194,195], provided the moduli at LCS are sufficiently massive, the stabilisation of this sector can be treated independently, ignoring consistently the presence of moduli near the conifold limit to leading order. Therefore, an interesting future direction would be to study the application of our results to characterise the spectrum of those complex structure at LCS for compactifications in a conifold-LCS regime, such as those described in [194,195].

Chapter 4

Racetrack potentials and the de Sitter swampland conjecture

After our thorough study of the complex structure and axiodilaton moduli sector, we now turn to work on same aspects of the stabilization procedure which include the Kähler sector. We will do this from a perspective of the *de Sitter Swampland* conjecture, which we will introduce below. In this chapter, we will be mostly interested in finding exact solutions which are critical points of the flux superpotential, with non-perturbative corrections taken into account in order to render the Kähler moduli massive. We will examine these particular solutions and check for the existence of de Sitter critical points and their validity from the effective field theory perspective. Moreover, we will also contrast them with the de Sitter Swampland conjecture and its refined counterpart.

This chapter is based on [197].

4.1 Introduction

It has recently been conjectured [54] that any potential consistent with quantum gravity should satisfy the bound

$$M_p \frac{|\nabla V|}{V} \geq c\,, \tag{4.1}$$

where c is a dimensionless constant of order unity. One of the obvious implications of this conjecture will be the impossibility of obtaining a metastable de Sitter vacua. However, the conjecture is much stronger than that: it also prohibits the existence of any critical point (saddle points) at positive values of the potential. This aspect of the conjecture is already under tension from several theoretical considerations that involve well known Standard Model physics [198–200]. In particular, one would need to introduce some specific couplings of the Higgs field in order to satisfy Eq. (4.1).

String theory is a consistent theory of quantum gravity, and if the conjecture is correct, any potential obtained in this theory would have to satisfy Eq. (4.1). This is particularly restrictive when we take into account the large number of 4-dimensional potentials that one could generate in the process of compactification from 10d. However, similar bounds

on the potential have been found earlier in some string theory compactifications [201]. It is therefore very important to investigate whether or not this general statement about low energy effective field theory is true in a generic situation. This has been recently discussed in several papers, e.g., [55–65], mostly in relation to the validity of the approximations to obtain a 4-dimensional de Sitter space minima.

In this chapter, we will focus our discussion on the existence of de Sitter saddle points in models of string compactification to demonstrate that the de Sitter conjecture is too restrictive. In fact, there is already some evidence in the literature for the existence of unstable de Sitter solutions, found from looking directly at the 10d equations of motion (see [202] and references therein). This seems to suggest that one could find a 4d dimensional version of a potential that could bring the spacetime to this form, therefore violating the de Sitter conjecture given by Eq. (4.1). However, it is not clear if those 10d solutions can be cast in a low energy effective field theory in 4d [203]. Thus it is still necessary and interesting to look for some other possible counterexamples to the conjecture.

One can also take a different perspective and think about the purely 4d effective theory that one obtains from compactication. This approach has been taken in several of the most-studied examples of de Sitter vacua in string theory, in particular the well known KKLT model [35] or the Large Volume Scenario [31,34,204], which we described in subsection 1.3.3. However, some of the ingredients in these constructions have been put into question by some authors [205] (see also [206]). It is therefore interesting to ask whether one can find de Sitter critical points in these constructions that violate the de Sitter swampland conjecture with all of the ingredients well under control. This question has been addressed by Conlon in [207] in the context of moduli potentials. His argument is based on the realization that in certain circumstances, the potential approaches zero from above along specific directions in field space, such as the internal volume or the dilaton. This fact, together with the existence of supersymmetric AdS minima in the interior of the moduli space, suggests that one should find a maximum of the potential somewhere between these two regions. This argument does not require the presence of any uplifting term in the effective potential and therefore seems more generic. In order to make the argument robust, one should show that the critical point is still there in the presence of several other fields, like the complex structure moduli and the other Kähler moduli. In this chapter, we will show that this is indeed possible in constructions of Type IIB with several complex structure moduli, the dilaton, and one Kähler moduli. We further find that the presence of de Sitter saddle points is quite generic in these constructions, which include (but are not limited to) the cases discussed by [207].

Furthermore, it has been argued in Ref. [63] that a form of the Weak Gravity Conjecture [52] will inhibit the possibility of obtaining a viable model of compactication with a Racetrack Potential. In the following, we will show that the form of the parameters imposed by the authors in Ref. [63] is in fact too restrictive, and one can easily find a set of coefficients that would not violate the Weak Gravity Conjecture.

The models we present here pass many requirements that one needs to impose to have some confidence on the results obtained from them. In particular we require that the following conditions are satisfied in our model:

- large enough internal volume

- weak coupling
- large complex structure values
- positivity of all the kinetic terms at the points of interest
- small periodicity of the axionic fields (a version of the Weak Gravity Conjecture)
- sub-Planckian energy densities
- discrete values of the fluxes and the superpotential.

This is quite a long list of demands. It is not completely clear, *a priori*, that one could satisfy all of them with the limited number of parameters present in our model. We will show that it is indeed possible to overcome these difficulties and find examples that respect all these conditions.

There are, however, some approximations that we have made in order to simplify the problem. In particular, we have modelled the Kähler moduli sector of the compactification manifold by a single complex field. We have also taken a simple model for the non-perturbative superpotential whose field dependence is restricted to this single Kähler moduli. One could in principle perform the same kind of calculations in a more realistic version of our model with two Kähler moduli and two complex structure fields, as was done in [99, 208], to investigate if the results in this chapter continue to hold in that case.

After the main part of this work was completed, a new version of the de Sitter Swampland Conjecture appeared in Ref. [66]. This is a much weaker version of this conjecture that allows for saddle points in de Sitter space, but imposes some restrictions on the curvature of the potential at those critical points. The arguments behind this new version of the conjecture are different in nature to the previous one and they are being actively investigated [209]. Given this situation, we feel that it is still important to give concrete examples that can firmly establish whether any of these conjectures are valid in its current form. Therefore this work provides evidence that the strong version of the conjecture, as stated in Eq. (4.1), is ruled out in string theory. We have also checked the form of the de Sitter saddle points we obtained in this model against the restrictions of the new conjecture, as reported in the final part of this chapter.

The rest of this chapter is organized as follows. In section 4.2, we construct several explicit examples of potentials with de Sitter saddle points in this context. In section 4.3, we discuss the validity of our solutions with respect to several possible constraints. In section 4.4, we investigate the form of the potentials around the de Sitter critical points and study them in connection to the refined version of the de Sitter Swampland Conjecture [66] . We conclude in section 4.5.

4.2 Explicit Examples for Type IIB compactification scenarios

In this chapter, we will be working with the well-studied orientifold model $\mathbb{WP}^4_{[11169]}$, which we thoroughly described in section 3.3, and has been widely used in the context of Kähler

moduli stabilization, see e.g. [45,100]. More concretely, we will apply the formulae concerning its supersymmetric truncation to two complex structure moduli[1] (in order to make the computational problem tractable). On the other hand, as we said in the previous section, the Kähler sector will be considered to be composed by only the overall volume modulus for simplicity.

As we discussed in section 1.3, due to the no-scale structure of the potential, supersymmetric vacua have flat directions along the Kähler fields, so one must go beyond the no-scale limit in order to stabilize the Kähler moduli. This can be done either by introducing perturbative corrections to the Kähler function [31], or by adding non-perturbative terms to the superpotential [35]. We will concentrate on non-perturbative terms in the simplest models of a single Kähler field, which take the form [35]

$$W_{\rm np} = \sum_i A_i e^{-a_i T} . \tag{4.2}$$

In the following, we will take A_i and a_i to be constants.

With the above ingredients in mind, we will study the $N = 1$ supergravity theory with the Kähler function

$$K(z_1, z_2, \tau, T) = -3\log(T + \overline{T}) - \log(-i(\tau - \bar{\tau})) + K_{cs}(z_1, z_2, \tau) \tag{4.3}$$

and superpotential

$$W(z_1, z_2, \tau, T) = W_{\rm flux}(z_1, z_2, \tau) + Ae^{-aT} + Be^{-bT} . \tag{4.4}$$

where K_{cs} is the Kähler potential for the complex structure at the LCS region, c.f. eq. (2.4), and the couplings have been described in eq. (3.23). We have denoted as $W_{\rm flux}$ the contribution of the fluxes to the superpotential, namely Gukov-Vafa-Witten superpotential described in (1.35), while the non-perturbative contributions have been explicitly written in (4.4). The latter give rise to the so-called "racetrack-type superpotential". This has been argued to arise from gaugino condensation in a stack of $D7$ branes wrapped around some internal cycles of the CY geometry [35].

This concludes the description of our model for this chapter, which is characterized by several parameters that we will fix in the following examples. It is important to note that even when one fixes the field space manifold and the D-brane content of our compactification scenario, we will still have a large number of possible potentials available due to the multitude of possible fluxes. We will use this fact to show that our conclusions are quite generic.

4.2.1 *Supersymmetric Vacua*

Let us denote by W_0 the value of the superpotential at tree-level no-scale vacua, which satisfy eqs. (1.37). We start our description of potentials with de Sitter saddle points by studying an

[1] In this chapter, as opposed to chapters 2 and 3, we will not constrain our complex structure moduli space to be one-dimensional. Therefore, even though we will be using the same CY orientifold as in the previous chapter, the region of the moduli space we will explore is quite different, and our previous results need not apply here.

example of fluxes that give rise to a vanishing tree-level flux superpotential, $W_0 = 0$. Using only the complex structure moduli (meaning without introducing any non-perturbative terms), it has been shown in ref. [45] that such vacua are possible if one chooses the flux numbers, $(f_A|f^B)$ and $(h_A|h^B)$, threading each cycle appropriately. For example, one can choose

$$(f_A|f^B) = (20,0,0|0,-69,-28)\,, \qquad (h_A|h^B) = (0,-4,0|49,18,6)\,. \tag{4.5}$$

to get $W_0 = 0$ at the solution of the no-scale vacuum equations (1.37).

Adding the non-pertubative potential with parameters[2]

$$A = -\frac{1}{100}\,, \qquad B = 1\,, \qquad a = \frac{2\pi}{100}\,, \qquad b = \frac{2\pi}{50}\,, \tag{4.6}$$

one can find a supersymmetric minima for all fields. In particular, we obtain $\mathrm{Re}[T] = T_R = 82.430$ and $\mathrm{Im}[T] = T_I = 0$ at an AdS supersymmetric minima. It is important to note that we have solved the complete set of supersymmetric equations for all fields, so in fact the superpotential at the true minimum has a tiny component due to the small correction to the supersymmetric equations introduced by the non-perturbative terms. However, this correction of the position of the minima in field space in the complex structure and the dilaton is quite small. This is useful since it allows us to first solve the equations for the dilaton and the complex structure with $W_{\rm np} = 0$, and then use this solution as our initial guess for the full solution.

4.2.2 de Sitter Critical Point

Looking at the asymptotic form of this potential at large values of T_R, one realizes that it approaches zero from above. However, the supersymmetric minimum we found before is at a negative value of V. This indicates, as figure 4.1 shows, that the potential should have a local maximum at some intermediate value of T_R. This is the same idea described in ref. [207] for the dilaton potential in a heterotic string compactification.

We have an expression for the scalar potential as a function of all the fields involved, so we can check that this maximum is indeed a critical point once we take into account all other directions. The locations of the dilaton and the complex structure moduli at the de Sitter critical point are slightly shifted from their values at the AdS supersymmetric vacuum. One can justify this by considering the differences in scales between the complex structure and dilaton masses and the Kähler fields.

As noted above, the values of the fluxes in this example are such that the solution respects supersymmetry even before introducing any non-perturbative corrections. In other words, $W_0 = 0$. This makes this solution free of any of the potential problems described in [37], where some concern was raised about the introduction of non-perturbative terms in the superpotential without taking proper account the possibility of other perturbative corrections due to supersymmetry breaking. See however the discussion in Ref. [38].

[2] Note that for a specific model of compactification, one may have to consider possible restrictions to the values of the exponentials of the superpotential due to the specific internal manifold. See for example the discussion in Ref. [99]. We will not take this into consideration here.

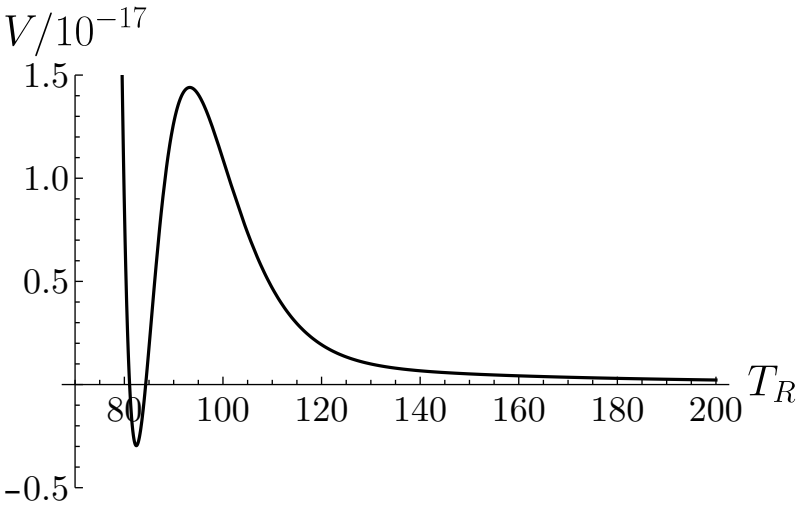

Figure 4.1: A plot of the $W_0 = 0$ case (Case 0) using the racetrack parameters from eq. (4.6). The nonperturbative correction results in an anti-de Sitter minimum. Because the potential asymptotically approaches zero from above, there must then be a maximum in T_R between this minimum and infinity. That maximum is in fact very near to a de Sitter saddle point.

We therefore conclude that it is possible to find true de Sitter saddle points in this type of scenario with many moduli fields. However, this example is somewhat special, since the main argument for the existence of the saddle point in the T_R direction relies on the vanishing of the tree level flux superpotential. In the following, we relax this condition to see how generic de Sitter saddle points are in our models.

4.2.3 *More general cases*

In the previous section, we gave a particular example of the parameters that lead to the existence of a de Sitter critical point following the description given by Conlon[3] [207]. We will now show that such critical points exist for a large volume of the parameter space of the models we are using.

Let us start by describing another way in which one could try to find a de Sitter critical point in our construction. Consider the situation incorporating the non-perturbative terms such that they yield a supersymmetric Mikowski vacuum. In other words, we will consider the case where the total superpotential (not only W_{flux}) at the vacuum is zero. This sounds like a good starting point if one wants to find a de Sitter saddle point: the potential around that minimum would be positive, but at large volume it should go back to zero, so it must turn around at some point. This, of course, only suggests the possibility of the existence of these points, and one will have to find explicit examples in the multifield potential. Here, we again use the $\mathbb{WP}^4_{[11169]}$ CY complex structure moduli to give such examples. This model has only two complex structure moduli, but it is already rich enough to demonstrate the generic existence of de Sitter critical points in the landscape.

[3] In Ref. [207], Conlon argued how one can find other examples where these de Sitter saddle points can appear by using α' corrections to the potential. This requires a specific sign of these corrections. Here we will show that these points appear generically in the racetrack models even ignoring these corrections.

Case #	$(f_A\|f^B)$	$(h_A\|h^B)$	W_0
0	$(20,0,0\|0,-69,-28)$	$(0,-4,0\|49,18,6)$	0
1	$(20,-1,-6\|12,-44,-14)$	$(-1,-4,3\|43,21,7)$	$-0.025920+i\,0.022994$
2	$(18,-2,-3\|16,-37,-10)$	$(-1,-4,3\|46,21,5)$	$-0.025987+i\,0.000443$
3	$(18,-1,-3\|14,-42,-15)$	$(-1,-4,3\|43,19,6)$	$-0.020426+i\,0.011213$

Table 4.1: The flux integer choices and initial W_0 (found from solving $D_I W_{flux}=0$ for $I\in\{\tau,z_i\}$) for all four cases we studied. The values of Eq. (4.7) were chosen such that the full potential $V(z_i,\tau,T)$ of Case 1 has a Minkowski supersymmetric minimum.

Finding a supersymmetric Minkowski vacuum can be achieved with our racetrack potential, as was shown in Ref. [210, 211], by adjusting the coefficients of our non-perturbative superpotential for a given W_0. In our case, we select

$$A=0.26050-i\,0.30090\,,\qquad B=-0.65453+i\,0.75603\,,\qquad a=\frac{2\pi}{300}\,,\qquad b=\frac{2\pi}{150}\,, \tag{4.7}$$

which were chosen based on a choice of fluxes

$$(f_A|f^B)=(20,-1,-6|12,-44,-12)\,,\qquad (h_A|h^B)=(-1,-4,3|43,21,7)\,, \tag{4.8}$$

which has an initial $W_0=-0.025920+i\,0.022994$. Looking at the full potential for these parameter values, we indeed find a de Sitter saddle point along the volume direction, as expected.

It may seem that this scenario is fine-tuned by the specific choice of our superpotential parameters (A,B,a,b), such that we obtain the Minkowski vacuum. Thus, we shall vary the flux numbers while keeping the racetrack potential fixed, with the requirement that we only consider relatively small values of $|W_0|$ in our examples. We have scanned a few sets of flux integer values to identify a few suitable candidates for our purposes. We shall consider four cases: the one with $W_0=0$ from before, the one with fluxes as in Eq. (4.8), and two others. These cases are detailed in Table 4.1.

We show in Fig. 4.2 the potential along the volume direction for all four cases, using always the racetrack parameters of Eq. (4.7). We find again a de Sitter critical point close to the minimum, where the potential is at an extremum in all field directions. There is another interesting point in this example for Cases 1–3. At large values of the volume, one finds another supersymmetric AdS critical point, so our de Sitter critical point is located in between these two supersymmetric points. This is a different asymptotic behavior than the one obtained Conlon [207] and in our previous section. This fact makes it harder to see how can one modify the potential to avoid the de Sitter critical point without also destroying the nearby supersymmetric points. As before, there is typically a small shift in the values of the moduli between the supersymmetric minima and the de Sitter critical point.

Furthermore, Cases 2 and 3 exhibit the same general behavior as Case 1, and so such behavior does not seem to be the result of fine-tuning. In a realistic model with many complex structure moduli, the distribution of vacua in the W_0 around the origin is flat [212], and the model we have chosen already allows for many minima around $|W_0|\approx 0$ [100]. This would mean that in reality, there would a very large number of these vacua with de Sitter critical points. Hence, the examples shown here are very generic in a typical CY.

Case #	τ	z_1	z_2	T
0	$-8.712\text{E-}4 + i\ 3.001$	$-1.000 - i\ 1.108\text{E-}4$	$-0.9999 + i\ 9.850\text{E-}5$	$62.22 - i\ 1.044\text{E-}3$
1	$-0.8120 + i\ 3.752$	$-1.383 - i\ 0.5176$	$-0.1546 + i\ 1.067$	$77.09 + i\ 0$
2	$-0.5595 + i\ 3.395$	$-1.225 - i\ 0.6514$	$-0.6160 + i\ 1.543$	$66.25 + i\ 5.737$
3	$-0.5748 + i\ 3.485$	$-1.304 - i\ 0.4232$	$-0.4240 + i\ 1.011$	$68.82 + i\ 2.727$

(a) Field values at the first (lower T_R) supersymmetric critical points

Case #	τ	z_1	z_2	T
0	$-8.929\text{E-}4 + i\ 3.001$	$-1.000 - i\ 1.136\text{E-}4$	$-0.9999 + i\ 1.010\text{E-}4$	$96.53 + i\ 5.127\text{E-}4$
1	$-0.8118 + i\ 3.752$	$-1.383 - i\ 0.5176$	$-0.1546 + i\ 1.067$	$96.53 + i\ 1.178\text{E-}3$
2	$-0.5593 + i\ 3.395$	$-1.225 - i\ 0.6514$	$-0.6159 + i\ 1.543$	$97.84 + i\ 3.846$
3	$-0.5747 + i\ 3.485$	$-1.304 - i\ 0.4232$	$-0.4240 + i\ 1.011$	$96.85 + i\ 1.963$

(b) Field values at the non-supersymmetric de Sitter saddle points.

Case #	τ	z_1	z_2	T
1	$-0.8110 + i\ 3.751$	$-1.383 - i\ 0.5175$	$-0.1546 + i\ 1.067$	$157.6 + i\ 3.882\text{E-}3$
2	$-0.5584 + i\ 3.395$	$-1.225 - i\ 0.6513$	$-0.6158 + i\ 1.543$	$189.7 - i\ 43.34$
3	$-0.5738 + i\ 3.484$	$-1.304 - i\ 0.4231$	$-0.4240 + i\ 1.010$	$194.9 - i\ 18.37$

(c) Field values at the second (higher T_R) supersymmetric anti-de Sitter minima.

Point	Case #	Masses							
1st SUSY	0	$5.791\cdot10^{-4}$	$5.790\cdot10^{-4}$	$2.846\cdot10^{-4}$	$2.845\cdot10^{-4}$	$1.510\cdot10^{-4}$	$1.510\cdot10^{-4}$	$9.744\cdot10^{-10}$	$8.462\cdot10^{-10}$
	1	$1.015\cdot10^{-2}$	$1.015\cdot10^{-2}$	$3.174\cdot10^{-4}$	$3.174\cdot10^{-4}$	$1.033\cdot10^{-4}$	$1.033\cdot10^{-4}$	$9.125\cdot10^{-11}$	$9.125\cdot10^{-11}$
	2	$1.813\cdot10^{-3}$	$1.813\cdot10^{-3}$	$4.155\cdot10^{-4}$	$4.154\cdot10^{-4}$	$1.523\cdot10^{-4}$	$1.523\cdot10^{-4}$	$4.292\cdot10^{-10}$	$3.799\cdot10^{-10}$
	3	$1.836\cdot10^{-3}$	$1.836\cdot10^{-3}$	$3.991\cdot10^{-4}$	$3.991\cdot10^{-4}$	$1.316\cdot10^{-4}$	$1.316\cdot10^{-4}$	$2.889\cdot10^{-10}$	$2.636\cdot10^{-10}$
de Sitter saddle	0	$1.551\cdot10^{-4}$	$1.550\cdot10^{-4}$	$7.622\cdot10^{-5}$	$7.614\cdot10^{-5}$	$4.045\cdot10^{-5}$	$4.040\cdot10^{-5}$	$\mathbf{-1.269\cdot10^{-10}}$	$1.178\cdot10^{-10}$
	1	$5.169\cdot10^{-3}$	$5.168\cdot10^{-3}$	$1.616\cdot10^{-4}$	$1.616\cdot10^{-4}$	$5.262\cdot10^{-5}$	$5.260\cdot10^{-5}$	$\mathbf{-2.514\cdot10^{-11}}$	$2.427\cdot10^{-11}$
	2	$5.630\cdot10^{-4}$	$5.628\cdot10^{-4}$	$1.290\cdot10^{-4}$	$1.289\cdot10^{-4}$	$4.730\cdot10^{-5}$	$4.726\cdot10^{-5}$	$\mathbf{-6.244\cdot10^{-11}}$	$5.866\cdot10^{-11}$
	3	$6.590\cdot10^{-4}$	$6.589\cdot10^{-4}$	$1.432\cdot10^{-4}$	$1.432\cdot10^{-4}$	$4.723\cdot10^{-5}$	$4.719\cdot10^{-5}$	$\mathbf{-5.101\cdot10^{-11}}$	$4.795\cdot10^{-11}$
2nd SUSY	1	$1.188\cdot10^{-3}$	$1.188\cdot10^{-3}$	$3.713\cdot10^{-5}$	$3.713\cdot10^{-5}$	$1.209\cdot10^{-5}$	$1.208\cdot10^{-5}$	$1.294\cdot10^{-12}$	$9.632\cdot10^{-13}$
	2	$7.720\cdot10^{-5}$	$7.720\cdot10^{-5}$	$1.769\cdot10^{-5}$	$1.769\cdot10^{-5}$	$6.484\cdot10^{-6}$	$6.483\cdot10^{-6}$	$3.801\cdot10^{-13}$	$3.065\cdot10^{-13}$
	3	$8.087\cdot10^{-5}$	$8.087\cdot10^{-5}$	$1.757\cdot10^{-5}$	$1.757\cdot10^{-5}$	$5.793\cdot10^{-6}$	$5.792\cdot10^{-6}$	$2.697\cdot10^{-13}$	$2.172\cdot10^{-13}$

(d) Scalar field mass spectra at the critical points. Eigenvalues corresponding to the T_R direction for the de Sitter critical point have been highlighted in red. The eigenvectors corresponding to the last two masses of every row are almost aligned with T_R and T_I, respectively.

Table 4.2: Field values of z_1, z_2, τ, and T and scalar mass spectra at the various critical points we illustrate in figs. 4.2-4.4. While we report these values to five significant digits, all calculations were carried out to a precision of forty digits. While it is not always clear from these tables, owing to the low precision in the presentation, the τ, z_1, and z_2 values all change between critical points, and so these data should be taken to give the vicinity of the critical points.

We plot in Figs. 4.2 & 4.3 the potentials along the volume direction for the values of the moduli that correspond to the first supersymmetric critical point and the de Sitter .critical point. Finally, we plot in Fig. 4.4 the other supersymmetric AdS critical points that exist in all cases except the case with $W_0 = 0$. We give details about the location and mass spectra[4] of these points in table 4.2.

[4]The kinetic term in the action for the scalar fields is generically not in canonical form. In order to compute the eigenvalues with respect to the real and imaginary parts of all the moduli,we need to find a metric g_{ij} in field space such that $K_{I\bar{J}}\partial_\mu\Phi^I\partial^\mu\bar{\Phi}^{\bar{J}} = \frac{1}{2}g_{ij}\partial_\mu\phi^i\partial^\mu\phi^j$ where $\Phi^I = \{\tau, z_1, z_2, T\}$ and ϕ^i stands for the real or imaginary part of any moduli. Thus, the matrix from which the eigenvalues will be computed is $\mathcal{H}^i{}_j = g^{ik}(\partial_k\partial_j V - \Gamma^l_{kj}\partial_l V)$. Note that the second term will vanish if we are analyzing a critical point.

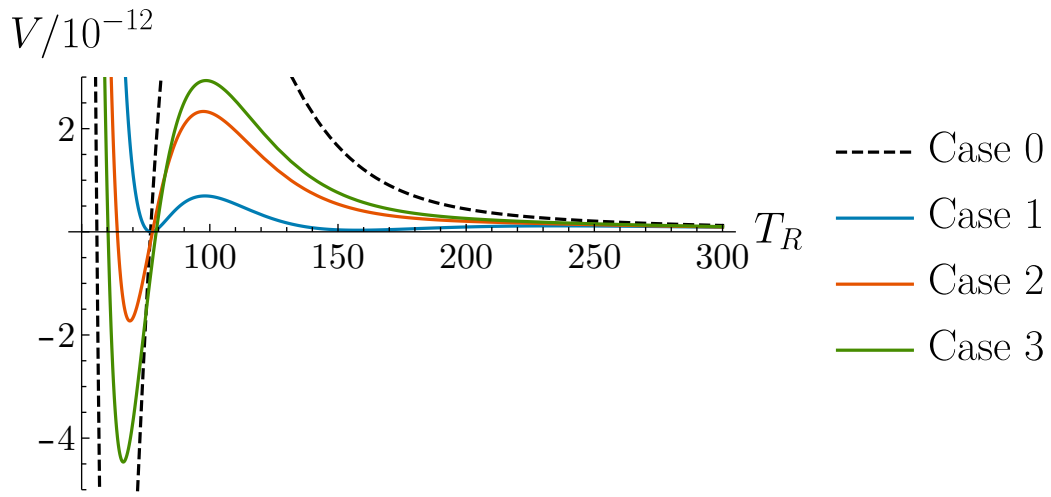

Figure 4.2: A plot of the potentials of Cases 0–3 with T_R varying and all other fields fixed at their first critical point values (vid. table 4.2(a)). All of the minima in this potential are anti-de Sitter, with the exception of Case 1, which is a Minkowski minimum.

4.3 Validity of the solutions

The values of the moduli at the minimum are constrained by several requirements so that one can trust the results given our approximations. The realizations we have studied here pass all of the following constraints.

One needs to find a minimum at a large value of the real part of T so that the internal volume is large in string units and one can trust the supergravity approximation. Our smallest T_R is ≈ 62.

The imaginary part of the dilaton should be large enough to be in the weak coupling regime. Similarly, the complex structure should be found in the region where the calculation of the periods that enter the Kähler and the superpotential can be trusted, i.e., instanton corrections should remain under control. Our smallest $\mathrm{Im}[\tau]$ is ≈ 3, and the z_1 all have real part greater than 1 in absolute units.

We also have to impose the positivity of all the kinetic terms for the moduli fields. This restricts some of the vacua that we have found numerically, forcing us to exclude them from consideration.

Another important point that has been discussed in the literature [63] is the possible trans-Planckian periodicity of the axion fields associated with the Kähler moduli. Models with that property violate a generalization of the Weak Gravity Conjecture and are therefore assumed to be part of the Swampland. This means that one should not consider such cases when looking for viable counterexamples of the de Sitter Swampland conjecture.

This added restriction, together with all the other conditions we would like to satisfy, puts some tension on the set of possible parameters that one can use. However it is not hard to find examples where the periodicities for the axions are sub-Planckian. In fact, all the numerical examples we give in this work avoid any violation of the Weak Gravity Conjecture. The harmonics of the axion can be directly computed from the scalar potential, and they

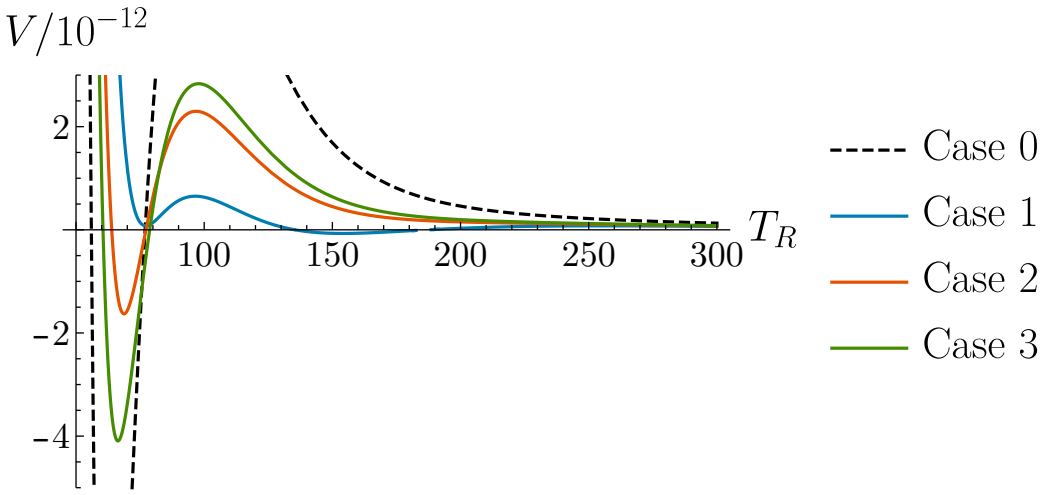

Figure 4.3: A plot of the potentials of Cases 0–3 with T_R varying and all other fields fixed at their de Sitter critical point values (vid. table 4.2(b)). All of the apparent maxima shown here are in fact saddle points once we account for all fields.

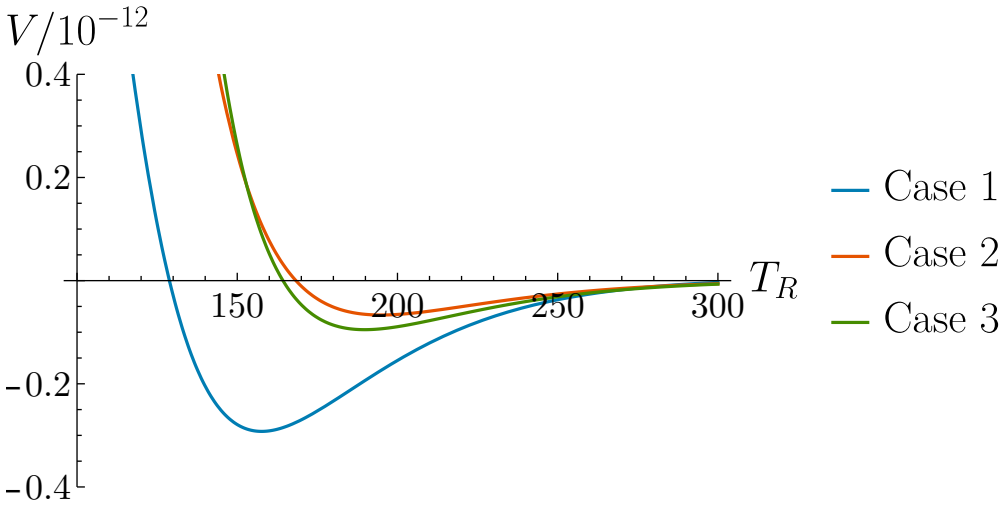

Figure 4.4: A plot of the potentials of Cases 1–3 with T_R varying and all other fields fixed at their second anti-de Sitter critical point values table 4.2(c). All cases are true minima once we account for all the fields.

should satisfy

$$aT_R > 1, \qquad bT_R > 1, \qquad (b-a)T_R > 1 \tag{4.9}$$

for the T_R at all critical points so all the terms in the potential for the axions have a sub-Planckian periodicity[5]. Finally, the de Sitter saddle points that we found are all at a sub-Planckian energy density, so this does not impose a serious restriction.

[5]Note that the dependence of this condition on T_R comes from imposing the periodicity on the canonically normalized axion fields.

4.4 de Sitter saddle points and the Refined de Sitter Conjecture

In the previous sections, we have shown that it is quite generic to obtain de Sitter critical points in constructions of moduli stabilization without much fine tuning. These points rule out the strong version of the de Sitter Conjecture.

A new version of the conjecture has appeared briefly afterwards that allows de Sitter saddle points as long as the the curvature of the potential is large along the unstable direction [66]. It states that at a saddle point, the potential will satisfy the relation

$$\text{Min}\left(V_{\phi\phi}\right) \leq -\frac{c'}{M_P^2} V\,, \tag{4.10}$$

where c' is a positive dimensionless constant of order 1 and $V_{\phi\phi}$ denotes the second derivative of the potential with respect to the canonically normalized fields, ϕ. This is directly related to one of the slow roll parameters in inflationary scenarios, η. This parameter is given by the ratio of the second derivative of the potential along the canonically normalized field direction and the potential itself. The new conjecture imposes that η should be large and negative along the unstable direction at those de Sitter critical points.

Using the form of the potential for all the moduli fields we obtained earlier, one can find in our model the eigenvalues of the squared masses of the canonically normalized fields around any critical point, and from there the values of η at those points. This calculation shows that the unstable directions in all de Sitter saddle points are in fact pretty much aligned with the direction that corresponds to the volume modulus. This is in agreement with the naïve expectation one gets by looking at the plots of the potential along the T_R direction.

We show in Table 4.3 the values of η for the four de Sitter critical points found earlier. It is clear from those results that all these points are in agreement with the weaker version of the de Sitter conjecture. However, this is to be expected in this simple model. The form of the kinetic term for this field is universal:

$$\frac{3}{4T_R^2}\left(\partial_\mu T_R \partial^\mu T_R\right), \tag{4.11}$$

and the value of the η parameter for the canonically normalized field along the T_R direction is in this case given by

$$\eta_{T_R} = \frac{2}{3}\, T_R^2 \left(\frac{V''}{V}\right), \tag{4.12}$$

where $V'' = \partial^2 V / \partial T_R^2$ and the contribution from the non-canonical kinetic term has been taken into account in the definition of η (see footnote 4). Because we need to have a large volume for consistency of the model, we conclude that it would be very difficult to have small enough values of η. This is not surprising, since our model, at this level, is nothing more than a supergravity model and as such is likely to be affected by the so-called eta-problem [213]. In fact one can show that, without introducing new ingredients, the kind of model we have been discussing would not lead to a region of small η parameter [214, 215], no matter what

Case #	0	1	2	3
η at de Sitter	-18.62	-38.58	-22.04	-22.20

Table 4.3: Values of the η-parameter for all cases at the de Sitter saddle points.

numerical parameters we use for the model. However, it is clear that there are a number of possible extensions of this model that would allow for flat enough de Sitter critical points, possibly involving some fine tuning of the potentials along the axionic directions.

One example of this is given by the Racetrack Inflation models [208, 216] where an uplifting term was included in the discussion. It is quite remarkable that this simple modification allows for a realistic model of inflation to be implemented. We have not included such terms here, since our focus in this chapter was to show the generic existence of de Sitter saddle points in some of the most conservative constructions in Type IIB compactification.

4.5 Discussion

In this chapter, we have given explicit examples of de Sitter critical points in models of compactification with racetrack potentials. These points violate the de Sitter Swampland Conjeture given by Eq. (4.1). We argue that in a generic CY with many moduli fields, there would be large numbers of these de Sitter critical points for generic values of the parameters of the racetrack superpotential and varying sets of flux numbers. We have shown this explicitly for a limited case, with only two complex structure moduli, to illustrate our point. For simplicity we have used a single-Kähler model, but we expect that one would be able to do the same exercise in the case of two Kähler [208].

The de Sitter critical points found in our model satisfy the weaker version of the de Sitter Conjecture given by Eq. (4.10). This is to be expected, given the nature of the unstable field direction and the fact that we only use a purely supergravity Lagrangian. However, given that the de Sitter Swampland Conjecture seems to be easily violated by these points, it would not be hard to envision cases where there will be flat enough saddle points once one introduces more ingredients to the Lagrangian, similar to what happens in models such as Racetrack Inflation [208, 216] .

We have also shown that one can find models of flux compactifications with many moduli which are fully compatible with all the constraints that one would normally like to impose in order to have control of the theory. In particular, we have shown that it is possible to find viable models of compactification that satisfy a version of the Weak Gravity Conjecture. This suggests that these types of models may be among the most interesting ones to find a de Sitter vacua in Type IIB compactifications. This has been studied in several scenarios in Ref. [217], where de Sitter vacua are found in models with racetrack potentials of the kind discussed in Ref. [210] and several uplifting mechanisms.

Finally, let us note that a straightforward continuation of this work would be to apply it to the compactification scheme presented in chapter 3, where the complex structure moduli space of the $\mathbb{WP}^4_{[11169]}$ orientifold was further reduced to an effectively single direction. This would allow us to have a model with *all* moduli stabilized, which would make for an extremely interesting setup to test, for example, uplifting mechanisms. This goal, however,

is far from being easy; among other issues, as we mentioned in the previous chapters, the stabilization of the Kähler sector is expected to lift the degeneracy of the truncated directions of the complex structure sector.

Part III

Cosmological aspects of the Landscape

Chapter 5

Slepian models for Gaussian Random Landscapes

Up until this moment, we have worked out the effective field theory of Type IIB String Theory in a completely analytical fashion, using the machinery described in chapter 1. However, in order to be able to have some computational control over the huge plethora of moduli, we have been forced to resort to supersymmetric truncations of this spectrum, either alluding to symmetries at special points of the Landscape, or to special ansatze of fluxes and field values.

Clearly, these schemes are too restrictive in order to analyze the Landscape in its full glory, and some other strategy may be required in order to account for the complexity which arises from the hundreds of moduli present in the theory. A possible course of action is to consider the Landscape to be a random function. While this idea may seem to be too simplistic in comparison with what we examined in the previous part of this thesis, it proves to be an interesting toy model in which to explore the phenomenological properties of the Landscape from a cosmological perspective. However, phenomenologically interesting scalar potentials are highly atypical in generic random landscapes. In this chapter, we will develop the mathematical techniques to generate constrained random potentials, i.e. *Slepian models*, which can globally represent low-probability realizations of the Landscape. We will give analytical as well as numerical methods to construct these Slepian models for constrained realizations of a full Gaussian random field around critical as well as inflection points. We will use these techniques to numerically generate, in an efficient way, a large number of minima at arbitrary heights of the potential and calculate their non-perturbative decay rate. Furthermore, we will also illustrate how to use these methods by obtaining statistical information about the distribution of observables in an inflationary inflection point constructed within these models.

This chapter is based on [117].

5.1 Introduction

The low energy description of many higher dimensional theories involve a large number of fields (moduli fields) that need to be stabilized. This is normally achieved by the existence of

a potential that fixes the values of these fields to a local minimum of that potential function. As we have discussed thoroughly in this thesis, a typical example of such a procedure can be found in String Theory compactification scenario, where the typical number of moduli fields in these cases is quite large, reaching often the order of a few hundred. This makes prohibitively difficult to study these potentials in detail and one is forced to look for simple models where the field space has been truncated to a small subset of fields. Alternatively, one can try to study these models by taking a more statistical approach, where the scalar potential is regarded as a random field whose sample space is the set of $4d$ low-energy effective potentials. These ideas have been pursued in relation to the study of the stability of critical points in these potentials in [46,134,171], as well as the description of cosmological models for the early universe in [102,103,174].

In many of these studies one is interested in particular points of the landscape such as, for example, a minimum with some value of its cosmological constant, or an inflection point with a particular set of conditions in its derivatives necessary for it to sustain inflation. However, depending on the restrictions imposed, it may be very difficult to obtain an example of the potential with these characteristics by producing random realizations of the scalar potential. Indeed, metastable de Sitter vacua and inflationary points compatible with observations are very rare in generic landscapes, with probabilities scaling as $P \sim \exp(-N_f^p)$, where N_f is the number of scalar fields in the theory, and $p > 0$ is a number of order one [105,108,109,123,177,218]. To obtain realizations with the desired properties, one can of course use a Taylor expansion around the point in question and take into account the probability distribution for its coefficients [106,112]. However this becomes quite complicated as one increases the number of fields and the field range that one is interested in[1]. Moreover, with this type of procedures it is not possible to capture correctly the global properties of the scalar potential, which are essential to study quantum decay processes in the landscape. Here we present a different strategy to generate these potentials that locally will be constrained to have a particular form, but that globally will still represent a faithful realization of the random landscape, the so-called *Slepian models* [219].

Several different methods have been suggested as a way to represent these random potentials in the landscape. In this work, we will concentrate on potentials described by Gaussian Random Fields (GRFs). This is based on the assumption that the $4d$ potential can be thought of as a sum of many different terms, of classical and quantum origin, coming from the compactification mechanism rendering the final result a Gaussian random field. This type of models have also been studied in connection to the distribution of vacua and its stability [178,218,220] as well as inflation [106,112–114,116] in the landscape. As an illustration of the mathematical techniques presented here for the construction of constrained GRFs we develop Slepian models that are locally described by critical points (maxima, minima and saddle points) as well as inflection points and use these realizations to extract important statistical information about them.

In particular, we will first study the quantum mechanical stability of local minima in these landscapes. In order to do so, we will compute numerically the decay rate of these minima using the quantum tunneling techniques first described in a series of papers in [67,68]. The result of this quantum instability is the creation of a bubble instanton that interpolates

[1] For another method of generating a specific class of constrained Gaussian random fields, see [116].

between the false vacuum and the true vacuum states. Using these Euclidean methods one can evaluate the probability of this decay channel and therefore estimate the lifetime of any specific vacuum. The calculation of these tunneling events in a multidimensional potential is however notoriously difficult. Recently some work on this direction has been done in relation to the stability of vacua in models with large number of dimensions in field space. It has been argued that the probability of the decay depends exponentially on the number of fields although the particular scaling is still uncertain [221–224].

In this chapter we will study these tunneling events in models of Gaussian random potentials. In particular we are interested in studying the dependence of the tunnelling rate with the height of the potential at the false vacuum. For large values of the cosmological constant this calculation would be impossible without constraining methods, since the number of these minima is negligible compared to the minima at lower values of the field. Our techniques allowed us to efficiently generate the same number of minima for different heights and have a good sample of cases from where we can extract statistical information.

Our second application involves the generation of inflection points. These are some of the most likely points in the landscape where cosmological inflation can happen. However this does not mean that an arbitrary inflection point would lead to inflation. Obtaining a successful inflationary period consistent with the current cosmological observations still requires some amount of fine tuning of the potential around the inflection point. Therefore, to characterise the distribution of observables for these inflationary models in the landscape one should again use some sort of constraining method, and look at a particular set of non-generic inflection points. In the present chapter we will explore the dependence of the observable parameters of inflation to its initial conditions in the landscape. In particular we will take the initial conditions for the fields to be the ones determined by the exit point of an instanton describing the transition from a nearby parent false vacuum. Note that in order to perform this analysis, one requires not only the knowledge of the potential around the inflection point but also its relation to nearby minima. Hence our method, which accurately captures the global statistical properties of the potential, is particularly suitable to carry out this investigation. It is worth noting that, to the best of our knowledge, this is the first time that an Slepian model for inflection points is presented in the literature. The effect of the tunneling in the initial stages of inflation has also been discussed in [87, 100, 112, 225].

The remaining of this chapter is organized as follows. In section 5.2 we introduce the notation that we will be using for describing our random potential function as a GRF. In section 5.3 we will outline the method for generating constrained random potentials as Slepian models. In section 5.4, we implement these ideas for a $2d$ field space landscape and generate a large set of random potentials with a minimum at a specific point in field space. This allows us to compute the tunneling paths from these minima and determine the statistics of the decay rate. In section 5.5, we condition the random potential to have an inflection point suitable for inflation, and study the effect of the initial conditions set by the tunneling process from a nearby minimum. We conclude in section 5.6 with some comments on the results and some further ideas that can be implemented with these numerical techniques. Some of the mathematical details and numerical proofs have been left for the appendices. In the present work, unless otherwise stated, we will use reduced Planck units $M_{\rm pl}^{-2} = 8\pi G/(\hbar c) = 1$.

5.2 Preliminaries for Gaussian Random Fields

In this chapter we will take our random potential, $V(\boldsymbol{\phi})$, to be a Gaussian random field defined over a N-dimensional field space, which we will parametrize with the vector $\boldsymbol{\phi} = \{\phi^i\}$, with $i = 1, \ldots, N$. Furthermore, we will consider the probability distribution for the random potential to be homogeneous and isotropic, so its covariance function will only depend on the distance between the points at which it is evaluated, in other words, it is of the form

$$\langle V(\boldsymbol{\phi_1}) V(\boldsymbol{\phi_2}) \rangle = C(|\boldsymbol{\phi_1} - \boldsymbol{\phi_2}|) \, . \tag{5.1}$$

We will additionally require the potential to have a null mean:

$$\langle V(\boldsymbol{\phi}) \rangle = 0 \, . \tag{5.2}$$

In the rest of this work we will evaluate our expressions using the following simple covariance function:

$$C(\boldsymbol{\phi}) = U_0^2 \exp\left(-\frac{\boldsymbol{\phi}^2}{2\Lambda^2}\right) , \tag{5.3}$$

for the case of $N = 2$ field space dimensions. The parameter U_0 sets the energy scale of the potential while Λ represents the correlation length in field space. It is important to realize that the techniques used in this work are generic and can be applied to other interesting situations like, for example, non-Gaussian covariance functions so in this sense these constructions are quite more generic than the ones presented in [116]. We have decided to use the simple Gaussian covariance function since it considerably simplifies some of the expressions in this chapter.

In the following we will be interested in the value of the field and its derivatives at a particular point in field space, which we can take to be $\boldsymbol{\phi} = 0$ without loss of generality, and we will refer to it as the center of field space. Following [106, 112], let us introduce the following definitions for the value of the potential and its derivatives:

$$u = V(\boldsymbol{\phi})|_{\boldsymbol{\phi}=\mathbf{0}}, \quad \eta_i = \left.\frac{\partial V(\boldsymbol{\phi})}{\partial \phi^i}\right|_{\boldsymbol{\phi}=\mathbf{0}}, \quad \zeta_{ij} = \left.\frac{\partial^2 V(\boldsymbol{\phi})}{\partial \phi^i \partial \phi^j}\right|_{\boldsymbol{\phi}=\mathbf{0}}, \quad \rho_{ijk} = \left.\frac{\partial^3 V(\boldsymbol{\phi})}{\partial \phi^i \partial \phi^j \partial \phi^k}\right|_{\boldsymbol{\phi}=\mathbf{0}} .$$

Furthermore, we will denote the eigenvalues of the Hessian matrix by λ_i with $i = 1, 2$ which will single out the directions 1, 2 in our field space. Note that the derivatives of the scalar potential are also Gaussian random variables, and therefore any collection of the previous quantities forms a Gaussian random vector. In appendix E.4 we will give the expressions for the correlators between these different derivatives of the potential as a function of the derivatives of the covariance function $C(\boldsymbol{\phi})$. These correlations will play an important role in some parts of our discussions.

5.3 Slepian Models for constrained Gaussian random fields

A key point in our construction of the GRF rests on the fact that a conditioned GRF maintains its Gaussian nature. More specifically, homogeneous and isotropic processes (such as the GRFs we are dealing with) can be conditioned using the Kac-Rice formula [226] in order to obtain new mean and covariance functions which generate GRFs with the required constraints.[2] The models for stochastic processes dealing with conditional events and crossings were pioneered by David Slepian [219], and have thus been coined in the mathematical literature as *Slepian models*.

We can describe these constrained processes in a generic form in the following way. For simplicity, let us consider first a Gaussian random p-dimensional vector, composed of jointly Gaussian variables, $\boldsymbol{x}^T = (x_1, \ldots, x_p)$, whose probability distribution function (PDF) is given by,

$$f(\boldsymbol{x}) = \frac{1}{(2\pi)^{p/2}\sqrt{\det \Sigma}} \exp\left[-\frac{1}{2}(\boldsymbol{x}-\boldsymbol{\mu})^T\, \Sigma^{-1}\, (\boldsymbol{x}-\boldsymbol{\mu})\right] \tag{5.4}$$

where $\mu = \langle \boldsymbol{x} \rangle$ is the mean *vector* and Σ is the *covariance matrix*, whose elements are given by

$$\Sigma_{ab} = \big\langle (x_a - \mu_a)(x_b - \mu_b) \big\rangle . \tag{5.5}$$

with $a, b = 1, \ldots, p$.

Let us now consider the following decomposition of the random vector $\boldsymbol{x} = (\boldsymbol{x_1}, \boldsymbol{x_2})$, where $\boldsymbol{x_2}$ are p_c components of the vector $\boldsymbol{x}$ that will be constrained by a condition $\boldsymbol{x_2} = \tilde{\boldsymbol{x}}$, and $\boldsymbol{x_1}$ are the remaining $p - p_c$ unconstrained elements. One can show [170, 226] that the distribution probability for $\boldsymbol{x_1}$ holding $\boldsymbol{x_2}$ fixed to the desired values is given by,

$$\tilde{f}(\boldsymbol{x}_1 | \boldsymbol{x}_2 = \tilde{\boldsymbol{x}}) = \frac{1}{(2\pi)^{\frac{p-p_c}{2}}\sqrt{\det \tilde{\Sigma}}} \exp\left[-\frac{1}{2}\left(\boldsymbol{x}_1 - \tilde{\boldsymbol{\mu}}\right)^T \tilde{\Sigma}^{-1} \left(\boldsymbol{x}_1 - \tilde{\boldsymbol{\mu}}\right)\right], \tag{5.6}$$

which shows that the distribution for the variables $\boldsymbol{x_1}$ is indeed a Gaussian distribution but now with a mean and covariance functions given in terms of the original ones as

$$\tilde{\boldsymbol{\mu}} = \boldsymbol{\mu}_1 + \Sigma_{12}\Sigma_{22}^{-1}(\tilde{\boldsymbol{x}} - \boldsymbol{\mu}_2) \qquad , \qquad \tilde{\Sigma} = \Sigma_{11} - \Sigma_{12}\Sigma_{22}^{-1}\Sigma_{21} \, , \tag{5.7}$$

where $\boldsymbol{\mu_1}$ and $\boldsymbol{\mu_2}$ are the means of the vectors $\boldsymbol{x_1}$ and $\boldsymbol{x_2}$ respectively, and

$$\begin{aligned} \Sigma_{11} &= \big\langle (\boldsymbol{x_1} - \boldsymbol{\mu_1})(\boldsymbol{x_1} - \boldsymbol{\mu_1}) \big\rangle , \\ \Sigma_{12} &= \Sigma_{21} = \big\langle (\boldsymbol{x_1} - \boldsymbol{\mu_1})(\boldsymbol{x_2} - \boldsymbol{\mu_2}) \big\rangle , \\ \Sigma_{22} &= \big\langle (\boldsymbol{x_2} - \boldsymbol{\mu_2})(\boldsymbol{x_2} - \boldsymbol{\mu_2}) \big\rangle . \end{aligned} \tag{5.8}$$

This is possible because one can always find a new Gaussian random vector $\boldsymbol{x}' = (\boldsymbol{x}'_1, \boldsymbol{x}'_2)$, connected to the original one with a non-singular linear transformation $\boldsymbol{x}' = A \cdot \boldsymbol{x}$, such that $\boldsymbol{x}'_2 = \boldsymbol{x_2}$ is uncorrelated to $\boldsymbol{x}'_1$. We show in appendix E.2 a proof of this statement. In the rest of the chapter we will use this fact in several different ways, applying this technique for

[2] See a brief description of the Kac-Rice formula in the current context in appendix E.5.

Gaussian random vectors made of different quantities of our potential.

5.3.1 *Slepian models for critical points*

In this section we will use the methods described earlier to generate a Gaussian random field with a critical point with a specific height at the center, $\boldsymbol{\phi} = \mathbf{0}$. In other words, we will find a description of the new GRF conditioned so that the point at its center satisfies the following properties: $V(\mathbf{0}) = u$ and $V_i'(\mathbf{0}) = \eta_i = 0$ for $i = 1,2$. In order to do this we will follow the prescription used in the mathematical literature for maxima in GRF [227] and adapt it to our case. Let us start by introducing the following Gaussian random vector:

$$\boldsymbol{x} = \{V(\boldsymbol{\phi}_1), \ldots, V(\boldsymbol{\phi}_q), V(\mathbf{0}), \eta_1, \eta_2, \zeta_{11}, \zeta_{22}, \zeta_{12}\} \tag{5.9}$$

where we denote by $\boldsymbol{\phi}_a$, with $a = 1, \ldots, q$, the position in field space of a discrete set of q points. One can show that the Gaussian random vector $\boldsymbol{x}$ has zero mean, and a probability distribution that can be readily computed using the form of the covariance function and its derivatives. This is a somewhat lengthy calculation and we have given the general expression in appendix E.6. According to the description for constrained Gaussian random vectors given above this is all we need to obtain the new mean and covariance function for the new conditioned vector (and thus, also for the constrained GRF).

Using the results in appendix E.6, one can show that the new mean function for the GRF with the constrained conditions is given by,

$$\tilde{\mu}(\boldsymbol{\phi}) = e^{-\frac{\boldsymbol{\phi}^2}{2\Lambda^2}} \left[u\left(1 + \frac{\boldsymbol{\phi}^2}{2\Lambda^2}\right) + \frac{1}{2}\sum_{i=1}^{2} \phi_i^2 \lambda_i \right]. \tag{5.10}$$

This result corresponds to the particular choice of covariance function in eq. (5.3), and is written in terms of the the value of the field $V(\mathbf{0}) = u$ and the eigenvalues of the Hessian matrix at the center, λ_i, which are to be drawn from the distribution in eq. (5.12) below. The new covariance function is

$$\tilde{C}(\boldsymbol{\phi_1}, \boldsymbol{\phi_2}) = U_0^2 \exp\left[-\frac{|\boldsymbol{\phi_1}|^2 + |\boldsymbol{\phi_2}|^2}{2\Lambda^2}\right] \left(\exp\left[\frac{\boldsymbol{\phi_1}\cdot\boldsymbol{\phi_2}}{\Lambda^2}\right] - 1 - \frac{\boldsymbol{\phi_1}\cdot\boldsymbol{\phi_2}}{\Lambda^2} - \frac{(\boldsymbol{\phi_1}\cdot\boldsymbol{\phi_2})^2}{2\Lambda^4} \right), \tag{5.11}$$

which is no longer homogeneous, but it is still isotropic.

It is important to note that the eigenvalues of the Hessian are not statistically independent of the height of the potential. This is intuitively clear since, for example, one would expect the typical minimum at a large height to be quite shallow compared to the minima situated well bellow the mean value of the potential. This expectation can be translated to the existence of important correlations between the field and its second derivatives at a point, and in particular at critical points. In order to take this effect into account one can calculate the joint probability distributions for the Hessian eigenvalues (λ_i) and heights (u) at critical

points to obtain[3]

$$P_{u,\lambda}\, du \prod_i d\lambda_i = \mathcal{N} \exp\left[-\frac{u^2}{2U_0^2}\right] |\lambda_1 - \lambda_2| \prod_{i=1}^{2} |\lambda_i| \exp\left[-\left(\frac{\Lambda^2 \lambda_i + u}{2U_0}\right)^2\right] d\lambda_i\, du\,, \tag{5.12}$$

where $\mathcal{N}$ is a normalizing constant. This distribution includes all types of critical points, namely maxima, minima and saddle points. Depending on the kind we are interested in, we simply need to impose positivity or negativity conditions on the values of each λ_i.

Using these results we can generate a Gaussian random field with a critical point with the desired properties by the following procedure. Let us consider for example a minimum with fixed height u. Our first step will be to generate a set of eigenvalues drawn from the distribution (5.12) taking into account the value of u, imposing the non-negativity condition $\lambda_i \geq 0$, and fixing the normalization factor accordingly.

Using these values for λ_i we can then generate realizations of the potential using the expression

$$V(\boldsymbol{\phi}) = e^{-\frac{\boldsymbol{\phi}^2}{2\Lambda^2}} \left[u\left(1 + \frac{\boldsymbol{\phi}^2}{2\Lambda^2}\right) + \frac{1}{2}\sum_{i=1}^{2} \phi_i^2 \lambda_i \right] + \Delta(\boldsymbol{\phi}) \tag{5.13}$$

where we have denoted by $\Delta(\boldsymbol{\phi})$ an inhomogeneous, zero-mean Gaussian random field whose covariance function is given by $\tilde{C}(\boldsymbol{\phi_1}, \boldsymbol{\phi_2})$ in eq. (5.11). We show in fig. 5.1 an example of the different ingredients that make up a Slepian model for a local minimum in a $1d$ GRF. We can use a similar procedure to generate other critical points, such as saddle points with different number of negative eigenvalues, by generating the appropriate samples of λ_i's.

An important conclusion that can be derived from the Slepian model (5.13), first noticed in [227], is that for highly non-generic extrema $|u| \gg U_0$ (such as very low maxima or high minima), the shape of this GRF becomes very deterministic around the critical point, and it is described very accurately by the first two terms in eq. (5.13). Indeed, one can see from eq. (5.11) that the standard deviation of the random component $\Delta(\boldsymbol{\phi})$ is always smaller than U_0, and that it approaches zero near the extremum located at $\boldsymbol{\phi} = \mathbf{0}$ (see also fig. 5.1). Therefore the last contribution in (5.13) can be neglected in a neighbourhood of the extremum where $|\Delta(\boldsymbol{\phi})| \lesssim U_0 \ll |V(\mathbf{0})|$ holds. On the other hand, in the limit $|u| \gg U_0$ the eigenvalue distribution of the Hessian (5.12) is approximately given by[4]

$$P_\lambda\, d\lambda_1\, d\lambda_2 \sim |\lambda_1 - \lambda_2||\lambda_1||\lambda_2| \exp\left[-\frac{\Lambda^2 |(\lambda_1 + \lambda_2)u|}{2U_0^2}\right] d\lambda_1\, d\lambda_2\,, \tag{5.14}$$

which indicates that in this limit the magnitude of the eigenvalues is very suppressed $|\lambda_i| \ll U_0/\Lambda^2$. Then, as we mentioned above, for highly non-generic extrema the decomposition (5.13) is dominated by its deterministic part (the first term), what makes these Slepian models very predictive in those situations. As we shall see bellow, this result is particularly important when we consider the distribution of non-perturbative decay rates from minima with a

[3] See the calculation in appendix E.6.

[4] Note that for very high minima $u > 0$ and $\lambda_i > 0$, while for very low maxima all signs are reversed.

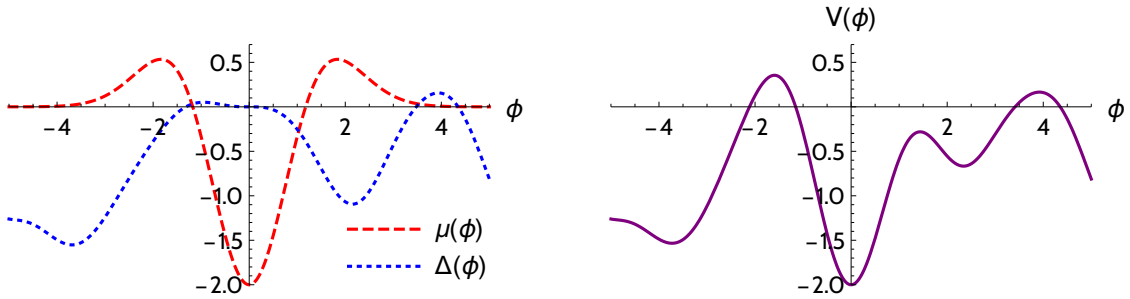

Figure 5.1: A 1d example of a Slepian model of a constrained minimum in a GRF. We show, for a particular realization, the two separate components of the construction on the left, namely, the constrained mean field form $\mu(\phi)$ in eq. (5.10) and the inhomogenous new GRF $\Delta(\phi)$ with covariance function given by eq. (5.11). The total GRF is shown on the right.

large vacuum energy. For an example of a realization with a high minimum see figure 5.2(a).

This deterministic character of large fluctuations of Gaussian Random Fields plays an important role in various areas of Cosmology, such as the analysis of the CMB data, and the study of Large Scale Structure formation in the universe (see e.g. [228–232]).

5.3.2 *Slepian models for inflection points*

As we discussed in the Introduction, we are also interested in inflection points in the landscape. The reason is that in a cosmological context these points could be one of the regions of the potential that give rise to a cosmological inflationary period. However, in order to be compatible with the latest cosmological observations, one needs to restrict the form of these inflection points. This leads us to consider an inflection point at $\boldsymbol{\phi} = 0$ as a realization of the GRF with a small gradient of the potential in the ϕ_1 direction, denoted by η_1, and the rest of the coefficients of the Taylor expansion of the field around that point of the form

$$\eta_2 = 0 \quad , \quad \lambda_1 = 0 \quad , \quad \lambda_2 > 0 \quad , \quad \eta_1 \cdot \rho_{111} > 0 \, . \tag{5.15}$$

The intuitive picture of these choices is clear, we are looking for a one dimensional inflection point that allows the slow-roll conditions to be satisfied along the direction ϕ^1 while the perpendicular directions have positive curvature. In other words, we are looking for a potential where inflation is effectively one dimensional locally. This also explains the last condition, which is imposed in order to allow for enough slow-roll inflation in the vicinity of this inflection point.

This is admittedly a very particular form of the potential around the inflection point and, even though it could be interesting to identify this type of points in a GRF in other contexts, we have not seen any studies of this class of constrained points on GRFs in the mathematical literature. However, it is not difficult to follow a similar procedure to the one for critical points in order to obtain Slepian models in this case. The first thing we should do is to enlarge the form of our initial Gaussian random vector (5.9), since we now want to constrain not only first derivatives but second derivatives as well. This suggests that we

should take the vector of the form,

$$\boldsymbol{x} = \{V(\boldsymbol{\phi}_1), \dots, V(\boldsymbol{\phi}_q), V(\mathbf{0}), \eta_1, \eta_2, \zeta_{11}, \zeta_{22}, \zeta_{12}, \rho_{111}, \rho_{122}, \rho_{222}, \rho_{112}\} \tag{5.16}$$

which, similarly to the critical point case, can now be conditioned to have the desired properties given in eq. (5.15).

Following the computations given in the appendix E.7 one arrives to the result that a GRF with an inflection point at $\boldsymbol{\phi} = \mathbf{0}$ is described by the expression

$$V(\boldsymbol{\phi}) = \exp\left[-\frac{\boldsymbol{\phi}^2}{2\Lambda^2}\right]\left((u + \boldsymbol{\phi}\cdot\boldsymbol{\eta})\left(1 + \frac{\boldsymbol{\phi}^2}{2\Lambda^2}\right) + \frac{1}{2}\sum_{i=1}^{2}\lambda_i {\phi_i}^2 + \frac{1}{6}\sum_{i,j,k=1}^{2}\phi_i\phi_j\phi_k\rho_{ijk}\right) + \Gamma(\boldsymbol{\phi})\,, \tag{5.17}$$

where $\Gamma(\boldsymbol{\phi})$ is an inhomogeneous zero-mean GRF with covariance function

$$\tilde{C}(\boldsymbol{\phi_1}, \boldsymbol{\phi_2}) = U_0^2 \exp\left[-\frac{|\boldsymbol{\phi_1}|^2 + |\boldsymbol{\phi_2}|^2}{2\Lambda^2}\right]\left(\exp\left[\frac{\boldsymbol{\phi_1}\cdot\boldsymbol{\phi_2}}{\Lambda^2}\right] - 1 - \frac{\boldsymbol{\phi_1}\cdot\boldsymbol{\phi_2}}{\Lambda^2} - \frac{(\boldsymbol{\phi_1}\cdot\boldsymbol{\phi_2})^2}{2\Lambda^4} - \frac{(\boldsymbol{\phi_1}\cdot\boldsymbol{\phi_2})^3}{6\Lambda^6}\right). \tag{5.18}$$

In these expressions u, λ_i and ρ_{ijk} should be drawn from the joint probability distribution for heights, first, second and third derivatives of the potential at inflection points[5]

$$P_{\rm inf}\, du\, d\lambda_2\, d\eta_1\, d\boldsymbol{\rho} = \mathcal{N}|\lambda_2|^2|\rho_{111}|\; P(u, \lambda_2 \mid \lambda_1 = 0)\; P\left(\eta_1, \rho_{ijk} \;\middle|\; \eta_2 = 0\right)\, du\, d\lambda_2\, d\eta_1\, d\boldsymbol{\rho} \tag{5.19}$$

where

$$P(u, \lambda_2 \mid \lambda_1 = 0)\; du\, d\lambda_2 = \mathcal{N}|\lambda_2| \exp\left[-\frac{4u^2 - 2\Lambda^2 u\lambda_2 - \Lambda^4\lambda_2^2}{2U_0}\right]\, du\, d\lambda_2,$$

$$P\left(\eta_1, \rho_{ijk} \;\middle|\; \eta_2 = 0\right)\, d\eta_1\, d\rho_{ijk} =$$

$$\mathcal{N} \exp\left[-\frac{\Lambda^2}{12U_0^2}\left(18\eta_1^2 + 6\Lambda^2\eta_1(\rho_{111} + \rho_{122}) + \Lambda^4\sum_{i,j,k=1}^{2}\rho_{ijk}^2\right)\right]\, d\eta_1\, d\rho_{ijk}\,. \tag{5.20}$$

In the last distribution, the condition $\eta_1 \cdot \rho_{111} > 0$ should also be imposed if one is interested in 'inflationary' inflection points.

We have checked the accuracy of these distributions by numerically computing them from a large set of generic (unconstrained) GRF examples. We have identified all the inflection points of our sample, and used this information to compute the distributions of the parameters of the inflection points we are interested in. See appendix F for the details of these numerical checks, which are summarised in figure F.2.

[5] See the computation of these distributions in appendix E.7.

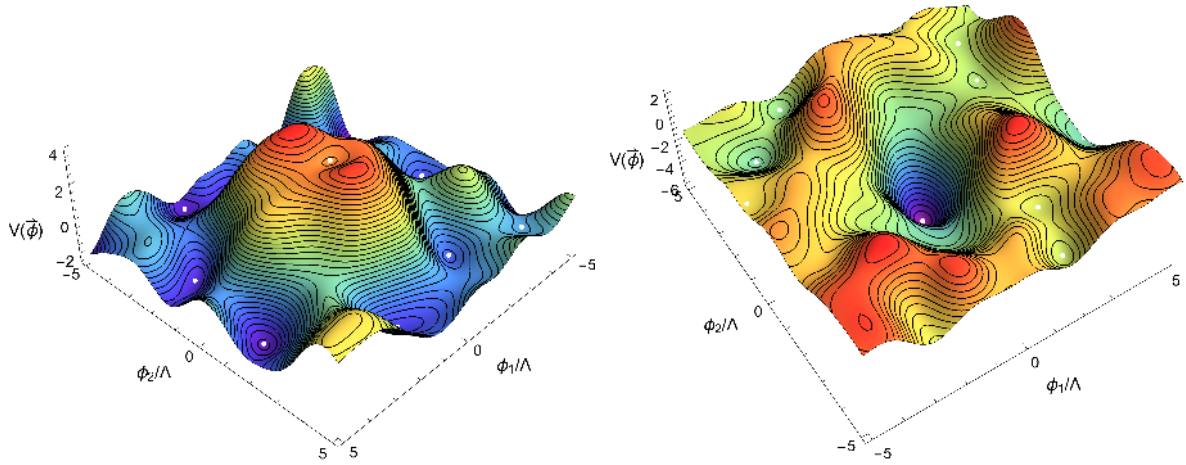

Figure 5.2: A pair of realizations of a 2d Gaussian random fields with zero mean, covariance function (5.3), and conditioned to have a minimum at center of height (in units of U_0) 4 (a) and -4 (b). The higher the minimum is, the lower its eigenvalues will typically be and vice versa (see text). The location of the minima of each realization has been marked with a white dot.

5.3.3 2D numerical implementation

All GRFs generated for this work were constructed following the Karhunen-Love expansion (see e.g. [170]), which is briefly described in appendix F. This algorithm generates values for a GRF discretized over a lattice which is to be interpolated afterwards.

Based in the criteria developed in [112], we used 5 lattice points per correlation length (25 per length squared). The resulting grid was then interpolated with fourth-order splines in order to analyse up to third-order derivatives of the field as faithfully as possible. The generated GRFs were found to follow successfully the initial mean and covariance function, as well as other properties such as the distribution of critical points and eigenvalues thereof.

Two examples of (rather extreme) GRFs generated following the steps in this section have been plotted in figure 5.2.

5.4 Tunneling in a Gaussian random landscape

A Gaussian random landscape possesses a large number of perturbatively stable minima. However, we know that quantum mechanically these vacua are not completely stable and can decay by the nucleation of a bubble of the new state. This means that a typical vacuum in our landscape will have many channels to decay into, each of them with a different probability. Here we would like to study the statistics of these decay channels in a controlled way by generating a large number of GRF realizations, and analyse their dependence on the parameters of the central minimum.

In order to do that we will use the instanton techniques described in section 1.5, where it was shown that for a given minimum of the potential the decay probability per unit time

and per unit volume is given by

$$\Gamma/V \sim Ae^{-S_E} \tag{5.21}$$

where S_E is the Euclidean action for the bounce solution that interpolates between the new state and the original one.[6]

In the absence of gravity, we found that the most likely decay channel is given by the $O(4)$-symmetric instanton solution in a 4-dimensional Euclidean spacetime; more concretely, the formalism we studied in the introductory chapter can be generalized to involve an arbitrary number of scalar fields. The equations of motion are then given by

$$\phi_i'' + \frac{3}{r}\phi_i' = \frac{\partial V(\boldsymbol{\phi})}{\partial \phi_i}\,, \tag{5.22}$$

where the prime denotes a derivative with respect to the radial coordinate in 4-dimensional Euclidean spacetime, r, and we have assumed that the fields $\boldsymbol{\phi}(r) = \{\phi^1(r), \ldots, \phi^N(r)\}$ are canonically normalized. Finally the boundary conditions are

$$\boldsymbol{\phi}(\infty) = \boldsymbol{\phi}_{FV} \qquad , \qquad \phi_i'(0) = 0. \tag{5.23}$$

where $\boldsymbol{\phi}_{FV}$ is the location of the false vacuum in field space, the minimum of the potential from which the decay happens. Once the field equations have been solved, the action in the exponent of (5.21) reads

$$S_E = 2\pi^2 \int_0^\infty dr\; r^3 \left[\frac{1}{2}|\boldsymbol{\phi}'|^2 + V(\boldsymbol{\phi}) - V(\boldsymbol{\phi}_{FV})\right]\,. \tag{5.24}$$

Computing the coupled system of the instanton equations (5.22) is no easy task; particularly, as the dimensionality of the field space grows, the solutions tend to be increasingly unstable. There are, however, several publicly available algorithms in the literature to tackle the problem (see, e.g., [77, 233]); additionally, some alternative methods have been recently proposed to find the action and escape point for the instanton, as in [234, 235].

In this work, we use AnyBubble [76] to compute the instanton actions for our realizations. AnyBubble is a Mathematica Package based on efficient numerical methods for the solution and optimization of the tunneling equations, see [76] for details.

In order to obtain statistics of the tunneling action in terms of the properties of the central minimum, we sampled false vacua with heights between -2 and 5 (in units of U_0, see eq. (5.3)) in uniform intervals. As explained in [112], we can write the Euclidean action as

$$S_E = \frac{\Lambda^4}{U_0}\bar{S} \tag{5.25}$$

so that $\bar{S}$ corresponds to the Euclidean action of a potential with covariance function (5.3) with $U_0 = \Lambda = 1$. Unless otherwise specified, all histograms corresponding to the action are given in terms of $\bar{S}$ due to numerical simplicity.

Following the procedure of the Slepian models described the previous sections, for each

[6] Here we will not be concerned with the prefactor A. See [68] for a detailed description of its computation.

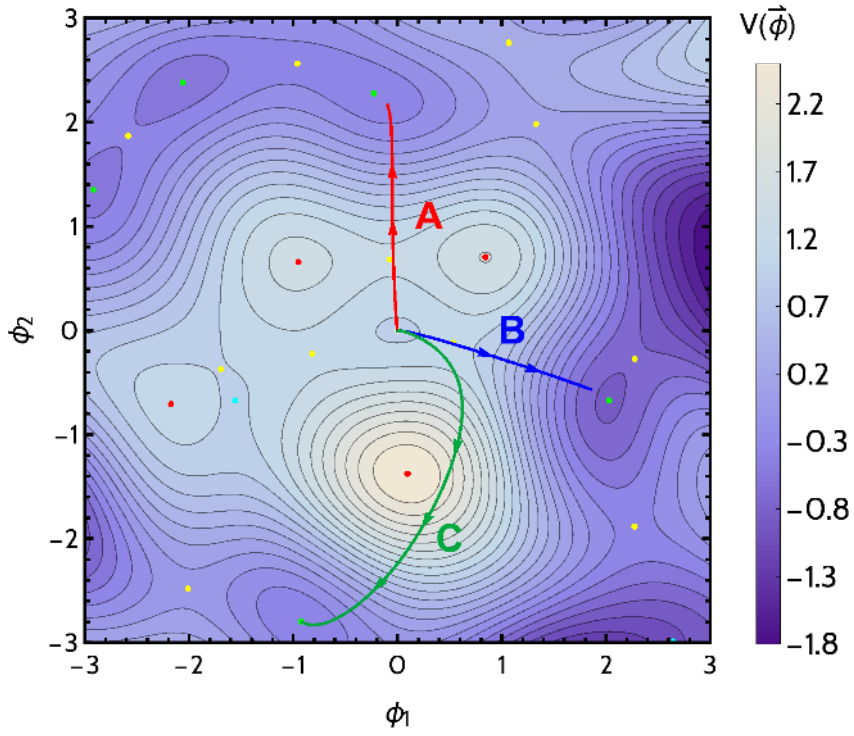

Figure 5.3: A typical example of the considered tunneling events. After generating a GRF with a minimum at the center with height 1 (in terms of U_0), we compute possible tunnelings with AnyBubble. The plot shows the GRF along with its minima (green), saddles (yellow), maxima (red) and inflection points (blue) as well as 3 of the instanton trajectories in field space for 3 decay channels.

value of the false vacuum height, we generated $2 \cdot 10^4$ Gaussian random field realizations centered around the minimum. All of these minima have the correct distribution of the Hessian eigenvalues, and the potentials are quite different from one another as one moves away from the minimum by one correlation length. This means that each realization has different vacua situated in different directions and lengths from the false vacuum, although the typical number of minima below $V(\boldsymbol{\phi}_{FV})$ is quite similar in all cases.

We can readily see the power of the machinery described in the previous section when constraining the field to have a minimum with a vacuum energy higher than $1.5U_0$. If we tried to find a minimum higher than that drawing samples from an unconstrained GRF, we would need to generate tens (if not hundreds) of random fields before finding a single minimum satisfying that condition, see figure F.1(a) in appendix F. For example, from equations (F.5), we can easily check that the probability of any minimum being higher than $5U_0$ is $\mathcal{O}(10^{-16})$, so finding one by chance happens to be quite remarkable. With the aid of conditioning methods, we are able to construct very efficiently large samples of random fields subject to a condition as difficult to meet as this one.

In order to study tunneling processes on each generated example, we identified all the minima near the center of field space and computed the tunneling rate between the central minimum (which always acts as a false vacuum, in our analysis) to all lower minima. An example of this procedure is plotted in figures 5.3 and 5.4, where we show the paths followed in field space by the different instanton decay channels. We have only considered

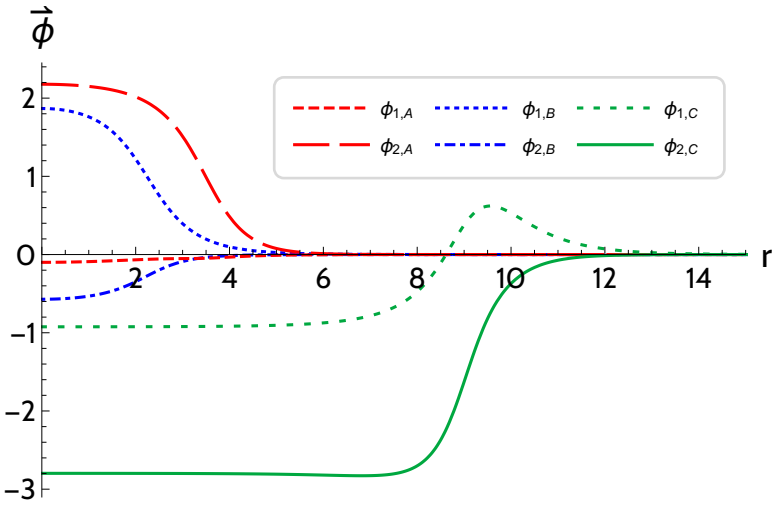

Figure 5.4: Field trajectories for the decays channels shown in fig. (5.3) in terms of the distance r in Euclidean space.

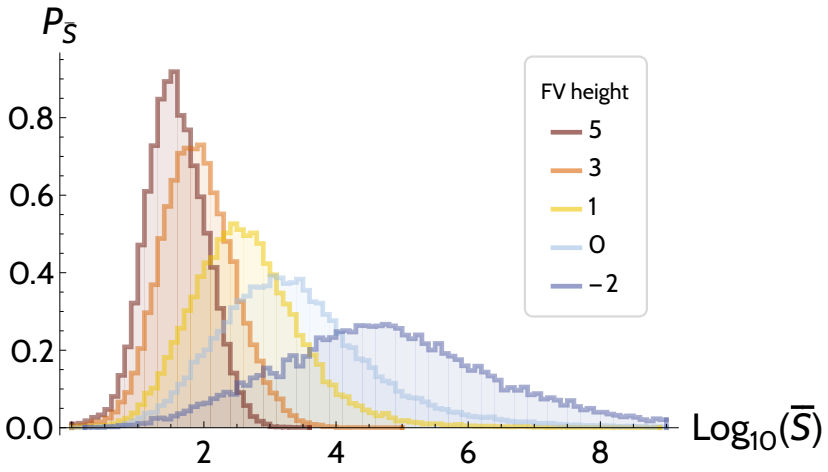

Figure 5.5: Obtained distribution of tunneling action ($\bar{S}$) in terms of false vacuum height.

tunneling to minima around the center to avoid problematic issues with minima close to the boundaries of our realizations.

5.4.1 Statistics of the instanton action

Dependence with the height

Figure 5.5 shows the resulting distributions[7] for the tunneling action, for different values of the false vacuum height. There is an interesting correlation between the mean and width of this distribution and the height of the false vacuum. Namely, we find that the higher the false vacuum is the lower the action and thus, the higher the probability of tunneling is. This behaviour is quite intuitive; as we can see from the examples in fig. 5.2, tunneling from a minimum high up in field space requires crossing a lower barrier to the true vacuum, which

[7] Unless otherwise specified, all histograms represent the normalized probability distribution function of the obtained results.

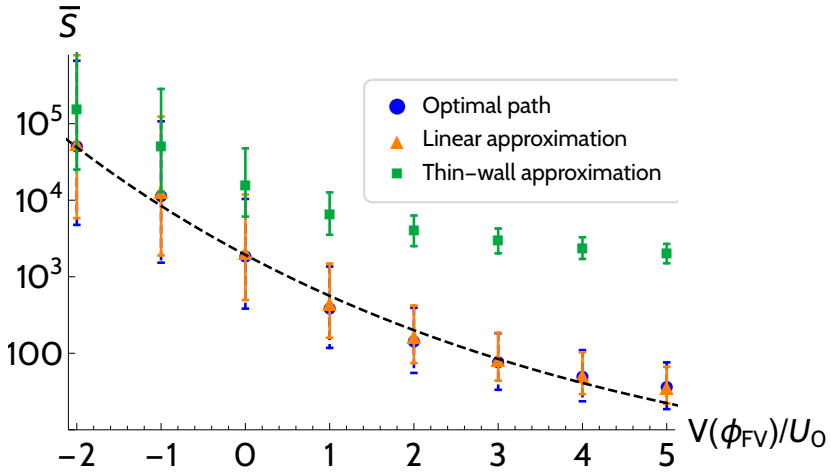

Figure 5.6: Evolution of the median of the action, with error bars representing data between the first and third quartiles of each distribution, for the optimal path, the linear (straight-path) and the thin wall approximations, along with a fitting curve (see (5.26)).

in turn results in a lower action for those transitions. Figure 5.6 (blue dots) shows the median of each distribution along with the range of actions between the first and third quartiles. We see, once again, that higher false vacua lead to lower and more deterministic values of the action.

The obtained data for each potential height was found to be easily fitted to a log-normal distribution. More specifically, the logarithm of the median of each distribution $\bar{S}_{\text{med}}$ (which, in this case, is very similar to the mean of $\log_{10}\bar{S}$) can be fitted by the following expression

$$\left\langle \log_{10}\bar{S}_{\text{med}} \right\rangle \approx 3.29\exp\left(-0.18\frac{V_{\text{fv}}}{U_0}\right) \tag{5.26}$$

where V_{fv} stands for the height of the false vacuum. As we see from figure 5.6, increasing V_{fv} reduces the width of the distribution significantly, thus increasing the predictive power of (5.26) for the expected value of the action. This enhancement of the predictability of the Slepian model for large values of V_{fv} corresponds precisely to what we anticipated in the previous section. Indeed, there we showed that near high minima the random potential becomes dominated by the first term in the decomposition (5.13), and therefore the landscape is very deterministic in a neighbourhood of false vacua with large V_{fv}. Consistent with this result, when studying the non-perturbative stability from these vacua we observe a reduction of the variance of tunneling actions for large heights of the false vacuum. This agreement also suggests that in the case of minima with a large V_{fv} the value of the instanton action is dominated by the local structure of the minimum. We will provide further evidence for this claim below.

5.4.2 *Approximations for the calculation of the action*

Due to the inherent instability of the equations to be solved to compute tunneling profiles, it is clear that as we increase the domain and dimensionality of the potential under study, the required computational time to solve the system will grow accordingly. Evidently,

this makes the study of higher-dimensional GRFs and their tunneling properties almost prohibitive in this sense. Motivated by these limitations, we turn to computing several different approximations of tunneling actions suggested in the literature, and compare them with our exact results.

Thin wall approximation

The thin-wall prescription was already discussed in the original papers by Coleman in [67]. In this approximation the instanton action is given in terms of the difference between potential at the false vacuum ($V_{\rm fv}$) and true vacuum ($V_{\rm tv}$) and σ, the tension of the wall interpolating between them, namely,

$$\bar{S}_{\rm tw} = \frac{27\pi^2\sigma^4}{2(V_{\rm fv}-V_{\rm tv})^3}, \qquad \sigma = \int_{\boldsymbol{\phi}_{TV}}^{\boldsymbol{\phi}_{FV}} d\phi\, \sqrt{2(V(\boldsymbol{\phi})-V(\boldsymbol{\phi}_{TV}))}\,. \tag{5.27}$$

This approximation is accurate as long as the difference between $V_{\rm fv}$ and $V_{\rm tv}$ is small.

We evaluated (5.27) for each bounce we previously found with AnyBubble in order to check this expression and its predictive power for GRFs. In the computation we restricted the field to a straight line in field space connecting the true and false vacua. Figure 5.6 shows the evolution of the median of $\bar{S}_{\rm tw}$ as a function of the false-vacuum height. While the width and median of the distribution in this case follow the same pattern as the optimal action, the values diverge rapidly from the optimal ones as the false vacuum height increases. This is not too surprising since, as one increases the height of the false vacuum minimum, the field can tunnel to a minimum with quite different values of the potential, what violates one of the premises of the thin wall approximation.

Straight-path approximation

While the thin-wall prescription provides a solid upper bound on the bounce action [236], it does not provide any useful estimation on the actual value on the bounce in our case. This fact calls for an alternative way to estimate the action, mostly for higher-dimensional landscapes.

A straightforward simplification to this problem was introduced in [237], which we will denote by *straight-path approximation*. This prescription is based on reducing the field space to a single straight line connecting the false and true vacua, thus making the problem of tunneling effectively one-dimensional. As can be seen from figure 5.3, this approximation may not be too unreasonable. Even though there are some paths which do curve over the field space, many (if not most) of them follow a straight trajectory in field space. Note, however, that this restriction in field space may yield effective potentials where the bounce does not exist or might even correspond to a different bounce in the full theory. For more details on the properties of this approximation, see [79].

For each optimal path, we considered a straight line in the two-dimensional GRF connecting the true and false vacua, and computed the corresponding estimate of the action, $\bar{S}_{\rm sp}$, in each case. In principle, $\bar{S}_{\rm sp}$ represents an upper bound on the optimal action $\bar{S}$, as the former only considers variations of the action in the direction of the straight path [237]. It is

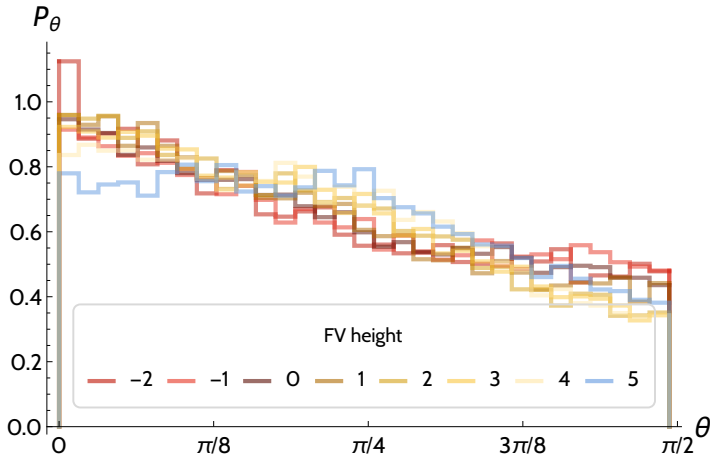

Figure 5.7: Exit angle distribution with respect to direction of the lowest eigenvalue for the instanton path of the most probable decay channel in each generated potential.

thus expected (and explicitly shown in [79]) that this approximation will diverge from the full solution as the dimensionality of the potential is increased.

We found that in this case the distribution of actions in terms of false vacuum height is identical to the optimal one shown in fig. 5.5, though slightly shifted to higher values. As we can see from fig. 5.6, the change in the median is minimal when the straight-path approximation is considered. Although, as we just mentioned, the straight-path approximation is not expected to give precise results for potentials in a higher field space dimension, this result suggests that it would be interesting to explore the validity of this method with GRFs in higher dimensions. Indeed, due to the computational complexity of such an analysis, a rough statistical estimate of the decay rate obtained with this approximation would still be very valuable.

5.4.3 *The lowest action*

In many circumstances one will be interested in the lowest action for a particular kind of minima. This will of course correspond to the path that would dominate the decay for those minima. In this subsection we will investigate the characteristics of such trajectories in field space.

Exit angle

An intuitive way to think about the most likely decay process would be to imagine that the tunneling occurs along the trajectory with the lowest barrier. One can check this idea in our case by first identifying the angle (in our $2d$ field space), θ, that the instanton trajectory makes with respect to the direction of the lowest eigenvalue of the Hessian at the minimum. A distribution of such angles obtained for different values of the height is plotted in figure 5.7. We see that there is a clear tendency of the tunnelings to occur around $\theta \approx 0$ but the correlation is not very strong.

Estimating the lowest action

The correlation of the instanton path with the lowest eigenvalue direction at the false vacuum suggests that one can try to estimate the lowest action by analyzing the potential along the lowest eigenvalue direction alone. This has been recently proposed in the context of the landscape in [224]. In the following we will use our large sample of realizations to test this idea in detail in our $2d$ GRF model of the landscape.

In order to evaluate the instanton action along the lowest eigenvalue direction we first take a slice of the potential along that direction and fit it to be of the form,

$$V_{le}(\phi_1) = V_0 + \frac{1}{2}\lambda_1\phi_1^2 + \frac{1}{3!}\rho_{111}\phi_1^3 + \frac{1}{4!}\delta\phi_1^4 \,. \tag{5.28}$$

Note that this procedure does not guarantee that the resulting one-dimensional potential is suitable for a tunneling process. In fact, in many cases the potential constructed this way does not have a lower minimum along this direction and therefore it cannot be used to estimate the decay rate. In the following we will only compute the instanton action in the successful cases where this $1d$ truncation gives an acceptable form.

Considering this simple form of the potential as the most likely exit path for the decay transition we can estimate the instanton action. In order to do that we will use the parametrization of the Euclidean action for the bounce that was obtained by Sarid in [80]. In our notation this becomes,

$$\bar{S}_S = \begin{cases} \frac{18\lambda_1}{\rho 111^2}\left(45.4 - 46.1 + \frac{2\pi^2}{12(1-4\kappa)^3} + \frac{16.5}{(1-4\kappa)^2} + \frac{28}{1-4\kappa}\right), & \kappa > 0 \\ \frac{18\lambda_1}{\rho 111^2} 45.4\left(1 + (\frac{136.2}{2\pi^2})^{1.1}|\kappa|^{1.1}\right)^{-1/1.1}, & \kappa \leq 0 \end{cases} \tag{5.29}$$

where

$$\kappa = \frac{3}{4}\delta\frac{\lambda_1}{\rho_{111}^2} \,. \tag{5.30}$$

We show in figure 5.8 the distributions of the lowest action from the exact computation and compare it to this estimate along the lowest barrier direction. We notice that the agreement between these two results is pretty good, what suggest that one can use this approximation to estimate the decay rate of vacua in a Gaussian random landscape. Moreover, it is worth noting that this approximation depends only on the local structure of the minimum, precisely where the Slepian model has a large predictive power for large values of $V_{\rm fv}$. The expression (5.29) becomes increasingly accurate for large values of the false vacuum energy $V_{\rm fv}$, what indicates that in this regime instanton action is mostly determined by the local form of the minimum. On the other hand, according to the Slepian model, the scalar potential around all high minima should look very similar in all realizations, with its shape dominated by the first term in (5.13). This explains why the distribution of instanton actions becomes more deterministic (fig. 5.5) for larger values of $V_{\rm fv}$, and therefore also the agreement between the Sarid approximation (5.29) for the *lowest action* and our fit in eq. (5.26) *for the median* of the distribution.

It would be interesting to check if this good agreement persists on a much larger landscape

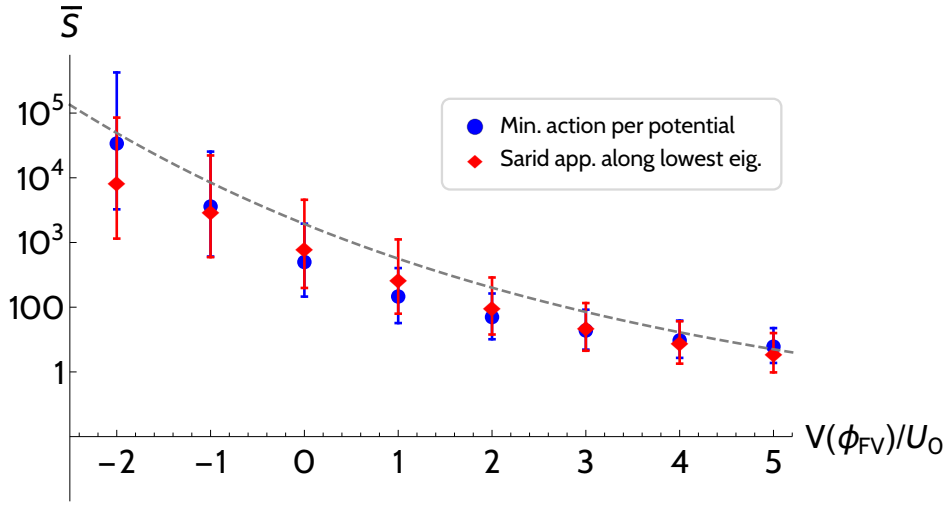

Figure 5.8: Distribution of lowest action per potential and Sarid approximation [80] along the lowest barrier direction, in terms of false vacuum height. The fit in eq. (5.26) is shown for comparison with previous results.

with hundreds of directions in field space,[8] and whether the approximation (5.29) can be used in combination with our Slepian model make robust predictions regarding the tunneling rates of high vacua.

5.5 Inflation in a Slepian Random Landscape

Up to now we have been using all the software and mathematical tools described above for the computation of bounce profiles and actions with Gaussian random fields conditioned to have a minimum at $\boldsymbol{\phi} = \mathbf{0}$. In this section, we turn to studying constrained GRFs with inflection points at the origin of field space focusing on their application to cosmological inflation.

Inflation in random potentials has already been extensively studied [106, 110, 112–114]. More specifically, inflation around inflection points has received special attention for being capable of sustaining enough e-folds to make contact with observations, while taking place in a small region of field space with an effectively one-dimensional potential.

While most of the obtained results and distributions seem promising, they have only been tested within Taylor expansions around these points, instead of using full GRFs. As we mentioned before, such methods do not capture correctly the global features of the potential, what is essential for characterising the non-perturbative stability of vacua. Therefore, this procedure is unsuitable for studying models of inflation where the initial conditions are determined by the decay of a parent false vacuum.

In this section we will apply Slepian models to constrain Gaussian random fields to have an inflection point with the desired properties to sustain inflation, and then we will study the dependence of its cosmological observables on the initial conditions, set by different

[8] Note that in our calculation we kept the quartic term of the potential while in reference [224] the authors drop this term arguing that for large number of fields (N) this coefficient becomes irrelevant. We have checked that in our case this is not the case and in order to obtain a good agreement it is necessary to take this term into account. This is due to the fact that we have limited our investigation to the N=2 case.

realizations of the parent vacuum.

5.5.1 1D Inflection point inflation

Let us briefly review the main results for one-dimensional inflection-point inflation (see appendix G and [114, 238] for more detailed explanations). Let us consider a potential of the form,

$$V(\phi) = u + \eta\phi + \frac{1}{6}\rho\phi^3 \,, \tag{5.31}$$

where, in order to satisfy the slow-roll conditions around the inflection point, we will assume that $\eta \ll u$. Note that we do not need to assume that the third derivative is too small. In fact, following typical conditions for a GRF we will consider the case where $u \ll \rho$. Taking this into account one can show that slow-roll inflation conditions will be satisfied in the interval

$$-\frac{u}{\rho} < \phi < \frac{u}{\rho} \,, \tag{5.32}$$

which together with the condition $u \ll \rho$ implies that we are describing small field inflation. Using the slow-roll conditions, it is easy to check that the expected number of e-folds, $N_{\rm exp}$, that can be achieved within that region is

$$N_{\rm exp} = \int_{-u/\rho}^{u/\rho} \frac{d\phi}{\sqrt{2\epsilon}} \approx \pi\sqrt{2}\frac{u}{\sqrt{\eta\rho}} - 4 \equiv N_{\rm max} - 4. \tag{5.33}$$

where $\epsilon = (V''(\phi)/\sqrt{2}V(\phi))^2$ and $N_{\rm max}$ is the maximal number of e-folds achievable in the whole potential. Moreover, defining

$$x \equiv \pi\frac{N_{\rm CMB}}{N_{\rm max}}, \qquad y \equiv \frac{N_{\rm max}}{2\pi}, \tag{5.34}$$

where $N_{\rm CMB}$ is the e-fold number at which the CMB scales leave the horizon, the spectral index of scalar perturbations can be shown to be given by

$$n_s = 1 + \frac{2}{y}\left(\frac{\tan x - y}{1 + y\tan x}\right) \,. \tag{5.35}$$

Finally, the amplitude of scalar perturbations can be expressed as

$$\Delta^2_{\mathscr{R}} = \frac{1}{12\pi^2}\frac{V^3(\phi)}{V'(\phi)^2} \approx \frac{N^4_{\rm CMB}\rho^2}{48\pi^2 u} f^2(x,y) \tag{5.36}$$

where

$$f(x,y) = \frac{\cos^2(x)(y\tan(x)+1)^2}{x^2(y^2+1)}. \tag{5.37}$$

satisfies $f(x,y) \sim 1$ for $y \gg 1$ and $x \sim 1$.

With these expressions at hand, we can easily obtain a set of parameters for the inflection

point (u, η and ρ) that are in agreement with the current cosmological observations [239], namely, $N_{\rm exp} > N_{\rm CMB} \approx 50$, $n_s \approx 0.965$ and $\Delta^2_{\mathscr{R}} \approx 2 \times 10^{-9}$ (see eq. (5.38) below).

5.5.2 *Numerical inflection points in a 2D Landscape*

We now want to embed $1d$ inflection-point inflation in our $2d$ GRF landscape. In order to do that we can follow the procedure explained in section 5.3.2 for Slepian models in the case of inflection points. In the notation introduced earlier, the $1d$ parameters $\eta = \eta_1$ and $\rho = \rho_{111}$, correspond to the derivatives along the flat direction of the multidimensional inflection point. Note that, in principle, u and ρ_{111} (when evaluated at the same point) are uncorrelated, but the same is not true for u and the second derivative along the inflaton direction λ_1; similarly η_1 and ρ_{111} are also correlated, see eq. (5.20). Here we are interested in studying the global properties of the landscape on the cosmological observables so we will focus on a particular type of inflection point where we have fixed its $1d$ parameters.

Following the steps from the previous section, we built two-dimensional GRFs with an inflection point whose inflating direction has fixed features. In the forthcoming sections we set

$$u = 0.5\ U_0\ , \quad \eta_1 = 6.8 \cdot 10^{-6}\ \frac{U_0}{\Lambda}\ , \quad \rho_{111} = 2.5\ \frac{U_0}{\Lambda^3} \tag{5.38}$$

where $U_0 = 6.0 \cdot 10^{-16}\ M_{\rm Pl}^4$ and $\Lambda = 0.5\ M_{\rm Pl}$ define the energy scale and correlation length respectively, with the Planck masses written explicitly for clarity.

Once u, η and ρ have been fixed, using the probability distributions listed in (5.19) and (5.20), we can obtain the remaining parameters of the two-dimensional inflection point set at the origin of field space $\boldsymbol{\phi} = \mathbf{0}$, and generate in a efficient way a large sample of GRFs with the listed properties.[9]

As an example, we show in figure 5.9 a field constructed with the above constraints. We then used AnyBubble to tunnel from a higher false vacuum to the central inflection point. We note that even though in every realization the inflection point has the same properties along the ϕ^1 direction up to third order, the potentials are different away from that point. This means that the false vacuum, which decays to the region around the inflection point, is located in a different place and it also has different features in each realization, e.g. vacuum energy and barrier height. Using AnyBubble we computed the exit points of a large set of realizations. After that we used these exit points of the instanton decay as the starting points of a Lorentzian evolution of a FRW universe with this potential.

In order to study the inflationary trajectory we used mTransport [240], a Mathematica code developed to compute inflationary observables. The cosmological evolution inside of a bubble universe created from tunneling is described by an open FRW universe [69]. Here, for simplicity, we used the flat-space approximation for the evolution of the cosmological interior of the bubble.[10]

[9] Note that following our earlier definition of the inflection point in our $2d$ landscape, we have set $\eta_2 = 0$ and $\lambda_2 > 0$.

[10] Note that in reality the initial cosmological evolution is dominated by the spatial curvature of the open FRW slices that describe the bubble interior. This will have some effect on the initial stages of the evolution of the scalar field in a multidimensional potential. See [100,113] for a discussion of these effects.

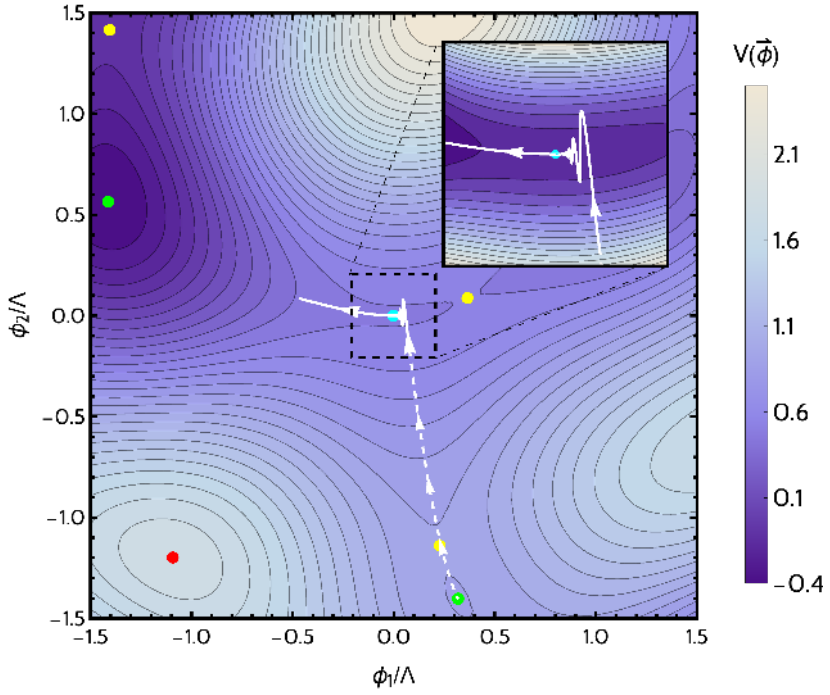

Figure 5.9: A Gaussian random field conditioned to have an inflection point in the middle. The dashed line represents the tunneling from a minimum to a lower inflection point. The inflationary slow-roll phase starts at the exit point, inflates for around 124 e-folds following the solid line, and evolves towards the closest minimum. We only show the inflationary part of the trajectory. Green, yellow and red dots represent minima, saddle points and maxima of the potential. The inflection point is marked with a blue dot.

In the example from figure 5.9, the dashed line represents the tunneling trajectory, while the solid one marks the inflationary one. We found this path to sustain a total of 124.1 e-folds and a spectral index of $n_s = 0.964$ at the observable scale.

5.5.3 *Statistics of inflationary parameters*

In order to test the method described above to generate inflationary random fields, we generated 5000 GRFs constrained to have an inflection point with the same properties as the one in the example of figure 5.9 (see eq. (5.38)). Next, in each of these realizations, we found all minima lying above the central inflection point and used anyBubble to compute the tunneling trajectory from the former to the latter in each case. Considering the exit point as the starting point of an inflationary phase, we used mTransport to find the number of e-folds, power spectrum, tensor-to-scalar ratio, spectral index and its running. The distributions of the e-fold number and the spectral index are shown in figure 5.10, for a pivot scale of 50 e-folds, whereas the action associated to the tunneling to the inflection point is shown in fig. 5.11. This is a different distribution than the ones we found earlier, since the common factor in these decays is the final point and we do not impose anything about the initial (false vacuum) state. It is interesting to see that this distribution is quite peaked around an action of the order of 10^3.

We have also obtained the distributions for the amplitude of scalar perturbations, tensor-

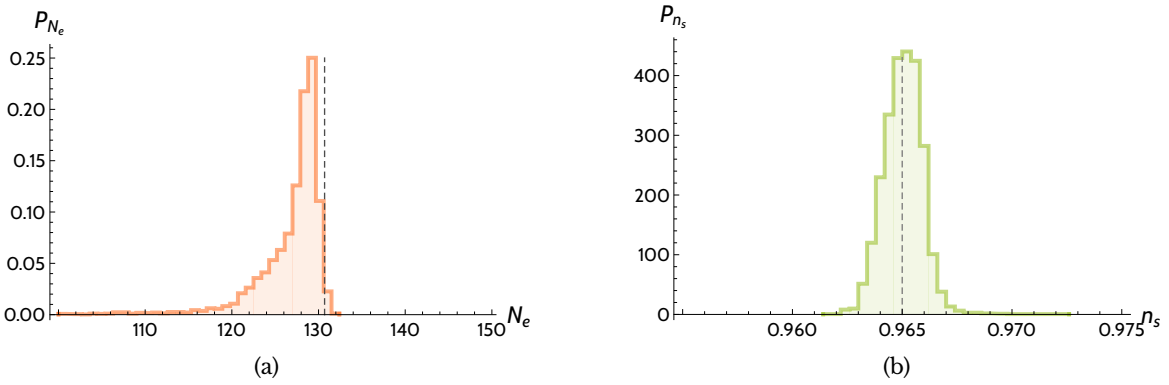

Figure 5.10: (a) Distribution of number of e-folds, with N_{exp} shown with a dashed line (b) Histogram of the obtained spectral index, with the analytic prediction marked with a dashed line. Both figures represent 4000 inflationary trajectories (see text).

to-scalar ratio and running of spectral index which turned out the be centered around the values

$$\Delta^2_{\mathscr{R}} = (2.02 \pm 0.04) \cdot 10^{-9}, \quad r = (8.0 \pm 0.1) \cdot 10^{-9} \quad \text{and} \quad \alpha = (-2.49 \pm 0.02) \cdot 10^{-3}, \tag{5.39}$$

respectively.[11] Our results in this section are fully compatible with the $1d$ studies in [112].

Finally, in fig. 5.12, we show several inflationary trajectories corresponding to tunnelings in different GRFs with an inflection point in the middle with the same features. Note that all trajectories, no matter how far they start from, have a similar behavior. After oscillating in the vertical ϕ_2 direction, they all stabilize around the inflection point and inflate along it. Most of the e-folds happen in the vicinity of the inflection point, as predicted by the analytic estimation.

We have obtained successful results from this analysis around 80% of the times. The rest of the times the procedure did not yield a cosmological solution in agreement with our universe either because inflation ended too soon or because the exit point was too far from the central inflection point and the inflaton trajectory went astray. The successful paths show very good agreement with the $1d$ results presented in the previous section. We see that even though some of the trajectories have some substantial deviation from the $1d$ inflationary direction, the cosmological observables are still in pretty good agreement with the single field inflection point inflation. The distributions of the results are quite peaked around their central values, so we can conclude that the dependence of the observables on the initial conditions seems to be quite mild.

It is important to remember that all these realizations have the same $1d$ inflection point parameters. In order to extract the complete statistical information about the predictions of a particular GRF we should combine these results with the ones obtained from inflection points with other parameters with their correct statistical weight. This is a much more

[11] The cosmological evolution of these Lorentzian trajectories continue after inflation until they reach a lower minimum. We have not fine-tuned this minimum to be in Minkowski space, so in general the evolution leads to eternal de Sitter or to an Anti-deSitter crunch. We are only interested in the statistics of the inflationary period so we have stopped this evolution after the field leaves the slow-roll regime.

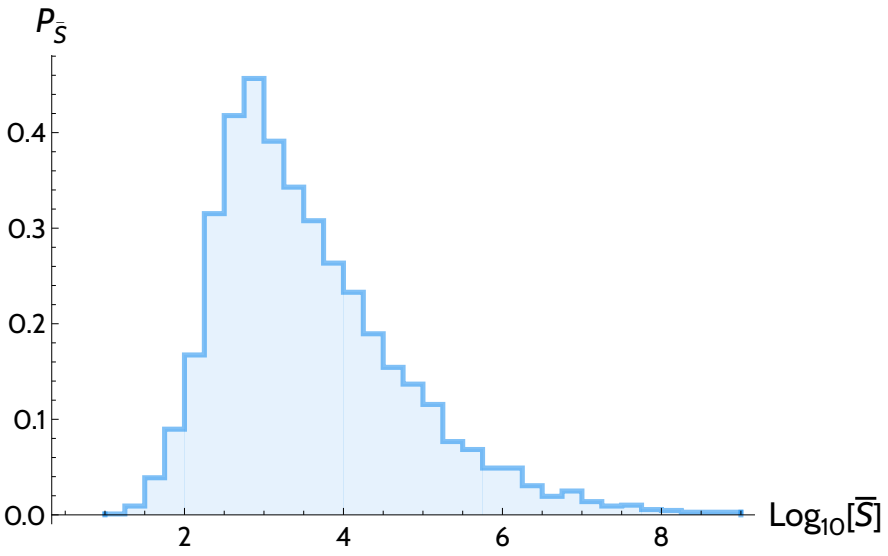

Figure 5.11: Distribution of the tunneling action from a minimum to the central inflection point, right before inflation begins.

numerically intensive problem and we leave it for a future publication.

5.6 Summary and conclusions

Slepian models are a powerful mathematical technique for modelling the statistics of random landscapes conditioned to satisfy a certain set of constraints. For this reason they are particularly useful to characterise phenomenologically interesting corners of the landscape, e.g. de Sitter vacua or inflationary regions consistent with the cosmological data, which are known to have highly suppressed probability to occur in generic random potentials. On the one hand, Slepian models provide a way to generate numerically large samples of a random landscape containing the region of phenomenological interest to be studied, regardless of the low probability of the realizations. On the other hand, this technique can also be used as an analytical description of conditioned random potentials, and thus to obtain valuable insight about properties of the landscape around these regions of interest. A particularly attractive feature of Slepian models, as opposed for example to the use of Taylor expansions, is that they can capture the global features of the random potential, and therefore they are specially useful for studying quantum mechanical instabilities in the landscape. In this chapter we have presented the mathematical techniques for studying conditioned Gaussian random landscapes. We have applied these method to condition a $2d$ random potential to have a de Sitter minimum with a specific vacuum energy and also to study $2d$ landscapes containing an inflection point capable of sustaining a period of inflation compatible with the data.

More specifically, regarding our discussion of de Sitter minima, we have considered the non-perturbative decay of these vacua to lower minima, and characterised the statistical distribution of their decay rate as a function of the height of the false vacuum. For this purpose we have used our Slepian model to generate numerically large samples of vacua with varying values of the vacuum energy, and then computed the corresponding decay rates

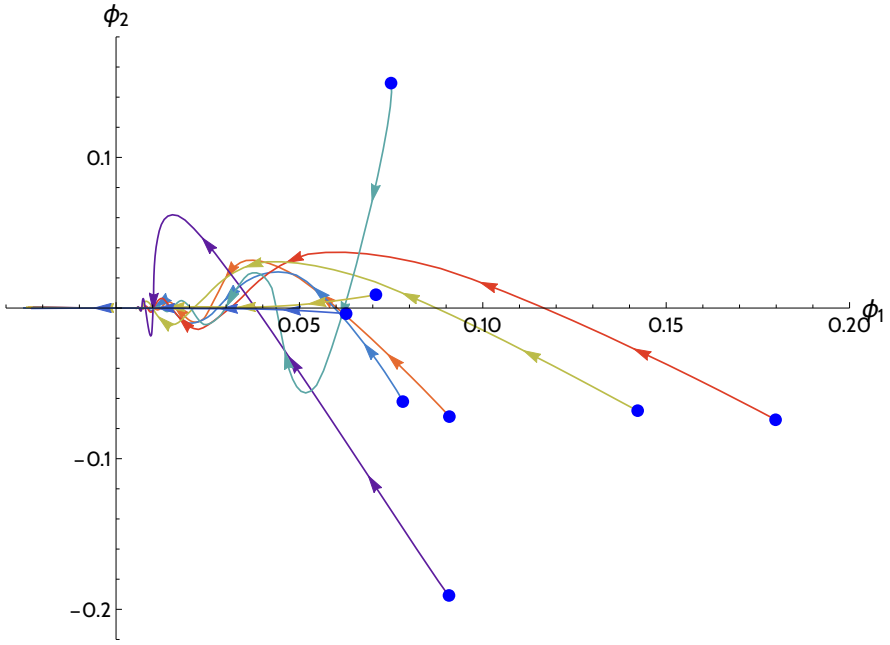

Figure 5.12: Showcase of several inflationary trajectories from different tunnelings to the central inflection point. Each exit point is marked by a blue dot.

both solving the full instanton equations, and using various approximate methods present in the literature: the thin-wall approximation [67], the straight-path approximation [237], and the estimate proposed by Sarid [80] for the lowest instanton action (see eq. (5.29)).

Our analysis shows that the thin-wall approximation is in good qualitative agreement with the numerical results, but only provides an accurate estimate of the instanton action for minima with a relatively small vacuum energy. Indeed, consistently with the thin-wall prediction of the instaton action, we observe that the decay rate increases (on average) for increasing values false vacuum height. This can be understood noticing that, in a Gaussian random landscape, the barrier height that needs to be crossed to escape from the vacuum decreases when the vacuum energy of the minimum increases. However, for minima with a large vacuum energy the tunneling typically occurs to much lower vacua, what violates the assumptions of the thin-wall approximation, and thus it cannot provide a good quantitative estimate of the decay rate.

In the straight-path approximation one assumes the decay is effectively one-dimensional, so that it occurs along the line connecting the false and true vacua. We have shown that this simplification agrees remarkably well with the results of our full numerical analysis in all cases we studied in a $2d$ Gaussian landscape. It is interesting to check if this simplification still provides a rough estimate (see [79] for a discussion) for the instanton action in higher dimensional landscapes where the numerical resolution of the full instanton equations becomes prohibitively difficult. In the particular case of a Gaussian random landscape this approach is specially attractive, since the statistics of the random field along the straight line connecting the false and true vacua can be fully described by simply restricting its covariance function to that line. Therefore, if this method would prove useful to estimate the non-perturbative stability of vacua in large-dimensional Gaussian landscapes, it would not be necessary to produce a sample the full higher dimensional GRF, it would suffice to

generate one dimensional realizations of the random field with the same covariance.

Regarding the estimate of Sarid [80] for the lowest action (the most likely decay channel), our numerical analysis shows that this approximation provides an accurate quantitative estimate of the instanton action in the case of minima with a large vacuum energy. Interestingly, this estimate depends only on the form of the potential in a neighbourhood of the false vacuum which, according to the predictions of the Slepian model, does not experience large variations between different realizations. In plain words, all high minima look locally very similar to each other. Indeed, Gaussian random potentials conditioned to have high minima exhibit a very deterministic shape in a large region around it, which is dominated by the first term in equation (5.13). As we argued in the main text, combining the estimate of [80] for the lowest action, with the Slepian analysis one concludes that the distribution for the instanton actions should become increasingly peaked and deterministic for higher minima. Our numerical results, displayed in figures 5.5 and 5.8, match perfectly this expectation. This suggests that the estimate for the instanton action in eq. (5.29), in combination with the Slepian techniques, might also provide a very good prediction for the decay rates of high false vacua in higher dimensional landscapes. For this purpose, the alternative methods proposed in [116] to generate constrained multidimensional Gaussian random landscapes might also proof very useful.

With respect to our second application of Slepian models, the analysis of inflection point inflation in a Gaussian random landscape, we have considered the dependence of the cosmological observables on the initial conditions for inflation. This initial conditions in our model are determined by the exit point of a quantum tunnelling process from a parent false vacuum. This study would have been very difficult without the aid of our conditioning techniques, since generating numerically a large sample of potentials with an inflection point with the right properties is exceedingly costly in terms of computation time. With our methods, however, we were able to generate easily a large number of realizations of the landscape with an inflection point capable of sustaining more that 60 e-folds of inflation, and with observables consistent with the current cosmological data. Note also that the ability of Slepian models to reproduce faithfully the global features of the potential was also essential in this analysis, in particular for modelling the preinflationary phase of false vacuum decay. Our results are summarised by figure 5.10 and equation (5.39), which display the computed values of the cosmological observables. We see that the dependence of the inflationary parameters on the initial conditions is quite mild. The obtained distributions for the observables are very peaked around their expected value in the $1d$ slow roll model where inflation happens around the inflection point. The typical realizations in our landscape have some variation on the observable parameters ranging between 1% and 10% depending on the quantity under consideration. It is important to emphasise that in this study we kept fixed the local properties of the inflection point. In order to perform a complete characterisation of inflection point inflation in a Gaussian landscape we would also need to study the effect of changing the inflection point parameters on the observables. We will leave this analysis for a later publication.[12]

[12] A realistic study of the observable parameters of inflation in this model should also include a prescription to calculate their probability distribution in the multiverse. This will require the introduction of a measure. Here we have not discussed this issue any further. (See [241] for a detailed description of the proposed prescriptions.)

Finally, one may also use the techniques presented in this work to analyze the possibility of a non-Gaussian Landscape. In fact similar methods have already been discussed in the mathematical literature for various non-gaussian random fields, and in particular were used to describe constrained extrema in these models [242–244]. One could in principle use the methods developed in those papers to implement a more accurate description of the String Theory Landscape potential or some sectors of it. This will allow us to explore the possibility that the results presented here could be modified by the relaxation of the Gaussian assumption. However the non-gaussian nature of the statistical description of the model seems to further complicate the calculations in a significant way in these cases so we will leave the implementation of these ideas for future work.

Chapter 6

Brane nucleation in supersymmetric models

In this final chapter we will explore an alternative mechanism to generate non-perturbative decays between vacua. In the following, we will combine the usual Coleman-deLuccia mechanism for false vacuum decay together with the Brown-Teitelboim scheme, where spherical membranes interpolate between vacua generated solely by three-form fluxes. We will derive an alternative approach for vacuum decay which combines both scalar fields *and* membranes, motivated by our previous analysis of flux compactifications. We have checked that the supersymmetric limit of such a setup leads to a flat membrane (i.e., of infinite radius), as expected in such transitions. Therefore, by parametrically breaking supersymmetry, we can generate decays connecting *different* vacua, generated by different fluxes. We will study these processes both with and without taking gravity into account, and we will give detailed examples to understand the physics behind these processes.

6.1 Introduction

As we have seen in chapters 1 and 5, false vacuum decay [67–69] is an essential tool for the exploration of the Landscape, with rich applications in Cosmology [87]. Using it in the Gaussian Random Landscapes of the previous chapter, we found that states emerging from a false vacuum may undergo an inflationary phase, which may well correspond to our Universe. However, as noted from the very beginning of that chapter, the scalar potentials we used there are simple models of the actual picture, where several ingredients such as form fields and membranes come into play to form the scalar potential in the effective field theory. Therefore, inspired by our previous research on the flux-generated String Theory Landscape, we aim to generalize false vacuum decay processes to include fluxes and other ingredients into this procedure, in order to construct more realistic transitions between vacua.

Regarding the non-perturbative stability of supersymmetric vacua against false vacuum decays, the non-gravitational case is quite trivial, since these minima must satisfy $V = |\partial_\phi W|^2 = 0$, meaning that they are always degenerate and thus no vacuum decay can happen. On the other hand, in [245, 246] it was shown that for the case of $\mathcal{N} = 1$ supergravity,

such a process cannot happen, since it would require a bubble of infinite radius, i.e., a domain wall. There exists no finite-radius decay which respects supersymmetry. Domain walls interpolating between supersymmetric vacua were developed in [247], for both the non-gravitational case and from the perspective of $\mathcal{N} = 1$ supergravity.

All of the processes above, when considered from the perspective of the flux Landscape, share a common property; namely, they all consider that the fluxes (which basically define the potential) remain constant in the process. It is therefore worthwhile studying how one may involve both scalar fields and fluxes in a non-perturbative quantum decay.

Actually, a process similar to the Coleman-deLuccia decay was studied by Brown and Teitelboim in [248, 249], where instead of fields, the authors studied the non-perturbative stability of a background composed of only 3-form fluxes. This was done as a motivation to study the neutralization of the cosmological constant, since in a 4-dimensional spacetime 3-forms contribute a constant potential term [250]. Therefore, it may be energetically favourable to tunnel a compact region of space from some value of a 3-form to another by the nucleation of a membrane coupled to said form. Most interestingly, such a process can be generalized to any dimension, and its 2-dimensional counterpart is equivalent to the Schwinger pair creation process [251] (however, this had been known for some time in the context of quantum creation of universes [252]).

All of the above ingredients come together when considering flux compactifications of String Theory, where 3-form fluxes are used to stabilize the extra directions of the theory into a compact manifold. As we mentioned in the introductory chapter, fluxes couple naturally to D-branes; on the other hand, in the process of the compactification hundreds of moduli arise, which parametrize the geometry of the internal manifold. Therefore, it may be worthwhile to investigate the interplay of all these ingredients from the EFT perspective of $\mathcal{N} = 1$ supergravity in $D = 4$ dimensions. In fact, the dynamics of membranes has been extensively studied in such a setup, see e.g. [253–255].

The inclusion of form fields within supersymmetry and supergravity multiplets has been around for quite some time [256, 257]. On the other hand, recent developments have been carried out in the connection between flux compactifications and three-form supergravity multiplets ([258], see [259] for a review). This has led to the inclusion of flat membranes in this setup to generate supersymmetric domain walls between flux vacua [260]. Similar processes involving membranes and axions have been studied [261–263] from the point of view of the Swampland program and Inflation.

In this work, we will give a pedagogical introduction on the inclusion of 3-form fields and membranes in supersymmetric setups (both without and with gravity included), and check the non-perturbative stability of flux-generated vacua. In order to do that, we will employ a combination of the Coleman-deLuccia and Brown-Teitelboim schemes for non-perturbative decays. Of course, as we said above, supersymmetric setups should be stable under false vacuum decay. Thus, we have included soft supersymmetry-breaking terms [264] into our Lagrangians, which can be made parametrically small, to see how false vacuum decay is affected by them. In such a setup, we have assumed the false vacuum state to be composed of a homogeneous and isotropic scalar field and 3-form. On the other hand, the instanton solution corresponds to a spherical brane coupled to the form, where the inside and the outside and the membrane are described by different flux values (as in the Brown-Teitelboim

instanton). This corresponds to a *different* potential at each side of the membrane, featuring distinct minima of the scalar field. We will check that it is energetically possible to carry out such a process and give detailed examples about these, both without and with gravity considered within the setup. We will also see that as we make the supersymmetry-breaking parameters go to zero, the expected brane-bubble's radius increases, which coincides with the infinite-radius (i.e. flat domain wall) solution of the supersymmetric limit.

This chapter is organized as follows. In section 6.2 we will explain the basics of supersymmetric domain walls in flat spacetime and how they can be thought of as the limiting cases of non-supersymmetric instantons. Furthermore, we will also see how flat membranes coupled to fluxes may generate domain walls, all the while leaving a part of the supersymmetry unbroken. In section 6.3, we will generalize these results by including soft supersymmetry-breaking terms. We will describe these instantons, which combine three-forms and scalar fields coupled to membranes and find that they tend asymptotically to the supersymmetric limit as the supersymmetry-breaking terms are dialled down. In section 6.4, we will review the existing theory on flat membranes in $\mathcal{N} = 1$, $D = 4$ Supergravity, and give a small example to check the main equations. In 6.5, we will follow the same steps as in the non-gravitational case to construct an instanton involving the scalar and form fields together with the membrane, given some ansatz for the metric in Euclidean space. We will check the main expressions with an example and find that we indeed can recover the supersymmetric setup as a limiting case. Finally, we will give some conclusions in section 6.6.

6.2 Global Supersymmetric Field Theories

As a warm-up exercise, before analysing theories including membranes, we will first check some basic results involving domain walls in supersymmetric theories, most of which may be found extensively detailed in [259]. Afterwards, we will see how supersymmetry-breaking terms affect the outcome of such a theory. This will help us build an intuition on what to expect once we include membranes.[1] In this chapter, we will work with theories involving a single scalar field; however, all of the results can be easily generalized to include more complex examples.

6.2.1 *A domain wall in an $\mathcal{N} = 1$ chiral superfield model*

We will start by considering the Lagrangian for the complex scalar field component of the chiral superfield, namely,

$$\mathcal{L} = -K_{\phi\bar{\phi}}\,\partial_\mu\phi\partial^\mu\bar{\phi} - K^{\phi\bar{\phi}}|W_\phi|^2 \tag{6.1}$$

where we have introduced the two functions that define the model: the Kahler function $K(\phi,\bar{\phi})$ and the holomorphic superpotential $W(\phi)$. We will denote their derivatives as $\partial_\phi\partial_{\bar{\phi}}K = K_{\phi\bar{\phi}} = 1/K^{\phi\bar{\phi}}$ and $W_\phi = \partial_\phi W(\phi)$, following the conventions of [265].

[1] It should be noted that in this context, domain walls refer to the scalar field profiles which interpolate between two minima of some potential; on the other hand, membranes are two-dimensional extended objects, with infinitesimal width. In the following sections we will consider both of them simultaneously.

The equations of motion for this theory are

$$K_{\phi\bar{\phi}}\partial_\mu\partial^\mu\phi - K_{\phi\phi\bar{\phi}}\partial_\mu\phi\partial^\mu\bar{\phi} + K_{\phi\bar{\phi}\bar{\phi}}(K^{\phi\bar{\phi}})^2|W_\phi|^2 - K^{\phi\bar{\phi}}W_\phi\overline{W}_{\bar{\phi}\bar{\phi}} = 0 \tag{6.2}$$

and its complex conjugate. These reduce to the usual Klein-Gordon equations for a complex scalar field if the kinetic term is canonical (which requires $K = \phi\bar{\phi}$) and a scalar potential given by $V(\phi,\bar{\phi}) = |W_\phi|^2$.

We are looking for a domain wall solution that interpolates between two supersymmetric minima, in other words, between two points whose superpotential satisfies $W_\phi(\phi_\pm) = 0$. Let us consider a flat domain wall whose transverse direction is given by the coordinate z. One can then show [247] that the static solution preserving half of the $N = 1$ supersymmetry solves the first-order equation

$$\partial_z\phi(z) = -e^{i\theta}K^{\phi\bar{\phi}}\overline{W}_{\bar{\phi}}(\phi(z)), \tag{6.3}$$

known as the BPS equation, where the phase θ is given by

$$e^{i\theta} = \frac{\Delta W}{|\Delta W|}, \qquad \text{where} \qquad \Delta W = W(\phi(z=\infty)) - W(\phi(z=-\infty)). \tag{6.4}$$

Of course, given appropriate boundary conditions, both the first-order and second-order equations should yield the same static solution for the domain wall. The tension of the domain wall in this model can be computed writing the energy per unit area as follows:

$$\sigma = \int dz\, T_{00} = -\int_{-\infty}^{\infty} dz\, K_{\phi\bar{\phi}}|\partial_z\phi(z) + e^{i\theta}K^{\phi\bar{\phi}}\overline{W}_{\bar{\phi}}(\phi(z))|^2 + 2\mathrm{Re}[e^{-i\theta}\Delta W] \tag{6.5}$$

which in the supersymmetric limit, where (6.3) holds, becomes

$$\sigma_{BPS} = 2|\Delta W| \tag{6.6}$$

Example. Double well potential

Let us illustrate all of the above by considering the following model:

$$K(\phi,\bar{\phi}) = \phi\bar{\phi}, \qquad W(\phi) = \left(\frac{1}{3}\phi^3 - a^2\phi\right) \tag{6.7}$$

where we are assuming that $a > 0$. The bosonic part of the Lagrangian for this supersymmetric theory is given by

$$\mathscr{L} = -\partial_\mu\phi\partial^\mu\bar{\phi} - |\phi^2 - a^2|^2. \tag{6.8}$$

The potential of the theory has been plotted in figure 6.1(a) (dashed line). The second-order equations of motion (6.2) read, in this case,

$$\partial_z^2\phi(z) - 2\bar{\phi}(\phi^2 - a^2) = 0. \tag{6.9}$$

Alternatively, we can write the first-order equations as

$$\partial_z \phi(z) = -(\bar{\phi}^2 - a^2) \tag{6.10}$$

where we can readily see that $\phi_\pm = \pm a$ are the two supersymmetric minima.

Let us choose[2] $e^{i\theta} = -1$. The solution of this equation is given by the real field configuration,

$$\phi(z) = a \tanh(az), \tag{6.11}$$

while the tension of this domain wall is given by

$$\sigma_{BPS} = 2|\Delta W| = \frac{8}{3} a^3 \tag{6.12}$$

As we mentioned earlier, this solution preserves some supersymmetry, so it is clear that it cannot represent the decay of the vacua. We can also see this noting that both vacua are supersymmetric, degenerate in energy and the wall is flat and infinite, so there is no way these vacua can decay.

On the other hand, the solution we found here is purely real. This is consistent with the potential we have since its form is such that perturbations around the solution in the imaginary field directions are stabilized. We can check this by expanding the potential in the real and imaginary parts of the field, namely

$$\phi(z) = \psi(z) + i\ s(z) \tag{6.13}$$

so the potential reads

$$V(\psi, s) = (\psi^2 - a^2)^2 + 2(\psi^2 + a^2)s^2 + s^4 \tag{6.14}$$

This is why we can concentrate on the solution along the $s = 0$ line. In all of the examples we show here, we have checked that this is indeed the case, therefore, in all of our illustrations we will simply draw the results concerning the real part of the fields.

Breaking Supersymmetry

We will break the supersymmetry of the theory by introducing several "soft supersymmetry-breaking terms" in the Lagrangian, of the form [264, 266]

$$S_{\text{soft}} = -\int d^4x \sqrt{-g} \left[\mu^2 \phi\bar{\phi} + b\left(\phi^3 + \bar{\phi}^3\right) \right] . \tag{6.15}$$

In the following, we will consider the coefficients to be small enough so that many of the properties of the solution found earlier will still hold. This means we will consider the case where $\mu^2 \ll a^2$ as well as $b \ll a$, see the coloured curves of 6.1(a).

[2] On the other hand, $e^{i\theta} = +1$ would yield the mirrored profile, often denoted as the anti-domain wall. This simply corresponds to flipping the boundary conditions imposed at $\pm\infty$.

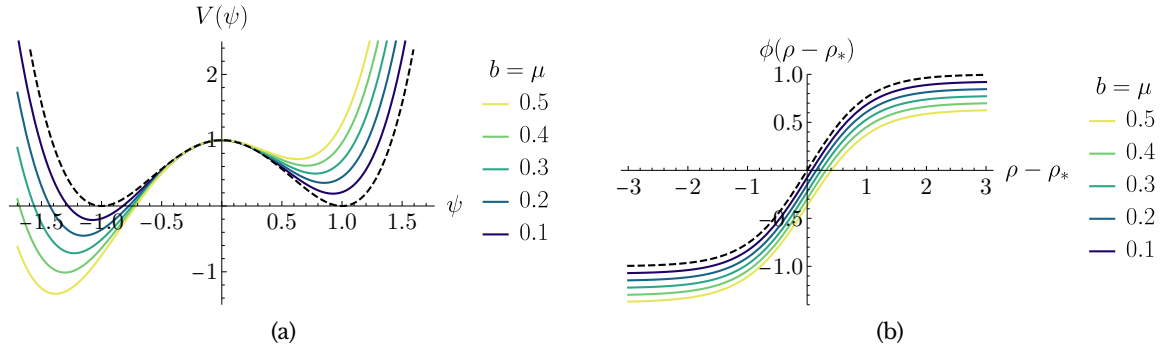

Figure 6.1: (a) Potential (6.19) with $a = 1$, for several supersymmetry-breaking parameters. (b) Solutions to (6.17), centered around the inflection point corresponding to each profile, labeled as ρ_*. The BPS limit is shown with a dashed line, representing the domain wall solution arising from the dashed potential in (a).

In this regime we can see that the theory still posses two minima given by

$$\phi_\pm = \pm a + \delta_\pm(\mu^2, b) \ , \tag{6.16}$$

where the solutions have only shifted slightly, so $|\delta_\pm / a| \ll 1$. The interesting point now is that both of these minima break supersymmetry. One can take $b < 0$ in such a way that the potential at ϕ_+ becomes slightly higher than the other minimum; this means that this vacuum will be unstable with respect to the nucleation of bubbles of the true vacuum at ϕ_-. Furthermore, the form of the supersymmetry-breaking terms allows for the tunneling to happen along the real direction of the field, see fig. 6.1(a).

In order to compute the probability of the decay and its profile in terms of the scalar field, we will resort to the usual methods developed by Coleman and collaborators [67, 68] in the context of False Vacuum Decay. Thus, we only have to extremize the Euclidean action associated to the Lagrangian (6.1) (plus the supersymmetry-breaking terms). Its actual value at the extremum will quantize the exponentially suppressed decay probability, while the equations of motion derived from it will give us a profile for the emerging scalar field. Assuming $O(4)$ symmetry in Euclidean space, the equations of motion for the field are

$$\phi'' + \frac{3}{\rho}\phi' = \frac{\partial V}{\partial \bar{\phi}} \tag{6.17}$$

where $\rho = \sqrt{\tau^2 + \boldsymbol{x}^2}$, τ being the Euclidean time $\tau = i\,t$ and primes denote derivatives with respect to ρ. This equation is to be solved considering the boundary conditions

$$\lim_{\rho\to\infty} \phi(\rho) = \phi_+ \ , \qquad \phi'(0) = 0. \tag{6.18}$$

Note that the Euclidean $O(4)$ symmetry will turn to $O(1,3)$ when transporting the solution back to Lorentzian space. Among other things, this will mean that the profile $\phi(\rho)$ obtained via (6.17) will correspond to the emergent scalar profile at $t = 0$; furthermore, this symmetry implies that the radius of the bubble so formed will accelerate towards the speed of light.

Following the example presented in the previous subsection, we will work with the

following potential

$$V(\phi,\bar{\phi}) = (\phi^2 - a^2)(\bar{\phi}^2 - a^2) + \mu^2\phi\bar{\phi} + b(\phi^3 + \bar{\phi}^3) \tag{6.19}$$

which already includes a contribution from supersymmetry-breaking terms within its definition.

In this one-dimensional setup, the profile of the scalar field can be easily found in Euclidean radial coordinates using an *undershoot/overshoot* algorithm [67], which we described in section 1.5. Essentially, since the boundary conditions (6.18) do not specify the initial starting point $\phi(0)$, we can first obtain a couple of points where the field either undershoots or overshoots the local maximum of $-V$ located at ϕ_{fv}. Iteratively reducing this field range, we will eventually find a starting point $\phi(0)$ which stays sufficiently close to ϕ_{tv} for large values of ρ. The solutions found this way have been contrasted with ones obtained using `AnyBubble` [76] and have been shown to be essentially identical.

Using this numerical algorithm, we can check that indeed the form of the domain wall forming the bubble does not change qualitatively in comparison to the supersymmetric case given above, see figure 6.1(b). It is also clear that dialing back the supersymmetric coefficients b, μ one will recover the supersymmetric vacua and therefore the configurations will be stable, since both minima will become degenerate.

6.2.2 *Supersymmetric membrane solution coupled to a 3-form potential*

In the previous subsection, we have seen how domain walls may be generated between degenerate vacua in supersymmetric theories. Furthermore, when supersymmetry-breaking terms are present, we have checked that the profiles of true vacuum bubbles tend towards the planar domain wall profiles as the supersymmetry-breaking terms are made smaller. Of course, when the vacuum is completely supersymmetric, the bubble radius is infinite and thus, no instanton exists.

In the following, we will introduce a final ingredient into our setup: a 2-dimensional membrane. As explained in the introduction, these objects couple naturally to 3-form fields [248, 249] and offer interesting ideas from a cosmological viewpoint. Furthermore, if their tension and couplings are chosen so that a part of the overall supersymmetry is conserved (see, e.g. [254]), one may couple this object to a supersymmetric theory which includes fluxes [258–260]. As we will review below, this allows us to divide our spacetime into two regions where the potential of a scalar field may be different on each side, allowing for transitions between vacua of *different* potentials.

In a non-gravitational setup, a possible global supersymmetric model for a fundamental membrane coupled to a 3-form potential, using a single real three-form per scalar field, i.e, $A_{\mu\nu\rho}$, and a complex scalar ϕ is of the form

$$S = S_{\text{bulk}} + S_{\text{membrane}} + S_{\text{boundary terms}}. \tag{6.20}$$

In appendix H, we show that such a theory can be written using chiral multiplets constructed out of vector ones. In that case, the bosonic content of the multiplet is simply given by complex scalar fields and auxiliary fields, the real part of which will be related to the field

strength of the 3-form. Thus, the simplest bulk action of a scalar field coupled to 3-forms, formed by so-called single 3-form multiplets, is given by

$$S_{\text{bulk}} = \int d^4x \left[-K_{\phi\bar{\phi}}\, \partial_\mu \phi \partial^\mu \bar{\phi} - \frac{1}{4\cdot 4!} K_{\phi\bar{\phi}}\, F^{\mu\nu\sigma\rho} F_{\mu\nu\sigma\rho} + \frac{1}{2\cdot 4!} \left(W_\phi + \overline{W}_{\bar{\phi}} \right) \epsilon^{\mu\nu\sigma\rho} F_{\mu\nu\sigma\rho} \right.$$
$$\left. + \frac{1}{4} K^{\phi\bar{\phi}} \left(W_\phi - \overline{W}_{\bar{\phi}} \right)^2 \right] \tag{6.21}$$

$$= \int d^4x \left[-K_{\phi\bar{\phi}} \partial_\mu \phi \partial^\mu \bar{\phi} + \frac{1}{4} K_{\phi\bar{\phi}} (*F_4)^2 + \frac{1}{2} (*F_4) \left(W_\phi + \overline{W}_{\bar{\phi}} \right) + \frac{1}{4} K^{\phi\bar{\phi}} \left(W_\phi - \overline{W}_{\bar{\phi}} \right)^2 \right] \tag{6.22}$$

where we have used[3] $F_{\mu\nu\rho\sigma} = \frac{1}{3!} \partial_{[\mu} A_{\nu\rho\sigma]}$ and its Hodge dual $*F_4 = \frac{1}{4!} \epsilon_{\mu\nu\rho\sigma} F^{\mu\nu\rho\sigma}$. It will also be useful to define the components of the Hodge-dual to the 3-form, $A_\mu = \frac{1}{3!} \epsilon_{\mu\nu\rho\sigma} A^{\nu\rho\sigma}$, since it allows us to write $*F_4 = \partial_\mu A^\mu$. As usual, K and W are the Kähler potential and superpotential, respectively, which define the supersymmetric model for the field ϕ, with subscripts denoting partial derivatives with respect to said field.[4]

As we show in appendix H, the boundary terms required to make the variation of the action well defined are given by

$$S_{\text{bd}} = \frac{1}{2\cdot 3!} \partial^\mu \left[A^{\nu\rho\sigma} \left(K_{\phi\bar{\phi}} F_{\mu\nu\rho\sigma} + \epsilon_{\mu\nu\rho\sigma} \left(W_\phi + \overline{W}_{\bar{\phi}} \right) \right) \right] \tag{6.23}$$

$$= -\frac{1}{2} \int d^4x\, \partial^\mu \left[A_\mu \left(K_{\phi\bar{\phi}} (*F_4) - W_\phi - \overline{W}_{\bar{\phi}} \right) \right] \tag{6.24}$$

Quite interestingly, as we review in appendix H (see also, for example, [258, 260]), when the 3-form is set on-shell the bulk action and the boundary term (which is required to make the variational problem well posed, see [249, 267]) reduce to the usual theory for a complex scalar field, albeit with a potential given by

$$V(\phi, \bar{\phi}) = \left| W_\phi - n \right|^2 \tag{6.25}$$

where $n \in \mathbb{R}$ is constant, arising from integrating the equation of motion corresponding to the 3-form field. Therefore, the fluxes yield a linear contribution to the effective superpotential of the scalar field. Of course, if these fluxes are assumed to arise from a flux compactification scheme, then we should expect $n \in \mathbb{Z}$, c.f. equation (1.33); in the following, we will consider them as such.

The piece of the action corresponding to the membrane is given by [249, 255]

$$S_{\text{memb.}} = -\int_{\mathcal{M}} d^3\xi \sqrt{-h}\, 2|q\phi| + \frac{q}{3!} \int_{\mathcal{M}} d^3\xi\, A_{\mu\nu\rho} \frac{\partial x^\mu}{\partial \xi^a} \frac{\partial x^\nu}{\partial \xi^b} \frac{\partial x^\rho}{\partial \xi^c} \epsilon^{abc}$$

$$= \int d^4x d^3\xi \sqrt{-g} \left[-\frac{\sqrt{-h}}{\sqrt{-g}} 2|q\phi| + \frac{q}{3!} A^\mu \epsilon_{\mu\nu\rho\sigma} \frac{\partial x^\nu}{\partial \xi^a} \frac{\partial x^\rho}{\partial \xi^b} \frac{\partial x^\sigma}{\partial \xi^c} \epsilon^{abc} \right] \delta^4(x - x(\xi))$$

[3] Here we have defined these quantities for a flat spacetime. They can be straightforwardly generalized to the case of curved space, see appendix H.

[4] For the sake of simplicity, we have written the theory in terms of a single scalar field, which may not appear to be explicitly invariant under field diffeomorphisms. This is not the case when the theory is written in terms of several chiral multiplets, see for example [259] for explicit details.

$$= \int d^4x\sqrt{-g}\left[-2|q\phi|J(x) + qA^\mu J_\mu(x)\right] \tag{6.26}$$

where h is the determinant of the induced metric on the membrane, $\mathscr{M}$ represents the membrane's worldvolume, ξ^i are the worldvolume coordinates and $x^\mu(\xi^i)$ represent the embedding functions of the membrane into the four-dimensional spacetime. Additionally, we have explicitly included the contribution of the spacetime metric for later use, and all the information regarding the shape of the membrane and its embedding in the ambient spacetime is stored in the functions $J(x)$ and J_μ, defined by

$$J(x) = \int d^3\xi \frac{\sqrt{-h}}{\sqrt{-g}}\delta^4(x - x(\xi)) \tag{6.27}$$

$$J_\mu(x) = \frac{1}{3!}\int d^3\xi\, \epsilon_{\mu\nu\rho\sigma}\frac{\partial x^\nu}{\partial\xi^a}\frac{\partial x^\rho}{\partial\xi^b}\frac{\partial x^\sigma}{\partial\xi^c}\epsilon^{abc}\delta^4(x - x(\xi)) \tag{6.28}$$

For example, for a flat membrane perpendicular to the z axis and located at $z = 0$, it is easy to check that $J(x) = \delta(z)$ and $J_\mu(x) = \delta^z_\mu\delta(z)$.

The first term of (6.26) is generally referred to as the Nambu-Goto term, which involves the tension of the membrane. In the case at hand, where a single complex scalar field is considered, the form of this tension is completely determined by requiring the preservation of supersymmetry [254] and it explicitly involves the value of the scalar field evaluated at the membrane worldvolume. Therefore, the field will be required to be non-zero at the membrane, in order to have a positive tension, and will be explicitly coupled to the membrane. We will see below that the appearance of the scalar field in this term will have interesting consequences on the emerging profile of the field across the membrane.

On the other hand, the second term, which is referred to as the Wess-Zumino term, gives a natural coupling between the 3-form and the worldvolume of the membrane, and is a straightforward generalization of the coupling term between a charged particle and the electromagnetic potential in electromagnetism. As shown in [248, 249], this term is responsible for the fluxes taking different values on both sides of the membrane. This will still be the case when scalar fields are included into the picture, and we will find that it has far-reaching consequences.

It is interesting to note that without the presence of the scalar field and membrane sources, the 3-form potential does not have any propagating degrees of freedom. The solutions of the 3-form field equations in this case are constant values of the field strength, $F^{\mu\nu\sigma\rho} = n\,\epsilon^{\mu\nu\sigma\rho}$; thus, when gravity is included, this corresponds to a contribution of the cosmological constant. Including the charged membranes allows the cosmological constant to change by the nucleation of these branes, which is essentially a higher-dimensional version of the Schwinger process [249, 252].

The equations of motion for the form field obtained by extremizing (6.20) with respect to A^μ yield

$$\partial_\mu\left(\frac{1}{2}K_{\phi\bar{\phi}}(*F_4) + \mathrm{Re}W_\phi\right) = qJ_\mu \tag{6.29}$$

For later convenience, it will be useful to define $J_\mu = \partial_\mu H$. Of course, in the flat membrane

case, this is simply $H(z) = \Theta(z)$, where $\Theta(x)$ is the usual Heavyside step function. With those definitions, we find the following equation of motion:

$$*F_4 = -2K^{\phi\bar{\phi}}\left(\mathrm{Re}W_\phi - (n + qH(x))\right) \tag{6.30}$$

Therefore, integrating out the form field from the full action and taking into account the contribution of the boundary term, we arrive to a theory for a complex scalar field of the form

$$S = \int d^4x\sqrt{-g}\left[-K_{\phi\bar{\phi}}\,\partial_\mu\phi\partial^\mu\bar{\phi} - K^{\phi\bar{\phi}}|\hat{W}_\phi|^2 - 2\left|q\phi\right|J(x)\right] \tag{6.31}$$

where $\hat{W}(\phi)$ is the following effective superpotential:

$$\hat{W}(\phi) \equiv W(\phi) - (n + qH(x))\phi. \tag{6.32}$$

One of the most interesting features of this result is that the membrane can now be thought to interpolate between to *distinct* scalar potentials $V_\pm = \left|\hat{W}_{\pm,\phi}\right|^2$ where the plus (minus) sign refers to the space with $z > 0$ ($z < 0$). Note that at each side of the membrane, the potential will be defined in terms of a flux which varies from one side to the other (namely, from n to $n + q$).

In the flat membrane case, the equations of motion for this theory follow from extremizing the action with respect to ϕ and assuming $\phi = \phi(z)$, we find:

$$K_{\phi\bar{\phi}}\partial_z^2\phi - K_{\phi\phi\bar{\phi}}|\partial_z\phi|^2 + K_{\phi\bar{\phi}\bar{\phi}}(K^{\phi\bar{\phi}})^2|\hat{W}_\phi|^2 - K^{\phi\bar{\phi}}\hat{W}_\phi\hat{\overline{W}}_{\bar{\phi}\bar{\phi}} - qe^{i\eta}\delta(z) = 0 \tag{6.33}$$

where $e^{i\eta} = \frac{q\phi}{|q\phi|}$ and, in this particular case,

$$\hat{W}(\phi) = W(\phi) - (n + q\Theta(z))\phi. \tag{6.34}$$

A particular solution of this equation of motion is also the solution of the first-order BPS equations [247, 259], obtained by requiring the preservation of part of the supersymmetry of the system:

$$\partial_z\phi + e^{i\eta}K^{\phi\bar{\phi}}\hat{\overline{W}}_{\bar{\phi}} = 0 \tag{6.35}$$

which is simply the generalization of (6.3) and includes the contribution of the membrane implicitly through the jump in the effective superpotential.

Example: quadratic superpotential

We will now consider a simple example for this model, which may also be found in [259] explained in full detail. In order to come as close as possible to the situation with the domain wall of the previous subsection, we will use

$$K(\phi,\bar{\phi}) = \phi\bar{\phi}, \qquad W(\phi) = \frac{1}{2}a\phi^2, \tag{6.36}$$

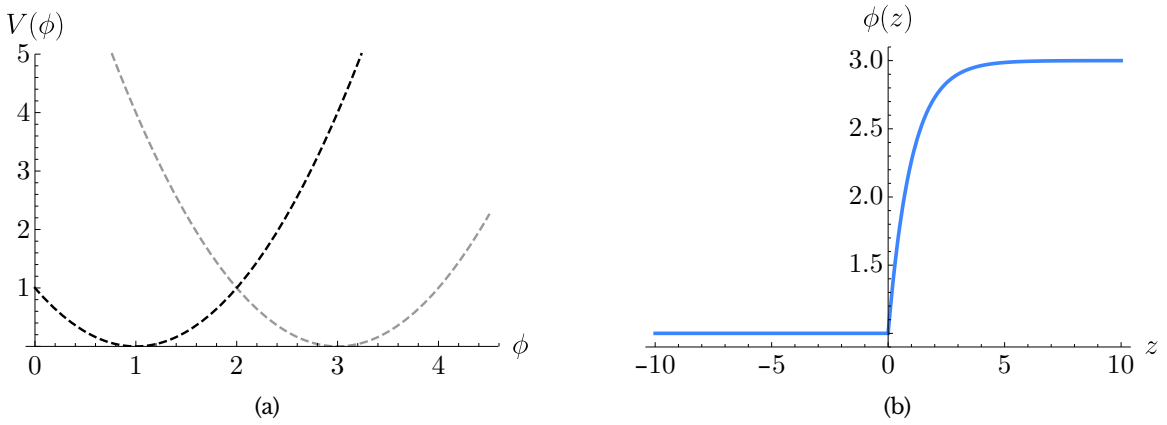

Figure 6.2: (a) Scalar potential, corresponding to eq. (6.37), with $n = 1$ and $q = 2$. The darker line represents the potential at $z < 0$, while the clearer one at $z > 0$. (b) Scalar field profile interpolating between the minima of the previous potential, with a membrane sitting at $z = 0$, see eq. (6.39).

where a is a constant with dimensions of energy; in the following, we will take $a = 1$. We will also assume the background flux is positive, $n > 0$, along with a flat membrane with $q > 0$ (so that $e^{i\eta} = 1$), with respect to the 3-form. On each side of the membrane, the theory for the scalar field is given by a different potential, namely we have

$$V_-(\phi) = |\phi - n|^2, \qquad V_+(\phi) = |\phi - (n+q)|^2. \tag{6.37}$$

for $z < 0$ and $z > 0$, respectively. This potential is shown in figure 6.2(a). As explained above, the perturbations of ϕ around its imaginary part are completely stabilized, and thus we will only consider the physics of its real part.

The BPS equation (6.35) yields

$$\begin{cases} \partial_z \phi(z) = -\bar{\phi}(z) + n & z < 0, \\ \partial_z \phi(z) = -\bar{\phi}(z) + n + q & z > 0. \end{cases} \tag{6.38}$$

This system is easily solved by considering the field to be real, imposing continuity at $z = 0$, and taking the field to asymptotically approach the supersymmetric minimum of the potential at each side of the membrane. This yields

$$\phi(z) = n + \Theta(z)\, q \left(1 - e^{-z}\right) \tag{6.39}$$

which we have plotted in figure 6.2(b). Indeed, the profile interpolates between the two different minima $\phi_\pm$ of their respective quadratic potentials on both sides of the brane. Notice the jump in the first derivative of the scalar field across the brane; as we will see below, this is entirely due to the tension of the membrane involving the scalar field ϕ.

One can also compute the tension of the membrane dressed with the scalar field, by integrating the energy of the whole system across the membrane. In the case at hand this

becomes

$$\sigma_{\text{DW+memb}} = 2\left|\frac{1}{2}(n+q)^2 - \frac{1}{2}n^2\right| = \left(2nq + q^2\right). \tag{6.40}$$

where we have noted that the superpotential is actually different at each side of the membrane. Note that this value is different from the one inferred from the Nambu-Goto contribution of the membrane which is $T_{\text{NG}} = 2nq$. If we consider the fact that the original flux (n) should be quantized in units of q and assume the situation where $n \gg q$, we notice that the correction to the tension is therefore small compared to the NG one.

6.3 Tunneling from a supersymmetry-breaking vacuum

Now that we have studied the interplay of scalar fields and fluxes in the presence of a static membrane, we are ready to take another step forward. In the following, we will analyze how the Coleman-de Luccia [67, 69] and Brown-Teitelboim [248, 249] schemes can be combined to yield a very interesting perspective on membrane nucleation in the presence of scalar fields.

In order to have a potential with non-degenerate vacua, we will add soft supersymmetry-breaking terms to the Lagrangian to get some shifted new minima which will expicitly break supersymmetry. This will allow the false vacuum solution (the highest of the two minima) to decay to the other vacuum by the formation of a membrane bubble that interpolates between them. This membrane bubble will have a structure locally similar to the flat membrane solution found earlier and should approach the supersymmetric profile as the supersymmetry-breaking terms are dialled down.

In order to study the tunneling from a state with the field in the false vacuum everywhere in space to a state with a spherical membrane coupled to the field, we will apply Euclidean methods and assume $O(4)$ symmetry as in the usual false vacuum decay process. In this setup, the membrane is a static 3-sphere. Using the conventions of [249], the Euclidean action can be found to be

$$\begin{aligned} S_E = &\int d^4x_E \sqrt{g_E}\left[K_{\phi\bar{\phi}} g_E^{\mu\nu}\partial_\mu\phi\partial_\nu\bar{\phi} - \frac{1}{4}K_{\phi\bar{\phi}}(*F_4)^2 + \frac{1}{2}(*F_4)\left(W_\phi + \overline{W}_{\bar{\phi}}\right) - \frac{1}{4}K^{\phi\bar{\phi}}\left(W_\phi - \overline{W}_{\bar{\phi}}\right)^2\right] \\ &+ \int d^4x\sqrt{g_E}\left[2|q\phi|J(x) + qA^\mu J_\mu(x)\right] + S_{\text{soft}} + S_{\text{bd}} \end{aligned} \tag{6.41}$$

where g_E represents the metric of Euclidean space[5] and S_{soft} represents the soft supersymmetry-breaking terms discussed in eq. (6.15).

Assuming spherical symmetry, the Euclidean metric will be given by

$$ds^2 = d\rho^2 + \rho^2 d\Omega_3^2 \tag{6.42}$$

[5] In the conventions of [249], the fully spatial components of $A^{\mu_1\mu_2\mu_3}$ are substituted by $iA^{\mu_1\mu_2\mu_3}$ in order to leave F^{0123} invariant under Wick rotations. Using the Hodge duals, this means that $*F_4 = \frac{1}{4!}\sqrt{-g}\epsilon_{\mu\nu\rho\sigma}F^{\mu\nu\rho\sigma} = -\sqrt{-g}F^{0123}$ should be left invariant as well. Note, however, that in Euclidean space we have $\epsilon_{0123} = \epsilon^{0123} = 1$, so $*F_4$ picks up a minus sign when described in Euclidean coordinates.

where $d\Omega_3$ represents the surface element of a 3-sphere. Recall, from our previous discussions on false vacuum decays using only scalar fields, that the false vacuum bubbles that we studied that may be thought of as bubbles of fixed radius (as in the thin-wall approximation). Therefore, the radius of the membrane in Euclidean space should also be a constant, which we will denote by R. Of course, once we Wick-rotate back to Lorentzian space, this $O(4)$ symmetry in Euclidean space will turn to $O(1,3)$ symmetry in Lorentzian space.

On the other hand, from the definition of $*F_4$ we easily see that

$$*F_4 = \frac{1}{\rho^3}\partial_\rho(\rho^3 A^\rho) \tag{6.43}$$

Integrating out the form fields as in the previous section using their equations of motion

$$*F_4 = D_\mu A^\mu = \frac{1}{\rho^3}\partial_\rho(\rho^3 A^\mu) = 2K^{\phi\bar{\phi}}\left(\mathrm{Re}W_\phi - n - q\Theta(\rho - R)\right)\,, \tag{6.44}$$

gives the straightforward counterpart of (6.31) for a static and spherical setup in Euclidean signature:

$$S_E = 2\pi^2 \int d\rho\ \rho^3 \left[K_{\phi\bar{\phi}}\left|\frac{d\phi}{d\rho}\right|^2 + V(\phi,\bar{\phi}) + 2\left|q\phi\right|\delta(\rho - R)\right]. \tag{6.45}$$

In the previous expression, V also includes the contribution from the supersymmetry-breaking terms in (6.15), namely

$$V = K^{\phi\bar{\phi}}\left|\hat{W}_\phi\right|^2 + \mu^2\phi\bar{\phi} + b(\phi^3 + \bar{\phi}^3), \qquad \hat{W} \equiv W - (n + q\Theta(r - R))\phi. \tag{6.46}$$

The equation of motion for the complex scalar field is then

$$\frac{1}{\rho^3}\partial_\rho\left(\rho^3 K_{\phi\bar{\phi}}\frac{d\phi}{d\rho}\right) = K_{\phi\bar{\phi}\bar{\phi}}\left|\frac{d\phi}{d\rho}\right|^2 + \frac{\partial V}{\partial\bar{\phi}} + qe^{i\eta}\delta(\rho - R) \tag{6.47}$$

where $e^{i\eta} = \frac{q\phi}{|q\phi|}$. This equation is greatly simplified if the kinetic term of the scalar field is in canonical form, namely if $K = \phi\bar{\phi}$ so that $K_{\phi\bar{\phi}} = 1$. In that particular case, the equation of motion for the scalar field reads

$$\frac{d^2\phi}{d\rho^2} + \frac{3}{\rho}\frac{d\phi}{d\rho} = \frac{\partial V}{\partial\bar{\phi}} + qe^{i\eta}\delta(\rho - R)\,, \tag{6.48}$$

which should be solved with the boundary conditions (6.18). This last equation is quite similar to the one which is generally used for false vacuum decay, see eq. (6.17); the only difference is that here we have derived it for a complex scalar field and that it has a contribution proportional to Dirac Delta function, due to the presence of a membrane of radius R.

To find the instanton solution in this case we should proceed with a little bit of care since the potential for the scalar field will be different on both sides of the wall. Most notably, the true and false vacuum of the theory now belong to two different potentials, as opposed to the usual case where they are both local minima of the same function.

We should integrate this equation starting at the true vacuum state at the center of the

bubble at $\rho = 0$ up to some distance ρ_*. At that point we should change the potential and integrate the new equations of motion with the new form of the potential $V_+(\phi)$ ending up in the false vacuum state. From our experience with the static flat membrane, we know that the field undergoes a jump in its first derivative at membrane crossing. We should expect a similar effect for the spherical membrane as well. In fact, integrating (6.48) between $R-\epsilon$ and $R+\epsilon$, where R is the radius of the Euclidean membrane, and making $\epsilon \to 0$, assuming ϕ is everywhere continuous, we find

$$\lim_{\epsilon\to 0}\left[\partial_\rho\phi(R+\epsilon) - \partial_\rho\phi(R-\epsilon)\right] = qe^{i\eta} \tag{6.49}$$

across the membrane. Note that this effect is entirely due to the presence of the scalar field in the Nambu-Goto term of the action (6.45).

This procedure has a free parameter: the radius of the membrane bubble, R. There are actually three different methods one can use to fix it in this non-gravitational case. First and foremost, one can evaluate the Euclidean action (6.45) at the solution as a function of this parameter. More concretely, the correct profile of the instanton that describes the quantum instability of the vacuum is the one that extremizes the tunneling probability (see eq. (1.59)), which is given in terms of

$$B = 2\pi^2\int_0^\infty d\rho\ \rho^3\left[K_{\phi\bar\phi}\left|\frac{d\phi}{d\rho}\right|^2 + V(\phi,\bar\phi) + 2\left|q\phi\right|\delta(\rho-R) - V_{\rm fv}\right] \tag{6.50}$$

where $V_{\rm fv}$ corresponds to the minimum of the potential outside the membrane.

One can also formulate this problem in terms of the energy difference between the false vacuum state and the state at the moment of emergence of the bubble in Lorentzian space. Indeed, there should be no energy loss or gain for the instanton solution at its emergence, and therefore the correct profile corresponds to the roots of the energy density difference, defined by

$$\Delta E = \int dV\,(T_{00} - V_{\rm fv}) = 4\pi\int_0^\infty dr\ r^2\left[K_{\phi\bar\phi}\left|\frac{d\phi}{dr}\right|^2 + V(\phi,\bar\phi) + 2\left|q\phi\right|\delta(r-R) - V_{\rm fv}\right]_{t=0}. \tag{6.51}$$

This expresion can be easily evaluated from the Euclidean solution since, as we commented in chapter 1, the profile obtained in Euclidean space corresponds to the profile of the emerging bubble in Lorentzian space at $t = 0$.

Finally, the radius of the membrane may also be fixed using its equation of motion. Varying the contribution of the spherical membrane to the action (6.41), we find

$$\left[\frac{3\left|q\phi\right|}{R} + \partial_\rho\left|q\phi\right| + \frac{q}{2}(*F_4)\right]_{\rho=R} = 0 \tag{6.52}$$

where all terms are evaluated at the membrane position. The Heaviside step function is regularized as $\Theta(0) = 1/2$, so the second and third terms in the equation above should be evaluated as the mean of each term with respect to its values to the left and right of the membrane. Note that this criterion is consistent with the one taken in the Brown-Teitelboim

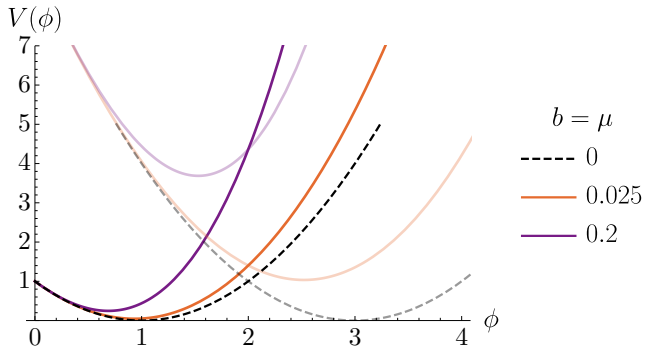

Figure 6.3: Scalar potential (6.54) for $n = 1$, $q = 2$ and some values of the supersymmetry-breaking parameters. The darker curve shows the potential inside the membrane ($\rho < R$), while the lighter one represents the potential outside it ($\rho > R$).

scheme, where the field strength at the membrane is also taken as the average of both sides. In our case, this particularly means that, using (H.23),

$$*F_4|_{\rho=R} = 2K^{\phi\bar{\phi}}\left(\mathrm{Re}W_\phi - n - \frac{q}{2}\right)_{\rho=R}. \tag{6.53}$$

Note, however, that eq. (6.52) does not provide any preliminary information about the value of the membrane radius, since it depends on the scalar field profile, which is unknown a priori. Therefore, one must still find the profile for several radii and either extremize B, find roots of ΔE and check the validity of (6.52).

6.3.1 *Example: quadratic superpotential*

In order to check the scheme above, we applied it to the supersymmetric model defined by (6.36), albeit with the inclusion of soft supersymmetry-breaking terms. In this case, the effective potential of the theory is

$$V(\phi,\bar{\phi}) = \left|\phi - \left(n + q\Theta(r-R)\right)\right|^2 + \mu^2\phi\bar{\phi} + b(\phi^3 + \bar{\phi}^3) \tag{6.54}$$

which is shown in figure 6.3 along the real part of ϕ. Once again, we will not consider the imaginary part of the scalar field, since the system is perturbatively stable along that direction.

As we said above, the radius of the membrane corresponding to the instanton solution is unknown, in principle. Therefore, for some supersymmetry-breaking parameter values b and μ, we computed the scalar field profiles for several R and used all three methods described above (namely, the radius should extremise the Euclidean action difference B, have no energy cost, i.e., $\Delta E = 0$, and the profile should satisfy eq. (6.52)) to find the correct membrane radius.

For a fixed membrane of radius R and for any parameters b and μ, we used the undershoot-overshoot algorithm described above to find the numerical profile of the scalar field. Of course, in so doing, one should take into account the jump on the first derivative of the profile at $\rho = R$, see eq. (6.49), and that the potential used for the evolution actually changes

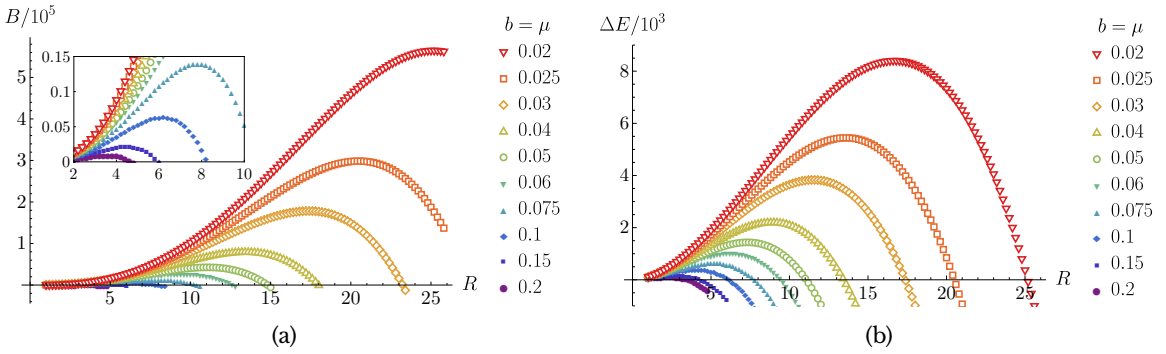

Figure 6.4: (a) Euclidean action and (b) energy difference with respect to the background, for solutions of the equation of motion (6.48), with $n = 1$, $q = 2$ and several values for R, b and μ. Note that the maxima of the Euclidean action correspond to the zeroes of ΔE, see figure 6.5.

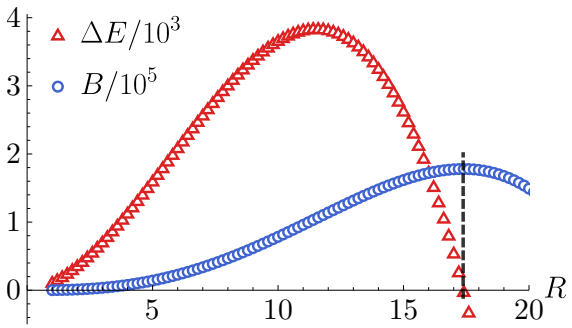

Figure 6.5: Energy and euclidean action difference with respect to the false vacuum state for several radii, in the case where $\mu = b = 0.03$. The maximum of B coincides with the root of ΔE, as expected.

when crossing the membrane. The resulting profiles were then used to corroborate which membrane radius corresponds to each choice of supersymmetry-breaking parameters. Our results are shown in figure 6.4. In fig. 6.4(a), we can clearly see that the maximum Euclidean action B of each branch is reached at an ever higher value of R as we tune down the supersymmetry-breaking parameters, just as we predicted above. We also checked the variation in the total energy of the profile with respect to the background at the time of nucleation, see figure 6.4(b); in all cases, the value of R corresponding to no energy loss or gain with respect to the background also corresponds to the maximum of the Euclidean action, see figure 6.5 for an explicit example.

The profiles corresponding to membrane-radii which extremized S_E (or satisfied any of the equivalent conditions) have been plotted in figure 6.6(a). As expected, as the supersymmetry-breaking parameters are made smaller, the radius of the emerging membrane increases and the scalar field profiles progressively tend towards the BPS solution derived above, as shown in fig. 6.6(b). A curious feature of these profiles is that, when considered as a particle in the inverted potential $-V$, they first tend to get away from the false vacuum, only to then be projected in the $r > R$ potential with enough velocity to asymptotically reach the false vacuum.

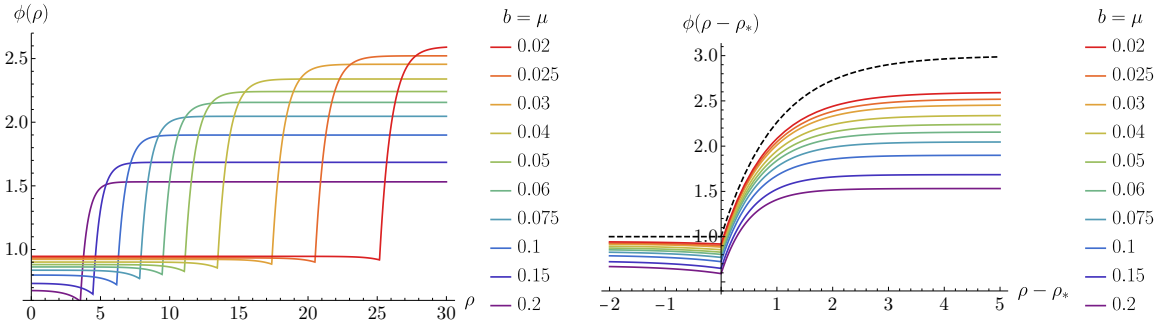

(a) (b)

Figure 6.6: (a) Scalar field profiles corresponding to each maximum Euclidean action for some supersymmetry-breaking parameters. (b) The same profiles as before, centered around the membrane radius corresponding to each profile. The dashed line represents the BPS solution from eq. (6.39), with $n = 1$ and $q = 2$, which is clearly the asymptotic behaviour of the profiles as the supersymmetry-breaking parameters b and μ tend to 0.

6.4 Flat membranes and domain walls in Supergravity

We now turn to study the same setup as in the previous section, with gravity taken into consideration. We will work in the context of $\mathcal{N} = 1$, $D = 4$ Supergravity coupled to chiral matter. We will be interested in generalizing the false vacuum decay discussed in the previous section to include gravity. However, before analysing more generic situations, we will first study the supersymmetric limit of flat membrane solutions in supergravity. Thus, in this section, we will start by analizing the action of the system composed by scalar fields, real three-forms and flat membranes in a spacetime of Lorentzian signature.

The action is once again given by

$$S = S_{\text{bulk}} + S_{\text{membrane}} + S_{\text{boundary terms}}. \tag{6.55}$$

As we review in appendix H, the bosonic part of the supersymmetric bulk action of the system, which includes gravity, scalar fields and 3-forms, is given by[6]

$$S_{\text{bulk}} = \int d^4x\sqrt{-g}\left[\frac{1}{2}R - K_{\phi\bar{\phi}}\partial_\mu\phi\partial^\mu\bar{\phi} - \frac{1}{3}e^{-K}(M + K_{\bar{\phi}}\overline{\mathscr{F}})(\overline{M} + K_\phi\mathscr{F}) - M\overline{W} - \overline{M}W \right.$$
$$\left. + e^{-K}K_{\phi\bar{\phi}}\mathscr{F}\overline{\mathscr{F}} + \mathscr{F}W_\phi + \overline{\mathscr{F}}\overline{W}_{\bar{\phi}}\right] \tag{6.56}$$

where

$$\mathscr{F} = \frac{1}{2}\left(D_\mu A^\mu + i\mathrm{d}\right) + \frac{2}{3}\bar{\phi}M + \frac{1}{3}\phi\overline{M}. \tag{6.57}$$

and we are using natural units with $M_{\text{Pl}} = 1$. In the above equations, R is the Ricci scalar, M is a complex scalar auxiliary field of the minimal supergravity multiplet, d is a real scalar auxiliary field and A^μ is the Hodge dual of the three-form of this setup. Just as in the non-

[6] Once again, the invariance under field redefinitions can be made explicit for more general systems, see [258, 259].

gravitational case, boundary terms must be included in the full action to ensure the variation of the action with respect to the form field is well posed. Note that the boundary terms will also include the Gibbons-Hawking term [268] in order for the variations with respect to the metric to be well defined.

The action of the membrane can be fixed by requiring the system to leave a fraction of the supersymmetry invariant after its inclusion, for the case of a flat membrane. When gravity is included in the system, it reads

$$\begin{aligned} S_{\text{memb.}} &= -\int_{\mathscr{M}} d^3\xi \sqrt{-h}\, 2e^{K/2}|q\phi| + \frac{q}{3!}\int_{\mathscr{M}} d^3\xi A_{\mu\nu\rho}\frac{\partial x^\mu}{\partial \xi^a}\frac{\partial x^\nu}{\partial \xi^b}\frac{\partial x^\rho}{\partial \xi^c}\epsilon^{abc} \\ &= -\int d^4x\sqrt{-g}\left[-2e^{K/2}|q\phi|J(x) + qA^\mu J_\mu(x)\right] \end{aligned} \tag{6.58}$$

where $J(x)$ and $J_\mu(x)$ have been defined in (6.28). Notice that the Nambu-Goto term now includes an exponential contribution in terms of the Kähler potential.[7]

It is easy to check that setting the form field and auxiliary fields on-shell and taking into account the contribution of the boundary terms, the action reads [260]

$$S = \int d^4x\sqrt{-g}\left[\frac{R}{2} - K_{\phi\bar{\phi}}\partial_\mu\phi\partial^\mu\bar{\phi} - V(\phi,\bar{\phi}) - 2\, e^{K/2}\left|q\phi\right| J(x)\right] + S_{\text{GH}} \tag{6.59}$$

where S_{GH} represents the Gibbons-Hawking boundary term, $V(\phi,\bar{\phi})$ is the usual $\mathcal{N}=1$, $D=4$ matter-coupled supergravity scalar potential

$$V(\phi,\bar{\phi}) = e^K\left[D_\phi\hat{W}K^{\phi\bar{\phi}}D_{\bar{\phi}}\hat{\bar{W}} - 3|\hat{W}|^2\right] \tag{6.60}$$

We have also denoted the usual Kähler-covariant derivative as $D_\phi = \partial_\phi + K_\phi$, and the potential is given in terms of the following effective superpotential:

$$\hat{W} = W - (n + qH(x))\phi. \tag{6.61}$$

where, just as in the non-gravitational case, we have defined $J_\mu = \partial_\mu H$, so that with a flat membrane we have $H(x) = \Theta(z)$, if it stands at $z=0$. Therefore, we retrieve the usual matter-coupled supergravity action, with a slightly modified superpotential due to the presence of three-form fluxes. The overall scalar potential will be different on both sides of the membrane and therefore we might find a profile which interpolates between supersymmetric minima of *different* potentials.

Let us begin with the case of a flat membrane interpolating between two supersymmetric vacua. Let us assume this static membrane sits at $z=0$. In order to study the profile across such a membrane, we will assume the following ansatz for the metric[8] [260]:

$$ds^2 = e^{2D(z)}(-dt^2 + dx^2 + dy^2) + dz^2 \tag{6.62}$$

[7] The exponential factor $e^{K/2}$ arises due to the super-Weyl rescaling and field redefinitions required to bring the action to Einstein frame, see appendix H for more detail.

[8] Note that with this choice of metric we will have $\sqrt{-h} = \sqrt{-g}$ when we evaluate the factors at $z=0$.

so that $\sqrt{-g} = e^{3D(z)}$. Let us turn to study the equation of motion for the scalar field, which is

$$\frac{1}{\sqrt{-g}}\partial_\mu\left(\sqrt{-g}K_{\phi\bar{\phi}}g^{\mu\nu}\partial_\nu\phi\right) = K_{\phi\bar{\phi}\bar{\phi}}\partial_\mu\phi\partial^\mu\bar{\phi} + \frac{\partial V}{\partial\bar{\phi}} + e^{K/2}\left[K_{\bar{\phi}}|q\phi| + qe^{i\eta}\right]\delta(z). \quad (6.63)$$

where $e^{i\eta} = \frac{q\phi}{|q\phi|}$. It is natural to assume that scalar field only depends on the transverse coordinate to the membrane, i.e., $\phi = \phi(z)$. Hence, the field obeys

$$\partial_z(K_{\phi\bar{\phi}}\partial_z\phi) + 3K_{\phi\bar{\phi}}\,\partial_z D\,\partial_z\phi = K_{\phi\bar{\phi}\bar{\phi}}\left|\partial_z\phi\right|^2 + \frac{\partial V}{\partial\bar{\phi}} + e^{K/2}\left[K_{\bar{\phi}}\left|q\phi\right| + qe^{i\eta}\right]\delta(z). \quad (6.64)$$

On the other hand, the Einstein equations for the metric can be combined to give

$$\partial_z^2 D + 3(\partial_z D)^2 = -V - e^{K/2}\left|q\phi\right|\delta(z) \quad (6.65)$$

Note that the deltas at $z = 0$ will yield jumps in the first derivative of both ϕ, as in the non-gravitational case, and in the scale factor D.

A supersymmetric and static domain wall may occur between non-degenerate minima, since essentially the gravitational contribution may compensate the difference in scalar potential between both vacua [247]. If supersymmetry is partly conserved across the profile of the domain wall, then the minima are bound to be either Minkowski or AdS vacua (note, however, that no supersymmetric domain wall may interpolate between two Minkowski vacua when gravity is included [247]).

With these remarks at hand, the BPS equations acquire the form [247, 259, 260]

$$\phi'(z) = \mp e^{K/2}e^{i\arg(\hat{W})}K^{\bar{\phi}\phi}D_{\bar{\phi}}\hat{W} \quad (6.66)$$

$$D'(z) = \pm e^{K/2}|\hat{W}| \quad (6.67)$$

where primes denote derivatives with respect to z, and the second equation is simply a first integral of (6.65). If we only consider the physics of the real part of ϕ, then, of course, $e^{i\arg(\hat{W})} \to \mathrm{sign}(\hat{W})$. It is convenient to write these equations in terms of

$$\mathcal{Z} \equiv e^{K/2}\hat{W}. \quad (6.68)$$

Note that the value of the scalar potential at supersymmetric critical points is then given by $V_{\mathrm{susy}} = -3|\mathcal{Z}|^2$. Indeed, in terms of $\mathcal{Z}$, the equations above read

$$\phi'(z) = \mp 2K^{\bar{\phi}\phi}\partial_{\bar{\phi}}|\mathcal{Z}| \quad (6.69)$$

$$D'(z) = \pm|\mathcal{Z}| \quad (6.70)$$

The sign choice to be used can be easily identified using these equations. First of all, we should note that since the membrane we are working with has a positive tension $\mathcal{T}$, we should expect the second derivative of the scale factor D to be always negative (see, for example, [269]). It is clear, then, that the behavior of $|\mathcal{Z}|$ around the membrane will define the correct sign to choose in the BPS equations. Furthermore, it can be explicitly checked

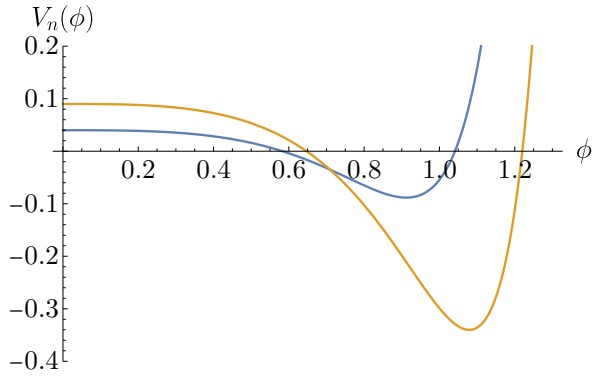

Figure 6.7: Scalar potential for the model described in this section. The blue curve corresponds to a flux integer of $n = 2$, while the orange one refers to $n = 3$.

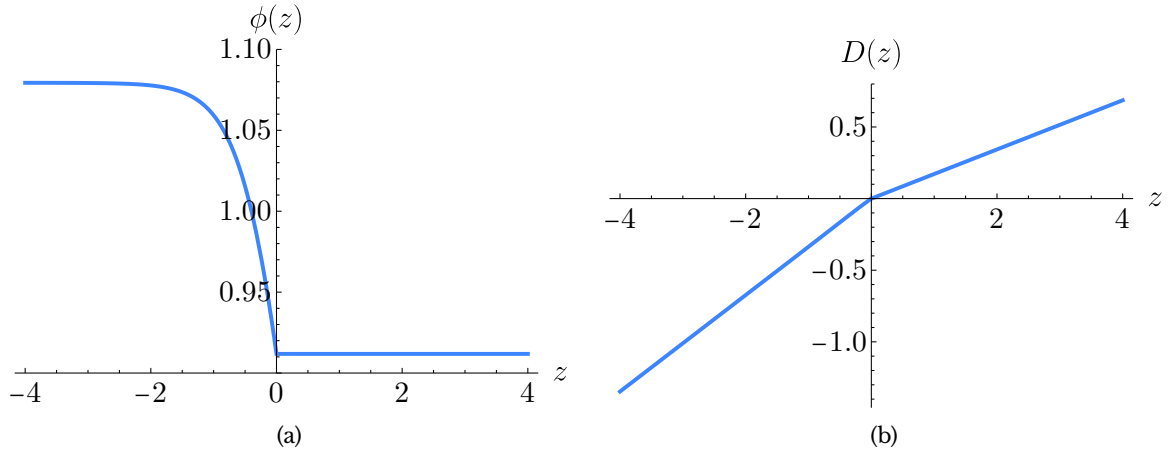

Figure 6.8: Solution of the BPS equations to the model defined in (6.71), for (a) the scalar field (b) the scale factor, for the metric defined in (6.62). The potential at $z < 0$ corresponds to the case $n = 3$, while $z > 0$ corresponds to $n = 2$; thus, the membrane is charged with $q = -1$.

from the definition of $\mathcal{Z}$ that, provided it is nowhere vanishing, it will increase or decrease monotonically along the z axis [260]. This means that if $|\mathcal{Z}|_{-\infty} < |\mathcal{Z}|_{+\infty}$, we should be using the lower sign (so D' experiences a downward jump at the membrane). Otherwise, we will need to use the upper sign. In case $|\mathcal{Z}|$ does have some root at, say, $z = z_0$, we will need to switch the sign of the BPS equations after crossing it. For more detail on these equations, see e.g. [247, 260].

6.4.1 *Example: quartic superpotential*

The above equations can be used to find the profiles of a scalar field interpolating between different minima of the model defined by[9]

$$K(\phi,\bar{\phi}) = \phi\bar{\phi} - \ln(100)M_{\rm Pl}^2, \qquad W(\phi) = M_{\rm Pl}^{-1}\phi^4. \tag{6.71}$$

where we have restored the Planck mass momentarily in order to show explicitly the energy scales involved in this example. The scalar potential defined by this Kähler potential and superpotential is shown in figure 6.7, once the 3-form has been integrated out. The minimum featured by each branch can be shown to be supersymmetric, i.e., it satisfies $D_\phi W = 0$.

Going back to units where $M_{\rm Pl} = 1$, the numerical BPS profile arising from this potential for both the scalar field and the scale factor D is shown in figure 6.8, where we have placed the lower minimum to the left (for easier comparison later on). We have also explicitly checked that the second-order equations (6.64) and (6.65), which explicitly incorporate the first-derivative jumps as Dirac deltas, yield exactly the same profiles.

6.5 Membrane nucleation in Supergravity

In the following we will generalize the procedure above to spherical membranes, just as in the previous part of this chapter. Following the usual Coleman-de Luccia scheme, we will turn to Euclidean space. Assuming $O(4)$ symmetry on our whole setup, the metric reads

$$ds^2 = d\chi^2 + \rho(\chi)^2 d\Omega_3^2, \qquad d\Omega_3 = d\varphi_1^2 + \sin^2\varphi_1 d\varphi_2^2 + \sin^2\varphi_1 \sin^2\varphi_2 d\varphi_3^2. \tag{6.72}$$

Of course, we should expect the solutions involving spherical membranes to approach the ones obtained for a flat membrane as the radius of the bubble increases.

The Euclidean action of our system will be

$$S_E = S_{\rm bulk,E} + S_{\rm memb,E} + S_{\rm soft,E} + S_{\rm bd,E} \tag{6.73}$$

where $S_{\rm bulk,E}$, $S_{\rm soft,E}$ and $S_{\rm bd,E}$ represent the straightforward Euclideanization of the bulk, soft supersymmetry-breaking terms and boundary terms of the action. On the other hand, the Euclidean membrane action, assuming a spherical setup, will be given by

$$S_{\rm memb,E} = 2\pi^2 \int d\chi\ \rho(\chi)^3 \left[2e^{K/2}|q\phi| + qA^\rho\right]\delta(\chi - R) \tag{6.74}$$

Thus, the membrane radius simply represents a fixed radial coordinate value.

Integrating out the form fields, we will retrieve the gravitational counterpart of (6.45),

[9] As shown in [260], shifting the Kähler potential by a constant, $K \to K + K_0$ rescales the scalar potential as $V \to e^{K_0}V$ and the length scales as $\chi \to e^{-K_0/2}\chi$. Furthermore, the supersymmetric action scales like $S \to e^{-K_0}S$. In case the supesymmetry-breaking parameter μ, for example, is contained within the action, then we should also require $\mu \to e^{K_0/2}\mu$. In order for this rescaling to be as simple as possible, we have chosen the constant below. This allows us to keep the energy density and the Nambu-Goto tension sub-Planckian.

namely:

$$S_E = \int d^4x\sqrt{g}\left[-\frac{R}{2} + K_{\phi\bar{\phi}}g^{ab}\partial_a\phi\partial_b\bar{\phi} + \tilde{V}(\phi,\bar{\phi})\right] + 2\int_{\mathcal{M}} d^3\xi\sqrt{h}e^{K/2}|q\phi| + S_{\rm GH} \quad (6.75)$$

where[10]

$$\tilde{V} = e^K\left(K^{\phi\bar{\phi}}\left|D_\phi\hat{W}\right|^2 - 3\left|\hat{W}\right|^2\right) + \mu^2\phi\bar{\phi}, \qquad \hat{W} \equiv W - (n + q\Theta(r-R))\phi. \quad (6.76)$$

As we will see afterwards, the Gibbons-Hawking boundary term will become important once we need to evaluate the actual value of the Euclidean action.

Just as we did above, we will be interested in investigating this decaying process in terms of soft supersymmetry breaking parameters added to the original scalar potential. That way, we will be able to see the flat membrane limit as the supersymmetric limit of this process.

We can obtain the equation of motion corresponding to the complex scalar field by extremizing (6.75) with respect to $\bar{\phi}$, which yields, assuming $\phi = \phi(\chi)$,

$$\partial_\chi\left(K_{\phi\bar{\phi}}\partial_\chi\phi\right) + \frac{3\,\partial_\chi\rho}{\rho}K_{\phi\bar{\phi}}\partial_\chi\phi = K_{\phi\bar{\phi}\bar{\phi}}\left|\partial_\chi\phi\right|^2 + \frac{\partial\tilde{V}}{\partial\bar{\phi}} + e^{K/2}\left[K_{\bar{\phi}}|q\phi| + qe^{i\eta}\right]\delta(\chi - R). \quad (6.77)$$

If we consider a canonical kinetic term on the fields, that is, $K(\phi,\bar{\phi}) = \phi\bar{\phi}$, then this equation reduces to

$$\phi'' + \frac{3\rho'}{\rho}\phi' = \frac{\partial\tilde{V}}{\partial\bar{\phi}} + e^{|\phi|^2/2}\left[\phi|q\phi| + qe^{i\eta}\right]\delta(\chi - R). \quad (6.78)$$

where primes denote derivatives with respect to the radial coordinate χ. Note that this equation corresponds to the usual one to be solved in Coleman-deLuccia vacuum transitions with complex scalar fields, save for the last term.

On the other hand, we can obtain the equations of motion for the scale factor through the extremization of (6.75) with respect to $g^{\mu\nu}$. Indeed, noting that the Ricci scalar and some components of the Ricci tensor are given by

$$R = -\frac{6}{\rho^2}\left(-1 + (\rho')^2 + \rho\rho''\right), \quad R_{\chi\chi} = -\frac{3\rho''}{\rho}, \quad R_{\varphi_1\varphi_1} = 2 - 2(\rho')^2 - \rho\rho'', \quad (6.79)$$

we find that the $\chi\chi$-component of the Einstein equation is given by

$$(\rho')^2 = 1 + \frac{\rho^2}{3}\left(K_{\phi\bar{\phi}}|\phi'|^2 - \tilde{V}\right) \quad (6.80)$$

while the $\varphi_1\varphi_1$-component yields

$$2\rho\rho'' + (\rho')^2 - 1 = -\rho^2\left(\tilde{V} + K_{\phi\bar{\phi}}|\phi'|^2\right) - 2\rho^2e^{K/2}|q\phi|\delta(\chi - R). \quad (6.81)$$

[10] We have omitted the supersymmetry-breaking cubic term for simplicity, as its effect (in this model, at least) was identical to turning on the quadratic term.

Both of these equations can be combined into

$$\rho'' = -\frac{1}{3}\rho\left(2K_{\phi\bar{\phi}}|\phi'|^2 + \tilde{V}\right) - \rho e^{K/2}|q\phi|\delta(\chi - R), \tag{6.82}$$

which we found to be numerically more stable than the former ones. Note that the deltas at $\chi = R$ will yield jumps in the first derivative of both ϕ and ρ, just as with the flat membrane.

Finally, note that the radius of the membrane, R, is still a free parameter of our system. Therefore, in order to fix it, we can take a similar approach as the one we took in the non-gravitational case. Namely, we can try solving the equations for several choices of R and find which one extremizes the Euclidean action (6.75). Another way to find the correct R for the instanton solution involves extremizing the action of the membrane (6.74) with respect to the radius. Doing so, we find

$$\left[3e^{K/2}\left|q\phi\right|\frac{\partial_\chi\rho}{\rho} + \partial_\rho\left(e^{K/2}\left|q\phi\right|\right) + \frac{q}{2}(*F_4)\right]_{\chi=R} = 0 \tag{6.83}$$

where, as in non-gravitational case, all discontinuous quantities at the membrane's position are evaluated through their means taken at each side, and the Lorentzian bulk solution for $*F_4$ has been obtained in (H.64), which depends explicitly on ϕ, and its constant n should be replaced by $n + q\Theta(r - R)$.

6.5.1 *Example: quartic superpotential*

In this subsection, we will apply the machinery described above to the simple model of eq. (6.71). In order to analyze the tunneling events in terms of the supersymmetry breaking parameter μ, we will have to take into account that the geometry of the Euclidean space will depend on the sign of the potential at the false vacuum, i.e., for $V_{\text{fv}} < 0$, the background will be a non-compact space, $V_{\text{fv}} = 0$ corresponds to the flat, Minkowskian background (which may be considered as a limiting case from AdS space in Euclidean signature), while $V_{\text{fv}} > 0$ will yield a compact space for the background [72].

All of the examples below were solved numerically using a simple overshoot-undershoot algorithm to find the correct initial condition for the scalar field. Note that, as far as the initial conditions for χ are concerned, the consistency of the equations of motion for the scale factor ρ will always require $\rho(\chi) = \chi + \mathcal{O}(\chi^3)$ for $\chi \to 0$, see [72] for further detail.

AdS/Minkowski to AdS transitions

As we mentioned above, this tunneling event occurs within a non-compact space. Therefore, the integral of the Euclidean action corresponding to the event with a membrane of coordinate radius R will diverge in general:

$$\begin{aligned} S_E &= 2\pi^2\int_0^\infty d\chi\left[\rho^3\left(|\phi'|^2 + \tilde{V}(\phi,\bar{\phi})\right) + 3\left(\rho^2\rho'' + \rho(\rho')^2 - \rho\right)\right] + 4\pi^2\left[\rho^3 e^{K/2}|q\phi|\right]_{\chi=R} + S_{\text{GH}} \\ &= 2\pi^2\int_0^\infty d\chi\left[\rho^3\left(|\phi'|^2 + \tilde{V}(\phi,\bar{\phi})\right) - 3\left(\rho(\rho')^2 + \rho\right)\right] + 4\pi^2\left[\rho^3 e^{K/2}|q\phi|\right]_{\chi=R} \end{aligned} \tag{6.84}$$

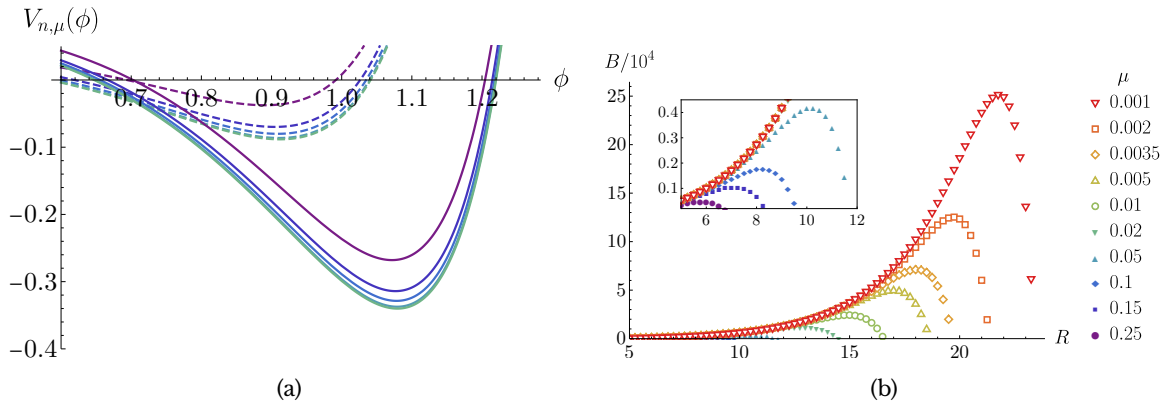

Figure 6.9: (a) Scalar potential for $n = 2$ (dashed) and $n = 3$ (solid). (b) Euclidean action for different fixed membrane radii R for a list of supersymmetry breaking parameters μ. The color corresponding to each μ is the same for both figures. Note that the radius R which extremizes the action increases as we diminish the supersymmetry-breaking parameter μ.

where, in the last step, the term we have integrated out cancels the contribution from the GH term (see [72, 270]). On the other hand, the integral corresponding to the background will also diverge:

$$S_{E,\text{bg}} = 2\pi^2 \int_0^\infty d\chi \left[\rho_{\text{fv}}^3 V_{\text{fv}} - 3\left(\rho_{\text{fv}}(\rho'_{\text{fv}})^2 + \rho_{\text{fv}}\right)\right], \tag{6.85}$$

where

$$\rho_{\text{fv}}(\chi) = \sqrt{\frac{3}{-V_{\text{fv}}}} \sinh\left(\frac{\chi}{\sqrt{\frac{3}{-V_{\text{fv}}}}}\right) \tag{6.86}$$

can be easily obtained plugging a constant and negative potential $V_{\text{fv}} < 0$ in (6.80). If the false vacuum is Minkowskian, then we will have

$$\rho_{\text{fv}}(\chi) = \chi, \tag{6.87}$$

which will also give an infinite contribution to the Euclidean action. However, the physically relevant quantity, which is the difference between these two actions (related to the tunneling rate from a background corresponding to the false vacuum, to a solution with a membrane separating two different potentials) is finite.

The key to computing this difference correctly lies in performing the integrations up to a certain ρ_{max}, such that its corresponding radial coordinate χ_{max} satisfies $\chi_{\text{max}} \gg R$, see [270] for more detail and an explicit proof of the convergence of this difference.

In figure 6.9 we show the result of computing this difference for several membrane radii and supersymmetry breaking parameter values. We can clearly see that the difference between actions is finite and reaches a maximum at a certain R, depending on μ. Furthermore, as the potential tends towards its original and supersymmetric form, the radius of the membrane interpolating between both branches of the scalar potential gets bigger, consistent with our expectations.

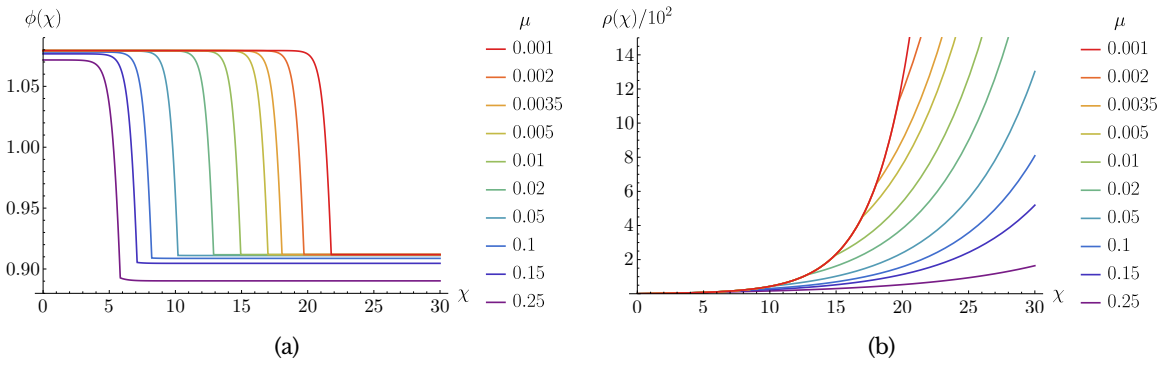

Figure 6.10: Evolution of (a) scalar field and (b) scale factor, for different supersymmetry parameters μ. Each case corresponds to the radius of maximum Euclidean action obtained in figure 6.9.

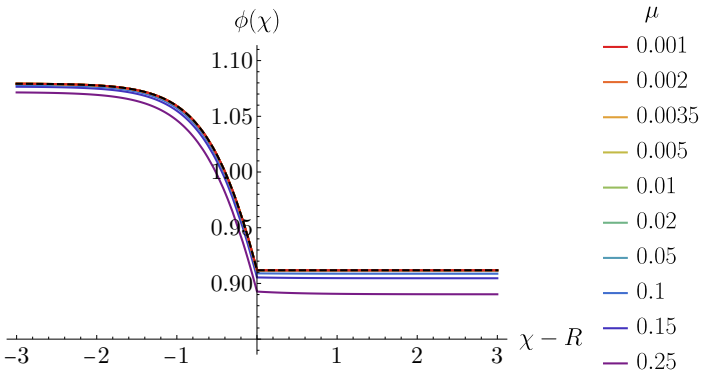

Figure 6.11: Evolution of scalar field for different supersymmetry parameters μ and around the membrane (i.e., R corresponds to the membrane's radial coordinate). The BPS case has been singled out with a dashed black line.

The profiles for both the scalar field and the scale factor corresponding to the radii with maximum Euclidean action difference for each μ are shown in figure 6.10. The scalar field profiles are all quite similar in shape, with the only differences resting on the positions of the true and false vacuum, and in the radius where the jump happens. On the other hand, the scale factor shows very clearly where the jump happens as well, and the exponential behaviour seems to pick up quite fast once the membrane has been crossed. All the profiles shown in fig. 6.10 satisfy equation (6.83).

In order to compare all these profiles with the limiting BPS case, we show in figure 6.11 a close-up plot around the membrane for all of them. Essentially, we see that the BPS profile is actually a limiting case for the scalar field, which concurs with our results in the non-gravitational case.

Tuning the supersymmetry-breaking parameter μ, we also analyzed an almost Minkowskian false vacuum ($\mu = 0.33$), see figure 6.12(a). Note that Minkowski false vacua are still non-compact spaces, and thus they should be analyzed in exactly the same fashion as AdS vacua.

After computing the Euclidean action difference for several radii, we found that the radius with maximum Euclidean action was $R = 5.2$ in the Minkowskian case. The profiles corresponding to a setting with such a membrane are shown in figure 6.13.

Finally, as explicitly shown in [249, 270], the requirement of energy conservation can be

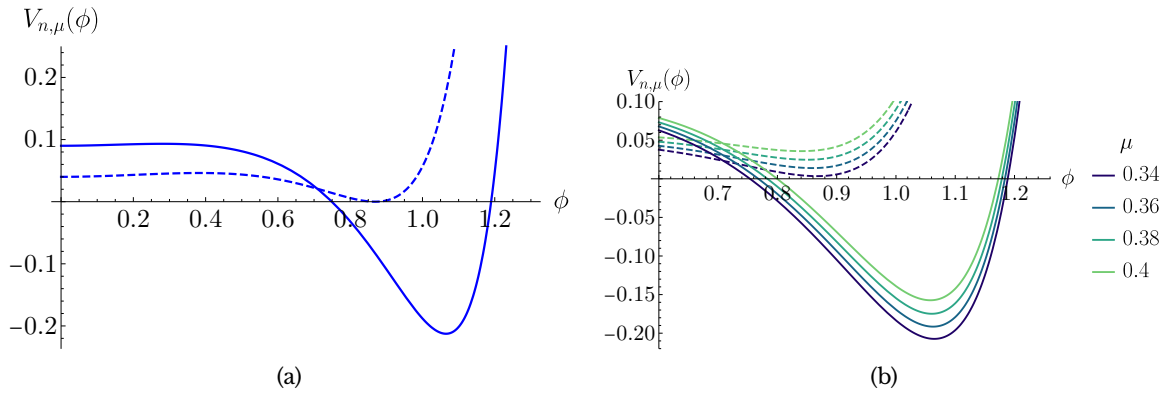

Figure 6.12: Scalar potential featuring (a) a Minkowskian false vacuum ($\mu = 0.33$) (b) Scalar potential with dS false vacua, for several supersymmetry breaking parameter values μ.

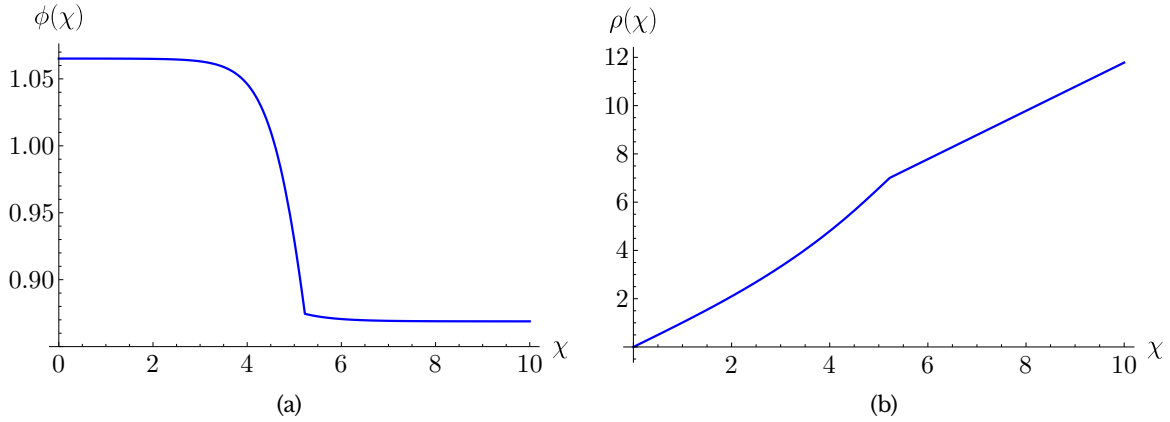

Figure 6.13: (a) Scalar field profile and (b) scale factor, for the potential shown in figure 6.12(a), corresponding to the membrane radius which maximized the Euclidean action difference.

generalized to tunnellings where gravitational effects are considered and the false vacuum is Minkowskian, by requiring the ADM mass vanishes. In our case, identifying the Euclidean ρ coordinate with the Lorentzial radial one, r, and taking the $\tau = 0$ spacelike surface, this implies[11]

$$\int dV\, T_{00} = 4\pi \int d\rho \rho^2 T_{00} = 4\pi \int_0^\infty d\chi\ \rho' \rho^2 \left[\left|\phi'\right|^2 + \tilde{V} + 2|q\phi| e^{K/2}\, \delta(\xi - R) \right] = 0. \tag{6.88}$$

We have checked that this condition is satisfied for the solution depicted in figure 6.13.

dS to AdS transitions

By making the supersymmetry-breaking parameter μ sufficiently big, we can actually make the false vacuum lie in a positive potential value, while the true vacuum rests at $V < 0$. As opposed to the previous cases, the compact geometry of this kind of instantons imposes

[11] As we mentioned above, $\rho'(R)$ should be evaluated as the mean between the derivative of the scale factor right before and after the membrane radius. Recall that this arises from our regularization of the Heaviside step function.

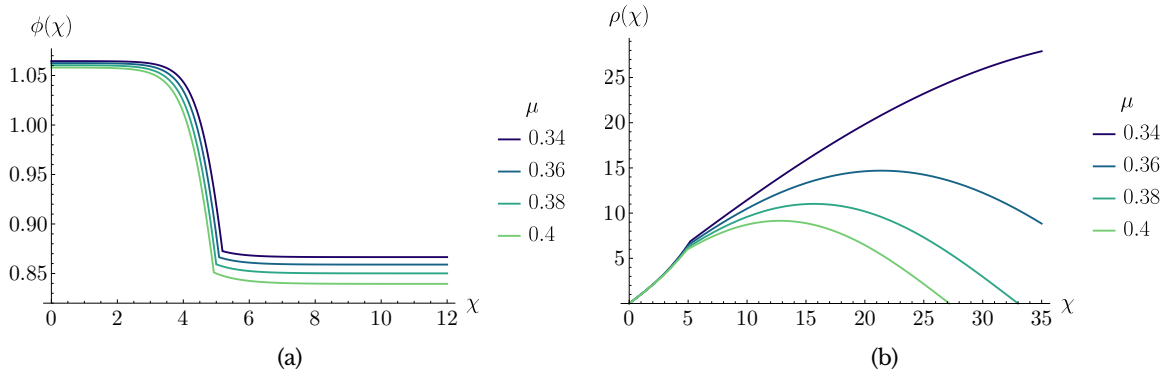

Figure 6.14: (a) Scalar field profile and (b) scale factor, for the dS → AdS decays between the potentials depicted in fig. 6.12(b). All profiles plotted here satisfy $\rho(\chi_{max}) = 0$ and $\rho'(\chi_{max}) = -1$ simultaneously.

boundary conditions at both the origin and the maximum value of the radial coordinate (see, e.g., [72]), where $\rho(0) = \rho(\chi_{\rm max}) = 0$. Of course, the Euclidean action (6.84) will be integrated up to $\chi_{\rm max}$. Indeed, the background consisting of a constant scalar potential $V_{\rm fv} > 0$ is described, in terms of our ansatz (6.72), by the following scale factor:

$$\rho_{\rm fv} = \sqrt{\frac{3}{V_{\rm fv}}}\sin\left(\frac{\chi}{\sqrt{\frac{3}{V_{\rm fv}}}}\right), \quad \chi \in [0, \chi_{\rm max}] \tag{6.89}$$

where $\chi_{\rm max}$ represents the first positive and non-zero root of $\rho_{\rm fv}$. Furthermore, the integral of the background action can be found analytically, and is given by

$$S_{\rm bg} = -\frac{24\pi^2}{V_{\rm fv}}. \tag{6.90}$$

Since the whole instanton is compact in dS → AdS decays, the only boundary conditions we can impose on the scalar field are[12] $\phi'(0) = \phi'(\chi_{\rm max})$=0. On the other hand, in order to find a non-singular instanton, for $\chi \to \chi_{\rm max}$ one must also require $\rho'(\chi) = -1 + \mathcal{O}((\chi - \chi_{\rm max})^3)$. We have found these requirements to be so restrictive, that for each potential in terms of μ shown in figure 6.12(b), only a *single* membrane radius solved the equations of motion correctly with respect to all of these boundary conditions.

The profiles of the scalar field and scale factor are shown in figure 6.14. The geometries shown in fig. 6.14(b) have been numerically shown to satisfy $\rho'(\chi_{\rm max}) = -1$. In all cases, the scale factor clearly shows an Euclidean AdS space starting at $\chi = 0$, which evolves up to the membrane radius, from where a compact Euclidean dS evolution follows.[13]

[12] Note that, in our case where a membrane is present, each of these boundaries is defined with respect to a different scalar potential (since the flux is different at each side of the membrane). Regardless, both $\phi(0)$ and $\phi(\chi_{\rm max})$ should lie close enough to the minimum of their respective potentials.

[13] Note that these profiles are full numerical solutions to the instanton equations; i.e., no thin-wall approximation has been used in order to compute either the scalar field or the scale factor.

6.6 Conclusions

In this chapter, we have studied a combination of the Coleman-deLuccia [67, 69] and Brown-Teitelboim [248, 249] formalisms for vacuum decay using both scalar fields *and* membranes, motivated from our study of flux compactifications. We have reviewed the existing theory on single three-form multiplets [258] which combines scalar fields and real three-form fields in a supersymmetric fashion, in the context of $\mathcal{N} = 1, D = 4$ supersymmetry and supergravity. Such a system has been studied with the inclusion of flat supersymmetric membranes in [260], which allows for interpolations between vacua defined by different potentials related by flux integers.

We have shown that adding soft supersymmetry-breaking terms to such a theory allows for rich phenomenological applications. Indeed, these terms enable false vacuum decays to occur through the nucleation of membranes. We have studied such systems using Euclidean methods and found the instanton solutions involving the form fields, scalar fields and membranes, both without and with gravity included. Furthermore, we have checked that we retrieve the correct supersymmetric limit as the supersymmetry-breaking terms are made smaller, so the flat membrane case can be taken as the limiting instanton solution corresponding to a membrane with infinite radius.

Recall from our discussion in chapter 1 that these processes have very interesting applications from a cosmological viewpoint [87], as they can naturally incorporate an emerging universe with an inflationary period. In this work we have only investigated transitions between very simple potentials, however, more phenomenologically interesting results may be obtained by considering more involved models. The transitions studied in this work essentially generalize the false vacuum decays we have studied in previous chapters, as these new ones naturally incorporate the contributions of the three-forms to the flux potential and the membranes which allow for transitions between them. On another note, recent proposals [271] have investigated the possibility of embedding the Universe within a positively curved membrane created due to a false vacuum decay in a higher-dimensional theory. While we have studied these models in a four-dimensional environment, it could be interesting to generalize our results to higher dimensions to check the compatibility of these processes with the ones discussed in [271].

From a numerical perspective, we should note that the models we have solved here were quite simple, in that they only involved a single (effectively real) scalar field. Such models are quite easy to solve using an undershoot/overshoot algorithm, even when membranes and gravity are present in the setup. However, as we know from the previous chapter, solving non-perturbative decays with two or more scalar fields is no simple matter. Thus, it might be useful to construct algorithms to compute false vacuum decays which effectively incorporate the first-derivative jumps on both the scalar fields and the scale factor.

Of course, the examples we have explored here can be generalized in several ways, aside from using more involved superpotentials. For once, we have broken supersymmetry by including explicit soft supersymmetry-breaking terms, motivated from phenomenological considerations [264]. However, recall that the tension of the membrane was chosen so that when flat branes are considered, the whole system of scalar fields, form fields and the membrane preserve half of the supersymmetry. Therefore, another interesting direction to

explore would consist on breaking supersymmetry by somehow detuning the Nambu-Goto term of the membrane.

Finally, in the models explored here we have considered single three-form multiplets, which allow for one real three-form field for each complex scalar field in the model (see appendix H and [258]). However, from our discussion in part II, we know that in a general flux Landscape of type IIB compactifications, we require $2h^{1,2}+2$ real (and integer) fluxes, where $h^{1,2}$ is the number of complex structure moduli. In order to build such a model in the context of three-form supergravity, we will require so-called double three-form supergravity, which allows for the inclusion of *complex* three-forms in the multiplets (i.e., two real fluxes for each complex scalar field) plus a complex three-form coupled directly to the supergravity multiplet. Such a system has been considered in [272], where some restrictions have been pointed on the possible EFTs that may be considered as candidates for generating transitions between vacua with flat membranes. It may be interesting to re-check this restrictions when considering false vacuum decay mediated by supersymmetry-breaking spherical membranes.

Part IV

Final remarks

Chapter 7

General conclusions and outlook

In this thesis, we have explored several aspects of the String Theory Landscape, focusing on the properties of its vacuum solutions and their ties to phenomenological aspects of String Theory and Cosmology. As we have reviewed in chapter 1, the need to compactify the extra dimensions of String Theory leads us to this collection of potentials determined by the internal geometry of the compact dimensions and the fluxes required to stabilize them. Thus, a solid knowledge of the Landscape and its vacuum solutions is vital to construct phenomenologically acceptable scenarios which might link such a high energy theory with our observations.

The first block of this work has been devoted to the study of vacua and other points of interest of the String Theory Landscape, which we have constructed using the ingredients outlined in the introductory chapter. In chapter 2 we have reviewed how the symmetries of the flux Landscape can be used in our favour to truncate a subset of the moduli present in the theory. In those cases where the symmetries reduce all of the physics to a single effective dimension, we have been able to obtain the scalar mass spectrum of the axiodilaton and complex structure sector of any vacuum in the Large Complex Structure regime, along with their statistical properties. This information is of particular interest to construct vacua with *all* moduli stabilized, since systematic stabilization schemes of the Kähler sector may require the rest of the moduli to be completely stable against α' or instanton corrections. On the other hand, we have also been able to explore the properties of vacua with parametrically small instanton corrections (which allow for the best perturbative control of the EFT) by setting the flux $N_A^0 \equiv f_A^0 - \tau\, h_A^0 = 0$. In that particular case, we have found that all masses are of the order of the gravitino mass ($m_{3/2}$) except for a single one, which may be found to be parametrically massless.

Even though the conclusions of that particular chapter apply only to those models admitting a supersymmetric truncation to a single field, in chapter 3 we found that a particular ansatz on the fluxes and the fields actually constitutes such a truncation, without alluding to any symmetry of the moduli space. More concretely, the ansatz on the fluxes involves the condition $N_A^0 = 0$, so all the results and conclusions regarding that kind of vacua are applicable to *any Calabi-Yau orientifold* compactification of type IIB String Theory, provided one applies the ansatz described in (3.17). Therefore, we have found a particular region of the moduli space of any compactification where the complete mass spectrum of the axiodilaton

and complex structure sector can be found analytically, and it only depends on the vacuum expectation value of the surviving modulus. Furthermore, we have noted in our statistical analysis of the spectrum that as long as one stays away from the LCS point, where the above mentioned massless mode appears, all the masses are guaranteed to be of the order of $m_{3/2}$. Thus, as long as all corrections to the EFT are under control, one may safely proceed to the stabilization of the Kähler sector.

A natural continuation of the works presented in chapters 2 and 3 is then to find a systematic way of applying the results above to stabilize the Kähler sector of geometries where the complex structure sector can be reduced by a single field either due to symmetries or by the imposition of a special ansatz. In any case, as we noted in chapter 3, we expect the Large Volume Scenario for Kähler moduli stabilization to be an adequate scheme to perform this task, since our no-scale vacua satisfy, in general, $W_0 \sim \mathcal{O}(1)$. If this follow-up study were shown to be successful, it would give us a way to construct vacua with *all* moduli stabilized, and would provide an excellent stepping stone towards a phenomenologically consistent vacuum of String Theory.

On a related note, regarding the stabilization of the Kähler moduli, in chapter 4 we simultaneously considered the axiodilaton, complex structure fields and a single Kähler modulus in a simple compactification with non-perturbative terms included, giving rise to the so-called *Racetrack* potential. While this scheme lacks the complexity of the previous ones (and does not consider the truncated moduli of the complex structure sector), it gave us a useful arrangement to look for anti-de Sitter minima and de Sitter saddle points in the flux-induced scalar potential of the theory. This was done in the context of the strong de Sitter Swampland conjecture, stating that there should be no de Sitter critical points (neither minima, maxima nor saddle points) with a positive vacuum energy. Starting from some known solutions in the very model we worked with, we were able to tune the flux integers and racetrack parameters to generate models which not only featured supersymmetric minima, but also de Sitter saddle points. The latter, of course, violate the strong de Sitter conjecture, but are in agreement with the soft version of the statement. In any case, the model we have used in this chapter may be generalized in many ways, for example, by considering the complete Kähler structure of the geometry, or using any other truncation ansatze on the complex structure sector.

The second block of this thesis has been focused on the cosmological aspects of the String Theory Landscape, focusing on the physical processes and properties of minima and other interesting points. For that matter, in chapter 5, we have modelled the Landscape using Gaussian Random Fields, as a motivation to ease the study of higher-dimensional potentials without having to deal with all the intricacies of the high energy Physics behind them. In order to perform a more efficient study, we reviewed and developed conditioning techniques known as *Slepian models*. These allowed us to ease the analysis of minima and inflationary inflection points in random Landscapes, which generically become scarcer as the dimensionality of the potential grows, which makes their study quite prohibitive. Thanks to these conditioned potentials, we were able to fine tune the properties of these relevant points to suit our needs. As we saw in chapter 5, Slepian models allow for the generation of models which enable a local and global study of random potentials, thus enabling us to study false vacuum decay from conditioned minima and inflationary processes around

conditioned inflection points. Thanks to these conditioning techniques, we have been able to obtain accurate statistics using numerical software and check the validity of different approximations.

Of course, Slepian models still have a lot to offer. For once, they might be used as conditioning techniques to study random and non-gaussian potentials, which might be more suitable candidates for studying random models of the Landscapes. On the other hand, the Slepian models used here have been applied to only two-dimensional potentials, but they are in principle valid for any number of dimensions. We might then apply some of the most successful approaches to estimate the decay-rate of minima, for example, to those cases. Furthermore, a more in-depth study of inflation in these random potentials is still in order, since the cases we studied here only consider extremely fine-tuned inflection-points, which might yield phenomenologically acceptable observables. Therefore, developing a more intricate study of inflation which accounts for any kind of inflection point in the Landscape could provide insightful data about how likely each type of inflection point could occur in a random potential, as well as their inflationary properties.

Finally, on the topic of tunnelling instabilities, in chapter 6 we have developed a framework to consider instantons which involve scalar fields, membranes and fluxes, which may point toward a more realistic way of undergoing decays in the Landscape. We have shown that such instanton solutions exist in models where supersymmetry is explicitly broken, both with and without gravity included in the setup. Quite interestingly, membranes interpolate between regions described by different flux quanta (just as in the Brown-Teitelboim scheme), and scalar fields satisfy the usual boundary conditions of Coleman-deLuccia false vacuum decay. Furthermore, in all cases, as the supersymmetry-breaking terms are made smaller, we have found that the membrane radius of the solutions grows ever bigger, so the solutions have the correct asymptotic behaviour towards a flat supersymmetric domain wall.

Even though the models studied here are quite constrained by the requirement that bulk supersymmetry be preserved in the flat membrane case, this might prove to be a very interesting first step towards realistic transitions in the Landscape, where not only moduli are considered to be part of the decay, but also the fluxes threading the compact geometry. On the other hand, we have only considered very simple examples with a single flux and scalar field, but there is still room for generalizing these models. We could, for example, detune the membrane tension to break supersymmetry that way, or we could also use models with more fluxes and scalar fields, such as the ones we have considered in chapters 2-4, in order to construct realistic vacuum decays in phenomenologically interesting models of type IIB String Theory.

Part V

Appendices

Appendix A

Hodge decomposition of the flux vector

In this appendix we review the Hodge decomposition of the flux vector N [134]. This decomposition was used in section 2.4.4 of the main text, and is also the starting point for the derivations of the probability distributions of the type IIB flux ensemble.

The flux vector N has complex dimension $2h^{2,1}+2$ and transforms non-trivially under the symplectic group $\mathrm{Sp}(2h^{2,1}+2,\mathbb{Z})$, i.e., it is a *symplectic section*. As we reviewed in section 2.2, the set of $2h^{2,1}+2$ vectors $\mathscr{B}=\{\Pi,\overline{\Pi},D_a\Pi,D_{\bar{a}}\overline{\Pi}\}$ evaluated at any given point $\{\tau,z^a\}$ is also composed of symplectic sections, which can be shown to be linearly independent. In other words, the set $\mathscr{B}$ forms a basis in the space of sections. To prove the linear independence of the elements of $\mathscr{B}$ we introduce the symplectic product $\langle A,B\rangle$ of two sections A and B,

$$\langle A,B\rangle = A^T\cdot\Sigma\cdot B, \tag{A.1}$$

where Σ is the symplectic invariant matrix (1.27). Then, it can be checked from the definition of Π that the elements of $\mathscr{B}$ satisfy the orthogonality relations

$$\begin{aligned}
\langle\Pi,\overline{\Pi}\rangle &= \mathrm{i}e^{-K_{cs}},\\
\langle\overline{\Pi},\overline{\Pi}\rangle &= 0,\\
\langle\Pi,D_a\Pi\rangle &= 0,\\
\langle\Pi,D_{\bar{a}}\overline{\Pi}\rangle &= 0,\\
\langle D_a\Pi,D_b\Pi\rangle &= 0,\\
\langle D_a\Pi,D_{\bar{b}}\overline{\Pi}\rangle &= -\mathrm{i}e^{-K_{cs}}\delta_{a\bar{b}},
\end{aligned} \tag{A.2}$$

from which the linear independence of the set $\mathscr{B}$ follows. In this setting the Hodge decomposition of the flux vector can be obtained as the decomposition in the basis of sections $\mathscr{B}$,

$$N=\sqrt{4\pi}(a_0\Pi+\bar{b}_0\overline{\Pi}+a^aD_a\Pi+\bar{b}^aD_{\bar{a}}\overline{\Pi}). \tag{A.3}$$

Using these orthogonality relations it is straightforward to find that the coefficients $\{a_0,a^a,b_0,b^a\}$

are determined by the values of the superpotential and its derivatives at the point $\{\tau, z^a\}$

$$a^0 = -e^{K_{cs}} D_{\bar{0}} \overline{W}, \qquad \bar{b}^0 = ie^{K_{cs}} W, \qquad a^a = e^{K_{cs}} D_{\bar{0}} D_{\bar{a}} \overline{W}, \qquad \bar{b}^a = -ie^{K_{cs}} D_a W. \tag{A.4}$$

Therefore, the basis elements Π, $D_a\overline{\Pi}$, $D_{\bar{a}}\Pi$ and $\overline{\Pi}$ correspond to the $(3,0)$, $(1,2)$, $(2,1)$ and $(0,3)$ components of the flux $G_3 = F_3 - \tau H_3$, respectively. In particular, at no-scale vacua (1.37), which is the moduli space locus where the parts $(3,0)$ and $(1,2)$ of G_3 vanish (i.e., G_3 is "imaginary self-dual"), the Hodge decomposition reduces to

$$N = \sqrt{4\pi} e^{K_{cs}} (iW\,\overline{\Pi} + D_{\bar{0}} D_{\bar{a}} \overline{W}\, D_a \Pi)\,, \tag{A.5}$$

Substituting this expression into (1.41) we can obtain an expression for the $D3$-charge induced by imaginary self-dual fluxes:

$$\begin{aligned} N_{\text{flux}} &= -i4\pi e^{2K_{\text{cs}}+K_{\text{d}}} \left(|W|^2 \left\langle \Pi, \overline{\Pi} \right\rangle + |D_0 D_1 W|^2 \left\langle D_{\bar{1}} \overline{\Pi}, D_1 \Pi \right\rangle \right. \\ &\qquad \left. +2\text{Im}\left[\overline{W} D_{\bar{0}} D_{\bar{1}} \overline{W} \langle \Pi, D_1 \Pi \rangle \right] \right) \\ &= 4\pi e^{K_{\text{cs}}+K_{\text{d}}} \left(|W|^2 + |D_0 D_1 W|^2 \right), \end{aligned} \tag{A.6}$$

where, in the last step, we have applied the identities (A.2). Finally, using the definitions of the gravitino mass and m_{susy}, we find N_{flux} to be positive semidefinite, and given by

$$0 \leq N_{\text{flux}} = 4\pi \mathcal{V}^2 \left(m_{3/2}^2 + m_{\text{susy}}^2 \right) \leq L. \tag{A.7}$$

Appendix B

Numerical search of no-scale solutions in the octic

In this appendix we describe in detail the numerical method used in this work to obtain the ensemble of no-scale solutions for the $\mathbb{WP}^4_{[1,1,1,1,4]}$ model, also known as the octic. As discussed in section 2.5, this model features a single complex structure modulus and an axio-dilaton, which we seek to stabilize at no-scale configurations (1.37).

B.1 Polynomial homotopy continuation and Paramotopy

It can easily be checked, using the machinery described in section 2.2, that the no-scale conditions can be expressed as a system of non-linear polynomial equations near the LCS point, where the instanton contributions to the prepotential (2.1) can be neglected [166]. In the following we will denote this polynomial form of the no-scale conditions (1.37) by

$$P_i(z,\bar{z},\tau,\bar{\tau};f,h)=0, \quad i=\{1,2\}, \tag{B.1}$$

where f and h are the *quantized* flux vectors defined in (1.33), and which are subject to the *tadpole condition* (1.42). The main numerical difficulty of this problem lies in solving the polynomial system of equations (B.1) for the huge number of allowed choices of f and h.

In recent years, one of the most outstanding algorithms to solve systems of the form of (B.1) has been that of *polynomial homotopy continuation* (PHC), coined within the field of numerical algebraic geometry [164,165]. Schematically, this method works as follows:

1. Given the set of polynomial equations to be solved, $P(x)=0$, the first step is to construct an auxiliary system of equations, $Q(x)=0$, which is easily solvable and that has the same maximal number of solutions. We then define

$$H(x,t)=\gamma(1-t)Q(x)+tP(x), \tag{B.2}$$

which is known as the *homotopy* function, where $t\in[0,1]$ and γ is a random complex

number.[1]

Note that the roots of $H(x,0)$ correspond to those of $Q(x)$, while the roots of $H(x,1)$ are those of $P(x)$, the ones we are interested in.

2. Once the roots of $Q(x) \propto H(x,0)$ are determined, it can be shown that, as t increases, the roots of $H(x,t)$ will be continuously deformed from their original values [165]. Thus, we can easily track the path each solution takes as we vary t up to $t=1$, where the solutions correspond to the solutions to our problem.

Many different implementations of the PHC method can be found in the literature, such as `phcpy` [273], `StringVacua` [274], and `Bertini` [275]. In this work, we have used `Paramotopy`[2] [163], a highly efficient PHC-based algorithm specially suited for polynomial systems like (B.1) which depend on parameter tuples.

In short, `Paramotopy` works in two steps. Given a certain parametrically-dependent polynomial system $P(x;p)$, it first performs the above PHC algorithm for a random p_0. Once that has been solved, it performs the same algorithm for the homotopy

$$H(x,t;p_0,p) = \gamma(1-t)P(x;p_0) + tP(x;p) \tag{B.3}$$

where p corresponds to one of the parameter choices we are interested in. However, in this second run, the number of paths that have to be tracked is qualitatively smaller than in the first step, as only those paths that led to proper solutions of $P(x;p_0)$ have to be followed. In cases where the number of well-behaved paths is orders of magnitude lower than the maximum number of solutions, this second step proves to be crucial for an efficient solution [163].

B.2 Search for no-scale solutions in one-parameter models

In order to perform a consistent exploration of the moduli space vacua of the octic, we took random integer flux values from a uniform distribution, that the components of the flux vectors satisfy $f,h \in [-f_{max}, f_{max}]$. Only those flux tuples satisfying the tadpole condition

$$0 < h\cdot\Sigma\cdot f \leq L \tag{B.4}$$

were kept where, for our purposes, we took $L=972$, and chose $f_{max}=50$ to be sufficiently large for the distribution of the $D3$-charge N_{flux} (1.41) to converge to a flat distribution. This way, we avoid artificially induced boundary effects associated to having set a finite value for f_{max}.

For the case of generic flux vacua, we generated 10^7 flux tuples consistent with the tadpole condition. On the other hand, for the constrained case, we generated 10^6 consistent flux

[1] This parameter ensures no singularities will occur during the deformation of $Q(x)$ into $P(x)$. For more detail, see [165].

[2] Software available at `www.paramotopy.com`

tuples[3] following the algorithm above, while manually keeping $f_A^0 = h_A^0 = 0$.

With these parameter choices in hand, we employed `Paramotopy` to solve the system of no-scale conditions given by (1.37). Note that (1.37) involves both τ, z and $\bar{\tau}, \bar{z}$. One possibility to deal with this would be to solve for the real and imaginary parts of each variable. However, here we solved for barred and unbarred variables separately, and then only kept those solutions which actually satisfied the conjugation relation between the variables. We found that this second choice was easier to solve by the software, and kept the equations simple. The whole process took around 5 hours in a 46-core machine for the constrained ensemble (10^6 tuples) and 50 hours for the generic ensemble (10^7 tuples).

From the resulting ensemble of no-scale solutions, we only considered (in section 2.6) those with moderately small instanton corrections. When performing this cut in our ensemble data, we made sure that the EFT we used to describe the octic model is indeed reliable. The sizes of these corrections were considered *a posteriori*, once the tree-level equations had been solved. More specifically, at each of the obtained solutions, we computed the Kähler potential and Kähler metric, both neglecting entirely the instanton contributions to the prepotential and considering the leading correction (2.52). First, we selected only those solutions for which the Kähler metric was still well defined after including the corrections, i.e., where it was non-degenerate and positive. Then, with these solutions, we computed the gravitino mass $m_{3/2}$, rescaled Yukawa coupling $\mathring{\kappa}$, and Kähler metric (with and without considering the leading instanton), and selected those vacua where the relative corrections were $< 20\%$. The resulting ensemble of solutions is represented in blue in the histograms of figures 2.7, 2.8 (generic ensemble), and 2.11 (constrained ensemble).

B.3 Redundancies of the EFT and solution duplicates

As discussed in sections 2.2 and 2.5, the low energy supergravity description of type IIB string compactifications has two inherent redundancies: one associated with the modular $\mathrm{SL}(2,\mathbb{Z})$ transformations (1.39), and one associated with the symplectic transformations acting as in (1.28) and (1.38). Thus, no-scale solutions which can be related to each other by any combination of these transformations should be regarded as equivalent.

To avoid double-counting no-scale solutions related by the $\mathrm{SL}(2,\mathbb{Z})$ symmetry, we transported each solution to the fundamental domain of the modular group, given by the complex upper half-plane with $|\tau| > 1$ and $|\mathrm{Re}(\tau)| < 1/2$. This operation can be easily performed by successively applying the generators of the group, given by

$$\underset{\tau \to \tau + b}{T_b = \begin{pmatrix} 1 & b \\ 0 & 1 \end{pmatrix}} \quad , \quad \underset{\tau \to -1/\tau}{R = \begin{pmatrix} 0 & -1 \\ 1 & 0 \end{pmatrix}} \, . \tag{B.5}$$

Note that while these transformations change the value of f and h, it can be shown that the quantity N_{flux} remains invariant, so the transported solutions will nevertheless satisfy the

[3] Random fluxes are more prone to high corrections as opposed to those with $N_A^0 = 0$, mostly due to the difference in the number of solutions near the LCS point. Thus, to keep a considerable amount of solutions in the former case, we generated more flux tuples.

tadpole condition.

As for the symplectic transformations, at large complex structure the corresponding source of redundancy comes from the monodromy around the LCS point, which acts on the complex structure field z and the fluxes as [98,124,133,172]

$$z \to z - i\, n \qquad \equiv \qquad \begin{cases} N \to A^n \cdot N \\ \Pi \to A^n \cdot \Pi \end{cases} , \tag{B.6}$$

where $n \in \mathbb{Z}$ and

$$A = \begin{pmatrix} 1 & 0 & 0 & 0 \\ 1 & 1 & 0 & 0 \\ 4 & -2 & 1 & -1 \\ -4 & -2 & 0 & 1 \end{pmatrix} \tag{B.7}$$

for the octic[4]. This symmetry allows us to define a fundamental domain on the z plane, which we chose to lie at $|\mathrm{Im}(z)| \leq 1/2$.

Both sets of transformations, (B.5) together with (B.6) and (B.7) can be used to transport τ and z to their respective fundamental domains. Vacua with the same flux and moduli values (up to 10^{-8}, corresponding to the error estimate of `Paramotopy`) are then removed to avoid double-counting solutions in the numerical scan.

[4] See [124] for more detail on this and other one-parameter models.

Appendix C

Density distribution of no-scale flux vacua

In this appendix we present a derivation of the theoretical probability distributions for the density of no-scale vacua (2.57) and (2.70), which describe the generic ensemble and the one constrained by the condition $N_A^0 = 0$, respectively.

The proof below relies only on the continuous flux approximation, and closely follows the one presented in [46]. We begin by deriving the probability distribution for the variables (2.56) at no-scale vacua using the Hodge decomposition (A.3). We then combine the result with a generalised version of the Kac-Rice formula to derive the density of flux vacua. In each of these two steps, we will present the argument first for the generic ensemble, as obtained in [46], and then we will adapt the it to the case the constrained ensemble.

C.1 Derivation of the Denef-Douglas distribution

Following [46], our starting point is a flat distribution for the $4m = 4(h^{2,1}+1)$ integer flux parameters

$$\{f_A^I, h_A^I, f_I^B, h_I^B\}. \tag{C.1}$$

Note that this distribution also matches the numerical procedure we followed to obtain the ensemble in the $\mathbb{WP}^4_{[1,1,1,1,4]}$ model, where flux realisations are drawn from a flat distribution.

In addition, we will also consider the situation when the tadpole constraint is large, $L \gg 1$. In this case the typical values of these flux parameters are also large, and can be regarded as a continuous random variables. The corresponding probability distribution is therefore

$$d\mu_{\text{flux}}(f,h) = \mathcal{N}\,(df\,dh)^{4m}. \tag{C.2}$$

Begin by switching variables to the complex flux parameters $N = f - \tau h$ and their conjugates

$\overline{N} = f - \bar{\tau} h$. The associated Jacobian is

$$J = \frac{\partial(N_A, \overline{N}_A, N^B, \overline{N}^B)}{\partial(f_A, h_A, f^B, h^B)} = \begin{pmatrix} \frac{\partial(N_A, \overline{N}_A)}{\partial(f_A, h_A)} & 0 \\ 0 & \frac{\partial(N^B, \overline{N}^B)}{\partial(f^B, h^B)} \end{pmatrix}, \tag{C.3}$$

where

$$\frac{\partial(N_A, \overline{N}_A)}{\partial(f_A, h_A)} = \frac{\partial(N^B, \overline{N}^B)}{\partial(f^B, h^B)} = \begin{pmatrix} \mathbb{1} & \mathbb{1} \\ -\tau\mathbb{1} & -\bar{\tau}\mathbb{1} \end{pmatrix}. \tag{C.4}$$

Then,

$$\det(J) = \det \begin{pmatrix} 1 & 1 \\ -\tau & \bar{\tau} \end{pmatrix}^{2m} = (-2\mathrm{i}\mathrm{Im}\tau)^{2m}, \tag{C.5}$$

implying that the resulting probability distribution for $\{N, \overline{N}\}$ reads

$$d\mu_{\text{flux}}(N, \overline{N}) = \mathcal{N}\,(dN d\overline{N})^{4m} \mathrm{e}^{2mK_d}. \tag{C.6}$$

Next, we consider the change of variables between $\{N, \overline{N}\}$ and $\{Z_0, F_a, F_0, Z_a, c.c.\}$, defined by[1]

$$\begin{aligned} F_0 &\equiv \mathrm{e}^{K/2} D_0 W = -\mathrm{i}\mathrm{e}^{K/2} N^\dagger \cdot \Sigma \cdot \Pi, \\ F_a &\equiv \mathrm{e}^{K/2} D_a W = \mathrm{e}^{K/2} N^T \cdot \Sigma \cdot D_a \Pi, \\ Z_0 &\equiv \mathrm{e}^{K/2} W = \mathrm{e}^{K/2} N^T \cdot \Sigma \cdot \Pi, \\ Z_a &\equiv \mathrm{e}^{K/2} D_0 D_a W = -\mathrm{i}\mathrm{e}^{K/2} N^\dagger \cdot \Sigma \cdot D_a \Pi, \end{aligned} \tag{C.7}$$

where the components of the vectors have been expressed in a canonically normalised basis. Note that these definitions coincide with those in the main text, (2.56), up to a volume factor $\mathcal{V}$. Since the volume is independent of the complex structure moduli or the dilaton, the effect of the rescaling necessary to make contact with (2.56) amounts to a redefinition of the normalisation constant, and thus we will ignore the volume prefactor in the following. The Jacobian $J = \partial(Z_0, F_a, F_0, Z_a, c.c.)/\partial(N, \overline{N})$ of the transformation above reads

$$J = \mathrm{e}^{K/2} \begin{pmatrix} \Sigma \cdot \Pi & \Sigma \cdot D_a \Pi & 0 & 0 & 0 & 0 & \mathrm{i}\Sigma \cdot \overline{\Pi} & \mathrm{i}\Sigma \cdot D_{\bar{a}} \overline{\Pi} \\ 0 & 0 & -\mathrm{i}\Sigma \cdot \Pi & -\mathrm{i}\Sigma \cdot D_a \Pi & \Sigma \cdot \overline{\Pi} & \Sigma \cdot D_{\bar{a}} \overline{\Pi} & 0 & 0 \end{pmatrix}. \tag{C.8}$$

Then,

$$\det(J) = \mathrm{e}^{2mK} |\det M|^2. \tag{C.9}$$

[1] In the following derivations, in order to simplify the notation, we will ignore the overall $1/\sqrt{4\pi}$ factor in the definition of W (1.35), since it plays no role in the final result.

where

$$M \equiv \left(\Sigma\cdot\Pi, \quad \Sigma\cdot D_a\Pi, \quad i\Sigma\cdot\overline{\Pi}, \quad i\Sigma\cdot D_{\bar{a}}\overline{\Pi}.\right) \tag{C.10}$$

To compute the determinant, we use the trick

$$|\det M|^2 = |M^\dagger M| = |M^\dagger\cdot\Sigma\cdot M|\,, \tag{C.11}$$

since $|\Sigma| = 1$. Then, using the orthogonality properties of the basis $\{\Pi, \overline{\Pi}, D_a\Pi, D_{\bar{a}}\overline{\Pi}\}$ for the space of symplectic sections under the product defined by Σ, we obtain [46]

$$M^\dagger\cdot\Sigma\cdot M = \begin{pmatrix} e^{-K_{cs}} & 0 & 0 & 0 \\ 0 & -ie^{-K_{cs}}\delta_{a\bar{b}} & 0 & 0 \\ 0 & 0 & e^{-K_{cs}} & 0 \\ 0 & 0 & 0 & ie^{-K_{cs}}\delta_{a\bar{b}} \end{pmatrix}. \tag{C.12}$$

The determinant of this matrix is then $\det(M^\dagger\cdot\Sigma\cdot M) = e^{-2mK_{cs}}$. Using this result we find that the determinant of the Jacobian of the change of variables is

$$\det(J) = e^{2m(K_d+K_k)}\,, \tag{C.13}$$

and therefore, noting that the factor e^{2mK_d} cancels with that of (C.6), we find that the probability distribution on the variables $\{F_0, F_a, Z_0, Z_a\}$ is flat

$$d\mu_{\rm flux}(F_A, Z_A, \overline{F}_A, \overline{Z}_A) = \mathcal{N}\,(dF_A d\overline{F}_A dZ_A d\overline{Z}_A)^{4m} e^{-2mK_k}. \tag{C.14}$$

In these variables no-scale vacua correspond to those configurations with $F_A = 0$, and the tadpole constraint requires

$$N_{\rm flux} = Z_A\overline{Z}_A \equiv |Z|^2 \le L. \tag{C.15}$$

The no-scale conditions can be imposed by introducing a delta function $\delta^{2m}(F_A, \overline{F}_A)$ in (C.14), which is equivalent to considering simply the distribution

$$d\mu_{\rm flux}(Z_A, \overline{Z}_A)|_{\text{no-scale}} = \mathcal{N}\,(dZ_A d\overline{Z}_A)^{2m}\,. \tag{C.16}$$

In other words, the variables $Z_A = \{e^{K/2}W, e^{K/2}D_0D_aW\}$ and their complex conjugates form a set of $2(h^{2,1}+1)$ independent complex variables uniformly distributed on the sphere (C.15) defined by the tadpole constraint. We refer to the previous probability density function as the *Denef-Douglas distribution*.

C.2 Constrained flux distribution

We will now repeat the above computation for the constrained ensemble of vacua. We begin by noting that this constraint can be implemented in the continuous flux approximation

with Dirac delta functions as

$$d\mu_{\text{flux}}(f,h) = \mathcal{N}\,(df\,dh)^{4m}\,\delta(f_A^0)\delta(h_A^0)\,. \tag{C.17}$$

After changing to complex flux coordinates, we obtain

$$d\mu_{\text{flux}}(N,\overline{N}) = \mathcal{N}\,(dN\,d\overline{N})^{4m}\mathrm{e}^{2mK_d}\delta(N_A^0)\delta(\overline{N}_A^0)|J_0|\,, \tag{C.18}$$

where

$$|J_0| = \det\frac{\partial(N_A^0,\overline{N}_A^0)}{\partial(f_A^0,h_A^0)} = \det\begin{pmatrix}1 & 1\\ -\tau & -\bar{\tau}\end{pmatrix} = -2\mathrm{i}\,\mathrm{Im}(\tau), \tag{C.19}$$

and so

$$d\mu_{flux}(N,\overline{N}) = \mathcal{N}\,\mathrm{i}(dN\,d\overline{N})^{4m}\mathrm{e}^{(2m-1)K_d}\delta(N_A^0)\delta(\overline{N}_A^0)\,. \tag{C.20}$$

Using the Hodge decomposition of the flux vector

$$N = \mathrm{e}^{\frac{1}{2}(-K_k-K_d+K_{cs})}(-\overline{F}_0\Pi + \mathrm{i}Z_0\overline{\Pi} + \overline{Z}_a D_a\Pi - \mathrm{i}F_a D_{\bar{a}}\overline{\Pi})\,, \tag{C.21}$$

we can obtain the form of the constraint in terms of the variables $\{Z_A, F_A, \overline{Z}_A, \overline{F}_A\}$. It is given by

$$N_A^0 = \mathrm{e}^{\frac{1}{2}(-K_k-K_d+K_{cs})}(-\overline{F}_0 + \mathrm{i}Z_0 - \sqrt{3/(1-2\xi)}\overline{Z}_1 + \sqrt{3/(1-2\xi)}\mathrm{i}F_1) = 0\,. \tag{C.22}$$

We can implement this condition as a constraint on the variables

$$Z_0 = Z_0^*(Z_a,F_A)\,, \qquad \overline{Z}_0 = \overline{Z}_0^*(Z_a,F_A) \tag{C.23}$$

with the aid of Dirac delta functions, so that the final density function, written in terms of $\{Z_A, F_A, \overline{Z}_A, \overline{F}_A\}$, reads

$$d\mu_{\text{flux}} = \mathcal{N}\,\mathrm{i}(dF_A\,d\overline{F}_A\,dZ_A\,d\overline{Z}_A)^{4m}\mathrm{e}^{-K_{cs}}\delta(Z_0 - Z_0^*)\delta(\overline{Z}_0 - \overline{Z}_0^*)\,. \tag{C.24}$$

Here we have absorbed the Calabi-Yau volume factor, which is independent of the axio-dilaton and complex structure fields, in the normalisation constant.

C.3 Density of generic no-scale vacua

We now turn to the computation of the density of flux vacua in the generic ensemble. The number of no-scale vacua $\mathscr{C}_{\text{vac}}(N)$ for a given choice of flux N can be obtained using the generalised Kac-Rice formula [168,169]

$$\mathscr{C}_{\text{vac}}(N) = \int d^{2m}u\,\delta^{2m}(DW)\,|\det D^2W|\,, \tag{C.25}$$

with $u^A = \{\tau, z^i\}$ and

$$\delta^{2m}(DW) = \delta^m(D_A W)\,\delta^m(D_{\bar{A}}\overline{W}), \qquad D^2W = \begin{pmatrix} D_A D_{\bar{B}} W & D_A D_B W \\ D_{\bar{A}} D_{\bar{B}} \overline{W} & D_{\bar{A}} D_B \overline{W} \end{pmatrix}. \tag{C.26}$$

Let us now consider the total number of no-scale vacua in the ensemble of fluxes satisfying the tadpole constraint $N_{\rm flux} \leq L$, which is given by

$$\mathscr{C}_{\rm vac}(N_{\rm flux} \leq L) = \sum_N \Theta(N_{\rm flux} - L) \int d^{2m}u\, \delta^{2m}(DW) |\det D^2 W|\,. \tag{C.27}$$

Note that here we have chosen to count all choices of flux with equal weight, consistent with our initial assumption that fluxes are drawn from an underlying uniform distribution.

As discussed in [46], using the integral representation of the Heaviside theta function we can rewrite the previous formula as

$$\mathscr{C}_{vac}(N_{\rm flux} \leq L) = \frac{1}{2\pi \mathrm{i}} \int_C \frac{d\alpha}{\alpha} \mathrm{e}^{\alpha L^*} \mathscr{C}(\alpha) \tag{C.28}$$

with

$$\begin{aligned} \mathscr{C}(\alpha) &\equiv \sum_N \int d^{2m}u\, \mathrm{e}^{-\alpha N_{\rm flux}}\, \delta^{2m}(DW) |\det D^2 W| \\ &\approx \int (dN d\overline{N})^{4m} \int d^{2m}u\, \mathrm{e}^{-\alpha N_{\rm flux}}\, \delta^{2m}(DW) |\det D^2 W| \mathrm{e}^{2mK_d}\,, \end{aligned} \tag{C.29}$$

where in the last line we have approximated the sum over the integer fluxes by an integral with measure given by (C.6).

Expressing the gradient, DW, and the Hessian of the superpotential, D^2W, in a canonically normalised basis, we find

$$\begin{aligned} \mathscr{C}(\alpha) &= \int (dN d\overline{N})^{4m} \int d^{2m}u |\det g|\, \mathrm{e}^{-\alpha N_{\rm flux}}\, \delta^{2m}(D_a W) |\det \mathscr{H}|^{1/2} \mathrm{e}^{2mK_d} \\ &= \int (dZ dF)^{4m} \int d^{2m}u |\det g|\, \mathrm{e}^{-\alpha \mathscr{V}^2 |Z|^2}\, \delta^m(F_A) \delta^m(\overline{F}_A) |\det \mathscr{H}|^{1/2} \mathrm{e}^{-2mK_k} \\ &= \mathscr{V}^{4m} \int (dZ d\overline{Z})^{2m} \int d^{2m}u |\det g|\, \mathrm{e}^{-\alpha \mathscr{V}^2 |Z|^2}\, |\det \mathscr{H}|^{1/2}\,. \end{aligned} \tag{C.30}$$

In the second line, the term of the form e^{mK} arises as a result of the change of variables (C.7) in the argument of the delta function, which then is reabsorbed when expressing $\det D^2 W$ in terms of $\mathscr{H}$.[2] Rescaling $Z_A \to Z_A/(\mathscr{V}\sqrt{\alpha})$, it is possible to see that $\mathscr{C}(\alpha) = \mathscr{C}(1, \mathscr{V} = 1)\alpha^{-2m}$ and the overall volume factor disappears, so we can explicitly perform the integral in α to give

$$\mathscr{C}_{vac}(N_{\rm flux} \leq L) = \Lambda(L, m) \cdot \int d^{2m}u |\det g| \int (dZ d\overline{Z})^{2m}\, \mathrm{e}^{-|Z|^2}\, |\det \mathscr{H}|^{1/2}\,. \tag{C.31}$$

[2] Recall that in canonically normalized coordinates we have the relation $\mathscr{H} = \mathrm{e}^K (D^2W)^2 = (m_{3/2}\mathbb{1} + \mathscr{M})^2$, from (2.8).

where $\Lambda(L,m)$ is a constant depending on the tadpole parameter L and the moduli space dimension m. Consistent with the previous equation, the density of flux vacua is then defined by

$$d\mu_{\rm vac}(z,\tau) = \mathcal{N}\cdot d^{2m}u\,|\det g|\left[\int (dZd\overline{Z})^{2m}\,\mathrm{e}^{-|Z|^2}\,|\det\mathscr{H}|^{1/2}\right]. \tag{C.32}$$

C.4 Density of constrained vacua

For the ensemble with constrained fluxes the argument proceeds as before, but when changing to the variables (C.7) in (C.30), we should use the measure (C.24) rather than (C.16). As a result, the density of no-scale vacua is given by

$$d\mu_{\rm vac}(z,\tau) = \mathcal{N}\cdot d^{2m}u\,|\det g|\left[\int (dZd\overline{Z})^{2(m-1)}\,\mathrm{e}^{-|Z|^2}\,|\det\mathscr{H}|^{1/2}\mathrm{e}^{-K_{cs}}\right], \tag{C.33}$$

where the integral is over the subspace of $\{Z_A,\overline{Z}_A\}$ defined by the constraints (C.23) with $F_A=\overline{F}_A=0$ (no-scale conditions). In the case when the complex structure moduli space is one dimensional ($m=2$), the integral appearing in the previous equation reduces to

$$\int dZ_1 d\overline{Z}_1 \mathrm{e}^{-\frac{2(2-\xi)}{1-2\xi}|Z_1|^2}\,|Z_1|^4\left|1+\frac{9}{(1-2\xi)^2}-\frac{3(2+\mathring{\kappa}^2)}{(1-2\xi)}\right|\frac{\xi+1}{\xi}, \tag{C.34}$$

where we used the relation $|Z_0| = \sqrt{3/(1-2\xi)}|Z_1|$ (given in (2.46)) and the definition of the LCS parameter $\mathrm{e}^{-K_{cs}} = |2\mathrm{Im}\kappa_0|(\xi+1)/\xi$. Integrating the previous expression over the complex variable Z_1, and over the directions $\mathrm{Im}z$ and $\mathrm{Re}\tau$ we find

$$d\mu_{\rm vac}(z,\tau) = \mathcal{N}\cdot\frac{(1+\xi)}{(2-\xi)^2}\frac{1}{r^2s^2}drds, \tag{C.35}$$

expressed in terms of the variables (2.61), which agrees with (2.70).

Appendix D

Bounds on the LCS parameter

The theoretical distributions (2.57) and (2.70) were derived in order to have an analytical description of the ensemble of no-scale vacua, constructed as described in section 2.5 and appendix B. However, this characterisation is only a faithful representation of the Landscape in the regime of moduli space where both the EFT and the continuous flux approximation are valid.

Indeed, vacua with large instanton corrections should be discarded, since the EFT we used cannot be trusted in those cases. As the vacuum density functions (2.57) and (2.70) contain no information regarding the size of the instanton contributions, they are bound to be inaccurate in the regime where these corrections are large. Furthermore, from [145, 155], we know that in the generic ensemble the density of vacua should be suppressed with respect to the theoretical distribution (2.57), due to the breakdown of the continuous flux approximation. In this appendix we discuss the parameter space where the statistical description can be applied, providing an analytic estimate for this region in terms of the LCS parameter ξ for the octic.

D.1 No-scale equations near the LCS point

We begin by rewriting the no-scale equations (1.37) in the LCS limit in a more convenient way for the derivations below. In this regime, $\xi \to 0$, the Kähler potential of the complex structure sector can be expressed as

$$Y \equiv e^{-K_{cs}} \approx \frac{1}{6}\kappa_{ijk}(z^i + \bar{z}^i)(z^j + \bar{z}^j)(z^k + \bar{z}^k)\,, \tag{D.1}$$

and the canonically normalized Yukawa couplings satisfy [145, 155]

$$\kappa_{111} = \frac{2}{\sqrt{3}}Y\,, \qquad \kappa_{11\tilde{a}} = 0\,, \quad \kappa_{1\tilde{a}\tilde{b}} = -\frac{1}{\sqrt{3}}Y\delta_{\tilde{a}\tilde{b}}\,, \tag{D.2}$$

where the direction "1" corresponds to the no-scale direction (2.31) and $\tilde{a}, \tilde{b} = 2, \dots h^{2,1}$. We also have

$$z^a = \frac{\sqrt{3}}{2}\delta^a_1 + i\lambda^a\,, \qquad K_a = -\sqrt{3}\delta^a_1\,, \tag{D.3}$$

where z^a (with $a = 1,\dots,h^{2,1}$) are the canonically normalised fields at the vacuum, and $\lambda^a = \mathrm{Im}(z^a)$. After some algebra, it can be shown that the superpotential has the form

$$W = -\frac{i}{6}\kappa_{abc}N_A^0 z^a z^b z^c + \frac{1}{2}\kappa_{abc}N_A^a z^b z^c + i\left(\kappa_a N_A^0 - \kappa_{ab}N_A^b - N_a^B\right)z^a + \kappa_0 N_A^0 + \kappa_a N_A^a - N_0^B\,, \tag{D.4}$$

while the no-scale conditions (1.37) read

$$\begin{aligned} D_0 W &= -\frac{1}{6}\kappa_{abc}\overline{N}_A^0 z^a z^b z^c - \frac{i}{2}\kappa_{abc}\overline{N}_A^a z^b z^c + \left(\kappa_a \overline{N}_A^0 - \kappa_{ab}\overline{N}_A^b - \overline{N}_a^B\right)z^a \\ &\quad - i\kappa_0\overline{N}_A^0 - i\kappa_a\overline{N}_A^a + i\overline{N}_0^B = 0\,, \\ D_a W &= -\frac{i}{2}\kappa_{abc}N_A^0 z^b z^c + \kappa_{abc}N_A^b z^c + i\kappa_a N_A^0 - i\kappa_{ab}N_A^b - iN_a^B - \sqrt{3}W\delta_a^1 = 0\,. \end{aligned} \tag{D.5}$$

To analyse these equations it is convenient to introduce the flux parameter redefinitions

$$\hat{N}_0^B \equiv -\frac{1}{6}\kappa_{abc}N_A^0\lambda^a\lambda^b\lambda^c - \frac{1}{2}\kappa_{abc}N_A^a\lambda^b\lambda^c - \left(\kappa_a N_A^0 - \kappa_{ab}N_A^b - N_a^B\right)\lambda^a + \kappa_0 N_A^0 + \kappa_a N_A^a - N_0^B\,, \tag{D.6}$$

$$\hat{N}_a^B \equiv -\frac{1}{2}\kappa_{abc}N_A^0\lambda^b\lambda^c - \kappa_{abc}N_A^b\lambda^c - \kappa_a N_A^0 + \kappa_{ab}N_A^b + N_a^B\,. \tag{D.7}$$

Note that the flux parameters $\hat{f}_I^B$ and $\hat{h}_I^B$ in $\hat{N} = \hat{f} - \tau\hat{h}$ are still real, but are not integers in general. Using these new parameters, the superpotential now reads

$$W = \hat{N}_0^B - i\frac{\sqrt{3}}{2}\hat{N}_1^B + \left[\left(\frac{\sqrt{3}}{4}\lambda^1 - \frac{i}{8}\right)N_A^0 + \frac{\sqrt{3}}{4}N_A^1\right]Y \tag{D.8}$$

and the no-scale conditions are given by

$$\left[\left(\frac{1}{2}\lambda^1 + \frac{i}{4\sqrt{3}}\right)N_A^0 + \frac{1}{2}N_A^1\right]Y + i\hat{N}_1^B = -\frac{2}{\sqrt{3}}\hat{N}_0^B\,, \tag{D.9}$$

$$\left[\left(\frac{1}{2}\lambda^1 - \frac{i\sqrt{3}}{4}\right)N_A^0 + \frac{1}{2}N_A^1\right]Y + i\hat{N}_1^B = 2\sqrt{3}\hat{N}_0^B\,, \tag{D.10}$$

$$\left[\frac{1}{2}\lambda^{a'}N_A^0 + \frac{1}{2}N_A^{a'}\right]Y + i\hat{N}_{a'}^B = 0\,. \tag{D.11}$$

These expressions can be rewritten in a more compact way as

$$\boxed{\hat{N}_0^B = -\frac{i}{8}YN_A^0, \qquad \hat{N}_a^B = \frac{i}{2}Y\left(N_A^0\lambda^a + N_A^a\right).} \tag{D.12}$$

The second equation can be equivalently written, after contracting it with the vielbein e_i^a, as

$$\hat{N}_i^B = \frac{i}{2}Y\left(N_A^0\lambda^j + N_A^j\right)g_{ji}\,, \tag{D.13}$$

where we have used that $\hat{N}_a^B e_i^a = \hat{N}_i^B$, and $N_A^a e_i^a = N_A^j e_j^a e_i^a = N_A^j g_{ji}$, and similarly for the terms involving λ^a. The redefined fluxes can also be rewritten as

$$\begin{aligned}\hat{N}_0^B \equiv & -\frac{1}{6}\kappa_{ijk}N_A^0\lambda^i\lambda^j\lambda^k - \frac{1}{2}\kappa_{ijk}N_A^i\lambda^j\lambda^k - \left(\kappa_i N_A^0 - \kappa_{ij}N_A^j - N_i^B\right)\lambda^i \\ & + \kappa_0 N_A^0 + \kappa_i N_A^i - N_0^B\,,\end{aligned} \tag{D.14}$$

$$\hat{N}_i^B \equiv -\frac{1}{2}\kappa_{ijk}N_A^0\lambda^j\lambda^k - \kappa_{ijk}N_A^j\lambda^k - \kappa_i N_A^0 + \kappa_{ij}N_A^j + N_i^B\,. \tag{D.15}$$

D.2 Lower bound on the LCS parameter

We will now determine the regime of applicability of the continuous flux approximation near the LCS point on the generic flux ensemble, expressed as a lower bound for the LCS parameter ξ.

Let us first discuss the equation in (D.12) for $\hat{N}_0^B$ in the $\xi \to 0$ limit when $N_A^0 \neq 0$. From the definition of the LCS parameter ξ (2.25), we can rewrite Y as

$$Y = 2\,|\mathrm{Im}\kappa_0|\,\frac{1+\xi}{\xi} \approx 2\,|\mathrm{Im}\kappa_0|\,\xi^{-1} \tag{D.16}$$

in the LCS limit, that is, $\xi \to 0$. On the other hand, from the definition of N_A^0, we can obtain the following lower bound:

$$\left|N_A^0\right|^2 = (f_A^0 - \mathrm{Re}(\tau)h_A^0)^2 + \mathrm{Im}^2(\tau)(h_A^0)^2 \geq 1\,, \tag{D.17}$$

where in the last step we used $\mathrm{Im}(\tau) > 1$, as required for the vacua to be in the weak string coupling regime. This implies that at no-scale vacua near the LCS limit, we must have

$$|\hat{N}_0^B| \approx \frac{|\mathrm{Im}\kappa_0|\left|N_A^0\right|}{4\xi}\,. \tag{D.18}$$

Note that, since by assumption $|N_A^0| \neq 0$, the right hand side blows up when $\xi \to 0$, and so $|\hat{N}_0^B| \gtrsim \mathcal{O}(\xi^{-1})$, which will require some contributions in (D.7) to become large. From (D.17) we can see that the previous condition will be the least restrictive when $|N_A^0|$ and $\mathrm{Im}\tau$ are both $\mathcal{O}(1)$, leading to

$$|\hat{N}_0^B| \gtrsim \frac{|\mathrm{Im}\kappa_0|}{4\xi}\,. \tag{D.19}$$

In order to solve this condition, one could try to tune the parameters $\lambda^i = \mathrm{Im}z^i$ to be large, $\lambda^i = \mathcal{O}(\xi^{-1/3})$; however, in that case the cubic terms in (D.7) would dominate, and the first equation in (D.12) would become

$$\frac{1}{6}\kappa_{ijk}\lambda^i\lambda^j\lambda^k \overset{!}{\approx} \mathrm{i}\frac{|\mathrm{Im}\kappa_0|}{4\xi}\,, \tag{D.20}$$

which cannot be solved, as the left hand side is real and the right hand side purely imaginary.

This conclusion is in agreement with the results of [145,155], where it was shown that if the superpotential is dominated by its cubic term, the no-scale equations (1.37) cannot admit solutions in a neighbourhood of the LCS point.

As a consequence, we need terms with different powers of λ^i in (D.7) to be comparable and, assuming the constant coefficients of the prepotential to be $\mathcal{O}(1)$, due to the tadpole condition (1.41) we will typically have $|\hat{N}_0^B| = \mathcal{O}(\sqrt{N_{\text{flux}}})$. Combining all of this, we arrive at the bound we were looking for:

$$\xi \gtrsim \xi_{\text{min}}\big|_{N_A^0 \neq 0} \equiv \frac{|\text{Im}\kappa_0|}{4\sqrt{N_{\text{flux}}}}. \tag{D.21}$$

As an example, for the $\mathbb{WP}^4_{[1,1,1,1,4]}$ model, we have $N_{\text{flux}} = 972$ and $2|\text{Im}\kappa_0| \approx 2.9$, which implies

$$\xi_{\text{min}} = \mathcal{O}(10^{-2}). \tag{D.22}$$

In the case of the constrained ensemble, the previous argument does not apply. In the limit $\xi \to 0$ with $f_A^0 = h_A^0 = h_A^z = 0$ and

$$f_0^B = f_A^z\, k_z + \frac{h_0^B}{2(h_z^B)^2}\left[2h_z^B(f_z^B + f_A^z\, k_{zz}) - f_A^z\, h_0^B\, k_{zzz}\right], \tag{D.23}$$

the LCS parameter ξ can be used to parametrize no-scale solutions. This leads to a flat direction along $\text{Im}\tau \approx (\xi_0/\xi)^{1/3}|f_A^z/h_z^B|$, where $\xi_0 \equiv (3/2^4)|\text{Im}\kappa_0|k_{zzz}^2$, which allows solutions arbitrarily close to the LCS/weak-coupling limit.

D.3 Maximum value consistent with small instanton corrections

In this section, we give an upper bound ξ_{max}, independent of the flux vector N, by requiring the instanton corrections to the metric of the complex structure moduli space to remain small. As we mentioned above, the numerical analysis shows that the field space metric is typically the object where these corrections have the largest effect, and thus it is particularly suitable for estimating the regime of validity of the EFT. For convenience we will split the prepotential as

$$\mathcal{F}(z) = \hat{\mathcal{F}}(z) + \mathcal{F}_*(z) + \dots, \tag{D.24}$$

where $\hat{\mathcal{F}}$ is the perturbative part of the prepotential, and $\mathcal{F}_*$ denotes the leading term of the instanton contributions $\mathcal{F}_{\text{inst}}$. In the case of the octic model, near the LCS point the prepotential is given by (2.51) and (2.52), which have the form

$$\hat{\mathcal{F}}(z) = \frac{i}{6}\kappa_3 z^3 + \frac{1}{2}\kappa_2 z^2 + i\kappa_1 z + \frac{1}{2}\kappa_0, \qquad \mathcal{F}_*(z) = -\frac{i n_1}{(2\pi)^3} e^{-2\pi z}, \tag{D.25}$$

the latter being perturbatively small when compared to $\hat{\mathscr{F}}$ in the LCS regime. The period vector (1.31) is then split as

$$\Pi = \begin{pmatrix} 1 \\ iz \\ 2\mathscr{F} - z\partial_z\mathscr{F} \\ -i\partial_z\mathscr{F} \end{pmatrix} = \begin{pmatrix} 1 \\ iz \\ 2\hat{\mathscr{F}} - z\partial_z\hat{\mathscr{F}} \\ -i\partial_z\hat{\mathscr{F}} \end{pmatrix} + \begin{pmatrix} 0 \\ 0 \\ 2\mathscr{F}_* - z\partial_z\mathscr{F}_* \\ -i\partial_z\mathscr{F}_* \end{pmatrix} \equiv \hat{\Pi} + \Pi_* \,. \tag{D.26}$$

Keeping only to leading instanton contribution, the Kähler potential (2.4) is then

$$\begin{aligned} e^{-K_{cs}} &= i\,\Pi^\dagger\cdot\Sigma\cdot\Pi \approx i\,\hat{\Pi}^\dagger\cdot\Sigma\cdot\hat{\Pi} + i\,\hat{\Pi}^\dagger\cdot\Sigma\cdot\Pi_* + i\,\Pi_*^\dagger\cdot\Sigma\cdot\hat{\Pi} \\ &= e^{-\hat{K}} - 2\,\mathrm{Im}(\hat{\Pi}^\dagger\cdot\Sigma\cdot\Pi_*)\,, \end{aligned} \tag{D.27}$$

Defining $\mathscr{I} \equiv \mathrm{Im}(\hat{\Pi}^\dagger\cdot\Sigma\cdot\Pi_*)$ we obtain to leading order

$$K_{cs} \approx \hat{K} + 2\mathscr{I}e^{\hat{K}}. \tag{D.28}$$

Denoting the zeroth order metric and its leading instanton correction as

$$G_{z\bar{z}} \equiv \partial_z\partial_{\bar{z}}\hat{K}\,, \qquad g_{z\bar{z}} \equiv \partial_z\partial_{\bar{z}}(2\mathscr{I}e^{\hat{K}})\,, \tag{D.29}$$

we find that the field space metric is given by

$$\begin{aligned} \partial_z\partial_{\bar{z}}K_{cs} &\approx G_{z\bar{z}} + g_{z\bar{z}} \\ &= G_{z\bar{z}} + 2e^{\hat{K}}\left(G_{z\bar{z}}\mathscr{I} + \hat{K}_z\hat{K}_{\bar{z}}\,\mathscr{I} + \hat{K}_{\bar{z}}\mathscr{I}_z + \hat{K}_z\mathscr{I}_{\bar{z}} + \mathscr{I}_{z\bar{z}}\right), \end{aligned} \tag{D.30}$$

where subindices denote partial derivatives. Letting e_z^1 be a *real vielbein* with respect to the zero-order metric $G_{z\bar{z}}$ (so that $G_{1\bar{1}} = 1$), we then find

$$g_{1\bar{1}} = 2e^{\hat{K}}\left(\left(1 + (\hat{K}_1)^2\right)\mathscr{I} + \hat{K}_1\left(\mathscr{I}_1 + \mathscr{I}_{\bar{1}}\right) + \mathscr{I}_{1\bar{1}}\right), \tag{D.31}$$

where we used $\hat{K}_1 = e_1^z\hat{K}_z = e_{\bar{1}}^{\bar{z}}\hat{K}_{\bar{z}} = \hat{K}_{\bar{1}}$. The value of $\mathscr{I}$ and its partial derivatives are found by direct computation. Defining $\theta = 2\pi\mathrm{Im}(z)$ and using (2.26), we get

$$\mathscr{I} = -\frac{n_1}{4\pi^3}e^{-2\pi\mathrm{Re}(z)}(1 + 2\pi\mathrm{Re}(z))\cos(\theta)\,, \tag{D.32}$$

$$\mathscr{I}_1 + \mathscr{I}_{\bar{1}} = \frac{2n_1}{\pi}e^{-2\pi\mathrm{Re}(z)}\frac{\mathrm{Re}^2(z)}{x}\cos(\theta)\,, \tag{D.33}$$

$$\mathscr{I}_{1\bar{1}} = \frac{2n_1}{\pi}e^{-2\pi\mathrm{Re}(z)}\frac{\mathrm{Re}^2(z)}{x^2}\cos(\theta)\,. \tag{D.34}$$

From the analysis in section 2.4, we know that the relations

$$e^{\hat{K}} = \frac{1}{2|\mathrm{Im}\,\kappa_0|}\frac{\xi}{1+\xi}\,, \quad \hat{K}_1 = -\sqrt{\frac{3}{1-2\xi}}\,, \tag{D.35}$$

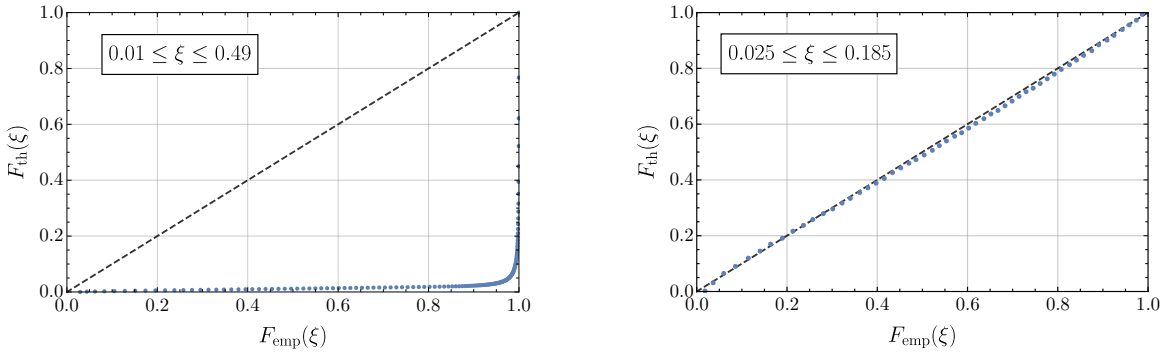

(a) (b)

Figure D.1: P-P plots of the theoretical distribution of ξ, (2.62), versus the data obtained within the generic ensemble for (a) $0.01 \leq \xi \leq 0.49$ and (b) $0.025 \leq \xi \leq 0.185$. For reference, we plot the curve $F_{th}(\xi) = F_{emp}(\xi)$ corresponding to perfect agreement with a dashed line. We find that the distribution only fits the data within the range plotted in (b).

$$x^2 = \frac{3(1-2\xi)}{(1+\xi)^2}\,, \quad \text{Re}\, z = \left(\frac{3|\text{Im}\,\kappa_0|}{2\kappa_3}\right)^{1/3} \frac{1}{\xi^{1/3}} \tag{D.36}$$

hold. Thus, substituting (D.32) through (D.36) into (D.31), and defining $\alpha \equiv \left(\frac{3|\text{Im}k_0|}{2k_3}\right)^{1/3}$, we get

$$g_{1\bar{1}} = -\frac{n_1\cos\theta}{6\pi^3|\text{Im}\,\kappa_0|}\frac{(2-\xi)\xi^{1/3}}{(1+\xi)(1-2\xi)}e^{-\frac{2\pi\alpha}{\xi^{1/3}}}\left((2\pi\alpha)^2(1+\xi)+3\xi^{2/3}+6\pi\alpha\xi^{1/3}\right).$$

Requiring the relative corrections to the canonically normalised metric to remain below 20% (or equivalently $|g_{1\bar{1}}| \leq 0.2$, since $G_{1\bar{1}} = 1$), we find

$$\xi \leq \xi_{\rm max} \approx 0.2\,. \tag{D.37}$$

D.4 Accuracy of the statistical description

The statistical description of the flux ensemble presented in section 2.6 relies on two assumptions: first that the prepotential defining the EFT (2.51) contains only polynomial terms (we neglect instanton contributions, $\mathscr{F}_{\rm inst} \equiv 0$), and second that the flux vector N can be regarded as a *continuous* random variable. These two conditions were imposed to make the problem analytically tractable, and also to simplify the numerical analysis so that the homotopy continuation methods could be applied. Thus, it is expected that, in the regimes of parameter space where the vacua fail to be consistent with these assumptions, we should observe discrepancies between the theoretical probability distributions and the histograms obtained from the numerical scan. Here, we present the method we used to identify these deviations in the data in a systematic way. For definiteness we will focus the discussion on the distribution of the LCS parameter ξ, whose theoretical distributions for the generic and constrained ensembles are given by (2.62) and (2.71), respectively.

As we discussed above, the predicted distribution cannot be applied in the whole domain

of ξ. Vacua near the conifold point $\xi_{\text{cnf}} \approx 0.39$ are prone to big instanton corrections while, for the generic ensemble, those in the LCS limit $\xi \to 0$ are expected to be suppressed due to the breakdown of the continuous flux approximation. Thus, we will now establish empirical bounds where the theoretical distributions for ξ are applicable. A widely used graphical method to verify how an empirical data distribution performs against a reference distribution is that of *P-P* plots (see, e.g., [276]). The method consists in plotting the empirical and theoretical cumulative distributions functions, $F_{\text{em}}(\xi)$ and $F_{\text{th}}(\xi)$, one against the other. If the agreement is perfect then the resulting plot is a straight line at 45 degrees.

As shown in figure D.1, in the generic ensemble case, the best agreement with the Denef-Douglas distribution was found for

$$0.025 \leq \xi \leq 0.185\,. \tag{D.38}$$

The large discrepancy observed in figure D.1(a) is due to the deficit of vacua near the LCS point in the generic ensemble. Note that these bounds are in very good agreement with the estimates (D.22) and (D.37) obtained above, which correspond to the limits of applicability of the continuous flux approximation and of the EFT, respectively.

A similar analysis shows that for the constrained ensemble, the theoretical and empirical distributions agree in the interval

$$5 \cdot 10^{-5} \leq \xi|_{N_A^0=0} \leq 0.185\,. \tag{D.39}$$

As can also be seen in the histograms of section 2.6, the Denef-Douglas distribution (2.57) provides an accurate description of the LCS parameter and other physical quantities (Yukawa couplings, scalar and fermion masses...) within the limits established above.

Appendix E

Construction of Slepian models

Throughout this appendix, we will give a detailed description of the tools and derivations needed in order to generate conditioned Gaussian random fields, such as the ones we have been using throughout the main text. We will be mainly following [170, 227].

E.1 Introductory remarks and some properties of Gaussian random variables

A random variable x is said to follow a *normal* or *Gaussian distribution* if its probability distribution function (PDF) is given by

$$f(x) = \frac{1}{\sqrt{2\pi\sigma^2}} e^{-\frac{(x-\mu)^2}{2\sigma^2}} \tag{E.1}$$

where $\mu = \langle x \rangle$ and $\sigma^2 = \left\langle (x-\mu)^2 \right\rangle$ are the mean and variance of the distribution, respectively. Likewise, a p-dimensional vector $\boldsymbol{x}^T = (x_1, \ldots, x_p)$ is defined as a Gaussian random vector (composed of jointly Gaussian variables) if every linear combination satisfies

$$\boldsymbol{a} \cdot \boldsymbol{x} = \sum_{i=1}^{p} a_i x_i \sim N(\tilde{\mu}, \tilde{\sigma}), \tag{E.2}$$

that is, it follows a normal distribution. The PDF of the whole vector is

$$f(\boldsymbol{x}) = \frac{1}{(2\pi)^{p/2}\sqrt{\det \Sigma}} \exp\left[-\frac{1}{2} (\boldsymbol{x} - \boldsymbol{\mu})^T \Sigma^{-1} (\boldsymbol{x} - \boldsymbol{\mu}) \right] \tag{E.3}$$

where $\boldsymbol{\mu} = \langle \boldsymbol{x} \rangle$ is the mean *vector* and Σ is the (non-degenarate) *covariance matrix*, whose elements are given by

$$\Sigma_{ij} = \left\langle (x_i - \mu_i)(x_j - \mu_j) \right\rangle. \tag{E.4}$$

E.2 Conditioned Gaussian random vectors

Let A be a $p \times p$ matrix and $\boldsymbol{x}^T = (x_1, \ldots, x_p)$ a Gaussian random vector. Then, by definition,

$$\boldsymbol{y} = A\boldsymbol{x} \quad \rightarrow \quad y_j = A_{ij} x_i \tag{E.5}$$

is also a Gaussian random vector with mean $\boldsymbol{\mu}'$ and covariance matrix Σ'. Since (E.5) is a linear transformation, the new mean is given by

$$\boldsymbol{\mu}' = A\boldsymbol{\mu}, \tag{E.6}$$

whereas the new covariance matrix is

$$\begin{aligned}
\Sigma'_{ij} &= \left\langle (y_i - \mu'_i)(y_j - \mu'_j) \right\rangle = \left\langle (x_a A_{ai} - \mu_b A_{bi})(x_c A_{cj} - \mu_d A_{dj}) \right\rangle \\
&= \langle x_a x_c \rangle A_{ai} A_{cj} - \mu_d \langle x_a \rangle A_{ai} A_{dj} - \mu_b \langle x_c \rangle A_{bi} A_{cj} + \mu_b \mu_d A_{bi} A_{dj} \\
&= \left\langle (x_a - \mu_a)(x_b - \mu_b) \right\rangle A_{ai} A_{bj} = (A^T)_{ia} \Sigma_{ab} A_{bj}
\end{aligned} \tag{E.7}$$

or, more compactly,

$$\Sigma' = A^T \Sigma A. \tag{E.8}$$

In order to introduce conditional probability notions to jointly Gaussian random variables, let us discuss some interesting properties of grouped random variables. If we split some Gaussian vector $\boldsymbol{x}$ into two parts, namely,

$$\boldsymbol{x} = (\boldsymbol{x}_1, \boldsymbol{x}_2) = \big((x_1, \ldots, x_d), (x_{d+1}, \ldots, x_p)\big) \tag{E.9}$$

then the mean vector and covariance matrix will also split accordingly:

$$\boldsymbol{\mu} = \big(\boldsymbol{\mu}_1, \boldsymbol{\mu}_2\big) = \big((\mu_1, \ldots, \mu_d), (\mu_{d+1}, \ldots, \mu_p)\big) \tag{E.10}$$

$$\Sigma = \begin{pmatrix} \Sigma_{11} & \Sigma_{12} \\ \Sigma_{21} & \Sigma_{22} \end{pmatrix}, \tag{E.11}$$

each block in Σ having the proper dimensions to accommodate the covariances among the vectors $\boldsymbol{x}^1$ and $\boldsymbol{x}^2$.

With these remarks at hand, let us perform a linear transformation on $\boldsymbol{x}$, choosing

$$A = \begin{pmatrix} \mathbb{1}_d & -\Sigma_{12}\Sigma_{22}^{-1} \\ 0 & \mathbb{1}_{p-d} \end{pmatrix}. \tag{E.12}$$

After some straightforward algebra, one can show that the new Gaussian vector $\boldsymbol{y}$ is

$$\boldsymbol{y}^T = \big(\boldsymbol{x}_1 - \Sigma_{12}\Sigma_{22}^{-1}\boldsymbol{x}_2, \boldsymbol{x}_2\big) = (\boldsymbol{y}_1, \boldsymbol{x}_2) \tag{E.13}$$

whose associated mean vector and covariance matrix are

$$\boldsymbol{\mu}'^{T} = \left(\boldsymbol{\mu}_1 - \Sigma_{12}\Sigma_{22}^{-1}\boldsymbol{\mu}_2, \boldsymbol{\mu}_2\right) \tag{E.14}$$

$$\Sigma' = \begin{pmatrix} \Sigma_{11} - \Sigma_{12}\Sigma_{22}^{-1}\Sigma_{21} & 0 \\ 0 & \Sigma_{22} \end{pmatrix}, \tag{E.15}$$

meaning that the new $\boldsymbol{y}_1$ and $\boldsymbol{x}_2$ are uncorrelated and, therefore, independent.

Given a bivariate joint probability distribution function $f(x_1, x_2)$, the conditional probability $f'(x_1|x_2 = \tilde{x})$ is defined by [277]

$$f'(x_1|x_2 = \tilde{x}) \equiv \frac{f(x_1, \tilde{x})}{\int dx_1\, f(x_1, \tilde{x})} = \frac{\int dx_2\, \delta(x_2 - \tilde{x}) f(x_1, x_2)}{\int dx_1\, dx_2\, \delta(x_2 - \tilde{x})\, f(x_1, x_2)}. \tag{E.16}$$

Let $\boldsymbol{x}$ be a Gaussian random vector, a subset of which has been set to $\boldsymbol{x}_2 = \tilde{\boldsymbol{x}}$. We could, in principle, substitute the value of the variables $\boldsymbol{x}_1$ into (E.3) and proceed with the remaining (and normalized) expression. However, more interesting conclusions can be drawn if the above results are applied. Instead of working with $\boldsymbol{x} = (\boldsymbol{x}_1, \boldsymbol{x}_2)$, let us use the PDF associated to $\boldsymbol{y} = A\boldsymbol{x}$, where A is given by (E.12):

$$\begin{aligned} f(\boldsymbol{y}) = &\frac{1}{(2\pi)^{p/2}\sqrt{\det\Sigma_{22}}\sqrt{\det(\Sigma_{11} - \Sigma_{12}\Sigma_{22}^{-1}\Sigma_{21})}} \\ &\exp\left[-\frac{1}{2}(\boldsymbol{y}_1 - \boldsymbol{\mu}'_1)^T(\Sigma_{11} - \Sigma_{12}\Sigma_{22}^{-1}\Sigma_{21})^{-1}(\boldsymbol{y}_1 - \boldsymbol{\mu}'_1) - \frac{1}{2}(\boldsymbol{x}_2 - \boldsymbol{\mu}_2)^T\Sigma_{22}^{-1}(\boldsymbol{x}_2 - \boldsymbol{\mu}_2)\right] \\ = &\tilde{f}(\boldsymbol{x}_1, \boldsymbol{x}_2) \end{aligned} \tag{E.17}$$

Fixing $\boldsymbol{x}_2 = \tilde{\boldsymbol{x}}$ and applying (E.16) to the resulting probability distribution function, we find

$$\tilde{f}'(\boldsymbol{x}_1|\boldsymbol{x}_2 = \tilde{\boldsymbol{x}}) = \frac{1}{(2\pi)^{d/2}\sqrt{\det\tilde{\Sigma}}} \exp\left[-\frac{1}{2}\left(\boldsymbol{x}_1 - \tilde{\boldsymbol{\mu}}\right)^T \tilde{\Sigma}^{-1}\left(\boldsymbol{x}_1 - \tilde{\boldsymbol{\mu}}\right)\right] \tag{E.18}$$

where

$$\tilde{\boldsymbol{\mu}} = \boldsymbol{\mu}_1 + \Sigma_{12}\Sigma_{22}^{-1}(\tilde{\boldsymbol{x}} - \boldsymbol{\mu}_2) \tag{E.19}$$

$$\tilde{\Sigma} = \Sigma_{11} - \Sigma_{12}\Sigma_{22}^{-1}\Sigma_{21} \tag{E.20}$$

From the expression above, we can conclude that *conditioned Gaussian random vectors retain their Gaussian nature* with mean and covariance matrix given by $\tilde{\boldsymbol{\mu}}$ and $\tilde{\Sigma}$ respectively.

E.3 Gaussian random fields

The idea of Gaussian random vectors can be generalized to random variables dependent on a certain set of parameters. Instead of having p Gaussian variables, we will have an infinite amount of them; the mean vector and covariance matrix will thus transform into a mean and covariance *functions*.

A Gaussian random field (GRF) $\{V(\boldsymbol{t}), t \in \mathbb{R}^n\}$ is defined as a function satisfying

$$\sum_{i=1}^{r} a_i V(\boldsymbol{t}_i) \sim N(\tilde{\mu}, \tilde{\sigma}) \quad \forall r \in \mathbb{N}, \quad \forall a_i \in \mathbb{R} \tag{E.21}$$

at every point of its domain. The mean function will be given by $\mu(\boldsymbol{t}) = \langle V(\boldsymbol{t}) \rangle$ whereas the covariance function must satisfy $C(\boldsymbol{t}, \boldsymbol{s}) = \langle V(\boldsymbol{t}) V(\boldsymbol{s}) \rangle$. If $C(\boldsymbol{t}, \boldsymbol{s}) = f(\boldsymbol{t} - \boldsymbol{s})$ the GRF is said to be *homogeneous*; if, on the other hand, $C(\boldsymbol{t}, \boldsymbol{s}) = g(\boldsymbol{t} \cdot \boldsymbol{s}, |\boldsymbol{t}|, |\boldsymbol{s}|)$ the field is *isotropic*. GRFs which are both homogeneous and isotropic are referred to as *stationary*, and satisfy

$$C(\boldsymbol{t}, \boldsymbol{s}) = C(|\boldsymbol{t} - \boldsymbol{s}|). \tag{E.22}$$

In the main text, we will we working with this last type of covariance function.

Finally, note that any GRF $V(\boldsymbol{t})$ with mean $\mu(\boldsymbol{t})$ can always be decomposed as

$$V(\boldsymbol{t}) = \mu(\boldsymbol{t}) + W(\boldsymbol{t}) \tag{E.23}$$

where $W(\boldsymbol{t})$ is a mean-zero GRF sharing the same covariance function $V(\boldsymbol{t})$. This construction will be useful to construct GRFs numerically (see appendix F).

E.4 Useful correlations

Since linear combinations of Gaussian variables are Gaussian as well, it is straightforward to see that the derivatives of Gaussian random fields at any point of their domain are Gaussian too. Some of the most important covariance functions relating different Gaussian variables are the following [170, sect. 5.5]:

$$\left\langle \frac{\partial^{\alpha+\beta} V(\boldsymbol{\phi})}{\partial^\alpha \phi_i \partial^\beta \phi_j} \frac{\partial^{\gamma+\delta} V(\boldsymbol{\phi})}{\partial^\gamma \phi_k \partial^\delta \phi_l} \right\rangle = (-1)^{\alpha+\beta} \frac{\partial^{\alpha+\beta+\gamma+\delta}}{\partial^\alpha \phi_i \partial^\beta \phi_j \partial^\gamma \phi_k \partial^\delta \phi_l} C(\boldsymbol{\phi}) \bigg|_{\boldsymbol{\phi}=\mathbf{0}}. \tag{E.24}$$

Let us change the notation to $\partial_{\phi_j} V(\mathbf{0}) = V'_j(\mathbf{0})$ and evaluate the previous expression for some useful cases:

$$\langle V(\mathbf{0}) V(\mathbf{0}) \rangle = U_0^2 \tag{E.25}$$

$$\langle V(\mathbf{0}) V'_i(\mathbf{0}) \rangle = \left\langle V'_i(\mathbf{0}) V''_{jk}(\mathbf{0}) \right\rangle = 0 \tag{E.26}$$

$$\left\langle V'_i(\mathbf{0}) V'_j(\mathbf{0}) \right\rangle = -\left\langle V(\mathbf{0}) V''_{ij}(\mathbf{0}) \right\rangle = -\frac{\partial^2 C(\mathbf{0})}{\partial \phi_i \partial \phi_j} = \alpha_2 \delta_{ij} \tag{E.27}$$

$$\left\langle V''_{ij}(\mathbf{0}) V''_{kl}(\mathbf{0}) \right\rangle = \frac{\partial^4 C(\mathbf{0})}{\partial \phi_i \partial \phi_j \partial \phi_k \partial \phi_l} = \begin{cases} \alpha_{22} & \text{if} \quad i = j \neq k = l \text{ (and perms.)} \\ \alpha_4 & \text{if} \quad i = j = k = l \\ 0 & \text{otherwise.} \end{cases} \tag{E.28}$$

$$\left\langle V(\mathbf{0}) V'''_{jkl}(\mathbf{0}) \right\rangle = \left\langle V''_{ij}(\mathbf{0}) V'''_{klm}(\mathbf{0}) \right\rangle = 0 \tag{E.29}$$

$$\left\langle V'_i(\mathbf{0}) V'''_{jkl}(\mathbf{0}) \right\rangle = -\left\langle V''_{ij}(\mathbf{0}) V''_{kl}(\mathbf{0}) \right\rangle = \begin{cases} -\alpha_{22} & \text{if} \quad i = j \neq k = l \text{ (and perms.)} \\ -\alpha_4 & \text{if} \quad i = j = k = l \\ 0 & \text{otherwise.} \end{cases} \tag{E.30}$$

$$\left\langle V'''_{ijk}(\mathbf{0}) V'''_{lmn}(\mathbf{0}) \right\rangle = -\frac{\partial^6 C(\mathbf{0})}{\partial\phi_i\partial\phi_j\partial\phi_k\partial\phi_l\partial\phi_m\partial\phi_n} = \begin{cases} \alpha_{222} & \text{if} \quad i=j\neq k=l\neq m=n \text{ (and perms.)} \\ \alpha_{24} & \text{if} \quad i=j\neq k=l=m=n \text{ (and perms.)} \\ \alpha_6 & \text{if} \quad i=j=k=l=m=n \\ 0 & \text{otherwise.} \end{cases} \tag{E.31}$$

In the above expressions, α_i, α_{ij} and α_{ijk} are numerical constants which depend only on the covariance function of the (unconstrained) Gaussian random field. Note that in the two-dimensional case α_{222} will be absent from all derivations, since the indices appearing in the correlation function between the third derivatives can only take two different values.

Note also that odd derivatives of the GRF are uncorrelated with even ones when they are evaluated at the same point in field space. This is due to the isotropy of the covariance function: if it is written as a power series, only even powers such as $\phi_i^2, \phi_i^2\phi_j^2$ will be involved. Therefore, only those correlations which end up involving even derivatives of the covariance function are non-zero.

This however, does not mean the fields $V(\boldsymbol{\phi})$ and, say, $V'_i(\boldsymbol{\phi})$ are completely uncorrelated. If we evaluate them at different points in field space, it can be shown [226, theorem 2.3] that

$$\left\langle V(\boldsymbol{\phi}) V'_i(\mathbf{0}) \right\rangle = -\frac{\partial}{\partial\phi_i} C(\boldsymbol{\phi}) \tag{E.32}$$

$$\left\langle V(\boldsymbol{\phi}) V''_{ij}(\mathbf{0}) \right\rangle = \frac{\partial^2}{\partial\phi_i\partial\phi_j} C(\boldsymbol{\phi}) \tag{E.33}$$

$$\left\langle V(\boldsymbol{\phi}) V'''_{ijk}(\mathbf{0}) \right\rangle = -\frac{\partial^3}{\partial\phi_i\partial\phi_j\partial\phi_k} C(\boldsymbol{\phi}) \tag{E.34}$$

therefore, a GRF and any of its derivatives are correlated as processes.

E.5 The Kac-Rice formula and conditioned Gaussian random fields

Consider a Gaussian random *vector* field with components $\mathcal{V}(\boldsymbol{\phi}) = \{V_1(\boldsymbol{\phi}), \dots, V_n(\boldsymbol{\phi})\}$. The multidimensional[1] Kac-Rice formula for this field gives us the expected number of times a certain event, say, $\mathcal{V}(\boldsymbol{\phi}) = \boldsymbol{u}$, happens in an interval $\boldsymbol{\phi} \in I$ of volume $\mathbb{V}$:

$$\mathbb{E}_{\#,I}\left[\mathcal{V}(\boldsymbol{\phi}) = \boldsymbol{u}\right] = \left\langle \int_I d\boldsymbol{\phi}\, |\det \mathcal{V}'(\boldsymbol{\phi})|\, \delta(\mathcal{V}(\boldsymbol{\phi}) - \boldsymbol{u}) \right\rangle \tag{E.35}$$

where $\det \mathcal{V}'(\boldsymbol{\phi})$ stands for the Jacobian determinant of the vector field[2], that is,

$$\mathcal{V}'(\boldsymbol{\phi}) = \begin{pmatrix} \partial_{\phi_1} V_1(\boldsymbol{\phi}) & \cdots & \partial_{\phi_1} V_n(\boldsymbol{\phi}) \\ \vdots & & \vdots \\ \partial_{\phi_n} V_1(\boldsymbol{\phi}) & \cdots & \partial_{\phi_n} V_n(\boldsymbol{\phi}) \end{pmatrix}. \tag{E.36}$$

[1] Note that this formula is only valid for fields mapping $\mathbb{R}^n \to \mathbb{R}^n$.

[2] For critical points, the Jacobian is identical to the Hessian of the GRF at the critical point.

If the field is *stationary*, that is, homogeneous and isotropic, we can simplify the expression above. Denoting $\mathcal{V}_\mathbf{0} = \mathcal{V}(\mathbf{0})$ and $\mathcal{V}'_\mathbf{0} = \mathcal{V}'(\mathbf{0})$, we find, assuming ergodicity,

$$\mathbb{E}_{\#,I}\left[\mathcal{V}(\boldsymbol{\phi}) = \boldsymbol{u}\right] = \mathcal{V} \int d\mathcal{V}_\mathbf{0}\, d\mathcal{V}_\mathbf{0}{}'\, |\det \mathcal{V}_\mathbf{0}{}'|\, \delta(\mathcal{V}_\mathbf{0} - \boldsymbol{u})\, P(\mathcal{V}_\mathbf{0}, \mathcal{V}_\mathbf{0}{}') \tag{E.37}$$

where the integral is performed over the whole domain of $\mathcal{V}_\mathbf{0}$ and $\mathcal{V}'_\mathbf{0}$ and $P(\mathcal{V}_\mathbf{0}, \mathcal{V}_\mathbf{0}{}')$ is the joint PDF of $\mathcal{V}_\mathbf{0}$ and its derivatives.

More than one simultaneous event can be considered in the expressions above by enlarging the vector $\mathcal{V}$ and introducing more Dirac deltas representing each event.[3]

While the above expression can certainly be used to obtain the number of times a certain event happens in a given interval, it can also be used to obtain distribution functions. More specifically, applying ergodicity theorems, it can be shown [226] that the probability of an event A happening, given that B has happened, that is, $P(A|B)$, can be obtained by

$$P(A|B) = \frac{\mathbb{E}_{\#,I}\left[A \cap B\right]}{\mathbb{E}_{\#,I}\left[B\right]}. \tag{E.38}$$

If A depends on continuous parameters (such as the position in field space of the GRF), then the expression above represents a probability distribution function.

E.6 Conditioned Gaussian random field for a critical point

With the tools presented in the sections above, we are now ready to begin conditioning GRFs. We can begin applying (E.38) and specializing it for critical points. We denote by A the event describing the field $V(\boldsymbol{\phi})$ taking a particular configuration, while B imposes $V(\mathbf{0}) \equiv V_0 = u$ and $V'_i(\mathbf{0}) \equiv \eta_i = 0$, that is, a critical point lying in the center of field space at height u. In order to proceed more easily, we shall discretize $V(\boldsymbol{\phi})$ as $\{V(\boldsymbol{\phi}_\mathbf{1}), \dots, V(\boldsymbol{\phi}_\boldsymbol{q})\} \equiv \{V_1, \dots V_q\} \equiv \boldsymbol{V}$.

In this case, the conditioning event involves the Gaussian random vector field $\mathcal{V} = \nabla V$, whose Jacobian is the Hessian of the original field V evaluated at $\boldsymbol{\phi} = \mathbf{0}$. Therefore, its determinant is simply the product of the eigenvalues of the Hessian evaluated at the origin, $\prod_{i=1}^{n} \lambda_i$.

Applying the Kac-Rice formula (E.37) into (E.38) yields

$$\begin{aligned} &P\Big(V(\boldsymbol{\phi})\Big|V_0 = u, \nabla V_0 = \mathbf{0}\Big) \equiv P_{cp}[V(\boldsymbol{\phi})] = \\ &= \frac{\displaystyle\int \prod_{i=1}^{n}\Big(d\eta_i \delta(\eta_i) d\lambda_i |\lambda_i|\Big)\, \Delta(\boldsymbol{\lambda})\, \delta(V_0 - u) \prod_{j=1}^{q}\left(d\tilde{V}_j \delta(\tilde{V}_j - V_j)\right) P\Big(V_0, \boldsymbol{V}, \boldsymbol{\eta}, \boldsymbol{\lambda}\Big)}{\displaystyle\int \prod_{i=1}^{n}\Big(d\eta_i \delta(\eta_i) d\lambda_i |\lambda_i|\Big)\, \Delta(\boldsymbol{\lambda})\, \delta(V_0 - u)\, P\Big(V_0, \boldsymbol{\eta}, \boldsymbol{\lambda}\Big)} \end{aligned} \tag{E.39}$$

[3] See, however, [226, ch.8] for a discussion on different types of conditioning events and how to deal with them. The reason why we consider the $V_0 = u$ event simply with a Dirac delta is that it is a *vertical window conditioning event*

$$= \mathcal{N} \int \prod_{i=1}^{n} (d\lambda_i |\lambda_i|)\, \Delta(\boldsymbol{\lambda}) P\Big(V(\boldsymbol{\phi}), \lambda_1, \dots, \lambda_n \;\Big|\; V_0 = u,\ \nabla V_0 = \mathbf{0}\Big) \tag{E.40}$$

where the integration domain will depend on the kind of critical point we are working with. $\Delta(\boldsymbol{\lambda}) \propto \prod_{i<j} |\lambda_i - \lambda_j|$ is the Jacobian of the variable change from components of the Hessian matrix to its eigenvalues, the proportionality constant depending on the dimensionality of the field space. For simplicity, the denominator in (E.39) has been considered as a normalization factor for the distribution in the numerator.

We can rewrite (E.39) in a more useful way:

$$P_{cp}[V(\boldsymbol{\phi})] = \prod_i \int d\lambda_i\ q_u(\lambda_1, \dots, \lambda_n)\ P\Big(V(\boldsymbol{t}) \;\Big|\; V_0 = u,\ \nabla V_0 = \mathbf{0},\ \lambda_1, \dots, \lambda_n\Big) \tag{E.41}$$

where

$$q_u(\lambda_1, \dots, \lambda_n) = \prod_i |\lambda_i|\ \Delta(\boldsymbol{\lambda})\ P\Big(\lambda_1, \dots, \lambda_n \;\Big|\; V_0 = u,\ \nabla V_0 = \mathbf{0}\Big) \tag{E.42}$$

represents the distribution of the Hessian eigenvalues at the origin for a critical point of height u. However, due to the homogeneous and isotropic nature of the original GRF, the latter distribution is valid for *any* critical point in the GRF, thus giving us a distribution for the parameters at critical points in the unconstrained field.

Equations (E.41) and (E.42) are central results in this derivation. Note that the $\prod_i |\lambda_i|\ \Delta(\boldsymbol{\lambda})$ factor is a direct consequence of the Kac-Rice formula, and as we shall explicitly see in appendix F, it carries important consequences in the distribution of the eigenvalues at critical points.

We can now see the power of this method. Assuming we have discretized our field space, we can readily compute the conditional probability distributions in (E.41) and (E.42) using the results from section E.2. This leads, together with (E.42), to a distribution from which we can draw eigenvalues for a minimum of height u. These can be plugged in (E.41) to generate iterations of GRFs with a minimum (or any other critical point) at their origin.

In order to apply all this machinery, let us introduce the following Gaussian random vector:

$$\{V(\boldsymbol{\phi}_1), \dots, V(\boldsymbol{\phi}_q), V(\mathbf{0}), V_1'(\mathbf{0}), \dots, V_n'(\mathbf{0}), V_{11}''(\mathbf{0}), \dots, V_{nn}''(\mathbf{0}), \underbrace{V_{12}''(\mathbf{0}), \dots, V_{(n-1)n}''(\mathbf{0})}_{V_{ij}''(\mathbf{0}) \quad i<j}\} \tag{E.43}$$

where we denote by $\boldsymbol{\phi}_q$ the position in field space of a discrete set of points whose center is located at $\mathbf{0}$, $V_i'(\mathbf{0})$ describes the first derivative along ϕ_i and $V_{ij}''(\mathbf{0})$ is the (i,j)-th element of the Hessian matrix. In order to unclutter the notation, we will compactify the previous vector as

$$\{\boldsymbol{V}, V(\mathbf{0}), \boldsymbol{V}'(\mathbf{0}), \boldsymbol{V}''(\mathbf{0})\} \tag{E.44}$$

which has dimension $q + 1 + n + n + \frac{1}{2}n(n-1)$. The mean of (E.43) is zero, and the covariance

matrix of these quantities can be computed from the results in section E.4:

$$\Sigma = \begin{pmatrix} S_{VV} & S_{V0} & S_{V1} & S_{V2} \\ S_{0V} & U_0^2 & \mathbf{0} & S_{02} \\ S_{1V} & \mathbf{0} & S_{11} & \mathbf{0} \\ S_{2V} & S_{20} & \mathbf{0} & S_{22} \end{pmatrix} \tag{E.45}$$

where

$$S_{02} = \begin{pmatrix} -\alpha_2 & \cdots & -\alpha_2 & 0 & \cdots & 0 \end{pmatrix} = S_{20}^T \tag{E.46}$$

$$S_{11} = \alpha_2 \times \mathbb{1}_n \tag{E.47}$$

$$S_{22} = \left(\begin{array}{cccc|cc} \alpha_4 & \alpha_{22} & \cdots & \alpha_{22} & & \\ \alpha_{22} & \alpha_4 & \cdots & \alpha_{22} & \multicolumn{2}{c}{0} \\ \vdots & \vdots & \ddots & \vdots & & \\ \alpha_{22} & \alpha_{22} & \cdots & \alpha_4 & & \\ \hline & & & & \alpha_{22} & 0 \\ & & 0 & & \ddots & \\ & & & & 0 & \alpha_{22} \end{array}\right) \tag{E.48}$$

$$S_{VV} = \begin{pmatrix} C(\mathbf{0}) & C(\boldsymbol{\phi_1} - \boldsymbol{\phi_2}) & \cdots & C(\boldsymbol{\phi_1} - \boldsymbol{\phi_q}) \\ C(\boldsymbol{\phi_2} - \boldsymbol{\phi_1}) & C(\mathbf{0}) & \cdots & C(\boldsymbol{\phi_2} - \boldsymbol{\phi_q}) \\ \vdots & \vdots & \ddots & \vdots \\ C(\boldsymbol{\phi_q} - \boldsymbol{\phi_1}) & C(\boldsymbol{\phi_q} - \boldsymbol{\phi_2}) & \cdots & C(\mathbf{0}) \end{pmatrix} \tag{E.49}$$

$$S_{0V} = \begin{pmatrix} C(\boldsymbol{\phi_1}) & C(\boldsymbol{\phi_2}) & \cdots & C(\boldsymbol{\phi_q}) \end{pmatrix} = S_{V0}^T \tag{E.50}$$

$$S_{1V} = \begin{pmatrix} -C_1'(\boldsymbol{\phi_1}) & -C_1'(\boldsymbol{\phi_2}) & \cdots & -C_1'(\boldsymbol{\phi_q}) \\ -C_2'(\boldsymbol{\phi_1}) & -C_2'(\boldsymbol{\phi_2}) & \cdots & -C_2'(\boldsymbol{\phi_q}) \\ \vdots & \vdots & \ddots & \vdots \\ -C_n'(\boldsymbol{\phi_1}) & -C_n'(\boldsymbol{\phi_2}) & \cdots & -C_n'(\boldsymbol{\phi_q}) \end{pmatrix} = S_{V1}^T \tag{E.51}$$

$$S_{2V} = \begin{pmatrix} C_{11}''(\boldsymbol{\phi_1}) & \cdots & C_{11}''(\boldsymbol{\phi_q}) \\ \vdots & \ddots & \vdots \\ C_{nn}''(\boldsymbol{\phi_1}) & \cdots & C_{nn}''(\boldsymbol{\phi_q}) \\ C_{12}''(\boldsymbol{\phi_1}) & \cdots & C_{12}''(\boldsymbol{\phi_q}) \\ \vdots & \ddots & \vdots \\ C_{(n-1)n}''(\boldsymbol{\phi_1}) & \cdots & C_{(n-1)n}''(\boldsymbol{\phi_q}) \end{pmatrix} = S_{V2}^T \tag{E.52}$$

In order to simplify the notation, since the jointly Gaussian probability distribution in

the end depends on two-point functions, we can actually write[4] (E.45) in the following way:

$$\Sigma = \left(\begin{array}{cc|ccc} U_0^2 & C(\boldsymbol{\phi_1}-\boldsymbol{\phi_2}) & C(\boldsymbol{\phi_1}) & S_{V1}(\boldsymbol{\phi_1}) & S_{V2}(\boldsymbol{\phi_1}) \\ C(\boldsymbol{\phi_2}-\boldsymbol{\phi_1}) & U_0^2 & C(\boldsymbol{\phi_2}) & S_{V1}(\boldsymbol{\phi_2}) & S_{V2}(\boldsymbol{\phi_2}) \\ \hline C(\boldsymbol{\phi_1}) & C(\boldsymbol{\phi_2}) & U_0^2 & \mathbf{0} & S_{02} \\ S_{1V}(\boldsymbol{\phi_1}) & S_{1V}(\boldsymbol{\phi_2}) & \mathbf{0} & S_{11} & \mathbf{0} \\ S_{2V}(\boldsymbol{\phi_1}) & S_{2V}(\boldsymbol{\phi_2}) & S_{20} & \mathbf{0} & S_{22} \end{array}\right) \tag{E.53}$$

where

$$S_{V1}(\boldsymbol{\phi}) = \begin{pmatrix} -C_1'(\boldsymbol{\phi}) & \cdots & -C_n'(\boldsymbol{\phi}) \end{pmatrix} = S_{1V}^T \tag{E.54}$$

$$S_{V2}(\boldsymbol{\phi}) = \begin{pmatrix} C_{11}''(\boldsymbol{\phi}) & \cdots & C_{nn}''(\boldsymbol{\phi}) & C_{12}''(\boldsymbol{\phi}) & \cdots & C_{(n-1)n}''(\boldsymbol{\phi}) \end{pmatrix} = S_{2V}^T \tag{E.55}$$

With these arrangements, the Gaussian random vector corresponding to (E.53) is

$$\left\{V(\boldsymbol{\phi}_1), V(\boldsymbol{\phi}_2), V(\mathbf{0}), \boldsymbol{V}'(\mathbf{0}), \boldsymbol{V}''(\mathbf{0})\right\}. \tag{E.56}$$

We have decomposed (E.53) into blocks so it can be plugged into (E.57) and (E.58) to obtain the mean function and covariance matrix of the conditioned process.[5] Using the results given above, one gets that the expectation value for the GRF around a critical point where $V_0 = u$ and $\boldsymbol{V_0'} = 0$, is given by,

$$\begin{aligned} \tilde{\mu}(\boldsymbol{\phi}) &= \mu(\boldsymbol{\phi}) + \begin{pmatrix} C(\boldsymbol{\phi}) & S_{V1}(\boldsymbol{\phi}) & S_{V2}(\boldsymbol{\phi}) \end{pmatrix} \begin{pmatrix} U_0^2 & \mathbf{0} & S_{02} \\ \mathbf{0} & S_{11} & \mathbf{0} \\ S_{20} & \mathbf{0} & S_{22} \end{pmatrix}^{-1} \begin{pmatrix} u \\ \mathbf{0} \\ \boldsymbol{h} \end{pmatrix} \\ &= \begin{pmatrix} C(\boldsymbol{\phi}) & S_{V2}(\boldsymbol{\phi}) \end{pmatrix} \begin{pmatrix} U_0^2 & S_{02} \\ S_{20} & S_{22} \end{pmatrix}^{-1} \begin{pmatrix} u \\ \boldsymbol{h} \end{pmatrix} \end{aligned} \tag{E.57}$$

where $\boldsymbol{h} = \{h_{11}, \ldots, h_{nn}, h_{12}, \ldots, h_{(n-1)n}\}$ represents a certain configuration of the Hessian components of the field around the origin.

Furthermore, the covariance function for the conditioned GRF is now

$$\begin{aligned} \tilde{C}(\boldsymbol{\phi_1}, \boldsymbol{\phi_2}) &= C(\boldsymbol{\phi_1}-\boldsymbol{\phi_2}) - \begin{pmatrix} C(\boldsymbol{\phi_1}) & S_{V1}(\boldsymbol{\phi_1}) & S_{V2}(\boldsymbol{\phi_1}) \end{pmatrix} \begin{pmatrix} U_0^2 & \mathbf{0} & S_{02} \\ \mathbf{0} & S_{11} & \mathbf{0} \\ S_{20} & \mathbf{0} & S_{22} \end{pmatrix}^{-1} \begin{pmatrix} C(\boldsymbol{\phi_2}) \\ S_{1V}(\boldsymbol{\phi_2}) \\ S_{2V}(\boldsymbol{\phi_2}) \end{pmatrix} \\ &= C(\boldsymbol{\phi_1}-\boldsymbol{\phi_2}) - \begin{pmatrix} C(\boldsymbol{\phi_1}) & S_{V2}(\boldsymbol{\phi_1}) \end{pmatrix} \begin{pmatrix} U_0^2 & S_{02} \\ S_{20} & S_{22} \end{pmatrix}^{-1} \begin{pmatrix} C(\boldsymbol{s}) \\ S_{2V}(\boldsymbol{\phi_2}) \end{pmatrix} \\ &\quad - S_{V1}(\boldsymbol{\phi_1}) S_{11}^{-1} S_{1V}(\boldsymbol{\phi_2}) \end{aligned} \tag{E.58}$$

[4] We basically have evaluated the first row for a given $\boldsymbol{\phi_1}$ and the first column for a given $\boldsymbol{\phi_2}$, just as in [227]. Doing so allows us to treat the independent variable as a continuous one, rather than a discrete one.

[5] Strictly speaking, we should be getting the mean and covariance of the random vector $\{V(\boldsymbol{\phi}_1), V(\boldsymbol{\phi}_2)\}$. Due to the isotropy of the GRF, $\boldsymbol{\phi}_1$ and $\boldsymbol{\phi}_2$ can be any points in field space. Thus, in order to unclutter the notation, we will only keep track of a single component of the resulting mean vector. Likewise, we will only keep the $\langle V(\boldsymbol{\phi}_1)V(\boldsymbol{\phi}_2)\rangle$ component of the covariance matrix.

We can also obtain (E.42), the distribution of eigenvalues at a critical point of a given height u, following the same steps as above, using as initial covariance matrix the bottom-right block of (E.53).

E.6.1 Analysis of a conditioned 2D Gaussian field

Let us apply these expressions to a two-dimensional isotropic and homogeneous GRF with covariance function

$$C(\boldsymbol{\phi}) = U_0^2 \exp\left(-\frac{\boldsymbol{\phi}^2}{2\Lambda^2}\right). \tag{E.59}$$

and zero mean. For this case, we obtain the conditioned mean from (E.57), which gives

$$\tilde{\mu}(\boldsymbol{\phi}) = e^{-\frac{\boldsymbol{\phi}^2}{2\Lambda^2}}\left[u\left(1+\frac{\boldsymbol{\phi}^2}{2\Lambda^2}\right)+\frac{1}{2}\begin{pmatrix}\phi_1 & \phi_2\end{pmatrix}\begin{pmatrix}h_{11} & h_{12}\\ h_{21} & h_{22}\end{pmatrix}\begin{pmatrix}\phi_1\\ \phi_2\end{pmatrix}\right], \tag{E.60}$$

where $h_{21} = h_{12}$, by definition. Since we are free to choose the basis of $\boldsymbol{\phi}$, in order to simplify the expression we will employ the eigenvector basis of the Hessian matrix, therefore transforming (E.60) to

$$\tilde{\mu}(\boldsymbol{\phi}) = e^{-\frac{\boldsymbol{\phi}^2}{2\Lambda^2}}\left[u\left(1+\frac{\boldsymbol{\phi}^2}{2\Lambda^2}\right)+\frac{1}{2}\sum_{i=1}^{2}\lambda_i\phi_i^2\right]. \tag{E.61}$$

where λ_i denote the two eigenvectors, drawn from (E.42) specialized to this case (see below). As for the conditioned covariance, from (E.58) we obtain

$$\tilde{C}(\boldsymbol{\phi_1},\boldsymbol{\phi_2}) = U_0^2 \exp\left[-\frac{|\boldsymbol{\phi_1}|^2+|\boldsymbol{\phi_2}|^2}{2\Lambda^2}\right]\left(\exp\left[\frac{\boldsymbol{\phi_1}\cdot\boldsymbol{\phi_2}}{\Lambda^2}\right]-1-\frac{\boldsymbol{\phi_1}\cdot\boldsymbol{\phi_2}}{\Lambda^2}-\frac{(\boldsymbol{\phi_1}\cdot\boldsymbol{\phi_2})^2}{2\Lambda^4}\right). \tag{E.62}$$

Note that the covariance function of the conditioned process is not homogeneous anymore! This, however, makes complete sense. We have actually made the center of every realization *special*, meaning that homogeneity is broken in this sense. In fact, the new covariance is isotropic with respect to $\boldsymbol{\phi} = \mathbf{0}$, further stating that the center of the GRF is somehow different from the rest of the points.

All the presented machinery works not only for minima, but also for maxima and saddle points as well; the only difference among these being the sign of each λ_i.

E.6.2 Distribution of heights and eigenvalues of the Hessian at a critical point

In order to calculate the probability distribution of the eigenvalues of the Hessian at a certain height of the potential at critical points we should pay attention to two ingredients. The first one is the fact that the height and the second derivatives are correlated, so we need to calculate the multivariate covariance function for these quantities together. Furthermore, we also want to calculate this at critical points which can be done with the use of the generalized Kac-Rice formula.

Assuming a critical point located at $\boldsymbol{\phi} = \mathbf{0}$, the probability distribution to be computed is

$$P\Big(V_0, \lambda_1, \lambda_2 \Big| \nabla V_0 = \mathbf{0}\Big) \tag{E.63}$$

We can easily compute the PDF by conditioning the following random vector:

$$\{V_0, h_{11}, h_{22}, h_{12}, \eta_1, \eta_2\} \tag{E.64}$$

of mean zero and covariance matrix

$$\left(\begin{array}{cc|c} U_0^2 & S_{02} & \mathbf{0} \\ S_{20} & S_{22} & \mathbf{0} \\ \hline \mathbf{0} & \mathbf{0} & S_{11} \end{array}\right) \tag{E.65}$$

Applying (E.19) and (E.20) to obtain the mean and covariance of the conditioned process and plugging them into (E.42), we get

$$P_{cp}(V_0, \lambda_1, \lambda_2)\, du \prod_{i=1}^{2} d\lambda_i = \mathcal{N}\, |\lambda_1||\lambda_2|\, \Delta(\boldsymbol{\lambda})\, P\Big(V_0, \lambda_1, \lambda_2 \Big| \nabla V_0 = \mathbf{0}\Big) \tag{E.66}$$

$$= \mathcal{N} |\lambda_1 - \lambda_2||\lambda_1||\lambda_2| \exp\left[-\frac{V_0^2}{2U_0^2} - \left(\frac{\Lambda^2 \lambda_i + V_0}{2U_0}\right)^2\right] d\lambda_i\, dV_0 \tag{E.67}$$

where $\mathcal{N}$ is a normalization factor and, in this two-dimensional example, $\Delta(\boldsymbol{\lambda}) = |\lambda_1 - \lambda_2| \cdot \pi/2$.

Setting V_0 to a constant value, say $V_0 = u$, in (E.67) yields the distribution $q_u(\lambda_1, \lambda_2)$, defined in (E.42). On the other hand, integrating out either V_0 or the eigenvalues, gives the marginal distribution for the remaining variables in critical points (see appendix F for more detail).

Another interesting application of (E.66) is that it can be used to count the expected number of critical points in a certain region of field space. For example, to compute the expected number of minima per correlation volume Λ^2 in the example above, a direct application of (E.37) yields

$$\begin{aligned} \frac{\mathbb{E}(\#_{min})}{\Lambda^2} &= \int_{-\infty}^{+\infty} du \int_0^{+\infty} d\lambda_1 \int_0^{+\infty} d\lambda_2 \frac{\pi}{2}\, \lambda_1 \lambda_2\, |\lambda_1 - \lambda_2| P\Big(V_0, \lambda_1, \lambda_2 \Big| \nabla V_0 = \mathbf{0}\Big) \\ &= \frac{1}{2\sqrt{3}}. \end{aligned} \tag{E.68}$$

In this case, the eigenvalues have been assumed to be positive. Setting other integration limits can give the expected number of maxima and saddle points, for example.

E.7 Conditioned Gaussian random field for an inflection point

We shall define an inflection point on our GRF as *a point where the gradient of the field points in the direction of a Hessian eigenvector whose corresponding eigenvalue is zero*. Furthermore, we will also demand that the non-zero eigenvalue of the Hessian to be positive at this point.

In order to do this we can expand the discussion of the previous section by taking into

account the third derivatives of the GRFs along with the lower ones. In order to simplify this description we will give a detail account of this construction for a $2d$ GRF only. Extending this to higher dimensions is straightforward. In particular we will be interested in the Gaussian random vector

$$\left\{V(\boldsymbol{\phi_1}), V(\boldsymbol{\phi_2}), V_0, V_1'(\mathbf{0}), V_2'(\mathbf{0}), V_{11}''(\mathbf{0}), V_{22}''(\mathbf{0}), V_{12}''(\mathbf{0}), V_{111}'''(\mathbf{0}), V_{122}'''(\mathbf{0}), V_{222}'''(\mathbf{0}), V_{112}'''(\mathbf{0})\right\} \tag{E.69}$$

whose components have zero mean. As for the covariance matrix, it can be expressed as

$$\Sigma = \left(\begin{array}{cc|cccc} U_0^2 & C(\boldsymbol{\phi}_1-\boldsymbol{\phi}_2) & C(\boldsymbol{\phi_1}) & S_{V1}(\boldsymbol{\phi_1}) & S_{V2}(\boldsymbol{\phi_1}) & S_{V3}(\boldsymbol{\phi_1}) \\ C(\boldsymbol{\phi_2}-\boldsymbol{\phi_1}) & U_0^2 & C(\boldsymbol{\phi}_2) & S_{V1}(\boldsymbol{\phi_2}) & S_{V2}(\boldsymbol{\phi_2}) & S_{V3}(\boldsymbol{\phi_2}) \\ \hline C(\boldsymbol{\phi_1}) & C(\boldsymbol{\phi_2}) & U_0^2 & \mathbf{0} & S_{02} & \mathbf{0} \\ S_{1V}(\boldsymbol{\phi_1}) & S_{1V}(\boldsymbol{\phi_2}) & \mathbf{0} & S_{11} & \mathbf{0} & S_{13} \\ S_{2V}(\boldsymbol{\phi_1}) & S_{2V}(\boldsymbol{\phi_2}) & S_{20} & \mathbf{0} & S_{22} & \mathbf{0} \\ S_{3V}(\boldsymbol{\phi_1}) & S_{3V}(\boldsymbol{\phi_2}) & \mathbf{0} & S_{31} & \mathbf{0} & S_{33} \end{array}\right) \tag{E.70}$$

where (for the 2D case)

$$S_{V3}(\boldsymbol{\phi}) = \begin{pmatrix} -C'_{111}(\boldsymbol{\phi}) & -C'_{122}(\boldsymbol{\phi}) & -C'_{222}(\boldsymbol{\phi}) & -C'_{112}(\boldsymbol{\phi}) \end{pmatrix} = S_{3V}^T \tag{E.71}$$

$$S_{13} = \begin{pmatrix} -\alpha_4 & -\alpha_{22} & 0 & 0 \\ 0 & 0 & -\alpha_4 & -\alpha_{22} \end{pmatrix} = S_{31}^T \tag{E.72}$$

$$S_{33} = \begin{pmatrix} \alpha_6 & \alpha_{24} & 0 & 0 \\ \alpha_{24} & \alpha_{24} & 0 & 0 \\ 0 & 0 & \alpha_6 & \alpha_{24} \\ 0 & 0 & \alpha_{24} & \alpha_{24} \end{pmatrix} \tag{E.73}$$

and the other matrix blocks have been defined in (E.46 - E.52).

Following the same steps as in the critical point case, we can obtain (for the covariance function (E.59)) the expression for a GRF once we conditioned everything up to the third derivative. In order to do this we can first compute the mean value of the GRF in the vicinity of our inflection point, which is given by

$$\tilde{\mu}(\boldsymbol{\phi}) = 0 + \begin{pmatrix} C(\boldsymbol{\phi}) & S_{V1}(\boldsymbol{\phi}) & S_{V2}(\boldsymbol{\phi}) & S_{V3}(\boldsymbol{\phi}) \end{pmatrix} \begin{pmatrix} U_0^2 & \mathbf{0} & S_{02} & \mathbf{0} \\ \mathbf{0} & S_{11} & \mathbf{0} & S_{13} \\ S_{20} & \mathbf{0} & S_{22} & \mathbf{0} \\ \mathbf{0} & S_{31} & \mathbf{0} & S_{33} \end{pmatrix}^{-1} \begin{pmatrix} u \\ \boldsymbol{\eta} \\ \boldsymbol{h} \\ \boldsymbol{\rho} \end{pmatrix} \tag{E.74}$$

$$= \begin{pmatrix} C(\boldsymbol{\phi}) & S_{V2}(\boldsymbol{\phi}) \end{pmatrix} \begin{pmatrix} U_0^2 & S_{02} \\ S_{20} & S_{22} \end{pmatrix}^{-1} \begin{pmatrix} u \\ \boldsymbol{h} \end{pmatrix} + \begin{pmatrix} S_{V1}(\boldsymbol{\phi}) & S_{V3}(\boldsymbol{\phi}) \end{pmatrix} \begin{pmatrix} S_{11} & S_{13} \\ S_{31} & S_{33} \end{pmatrix}^{-1} \begin{pmatrix} \boldsymbol{\eta} \\ \boldsymbol{\rho} \end{pmatrix}$$

$$= \exp\left[-\frac{\boldsymbol{\phi}^2}{2\Lambda^2}\right] \left((u + \boldsymbol{\phi}\cdot\boldsymbol{\eta}) \left(1 + \frac{\boldsymbol{\phi}^2}{2\Lambda^2}\right) + \frac{1}{2}\sum_{i=1}^{2} \lambda_i \phi_i^2 + \frac{1}{6}\sum_{i,j,k=1}^{2} \phi_i\phi_j\phi_k\rho_{ijk} \right), \tag{E.75}$$

where the basis of $\boldsymbol{\phi}$ has been chosen to be the eigenbasis of the Hessian matrix (whose components are described by $\boldsymbol{h}$ and its eigenvalues by λ_i) and we have denoted by $\boldsymbol{\eta}$ and $\boldsymbol{\rho}$ the components of the first and third derivatives at the origin along the eigenbasis.

The conditioned covariance, on the other hand, reads

$$\tilde{C}(\boldsymbol{\phi_1},\boldsymbol{\phi_2}) = C(\boldsymbol{\phi_1}-\boldsymbol{\phi_2}) - \begin{pmatrix} C(\boldsymbol{\phi_1}) & S_{V1}(\boldsymbol{\phi_1}) & S_{V2}(\boldsymbol{\phi_1}) & S_{V3}(\boldsymbol{\phi_1}) \end{pmatrix} \begin{pmatrix} U_0^2 & \mathbf{0} & S_{02} & \mathbf{0} \\ \mathbf{0} & S_{11} & \mathbf{0} & S_{13} \\ S_{20} & \mathbf{0} & S_{22} & \mathbf{0} \\ \mathbf{0} & S_{31} & \mathbf{0} & S_{33} \end{pmatrix}^{-1} \begin{pmatrix} C(\boldsymbol{\phi_2}) \\ S_{1V}(\boldsymbol{\phi_2}) \\ S_{2V}(\boldsymbol{\phi_2}) \\ S_{3V}(\boldsymbol{\phi_2}) \end{pmatrix}$$

$$= U_0^2 \exp\left[-\frac{|\boldsymbol{\phi_1}|^2+|\boldsymbol{\phi_2}|^2}{2\Lambda^2}\right]\left(\exp\left[\frac{\boldsymbol{\phi_1}\cdot\boldsymbol{\phi_2}}{\Lambda^2}\right] - 1 - \frac{\boldsymbol{\phi_1}\cdot\boldsymbol{\phi_2}}{\Lambda^2} - \frac{(\boldsymbol{\phi_1}\cdot\boldsymbol{\phi_2})^2}{2\Lambda^4} - \frac{(\boldsymbol{\phi_1}\cdot\boldsymbol{\phi_2})^3}{6\Lambda^6}\right) \tag{E.76}$$

which, once again, is isotropic around the origin of the field.

E.7.1 Probability distribution for the inflection point parameters

We can extend the treatment for the eigenvalues of the hessian that we did for the critical points to inflection points. The difference is that we will now impose that one of the eigenvalues vanishes while the other one is positive. Furthermore we will also impose that the gradient in the second eigenvalue direction also vanishes. These conditions have to be included in the calculation of the PDF of the parameters of the inflection points $(V_0, \eta_1, \lambda_2, \boldsymbol{\rho})$. Using a generalized version of the Kac-Rice procedure we arrive to,

$$P_{\rm inf}\, dV_0\, d\lambda_2\, d\eta_1\, d\boldsymbol{\rho} = \mathcal{N}|\lambda_2|^2|\rho_{111}|\, P\Big(V_0,\ \lambda_2 \mid \lambda_1 = 0\Big)\, P\left(\eta_1, \rho_{ijk} \,\middle|\, \eta_2 = 0\right) \tag{E.77}$$

where

$$P\Big(V_0,\ \lambda_2 \mid \lambda_1 = 0\Big)\, dV_0\, d\lambda_2 = \mathcal{N}\exp\left[-\frac{4V_0^2 - 2\Lambda^2 V_0\lambda_2 - \Lambda^4\lambda_2^2}{2U_0}\right] dV_0\, d\lambda_2 \tag{E.78}$$

$$P\left(\eta_1, \rho_{ijk} \,\middle|\, \eta_2 = 0\right)\, d\eta_1\, d\rho_{ijk} = \mathcal{N}\exp\left[-\frac{\Lambda^2}{12U_0^2}\left(18\eta_1^2 + 6\Lambda^2\eta_1(\rho_{111}+\rho_{122}) + \Lambda^4\sum_{i,j,k=1}^{2}\rho_{ijk}^2\right)\right] d\eta_1\, d\rho_{ijk} \tag{E.79}$$

In (E.77), one of the $|\lambda_2|$ factors comes from the Jacobian of the variable change to the eigenbasis of the Hessian (though with $\lambda_1 = 0$); the remaining $|\lambda_2||\rho_{111}|$ factor is just the determinant appearing in Kac-Rice's expression.

These last expressions can be used as in (E.68) to compute the expected number of inflection point per correlation volume Λ^2, which yields, for our choice of covariance function,

$$\frac{\mathbb{E}(\#_{ip})}{\Lambda^2} = \frac{\sqrt{5}-\sqrt{3}}{3\pi}. \tag{E.80}$$

Appendix F

Numerical implementation and tests of Slepian models

F.1 Generation of Gaussian random fields: Karhunen-Loève expansion

In order to generate realizations of two-dimensional Gaussian random fields, we resorted to the so-called spectral or Karhunen-Loève decomposition, due to its mathematical and computational simplicity.

Given a certain mean function $\mu(\boldsymbol{t})$, covariance function $C(\boldsymbol{t},\boldsymbol{s})$ and a discretized space $\{\boldsymbol{t}_a\}$ (where a runs over all n points in the lattice space) of a GRF, we can build the matrix $C_{ab} = C(\boldsymbol{t}_a,\boldsymbol{t}_b)$, which by construction is symmetric and positive definite; therefore, we can always decompose C_{ab} as

$$C = U\Lambda U^T \tag{F.1}$$

where $\Lambda = \mathrm{diag}(\lambda_1,\ldots,\lambda_n)$ is the diagonal eigenvalue matrix, consisting of non-negative entries, and U is constructed by inserting all eigenvectors along its rows. Since $\Lambda > 0$, we can further decompose C as

$$C = U\sqrt{\Lambda}\sqrt{\Lambda}U^T = \left(U\sqrt{\Lambda}\right)\left(U\sqrt{\Lambda}\right)^T = L\,L^T. \tag{F.2}$$

This procedure is tantamount to performing a Cholesky decomposition [278] on C; which is by far the most expensive step in this algorithm, in terms of computational cost.

Once we have computed L, constructing the GRF on the discretized space is straightforward. We only need to construct a random vector $\boldsymbol{\xi}$ of length n whose entries are *independently* distributed as Gaussian variables of zero mean and unit variance, and introduce the following variables:

$$V_a = \mu_a + L_{ab}\xi_b, \tag{F.3}$$

where $\mu_a = \mu(\boldsymbol{t}_a)$. It can be easily shown that this gives the correct correlations among the

values of the GRF evaluated at different points $\boldsymbol{t}_a$,

$$\begin{aligned}\langle (V_a-\mu_a)(V_b-\mu_b)\rangle &= \langle L_{ac}\xi_c L_{bd}\xi_d\rangle = L_{ac}L_{bd}\langle \xi_c\xi_d\rangle \\ &= L_{ac}L_{bd}\delta_{cd} = L_{ac}L_{bc} = L_{ac}L^T_{cb} = (LL^T)_{ab} = C_{ab} = C(\boldsymbol{t}_a,\boldsymbol{t}_b).\end{aligned} \tag{F.4}$$

The main advantage of using this procedure to generate GRFs is that the main computationally costly step, constructing the L matrix, needs to be performed only once. The rest of the algorithm is highly trivial from this perspective and allows for further simplification, as we have seen.

F.2 Numerical evaluations of Critical points

Using the expressions above we can compute the normalized distribution of heights of minima, maxima and saddle points for a $2d$ GRF,

$$\begin{aligned}P_{u,min}\ du &= \frac{\sqrt{3}}{4\pi U_0}e^{-u^2/U_0^2}\left(-\frac{2u}{U_0}+2\sqrt{\pi}\ e^{u^2/4U_0^2}\ \mathrm{erfc}\left[\frac{u}{2U_0}\right]+\sqrt{2\pi}\left(\frac{u^2}{U_0^2}-1\right)e^{u^2/2U_0^2}\ \mathrm{erfc}\left[\frac{u}{\sqrt{2}U_0}\right]\right)du \\ P_{u,max}\ du &= \frac{\sqrt{3}}{4\pi U_0}e^{-u^2/U_0^2}\left(\frac{2u}{U_0}+2\sqrt{\pi}\ e^{u^2/4U_0^2}\ \mathrm{erfc}\left[-\frac{u}{2U_0}\right]+\sqrt{2\pi}\left(\frac{u^2}{U_0^2}-1\right)e^{u^2/2U_0^2}\ \mathrm{erfc}\left[-\frac{u}{\sqrt{2}U_0}\right]\right)du \\ P_{u,sp}\ \ du &= \frac{\sqrt{3}}{2\sqrt{\pi}U_0}\exp\left[-\frac{3u^2}{4U_0^2}\right].\end{aligned} \tag{F.5}$$

Furthermore, we can also compute the marginal distribution for the Hessian eigenvalues at critical points regardless of their height. This distribution is given by,

$$\begin{aligned}P_{sp,\lambda_i}\ d\lambda_1\ d\lambda_2 &= \sqrt{\frac{3}{\pi}}\frac{\Lambda^{10}}{32U_0^5}\prod_{i=1}^{2}\left(|\lambda_i|\exp\left[-\frac{\Lambda^4}{8U_0^2}\lambda_i^2\right]\right)|\lambda_1-\lambda_2|\exp\left[-\frac{\Lambda^4}{16U_0^2}(\lambda_1-\lambda_2)^2\right]\ d\lambda_1\ d\lambda_2 \\ &= \frac{1}{2}P_{min,max,\lambda_i}\ d\lambda_1\ d\lambda_2.\end{aligned} \tag{F.6}$$

We have checked the distributions above with numerical realizations of unconstrained Gaussian random fields in Mathematica. Regarding the heights of critical points, the numerical results fit the analytical prediction perfectly, as shown in figure F.1(a).

As for the eigenvalue distribution, fig. F.1(b)-(d) shows that the histograms fit the analytical predictions perfectly once again. An important feature of these distributions is the fact that critical points with one of the eigenvalues close to zero or both eigenvalues close to each other are very rare; this effect (referred to as *eigenvalue repulsion*) is a direct consequence of the presence of the Vandermonde determinant in the distributions, as well as the Jacobian of the gradient field in the Kac-Rice formula.

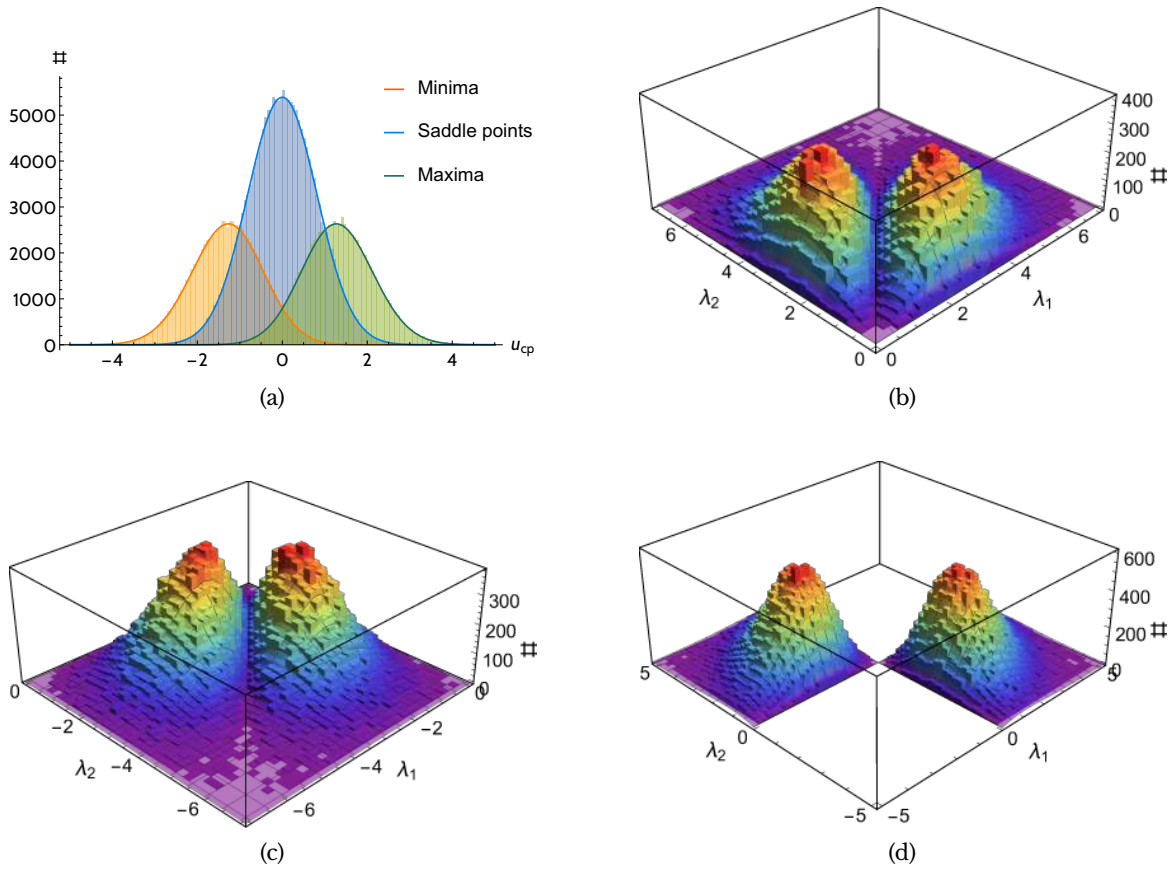

Figure F.1: Histograms of (a) heights and (b-d) eigenvalues for critical points, normalized to expected values, from a $10^5\Lambda^2$ GRF. Distributions (F.5) and (F.6) are plotted along with their respective histograms, normalized with respect to (E.68).

F.3 Numerical evaluations of Inflection points

Using the results given above, we can obtain the following distributions for the parameters of the inflection points in a typical GRF:

$$P_u\,du = \frac{3\sqrt{3}}{16\pi U_0^3}\exp\left[-\frac{u^2}{U_0^2}\right]\left(-2U_0u+\sqrt{\pi}(u^2+2U_0^2)\exp\left[\frac{u^2}{4U_0^2}\right]\operatorname{erfc}\left[\frac{u}{2U_0}\right]\right)du \tag{F.7}$$

$$P_{\lambda_2}\,d\lambda_2 = \sqrt{\frac{3}{\pi}}\frac{3}{16}\frac{\Lambda^6}{U_0^3}\lambda_2^2\exp\left[-\frac{3\Lambda^4}{16U_0^2}\lambda_2^2\right]d\lambda_2 \tag{F.8}$$

$$P_{\eta_1}\,d\eta_1 = \frac{(3+\sqrt{15})\Lambda}{12U_0^2}\exp\left[-\frac{5\Lambda^2}{4U_0^2}\eta_1^2\right]\left(\sqrt{\frac{12}{\pi}}U_0-3\Lambda\,|\eta_1|\exp\left[\frac{3\Lambda^2}{4U_0^2}\eta_1^2\right]\operatorname{erfc}\left[\frac{\sqrt{3}\Lambda}{2U_0}\,|\eta_1|\right]\right)d\eta_1 \tag{F.9}$$

$$P_{\rho_{111}}\,d\rho_{111} = \frac{(5+\sqrt{15})\Lambda^6}{60U_0^2}\,|\rho_{111}|\exp\left[-\frac{\Lambda^6}{30U_0^2}\rho_{111}^2\right]\operatorname{erfc}\left[\frac{\Lambda^3}{2\sqrt{5}U_0}|\rho_{111}|\right]d\rho_{111} \tag{F.10}$$

where the complementary error function is defined as

$$\operatorname{erfc}(x) = \frac{2}{\sqrt{\pi}}\int_x^\infty dt\,e^{-t^2}.$$

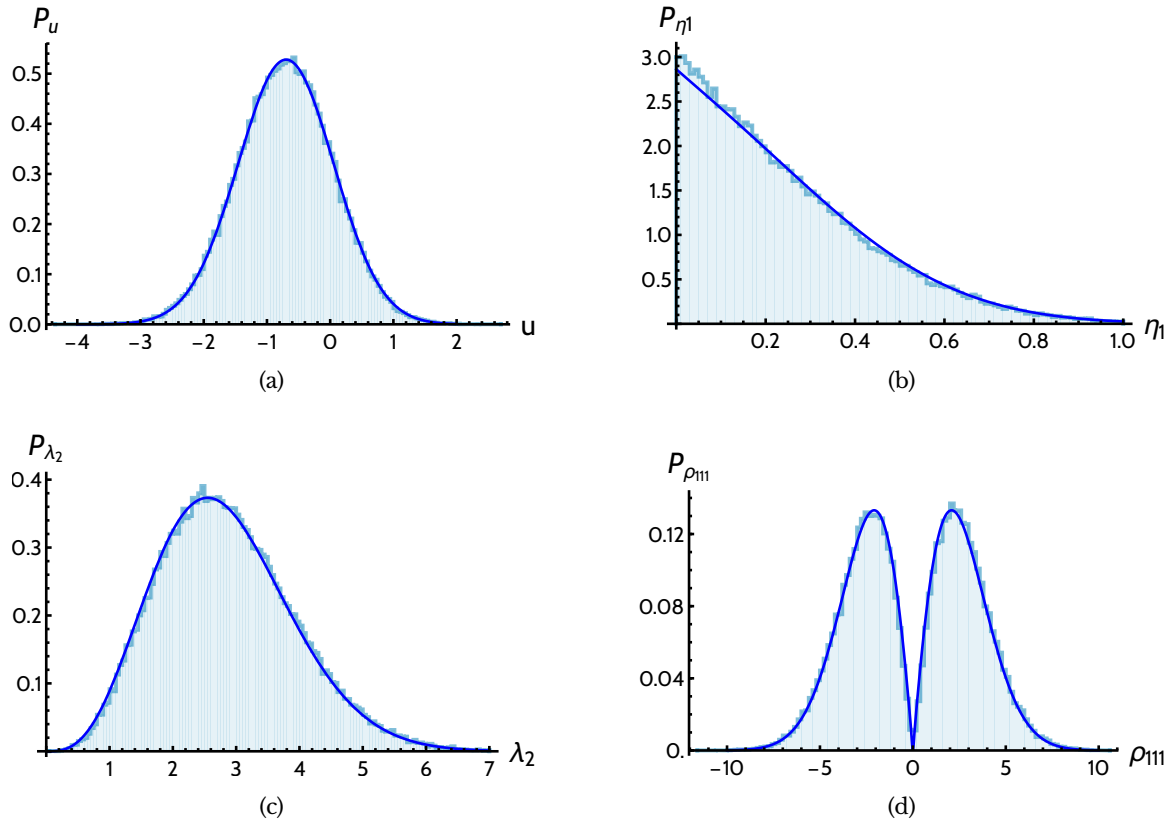

Figure F.2: Normalized histograms of (a) height (b) η_1 (c) λ_2 (d) ρ_{111} for inflection points and their expected PDFs (F.7)-(F.10), constrained by the condition $\lambda_2/\eta_1 > 4$.

Once again, we found these expressions to be fully consistent with the numerical results, as shown in figure F.2.

In order to find inflection points in our numerically generated potentials, we looked for roots of the system

$$\begin{cases} \boldsymbol{\eta}^T \mathscr{H} \boldsymbol{\eta} \\ \boldsymbol{\eta}^T \mathscr{H} \boldsymbol{\eta}_\perp \end{cases} \tag{F.11}$$

where $\mathscr{H}$ is the Hessian matrix, $\boldsymbol{\eta}^T = (\eta_1, \eta_2)$ represents the gradient at any point of the field and $\boldsymbol{\eta}_\perp^T = (-\eta_2, \eta_1)$. It can be easily shown that simultaneous roots of eq. (F.11) are either critical or inflection points.

Finding inflection points numerically is quite tricky and the algorithm sometimes incorporates spurious points that, upon further study, are proven to be fictitious inflection points. In order to make a proper comparison to the general expressions we have found analytically and avoid the inclusion of those spurious inflection points, we only considered those points which satisfied $\lambda_2/\eta_1 > 4$. This cut removes around 30% of the potential inflection points. Note that even though we might be removing a portion of real inflection points, the distributions above are still in perfect agreement with the analytic computations.

Appendix G

Inflection point inflation

In the following appendix, we will give a short summary of some important derivations and results concerning inflationary processes along inflection points. To this effect, we shall consider a cubic potential and perform several approximations in order to obtain closed-form results of some important parameters. We will be mainly following [114, 238].

Given the cubic potential

$$V(\phi) = U + \eta\phi + \frac{\rho}{6}\phi^3, \tag{G.1}$$

its slow-roll parameters are given by

$$\epsilon_v \equiv \frac{1}{2}\left(\frac{V'(\phi)}{V(\phi)}\right)^2 \approx \frac{1}{2}\left(\frac{\eta + \frac{\rho}{2}\phi^2}{U}\right)^2 \tag{G.2}$$

$$\eta_v \equiv \frac{V''(\phi)}{V(\phi)} \approx \frac{\rho}{U}\phi \tag{G.3}$$

where we have assumed the denominator to be approximately constant in both cases.

The maximum number of e-folds sustainable in this potential is

$$N_{\max} = \int_{-\infty}^{+\infty} \frac{d\phi}{\sqrt{2\epsilon_v}} \approx \int_{-\infty}^{+\infty} d\phi \frac{U}{\eta + \frac{\rho}{2}\phi^2} = \pi\sqrt{2}\frac{U}{\eta\rho}. \tag{G.4}$$

Slow-roll happens in the region

$$-U/\rho < \phi < U/\rho \tag{G.5}$$

so the number of e-folds that can be attained in that interval is

$$N_{\rm sr} = \int_{-U/\rho}^{U/\rho} \frac{d\phi}{\sqrt{2\epsilon_v}} \approx 2\sqrt{2}\frac{U}{\sqrt{\eta\rho}} \arctan\left(\frac{U}{\sqrt{2\eta\rho}}\right) \approx N_{\max} - 4. \tag{G.6}$$

Let us now consider the number of e-folds between the value of the field when the CMB

scale leaves the horizon, ϕ_*, and $\phi_{\rm end} \equiv -U/\rho$:

$$N_{\rm CMB} = \int_{\phi_{\rm end}}^{\phi_*} \frac{d\phi}{\sqrt{2\epsilon_v}} \approx \frac{N_{\rm max}}{\pi} \cdot \arctan\left(\sqrt{\frac{\rho}{2\eta}}\phi\right)\Bigg|_{\phi_{\rm end}}^{\phi_*} \tag{G.7}$$

In order to ease the notation, let us define

$$x \equiv \pi \frac{N_{\rm CMB}}{N_{\rm max}} \tag{G.8}$$

$$y \equiv \frac{N_{\rm max}}{2\pi} = \frac{U}{\sqrt{2\eta\rho}} \tag{G.9}$$

With these parameters, we can rewrite (G.7) as

$$\pi \frac{N_{\rm CMB}}{N_{\rm max}} = x = \arctan\left(\sqrt{\frac{\rho}{2\eta}}\phi_*\right) - \arctan\left(-\frac{U}{\rho}\sqrt{\frac{\rho}{2\eta}}\right) = \arctan\left(\sqrt{\frac{\rho}{2\eta}}\phi_*\right) - \arctan(-y) \tag{G.10}$$

We can now use the identity

$$\tan\left[\arctan(a) - \arctan(b)\right] = \frac{a-b}{1+ab} \tag{G.11}$$

so (G.10) can be recast as

$$\tan x = \frac{\sqrt{\frac{\rho}{2\eta}}\phi_* + y}{1 - \sqrt{\frac{\rho}{2\eta}}\phi_*\, y} \quad \longrightarrow \quad \sqrt{\frac{\rho}{2\eta}}\phi_* = \frac{\tan(x) - y}{1 + y\, \tan(x)} \tag{G.12}$$

In order to compute the spectral index, we will use

$$n_s - 1 = \left(2\eta_v - 6\epsilon_v\right)\big|_{\phi_*}\,. \tag{G.13}$$

During slow-roll, however, ϵ_v is negligible when compared with η_v so we can simplify the expression to

$$n_s \approx 1 + 2\eta_v(\phi_*) = 1 + \frac{2\rho}{U}\phi_* = 1 + 2\frac{\sqrt{2\eta\rho}}{U}\sqrt{\frac{\rho}{2\eta}}\phi_* = 1 + \frac{2}{y}\left(\frac{\tan(x) - y}{1 + y\, \tan(x)}\right) \tag{G.14}$$

Following a similar reasoning, we can give an estimate of the magnitude of scalar perturbations

$$\Delta^2_{\mathscr{R}} = \frac{1}{24\pi^2}\frac{V(\phi)}{\epsilon_v}\bigg|_{\phi_*} \approx \frac{U^3}{12\pi^2}\left(\eta + \frac{\rho}{2}\phi_*^2\right)^2 = \frac{U^3}{12\pi^2\eta^2}\left(1 + \left[\sqrt{\frac{\rho}{2\eta}}\phi_*\right]^2\right)$$

$$= \frac{U^3}{12\pi^2\eta^2} \frac{(1 + y\ \tan(x))^4}{\left[(1 + y\ \tan(x))^2 + (\tan(x) - y)^2\right]^2} \tag{G.15}$$

This last result can be rewritten in a more convenient form as

$$\Delta^2_{\mathscr{R}} \approx \frac{U^3}{12\pi^2\eta^2} \frac{\cos^4(x)\ (1 + y\ \tan(x))^4}{(1 + y^2)^2} = \frac{N^4_{\rm CMB}\rho^2}{48\pi^2 U} f^2(x, y) \tag{G.16}$$

where

$$f(x, y) = \frac{\cos^2(x)\ (1 + y\ \tan(x))^2}{x^2(1 + y^2)} \tag{G.17}$$

satisfies $f(x, y) \sim 1$ for $y \gg 1$ and $x \sim 1$.

Appendix H

Single three-form multiplets

In this appendix, we will briefly derive the simplest way to construct the supersymmetric Lagrangians used throughout chapter 6 which include 3-forms among their components. More specifically, we will work out the expressions for *single* 3-form multiplets, i.e., chiral superfields whose auxiliary field's real component is substituted by a 3-form (as opposed to *double* 3-form multiplets, where the auxiliary field's real and imaginary parts are replaced by 2 3-form fields). Most of the following formalism may be found in [254, 258, 259], and we will try to stick to the conventions of [265] unless otherwise stated.

H.1 Three-form multiplets in supersymmetry

In the superspace formalism, supersymmetric covariant derivatives are given by

$$D_\alpha = \partial_\alpha + i\sigma^\mu_{\alpha\dot\alpha}\bar\theta^{\dot\alpha}\partial_\mu, \qquad \overline{D}_{\dot\alpha} = -\partial_{\dot\alpha} - i\theta^\alpha\sigma^\mu_{\alpha\dot\alpha}\partial_\mu. \tag{H.1}$$

A *chiral* supefield is defined by the constraint $\overline{D}_{\dot\alpha}\Phi = 0$, and has the following component expansion in terms of the Grassmanian variables θ^α:

$$\Phi = \phi + \sqrt{2}\theta\psi + \theta\theta F + i\theta\sigma^\mu\bar\theta\partial_\mu\phi - \frac{i}{\sqrt{2}}\theta\theta\partial_\mu\psi\sigma^\mu\bar\theta + \frac{1}{4}\theta\theta\bar\theta\bar\theta\Box\phi \tag{H.2}$$

where $\phi(\boldsymbol{x})$ and $F(\boldsymbol{x})$ are complex scalar fields and $\psi(\boldsymbol{x})$ is a Weyl spinor. It is convenient to introduce ways to project out the components of the superfield, to keep track of its terms. The principal terms of the superfield expansion can thus be projected as follows:

$$\Phi| = \phi \tag{H.3}$$

$$\frac{1}{\sqrt{2}}D_\alpha\Phi| = \psi_\alpha \tag{H.4}$$

$$-\frac{1}{4}D^2\Phi\Big| = F, \tag{H.5}$$

where the vertical line means that we are taking the superfield with $\theta = \bar\theta = 0$.

Given some chiral superfields $\boldsymbol{\Phi} = \{\Phi^1, \ldots, \Phi^n\}$, the most general interacting supersym-

metric theory involving those can be written as

$$\mathscr{L} = \int d^2\theta d^2\bar{\theta}\; K(\mathbf{\Phi},\overline{\mathbf{\Phi}}) + \left[\int d^2\theta\; W(\mathbf{\Phi}) + \text{h.c.}\right] \tag{H.6}$$

$$= -K_{a\bar{b}}\partial_\mu\phi^a\partial^\mu\overline{\phi}^{\bar{b}} + K_{a\bar{b}}F^a\overline{F}^{\bar{b}} + F^a W_a + \overline{F}^a\overline{W}_a + \dots \tag{H.7}$$

where $a,b \in \{1,\dots,n\}$, $K(\mathbf{\Phi},\overline{\mathbf{\Phi}})$ is the *Kähler potential*, $W(\mathbf{\Phi})$ is the holomorphic *superpotential* and subscripts denote derivatives with respect to the scalar fields as in $K_{a\bar{b}} = \partial_{\phi^a}\partial_{\phi^b}K$. In (H.7) we have omitted the terms involving the fermionic fields for simplicity; unless otherwise stated, we will not consider them in the following computations.

It can be easily shown that, when the auxiliary fields are set on-shell with their respective equations of motion, the above Lagrangian reads

$$\mathscr{L}|_{\text{bos., on-sh.}} = -K_{a\bar{b}}\partial_\mu\phi^a\partial^\mu\overline{\phi}^{\bar{b}} - K^{a\bar{b}}W_a\overline{W}_{\bar{b}}. \tag{H.8}$$

where $K^{a\bar{b}}$ is the inverse of $K_{a\bar{b}}$.

H.1.1 Including 3-forms into the chiral multiplet

Chiral superfields are the most fundamental ingredients to construct supersymmetric theories, so we will be interested in finding ways to plug three-forms into them. As we will see shortly, the key idea in this respect will be to introduce those three-forms through their Hodge-dual one-form fields [256, 258]. Thus, we only need to find chiral superfields which include vector fields in their component expansion.

The easiest way to do this is through the inclusion of real scalar superfields (which are also used to describe vector multiplets). These are defined by the constraint $V = \overline{V}$ and have the following expansion in θ:

$$\begin{aligned} V(x,\theta,\bar{\theta}) =& C + i\theta\chi - i\bar{\theta}\bar{\chi} + i\theta\theta\bar{\phi} - i\bar{\theta}\bar{\theta}\phi - \theta\sigma^\mu\bar{\theta}\,v_\mu \\ &+ i\theta\theta\bar{\theta}\left[\bar{\lambda} + \frac{i}{2}\bar{\sigma}^\mu\partial_\mu\chi\right] - i\bar{\theta}\bar{\theta}\theta\left[\lambda + \frac{i}{2}\sigma^\mu\partial_\mu\bar{\chi}\right] + \frac{1}{2}\theta\theta\bar{\theta}\bar{\theta}\left[D - \frac{1}{2}\Box C\right]. \end{aligned} \tag{H.9}$$

Here $u(\boldsymbol{x})$ and $D(\boldsymbol{x})$ are real scalar fields, $\phi(\boldsymbol{x})$ is a complex scalar field, $v_\mu(\boldsymbol{x})$ is a real vector field and $\chi(\boldsymbol{x})$ and $\lambda(\boldsymbol{x})$ are Weyl spinors.

A special chiral superfield can easily be built out of this multiplet by defining[1]

$$Y := -\frac{i}{4}\overline{D}^2 V \tag{H.10}$$

(the prefactor is chosen for later convenience). It is easy to check that it fulfils the condition

[1] Note that this definition allows for some freedom in choosing V, since we can always redefine $V \to V + U$, where U satisfies $\overline{D}^2 U = 0$. This redefinitions correspond to the gauge symmetries associated to the vector fields of V. Furthermore, the definition of Y may be generalized to involve holomorphic functions of the scalar field, which allows for more complex models. See [258–260] for further detail.

$\overline{D}_{\dot{\alpha}} Y = 0$ from its definition. Its components can be projected using

$$Y| = -\frac{i}{4}\,\overline{D}^2 V\Big| = \phi \tag{H.11}$$

$$D_\alpha Y| = -\frac{i}{4}\,D_\alpha \overline{D}^2 V\Big| = \lambda_\alpha \tag{H.12}$$

$$-\frac{1}{4}\,D^2 Y\Big| = \frac{i}{16}\,D^2\overline{D}^2 V\Big| = \frac{1}{2}\left(\partial^\mu v_\mu + iD\right) \tag{H.13}$$

Note that, component-wise, Y is almost identical to the original chiral field Φ in that it contains a complex scalar field, a complex Weyl fermion and a complex auxiliary field, albeit in this case we are only interested in the real part of the latter.

For our purposes, it will be convenient to consider v_μ as the one-form associated through Hodge duality to a three-form. Indeed, the Hodge dual of the three-form is given by the following vector field[2]

$$(*A_3)_\mu \equiv A_\mu = \frac{1}{3!}\epsilon_{\mu\nu\rho\sigma}A^{\nu\rho\sigma} \tag{H.14}$$

where the indices have been raised using the flat spacetime metric. The divergence of this vector field is related to the Hodge dual of the 4-form field strength F_4, associated to $A_{\nu\rho\sigma}$ through[3]

$$*F_4 = \frac{1}{4!}\epsilon_{\mu\nu\rho\sigma}F^{\mu\nu\rho\sigma} = \partial_\mu A^\mu \tag{H.15}$$

With these expressions in hand, we find that if v_μ is identified with A_μ, i.e, with the Hodge dual of the 3-form field, the auxiliary field of the special chiral superfield Y reads

$$F_Y = -\frac{1}{4}\,D^2 Y\Big| = \frac{1}{2}\left(*F_4 + iD\right). \tag{H.16}$$

Since D does not enter the membrane part of the full action, we will be able to remove it from the action by solving its algebraic equations early on, leaving $*F_4$ untouched for its interplay with the scalar field and the membrane.

We can easily apply these expressions to a single three-form multiplet Y, with a certain Kähler potential $K(Y,\overline{Y})$ and superpotential $W(Y)$. Plugging the component fields of Y into the bosonic Lagrangian (H.7), we find

$$\begin{aligned}\mathscr{L}|_{\text{bos.}} &= -K_{\phi\bar{\phi}}\partial_\mu\phi\partial^\mu\bar{\phi} + \frac{1}{4}K_{\phi\bar{\phi}}\left(*F_4 + iD\right)\left(*F_4 - iD\right) + \frac{1}{2}\left(*F_4 + iD\right)W_\phi + \frac{1}{2}\left(*F_4 - iD\right)\overline{W}_{\bar{\phi}} \\ &= -K_{\phi\bar{\phi}}\partial_\mu\phi\partial^\mu\bar{\phi} + \frac{1}{4}K_{\phi\bar{\phi}}\left(*F_4\right)^2 + \frac{1}{2}\left(*F_4\right)\left(W_\phi + \overline{W}_{\bar{\phi}}\right) + \frac{1}{4}K_{\phi\bar{\phi}}D^2 + \frac{i}{2}D\left(W_\phi - \overline{W}_{\bar{\phi}}\right)\end{aligned} \tag{H.17}$$

[2] In our conventions, $\epsilon^{0123} = -\epsilon_{0123} = 1$ for Lorentzian coordinates (which we will use throughout this appendix), while $\epsilon^{0123} = \epsilon_{0123} = 1$ for Euclidean ones.

[3] We have omitted the contribution of the metric determinant in these expressions to clarify the definitions. In the case of a curved spacetime, these expressions are $(*A_3)_\mu \equiv A_\mu = \frac{1}{3!}\sqrt{-g}\epsilon_{\mu\nu\rho\sigma}A^{\nu\rho\sigma}$ and $*F_4 = \frac{1}{\sqrt{-g}}\partial_\mu(\sqrt{-g}A^\mu)$.

The equation of motion for the auxiliary field D reads

$$D = -iK^{\phi\bar{\phi}}\left(W_\phi - \overline{W}_{\bar{\phi}}\right) \tag{H.18}$$

which is completely algebraic, as expected. Plugging this into (H.17) yields

$$\mathscr{L}|_{\text{bos.}} = -K_{\phi\bar{\phi}}\partial_\mu\phi\partial^\mu\bar{\phi} + \frac{1}{4}K_{\phi\bar{\phi}}(*F_4)^2 + \frac{1}{2}(*F_4)\left(W_\phi + \overline{W}_{\bar{\phi}}\right) + \frac{1}{4}K^{\phi\bar{\phi}}\left(W_\phi - \overline{W}_{\bar{\phi}}\right)^2 \tag{H.19}$$

$$= -K_{\phi\bar{\phi}}\,\partial_\mu\phi\partial^\mu\bar{\phi} - \frac{1}{4\cdot 4!}K_{\phi\bar{\phi}}\,F^{\mu\nu\sigma\rho}F_{\mu\nu\sigma\rho} + \frac{1}{2\cdot 4!}\left(W_\phi + \overline{W}_{\bar{\phi}}\right)\epsilon^{\mu\nu\sigma\rho}F_{\mu\nu\sigma\rho} + \frac{1}{4}K^{\phi\bar{\phi}}\left(W_\phi - \overline{W}_{\bar{\phi}}\right)^2 \tag{H.20}$$

where, in the second step, we have rewritten the Hodge duals in terms of their original form-fields for clarity.

In order to proceed, recall that the physical field we wish to extremise in the action is not the field strength, but rather the three-form components $A_{\mu\nu\rho}$. In the following, it will be more convenient to work with the Hodge-duals A^μ since they appear directly in the definition of $*F_4$, i.e., eq. (H.15). The variation of (H.20) with respect to A_μ is

$$\begin{aligned}&\frac{1}{2}K_{\phi\bar{\phi}}(*F_4)\left(\partial^\mu\delta A_\mu\right) + \frac{1}{2}\left(\partial^\mu\delta A_\mu\right)\left(W_\phi + \overline{W}_{\bar{\phi}}\right)\\ &\quad = \delta A_\mu\left[\frac{1}{2}\partial^\mu\left(-K_{\phi\bar{\phi}}(*F_4) + W_\phi + \overline{W}_{\bar{\phi}}\right)\right] + \partial^\mu\left[\delta A_\mu\frac{1}{2}\left(K_{\phi\bar{\phi}}(*F_4) - W_\phi - \overline{W}_{\bar{\phi}}\right)\right] = 0\end{aligned} \tag{H.21}$$

We can clearly see that the first term in the r.h.s. will give us a new equation of motion, while the second one will produce a boundary term. As originally discussed in [249], in order to deal with the second term in (H.21) we will need to add a boundary term to our original Lagrangian to cancel this contribution. This not only ensures the consistency of the variational problem but, as we will see shortly, it will have a noticeable effect on the final, on-shell result. More concretely, the required boundary term is given by

$$\begin{aligned}\mathscr{L}_{bd} &= -\frac{1}{2}\partial^\mu\left[A_\mu\left(K_{\phi\bar{\phi}}(*F_4) - W_\phi - \overline{W}_{\bar{\phi}}\right)\right]\\ &= \frac{1}{2\cdot 3!}\partial^\mu\left[A^{\nu\rho\sigma}\left(K_{\phi\bar{\phi}}F_{\mu\nu\rho\sigma} + \epsilon_{\mu\nu\rho\sigma}\left(W_\phi + \overline{W}_{\bar{\phi}}\right)\right)\right]\end{aligned} \tag{H.22}$$

while the equation of motion for the form field is

$$\partial_\mu\left(\frac{1}{2}K_{\phi\bar{\phi}}(*F_4) + \text{Re}W_\phi\right) = 0 \;\rightarrow\; *F_4 = -2K^{\phi\bar{\phi}}\left(\text{Re}W_\phi - n\right) \tag{H.23}$$

where $n \in \mathbb{R}$ is a real constant.

Plugging this result into (H.20) and taking into account the non-vanishing contribution of the boundary term yields

$$\mathscr{L}|_{\text{bos.,on-sh.}} = -K_{\phi\bar{\phi}}\partial_\mu\phi\partial^\mu\bar{\phi} - K^{\phi\bar{\phi}}\left(W_\phi - n\right)\left(\overline{W}_{\bar{\phi}} - n\right). \tag{H.24}$$

From this final Lagrangian we can conclude that the contribution of 3-forms in a supersymmetric setup, results in a linear contribution to our original superpotential. Thus, setting the 3-forms on shell reduces the original theory to amodel of a scalar field described by the original Kähler potential and an effective superpotential given by

$$\hat{W}(\phi) \equiv W(\phi) - n\phi. \tag{H.25}$$

H.2 Three-form multiplets in supergravity

In this section we will follow a similar reasoning as the one above, with gravity included. We will first present the action for scalar multiplets described by generic chiral superfields, which we will later on generalize to include special chiral superfields which have vector or 3-form components among their bosonic ingredients. All of the results we present here have also been derived in [258, 259] using a super-Weyl invariant approach to matter-coupled supergravity, reaching the same conclusions.

We recall that supergravity can be described in terms of the superspace supervielbein $E_M^A(z)$ subject to a set of torsion constraints. After fixing the so-called Wess-Zumino gauge, its field content reduces to

- e_a^μ, the vielbein,
- ψ_α^μ, the gravitino,
- b^μ, a real vector auxiliary field,
- M, a complex scalar auxiliary field.

We construct a conveniently defined action in superspace in terms of $E_M^A(z)$ and generic chiral superfields (defined in curved supergravity superspace). The spacetime action for the component fields is then obtained upon finxing the Wess-Zumino gauge and integrating over the fermionic coordinates of superspace. In the conventions of [265], the spacetime Lagrangian of the bosonic sector of such an action reads

$$\begin{aligned}\frac{1}{\sqrt{-g}}\mathscr{L} = \frac{1}{2}Re^{-\frac{1}{3}K} + \Omega_{a\bar{b}}\partial_\mu\phi^a\partial^\mu\bar{\phi}^{\bar{b}} - \frac{1}{3}e^{-\frac{1}{3}K}\tilde{M}\tilde{\overline{M}} - \tilde{M}\overline{W} - \tilde{\overline{M}}W \\ + e^{-\frac{1}{3}K}K_{a\bar{b}}F^a\bar{F}^{\bar{b}} + F^a(W_a + K_aW) + \bar{F}^{\bar{b}}(\overline{W}_{\bar{b}} + K_{\bar{b}}\overline{W}) \\ -\frac{1}{9}\Omega b_\mu b^\mu - \frac{i}{3}b^\mu(\partial_\mu\phi^a\Omega_a - \partial_\mu\bar{\phi}^{\bar{b}}\Omega_{\bar{b}})\,,\end{aligned} \tag{H.26}$$

where

$$\Omega(\Phi,\bar{\Phi}) = -3e^{-\frac{1}{3}K(\Phi,\bar{\Phi})}, \qquad \tilde{M} = M + K_{\bar{a}}\bar{F}^{\bar{a}}\,, \qquad \tilde{\overline{M}} = \overline{M} + K_aF^a\,. \tag{H.27}$$

This actionis not written in Einstein frame. Therefore, it is customary to rescale the vielbein as follows:

$$e_\mu^a \mapsto e_\mu^a e^{\frac{1}{6}K}\,, \tag{H.28}$$

and to supplement this with a suitable transformation of the spin connection. Furthermore, rescaling the auxiliary fields as

$$F^i \mapsto F^i\, e^{-\frac{1}{6}K}\,, \qquad M \mapsto M\, e^{-\frac{1}{6}K}\,, \tag{H.29}$$

we arrive at the following action in Einstein frame

$$\begin{aligned}\frac{1}{\sqrt{-g}}\mathscr{L} =& \frac{1}{2}R - K_{a\bar{b}}\partial_\mu\phi^a\partial^\mu\bar{\phi}^{\bar{b}} - \frac{1}{3}\tilde{M}\bar{\tilde{M}} - e^{\frac{1}{2}K}\tilde{M}\overline{W} - e^{\frac{1}{2}K}\bar{\tilde{M}}W \\ &+ K_{a\bar{b}}F^a\overline{F}^{\bar{b}} + e^{\frac{1}{2}K}F^a(W_a + K_aW) + e^{\frac{1}{2}K}\overline{F}^{\bar{b}}(\overline{W}_{\bar{b}} + K_{\bar{b}}\overline{W})\,.\end{aligned} \tag{H.30}$$

Notice that in this last expression the auxiliary fields b^μ have been integrated out using their equations of motion. If we are dealing with minimal supergravity and scalar multiplets, $\tilde{M}$ and all F^i are independent, and the auxiliary field equations read

$$\tilde{M} = -3e^{\frac{1}{2}K}W\,, \qquad F^aK_{a\bar{b}} = -e^{\frac{1}{2}K}(\overline{W}_{\bar{b}} + K_{\bar{b}}\overline{W})\,. \tag{H.31}$$

Substituting this into (H.30) we find the well known matter-coupled $\mathcal{N}=1$, $D=4$ supergravity Lagrangian

$$\frac{1}{\sqrt{-g}}\mathscr{L} = \frac{1}{2}\mathscr{R} - K_{a\bar{b}}\partial_\mu\phi^a\partial^\mu\bar{\phi}^{\bar{b}} - V(\phi,\bar{\phi}) \tag{H.32}$$

where the potential is given by

$$V(\phi,\bar{\phi}) = e^K\left(D_aWK^{a\bar{b}}D_{\bar{b}}\overline{W} - 3|W|^2\right), \tag{H.33}$$

and $D_a = \partial_a + K_a$ are the usual Kähler-covariant derivatives.

H.2.1 Supergravity interacting with 3-form multiplets

Just as in the non-gravitational case, we will implicitly introduce three-forms by passing from generic to special chiral superfields. In this case, special chiral superfields describing single three-form multiplets are given by

$$S = -\frac{i}{4}(\overline{D}^2 - 8\mathscr{R})\mathscr{P}\,, \qquad \mathscr{P} = (\mathscr{P})^* \tag{H.34}$$

where $\mathscr{R}$ is the main chiral superfield of minimal supergravity and $\mathscr{P}$ is an unconstrained real superfield defined up to a real linear superfield

$$\mathscr{P} \mapsto \mathscr{P} + L, \qquad (\overline{D}^2 - 8\mathscr{R})L = 0 = (D^2 - 8\overline{\mathscr{R}})L. \tag{H.35}$$

This freedom can be used to fix the Wess-Zumino gauge, where

$$\mathscr{P}| = 0\,, \qquad D_\alpha\mathscr{P}| = 0\,, \qquad \overline{D}_{\dot{\alpha}}\mathscr{P}| = 0\,, \tag{H.36}$$

and the remaining part of the L symmetry, preserving this gauge, coincides with the 2-form gauge symmetry for the 3-form dual to vector component of the prepotential superfield,

$$\sigma^a_{\alpha\dot\alpha}[D^\alpha,\overline{D}^{\dot\alpha}]\mathscr{P}| = 4A^a\,, \qquad A^a = *(A_3)^a\,. \tag{H.37}$$

Using the gauge above, we find that the highest component of the special chiral superfield of S is given by (in the notation of [265])

$$\mathscr{F} \equiv F_S = -\frac{1}{4}D^2S| = \frac{i}{16}D^2\overline{D}^2\mathscr{P}| - \frac{i}{2}\mathscr{R}D^2\mathscr{P}| = \frac{1}{2}\left(D_\mu A^\mu + i\mathrm{d}\right) + \frac{1}{3}(s\overline{M} + 2\bar{s}M)\,. \tag{H.38}$$

where $s = S|$, M and $\overline{M}$ are the scalar auxiliary fields of minimal supergravity, d is a real auxiliary scalar field, $*F_4 = D_\mu A^\mu = \frac{1}{e}\partial_\mu(eA^\mu)$ and $e = \det e^a_\mu$.

Fixing the WZ gauge and integrating over the fermionic coordinates of superspace, in complete analogy with the case of generic scalar matter multiplets, we find from our original Lagrangian for bosonic fields of scalar multiplets interacting with supergravity (H.30):

$$\begin{aligned}\frac{1}{\sqrt{-g}}\mathscr{L} &= \frac{1}{2}Re^{-\frac{1}{3}K} + \Omega_{s\bar{s}}\partial_\mu s\partial^\mu\bar{s} - \frac{1}{3}e^{-\frac{1}{3}K}(M + K_{\bar{s}}\overline{\mathscr{F}})\,(\overline{M} + K_s\mathscr{F}) - M\overline{W} - \overline{M}W\\ &+e^{-\frac{1}{3}K}K_{s\bar{s}}\mathscr{F}\overline{\mathscr{F}} + \mathscr{F}W_s + \overline{\mathscr{F}}\overline{W}_{\bar{s}} - \frac{1}{9}\Omega b_\mu b^\mu - \frac{i}{3}b^\mu(\partial_\mu s\Omega_s - \partial_\mu\bar{s}\Omega_{\bar{s}}) + \frac{1}{\sqrt{-g}}\mathscr{L}_{bd}\,.\end{aligned} \tag{H.39}$$

Here we have explicitly written the corresponding boundary term needed to have a well-posed variational problem. Before substituting the expression for the F-components of the special chiral superfields, (H.38), we have to perform a Weyl rescaling of the fields with (H.28), which we need to consider carefully.

Super-Weyl transformations

In the previous section, when considering non-gravitational chiral superfields, we have assumed that Φ and its components ϕ and F are inert under Weyl transformations. This is a consistent assumption in the case of a generic chiral superfield.[4] However, since the chiral superfield S has been written in terms of a real superfield $\mathscr{P}$, it is important to check how rescalings of the supervielbein, i.e., *super-Weyl transformations*, act on them. These are defined via [265, 279]

$$E^a \;\mapsto\; \tilde{E}^a = e^{\Upsilon+\overline{\Upsilon}}E^a\,, \tag{H.40}$$

$$E^\alpha \;\mapsto\; \tilde{E}^\alpha = e^{2\overline{\Upsilon}-\Upsilon}\left(E^\alpha - \frac{i}{4}E^a\overline{\mathscr{D}}_{\dot\alpha}\overline{\Upsilon}\tilde{\sigma}_a^{\dot\alpha\alpha}\right), \tag{H.41}$$

$$\overline{E}^{\dot\alpha} \;\mapsto\; \tilde{\overline{E}}^{\dot\alpha} = e^{2\Upsilon-\overline{\Upsilon}}\left(\overline{E}^{\dot\alpha} + \frac{i}{4}E^a\tilde{\sigma}_a^{\dot\alpha\alpha}\mathscr{D}_\alpha\Upsilon\right), \tag{H.42}$$

[4] This can be checked by writing the chiral field in terms of an unconstrained complex superfield (with a similar definition as (H.34)). Choosing the Weyl weights of the transformation accordingly, it can be shown that a general chiral superfield Φ is invariant under these rescalings.

where Υ is a chiral superfield:

$$\overline{D}_{\dot{\alpha}}\Upsilon = 0\,, \qquad D_\alpha \overline{\Upsilon} = 0. \tag{H.43}$$

Those rescalings have to be supplemented with a shift of spin connection, the explicit form of which is not needed for our purposes (but see [265, 279] for more detail). On the other hand, it can be shown that supergravity chiral projector transforms in an inhomogeneous way as

$$(\overline{D}\overline{D} - 8\mathscr{R}) \mapsto e^{-4\Upsilon}(\overline{D}\overline{D} - \mathscr{R})e^{2\overline{\Upsilon}}, \qquad (DD - 8\overline{\mathscr{R}}) \mapsto e^{-4\overline{\Upsilon}}(DD - 8\overline{\mathscr{R}})e^{2\Upsilon}. \tag{H.44}$$

Note that since the definition of S involves this operator, it is guaranteed to transform non-trivially under super-Weyl transformations.

Indeed, in the light of (H.44), the only way to obtain a covariant super-Weyl transformation of the special chiral superfields (H.34) is to attribute to its real prepotential the transformation rule

$$\mathscr{P} \mapsto \mathscr{P}\, e^{-2\Upsilon - 2\overline{\Upsilon}}, \tag{H.45}$$

which results in

$$S \mapsto S e^{-6\Upsilon}. \tag{H.46}$$

We see that in this case the bosonic component of S will transform as[5]

$$s \mapsto s e^{-6\Upsilon|}\,. \tag{H.47}$$

We will be interested in purely bosonic transformations with

$$\Upsilon| = \frac{1}{12}K = \overline{\Upsilon}|\,, \qquad D_\alpha \Upsilon| = 0\,, \qquad D^2\Upsilon| = 0\,, \tag{H.48}$$

since, in that case,

$$e^a_\mu \;\mapsto\; e^a_\mu e^{\frac{1}{6}K} \tag{H.49}$$

as needed to write the Lagrangian in Einstein frame, just as in the case of supergravity interacting with chiral multiplets. However, $\mathscr{F}$ and M will also be affected by this transformation. We can easily derive the rescalings by studying

$$(D^2 - 8\overline{\mathscr{R}})S| = -4\mathscr{F} - 8\mathscr{R}S| = -4\mathscr{F} + \frac{4}{3}s\overline{M}. \tag{H.50}$$

Considering all of the above transformation laws, we can easily check that for the purely bosonic super-Weyl transformation, we find

$$s \;\mapsto\; e^{-\frac{1}{2}K} s \tag{H.51}$$

[5] We do not write the transformation of $P|$ because we use the Wess-Zumino like gauge with $P| = 0$.

$$\mathscr{F} \mapsto e^{-\frac{2}{3}K}\mathscr{F} \tag{H.52}$$

$$M \mapsto e^{-\frac{1}{6}K}M\,. \tag{H.53}$$

As far as the scalar field is concerned, it is convenient to combine the Weyl rescaling with the field redefinition

$$\phi \equiv e^{-\frac{1}{2}K}s \tag{H.54}$$

so that the kinetic term of ϕ field remains simple.

Taking all of the above into account and integrating out the auxiliary field b^μ using its algebraic equations of motion, we find that

$$\begin{aligned}\frac{1}{\sqrt{-g}}\mathscr{L} =& \frac{1}{2}R - K_{\phi\bar{\phi}}\partial_\mu\phi\partial^\mu\bar{\phi}^J - \frac{1}{3}(M + e^{-\frac{1}{2}K}K_{\bar{\phi}}\overline{\mathscr{F}})\,(\overline{M} + e^{-\frac{1}{2}K}K_\phi\mathscr{F})\\ &- e^{\frac{1}{2}K}M\overline{W} - e^{\frac{1}{2}K}\overline{M}W + e^{-K}K_{\phi\bar{\phi}}\mathscr{F}\overline{\mathscr{F}} + \mathscr{F}W_\phi + \overline{\mathscr{F}}\,\overline{W}_{\bar{\phi}} + \frac{1}{\sqrt{-g}}\mathscr{L}_{bd}.\end{aligned} \tag{H.55}$$

It is convenient to further redefine the supergravity auxiliary field M as

$$\check{M} \equiv Me^{\frac{1}{2}K} \tag{H.56}$$

which, taking into account the redefinition of the scalar field (H.54), allows us to write the auxiliary field of S as

$$\mathscr{F} = \frac{1}{2}\left(D_\mu A^\mu + i\mathrm{d}\right) + \frac{2}{3}\bar{\phi}\check{M} + \frac{1}{3}\phi\check{\overline{M}}. \tag{H.57}$$

In the end, the rescaled Lagrangian reads

$$\begin{aligned}\frac{1}{\sqrt{-g}}\mathscr{L} =& \frac{1}{2}R - K_{\phi\bar{\phi}}\partial_\mu\phi\partial^\mu\bar{\phi} - \frac{1}{3}e^{-K}(\check{M} + K_{\bar{\phi}}\overline{\mathscr{F}})\,(\check{\overline{M}} + K_\phi\mathscr{F}) - \check{M}\overline{W} - \check{\overline{M}}W\\ &+ e^{-K}K_{\phi\bar{\phi}}\mathscr{F}\overline{\mathscr{F}} + \mathscr{F}W_\phi + \overline{\mathscr{F}}\,\overline{W}_{\bar{\phi}} + \frac{1}{\sqrt{-g}}\mathscr{L}_{bd}.\end{aligned} \tag{H.58}$$

The boundary term can be obtained in the same fashion as in the previous section. Noting that the 3-form enters the action only through $D_\mu A^\mu$, varying the action for that field gives the following

$$\begin{aligned}\delta S =& \int d^4x\, e\, \frac{\partial\mathscr{L}}{\partial(D_\mu A^\mu)}\left(\frac{1}{e}\partial_\mu(e\,\delta A^\mu)\right)\\ =& -\int d^4x\, e\,\delta A^\mu\,\partial_\mu\left(\frac{\partial\mathscr{L}}{\partial(D_\mu A^\mu)}\right) + \int d^4x\,\partial_\mu\left(e\,\delta A^\mu\frac{\partial\mathscr{L}}{\partial(D_\mu A^\mu)}\right).\end{aligned} \tag{H.59}$$

Therefore, we conclude that the boundary term, which makes the variational problem well posed, reads

$$\mathscr{L}_{bd} = -\int d^4x\,\partial_\mu\left(e\,A^\mu\frac{\partial\mathscr{L}}{\partial(D_\mu A^\mu)}\right). \tag{H.60}$$

The equations of motion to solve are then

$$\frac{\partial \mathscr{L}}{\partial d} = 0, \qquad \frac{\partial \mathscr{L}}{\partial \check{M}} = 0, \qquad \frac{\partial \mathscr{L}}{\partial (D_\mu A^\mu)} = n, \tag{H.61}$$

where $n \in \mathbb{R}$. These algebraic equations are solved by

$$d = -iK^{\phi\bar{\phi}} e^K \left[D_\phi (W - n\phi) - \text{c.c.} \right] \tag{H.62}$$

$$\check{M} = e^K \left[D_\phi (W - n\phi) K^{\phi\bar{\phi}} K_{\bar{\phi}} - 3(W - n\phi) \right] \tag{H.63}$$

$$D_\mu A^\mu = e^K \left[3(W - n\phi)\bar{\phi} - (1 + \bar{\phi} K_{\bar{\phi}}) K^{\phi\bar{\phi}} D_\phi (W - n\phi) + \text{c.c.} \right] \tag{H.64}$$

where $D_\phi = \partial_\phi + K_\phi$ is the usual Kähler-covariant derivative. Plugging all these equations into (H.58) and taking into account the contribution of the boundary term yields

$$\frac{1}{\sqrt{-g}} \mathscr{L} = \frac{1}{2} R - K_{\phi\bar{\phi}} \partial_\mu \phi \partial^\mu \bar{\phi} - e^K \left(D_\phi \hat{W} K^{\phi\bar{\phi}} D_{\bar{\phi}} \hat{\bar{W}} - 3 \left| \hat{W} \right| \right) \tag{H.65}$$

where, exactly as in the non-gravitational case,

$$\hat{W} \equiv W - n\phi. \tag{H.66}$$

Therefore, after all the auxiliary fields' equations of motion have been applied, the contribution of the 3-form fields reduce to a simple linear term on the superpotential. The effective action for the scalar fields and gravity coincides with the usual $\mathcal{N} = 1$, $D = 4$ matter-coupled supergravity, albeit with a potential constructed from the new effective superpotential (H.66).

Bibliography

[1] J. Polchinski, *String theory. Vol. 1: An introduction to the bosonic string*, Cambridge Monographs on Mathematical Physics, Cambridge University Press (12, 2007), 10.1017/CBO9780511816079.

[2] J. Polchinski, *String theory. Vol. 2: Superstring theory and beyond*, Cambridge Monographs on Mathematical Physics, Cambridge University Press (12, 2007), 10.1017/CBO9780511618123.

[3] K. Becker, M. Becker and J.H. Schwarz, *String theory and M-theory: A modern introduction*, Cambridge university press (2006).

[4] R. Blumenhagen, D. Lüst and S. Theisen, *Basic concepts of string theory*, Theoretical and Mathematical Physics, Springer, Heidelberg, Germany (2013), 10.1007/978-3-642-29497-6.

[5] P. Di Vecchia and A. Schwimmer, *The Beginning of string theory: A Historical sketch*, *Lect. Notes Phys.* **737** (2008) 119 [0708.3940].

[6] P. Goddard, J. Goldstone, C. Rebbi and C.B. Thorn, *Quantum dynamics of a massless relativistic string*, *Nucl. Phys. B* **56** (1973) 109.

[7] E. Witten, *String theory dynamics in various dimensions*, *Nucl. Phys. B* **443** (1995) 85 [hep-th/9503124].

[8] M.J. Duff, *M theory (The Theory formerly known as strings)*, *Int. J. Mod. Phys. A* **11** (1996) 5623 [hep-th/9608117].

[9] A. Strominger, *Superstrings with Torsion*, *Nucl. Phys. B* **274** (1986) 253.

[10] B. de Wit, D.J. Smit and N.D. Hari Dass, *Residual Supersymmetry of Compactified D=10 Supergravity*, *Nucl. Phys. B* **283** (1987) 165.

[11] S.B. Giddings, S. Kachru and J. Polchinski, *Hierarchies from fluxes in string compactifications*, *Phys.Rev.* **D66** (2002) 106006 [hep-th/0105097].

[12] M. Grana, *Flux compactifications in string theory: A Comprehensive review*, *Phys. Rept.* **423** (2006) 91 [hep-th/0509003].

[13] M.R. Douglas and S. Kachru, *Flux compactification*, *Rev.Mod.Phys.* **79** (2007) 733 [hep-th/0610102].

[14] F. Denef, *Les Houches Lectures on Constructing String Vacua*, *Les Houches* **87** (2008) 483 [0803.1194].

[15] J. Polchinski, *Dirichlet Branes and Ramond-Ramond charges*, *Phys. Rev. Lett.* **75** (1995) 4724 [hep-th/9510017].

[16] E. Witten, *Bound states of strings and p-branes*, *Nucl. Phys. B* **460** (1996) 335 [hep-th/9510135].

[17] P. Candelas, G.T. Horowitz, A. Strominger and E. Witten, *Vacuum Configurations for Superstrings*, *Nucl. Phys. B* **258** (1985) 46.

[18] K. Becker, M. Becker and J.H. Schwarz, *String theory and M-theory: A modern introduction*, Cambridge University Press (12, 2006).

[19] S.-T. Yau, *On the ricci curvature of a compact kähler manifold and the complex monge-ampére equation, i*, *Communications on pure and applied mathematics* **31** (1978) 339.

[20] T. Hubsch, *Calabi-Yau manifolds: A Bestiary for physicists*, World Scientific (1992).

[21] P. Candelas and X. de la Ossa, *Moduli space of Calabi-Yau manifolds*, *Nucl.Phys.* **B355** (1991) 455.

[22] T.W. Grimm and J. Louis, *The Effective action of N = 1 Calabi-Yau orientifolds*, *Nucl.Phys.* **B699** (2004) 387 [hep-th/0403067].

[23] R. Blumenhagen, B. Kors, D. Lust and S. Stieberger, *Four-dimensional String Compactifications with D-Branes, Orientifolds and Fluxes*, *Phys. Rept.* **445** (2007) 1 [hep-th/0610327].

[24] P. Svrcek and E. Witten, *Axions In String Theory*, *JHEP* **06** (2006) 051 [hep-th/0605206].

[25] A. Arvanitaki, S. Dimopoulos, S. Dubovsky, N. Kaloper and J. March-Russell, *String Axiverse*, *Phys. Rev. D* **81** (2010) 123530 [0905.4720].

[26] M. Kreuzer and H. Skarke, *Complete classification of reflexive polyhedra in four-dimensions*, *Adv. Theor. Math. Phys.* **4** (2002) 1209 [hep-th/0002240].

[27] Y.-H. He, *The Calabi-Yau Landscape: from Geometry, to Physics, to Machine-Learning*, 1812.02893.

[28] B.S. Acharya, G. Kane and P. Kumar, *Compactified String Theories – Generic Predictions for Particle Physics*, *Int. J. Mod. Phys. A* **27** (2012) 1230012 [1204.2795].

[29] S. Gukov, C. Vafa and E. Witten, *CFT's from Calabi-Yau four folds*, *Nucl.Phys.* **B584** (2000) 69 [hep-th/9906070].

[30] A. Klemm, *Topological string theory on Calabi-Yau threefolds*, *PoS* **RTN2005** (2005) 002.

[31] J.P. Conlon, F. Quevedo and K. Suruliz, *Large-volume flux compactifications: Moduli spectrum and D3/D7 soft supersymmetry breaking*, *JHEP* **0508** (2005) 007 [hep-th/0505076].

[32] K. Becker, M. Becker, M. Haack and J. Louis, *Supersymmetry breaking and alpha-prime corrections to flux induced potentials*, *JHEP* **0206** (2002) 060 [hep-th/0204254].

[33] L. Anguelova, C. Quigley and S. Sethi, *The Leading Quantum Corrections to Stringy Kahler Potentials*, *JHEP* **10** (2010) 065 [1007.4793].

[34] V. Balasubramanian, P. Berglund, J.P. Conlon and F. Quevedo, *Systematics of moduli stabilisation in Calabi-Yau flux compactifications*, *JHEP* **0503** (2005) 007 [hep-th/0502058].

[35] S. Kachru, R. Kallosh, A.D. Linde and S.P. Trivedi, *De Sitter vacua in string theory*, *Phys.Rev.* **D68** (2003) 046005 [hep-th/0301240].

[36] V. Balasubramanian and P. Berglund, *Stringy corrections to Kahler potentials, SUSY breaking, and the cosmological constant problem*, *JHEP* **0411** (2004) 085 [hep-th/0408054].

[37] S. Sethi, *Supersymmetry Breaking by Fluxes*, *JHEP* **10** (2018) 022 [1709.03554].

[38] S. Kachru and S.P. Trivedi, *A comment on effective field theories of flux vacua*, *Fortsch. Phys.* **67** (2019) 1800086 [1808.08971].

[39] C. Vafa, *Evidence for F theory*, *Nucl. Phys. B* **469** (1996) 403 [hep-th/9602022].

[40] D. Baumann and L. McAllister, *Inflation and String Theory*, 1404.2601.

[41] A. Hebecker, *Lectures on Naturalness, String Landscape and Multiverse*, 2008.10625.

[42] G. Veneziano and S. Yankielowicz, *An Effective Lagrangian for the Pure N=1 Supersymmetric Yang-Mills Theory*, *Phys. Lett. B* **113** (1982) 231.

[43] C. Burgess, R. Kallosh and F. Quevedo, *De Sitter string vacua from supersymmetric D terms*, *JHEP* **0310** (2003) 056 [hep-th/0309187].

[44] L. Susskind, *The Anthropic landscape of string theory*, hep-th/0302219.

[45] F. Denef, M.R. Douglas and B. Florea, *Building a better racetrack*, *JHEP* **0406** (2004) 034 [hep-th/0404257].

[46] F. Denef and M.R. Douglas, *Distributions of flux vacua*, *JHEP* **0405** (2004) 072 [hep-th/0404116].

[47] W. Taylor and Y.-N. Wang, *The F-theory geometry with most flux vacua*, *JHEP* **12** (2015) 164 [1511.03209].

[48] M.R. Douglas, *The Statistics of string / M theory vacua*, *JHEP* **05** (2003) 046 [hep-th/0303194].

[49] C. Vafa, *The String landscape and the swampland*, hep-th/0509212.

[50] T.D. Brennan, F. Carta and C. Vafa, *The String Landscape, the Swampland, and the Missing Corner*, *PoS* **TASI2017** (2017) 015 [1711.00864].

[51] E. Palti, *The Swampland: Introduction and Review*, *Fortsch. Phys.* **67** (2019) 1900037 [1903.06239].

[52] N. Arkani-Hamed, L. Motl, A. Nicolis and C. Vafa, *The String landscape, black holes and gravity as the weakest force*, *JHEP* **06** (2007) 060 [hep-th/0601001].

[53] T. Banks and L.J. Dixon, *Constraints on String Vacua with Space-Time Supersymmetry*, *Nucl. Phys. B* **307** (1988) 93.

[54] G. Obied, H. Ooguri, L. Spodyneiko and C. Vafa, *De Sitter Space and the Swampland*, 1806.08362.

[55] U.H. Danielsson and T. Van Riet, *What if string theory has no de Sitter vacua?*, *Int. J. Mod. Phys. D* **27** (2018) 1830007 [1804.01120].

[56] A. Achúcarro and G.A. Palma, *The string swampland constraints require multi-field inflation*, *JCAP* **02** (2019) 041 [1807.04390].

[57] K. Dasgupta, M. Emelin, E. McDonough and R. Tatar, *Quantum Corrections and the de Sitter Swampland Conjecture*, *JHEP* **01** (2019) 145 [1808.07498].

[58] Y. Akrami, R. Kallosh, A. Linde and V. Vardanyan, *The Landscape, the Swampland and the Era of Precision Cosmology*, *Fortsch. Phys.* **67** (2019) 1800075 [1808.09440].

[59] M. Cicoli, S. De Alwis, A. Maharana, F. Muia and F. Quevedo, *De Sitter vs Quintessence in String Theory*, *Fortsch. Phys.* **67** (2019) 1800079 [1808.08967].

[60] R. Kallosh and T. Wrase, *dS Supergravity from 10d*, *Fortsch. Phys.* **67** (2019) 1800071 [1808.09427].

[61] R. Kallosh, A. Linde, E. McDonough and M. Scalisi, *4D models of de Sitter uplift*, *Phys. Rev. D* **99** (2019) 046006 [1809.09018].

[62] J. Moritz, A. Retolaza and A. Westphal, *Toward de Sitter space from ten dimensions*, *Phys. Rev. D* **97** (2018) 046010 [1707.08678].

[63] J. Moritz and T. Van Riet, *Racing through the swampland: de Sitter uplift vs weak gravity*, *JHEP* **09** (2018) 099 [1805.00944].

[64] J. Moritz, A. Retolaza and A. Westphal, *On uplifts by warped anti-D3-branes*, *Fortsch. Phys.* **67** (2019) 1800098 [1809.06618].

[65] L. Heisenberg, M. Bartelmann, R. Brandenberger and A. Refregier, *Dark Energy in the Swampland*, *Phys. Rev. D* **98** (2018) 123502 [1808.02877].

[66] H. Ooguri, E. Palti, G. Shiu and C. Vafa, *Distance and de Sitter Conjectures on the Swampland*, *Phys. Lett. B* **788** (2019) 180 [1810.05506].

[67] S.R. Coleman, *The Fate of the False Vacuum. 1. Semiclassical Theory*, *Phys. Rev.* **D15** (1977) 2929.

[68] C.G. Callan, Jr. and S.R. Coleman, *The Fate of the False Vacuum. 2. First Quantum Corrections*, *Phys. Rev.* **D16** (1977) 1762.

[69] S.R. Coleman and F. De Luccia, *Gravitational Effects on and of Vacuum Decay*, *Phys. Rev.* **D21** (1980) 3305.

[70] S.R. Coleman, V. Glaser and A. Martin, *Action Minima Among Solutions to a Class of Euclidean Scalar Field Equations*, *Commun. Math. Phys.* **58** (1978) 211.

[71] S. Coleman, *Aspects of Symmetry: Selected Erice Lectures*, Cambridge University Press, Cambridge, U.K. (1985), 10.1017/CBO9780511565045.

[72] E.J. Weinberg, *Classical solutions in quantum field theory: Solitons and Instantons in High Energy Physics*, Cambridge Monographs on Mathematical Physics, Cambridge University Press (9, 2012), 10.1017/CBO9781139017787.

[73] T. Banks, C.M. Bender and T.T. Wu, *Coupled anharmonic oscillators. 1. Equal mass case*, *Phys. Rev. D* **8** (1973) 3346.

[74] L.D. Landau and E.M. Lifshitz, *Mechanics: Volume 1*, vol. 1, Butterworth-Heinemann (1976).

[75] K. Blum, M. Honda, R. Sato, M. Takimoto and K. Tobioka, *O(N) Invariance of the Multi-Field Bounce*, *JHEP* **05** (2017) 109 [1611.04570].

[76] A. Masoumi, K.D. Olum and B. Shlaer, *Efficient numerical solution to vacuum decay with many fields*, *JCAP* **1701** (2017) 051 [1610.06594].

[77] C.L. Wainwright, *CosmoTransitions: Computing Cosmological Phase Transition Temperatures and Bubble Profiles with Multiple Fields*, *Comput. Phys. Commun.* **183** (2012) 2006 [1109.4189].

[78] R. Sato, *SimpleBounce : a simple package for the false vacuum decay*, *Comput. Phys. Commun.* **258** (2021) 107566 [1908.10868].

[79] A. Masoumi, K.D. Olum and J.M. Wachter, *Approximating tunneling rates in multi-dimensional field spaces*, *JCAP* **1710** (2017) 022 [1702.00356].

[80] U. Sarid, *Tools for tunneling*, *Phys. Rev.* **D58** (1998) 085017 [hep-ph/9804308].

[81] K.-M. Lee and E.J. Weinberg, *Decay of the True Vacuum in Curved Space-time*, *Phys. Rev. D* **36** (1987) 1088.

[82] J. Garriga and A. Vilenkin, *Recycling universe*, *Phys. Rev. D* **57** (1998) 2230 [astro-ph/9707292].

[83] A.H. Guth, *The Inflationary Universe: A Possible Solution to the Horizon and Flatness Problems*, *Phys.Rev.* **D23** (1981) 347.

[84] A.H. Guth and E.J. Weinberg, *Could the Universe Have Recovered from a Slow First Order Phase Transition?*, *Nucl. Phys. B* **212** (1983) 321.

[85] D. Baumann, *TASI Lectures on Inflation*, 0907.5424.

[86] V. Mukhanov, *Physical foundations of cosmology*, Cambridge Univ. Pr., Cambridge, UK (2005).

[87] B. Freivogel, M. Kleban, M. Rodriguez Martinez and L. Susskind, *Observational consequences of a landscape*, *JHEP* **03** (2006) 039 [hep-th/0505232].

[88] A.D. Linde, *Inflation, quantum cosmology and the anthropic principle*, hep-th/0211048.

[89] A.D. Linde, *Inflationary Cosmology*, *Lect. Notes Phys.* **738** (2008) 1 [0705.0164].

[90] M. Yamaguchi, *Supergravity based inflation models: a review*, *Class.Quant.Grav.* **28** (2011) 103001 [1101.2488].

[91] R. Bousso, D. Harlow and L. Senatore, *Inflation after False Vacuum Decay: observational Prospects after Planck*, *Phys. Rev. D* **91** (2015) 083527 [1309.4060].

[92] R. Bousso, D. Harlow and L. Senatore, *Inflation After False Vacuum Decay: New Evidence from BICEP2*, 1404.2278.

[93] S. Cespedes, S.P. de Alwis, F. Muia and F. Quevedo, *Lorentzian Vacuum Transitions: Open or Closed Universes?*, 2011.13936.

[94] J.J. Blanco-Pillado, K. Sousa, M.A. Urkiola and J.M. Wachter, *Towards a complete mass spectrum of type-IIB flux vacua at large complex structure*, *JHEP* **04** (2021) 149 [2007.10381].

[95] A. Westphal, *de Sitter string vacua from Kahler uplifting*, *JHEP* **03** (2007) 102 [hep-th/0611332].

[96] A. Giryavets, S. Kachru, P.K. Tripathy and S.P. Trivedi, *Flux compactifications on Calabi-Yau threefolds*, *JHEP* **0404** (2004) 003 [hep-th/0312104].

[97] A. Giryavets, S. Kachru and P.K. Tripathy, *On the taxonomy of flux vacua*, *JHEP* **08** (2004) 002 [hep-th/0404243].

[98] O. DeWolfe, A. Giryavets, S. Kachru and W. Taylor, *Enumerating flux vacua with enhanced symmetries*, *JHEP* **0502** (2005) 037 [hep-th/0411061].

[99] J. Louis, M. Rummel, R. Valandro and A. Westphal, *Building an explicit de Sitter*, *JHEP* **1210** (2012) 163 [1208.3208].

[100] J.J. Blanco-Pillado, M. Gomez-Reino and K. Metallinos, *Accidental Inflation in the Landscape*, *JCAP* **1302** (2013) 034 [1209.0796].

[101] M. Cicoli, D. Klevers, S. Krippendorf, C. Mayrhofer, F. Quevedo et al., *Explicit de Sitter Flux Vacua for Global String Models with Chiral Matter*, *JHEP* **1405** (2014) 001 [1312.0014].

[102] M. Tegmark, *What does inflation really predict?*, *JCAP* **0504** (2005) 001 [astro-ph/0410281].

[103] R. Easther and L. McAllister, *Random matrices and the spectrum of N-flation*, *JCAP* **0605** (2006) 018 [hep-th/0512102].

[104] D. Battefeld, T. Battefeld and S. Schulz, *On the Unlikeliness of Multi-Field Inflation: Bounded Random Potentials and our Vacuum*, *JCAP* **1206** (2012) 034 [1203.3941].

[105] M.C.D. Marsh, L. McAllister, E. Pajer and T. Wrase, *Charting an Inflationary Landscape with Random Matrix Theory*, *JCAP* **1311** (2013) 040 [1307.3559].

[106] A. Masoumi, A. Vilenkin and M. Yamada, *Inflation in random Gaussian landscapes*, *JCAP* **1705** (2017) 053 [1612.03960].

[107] G. Wang and T. Battefeld, *Random Functions via Dyson Brownian Motion: Progress and Problems*, *JCAP* **1609** (2016) 008 [1607.02514].

[108] F.G. Pedro and A. Westphal, *Inflation with a graceful exit in a random landscape*, *JHEP* **03** (2017) 163 [1611.07059].

[109] B. Freivogel, R. Gobbetti, E. Pajer and I.-S. Yang, *Inflation on a Slippery Slope*, 1608.00041.

[110] T. Bjorkmo and M.C.D. Marsh, *Manyfield Inflation in Random Potentials*, *JCAP* **1802** (2018) 037 [1709.10076].

[111] M. Dias, J. Frazer and M.c.D. Marsh, *Seven Lessons from Manyfield Inflation in Random Potentials*, *JCAP* **1801** (2018) 036 [1706.03774].

[112] A. Masoumi, A. Vilenkin and M. Yamada, *Initial conditions for slow-roll inflation in a random Gaussian landscape*, *JCAP* **1707** (2017) 003 [1704.06994].

[113] A. Masoumi, A. Vilenkin and M. Yamada, *Inflation in multi-field random Gaussian landscapes*, *JCAP* **1712** (2017) 035 [1707.03520].

[114] J.J. Blanco-Pillado, A. Vilenkin and M. Yamada, *Inflation in Random Landscapes with two energy scales*, *JHEP* **02** (2018) 130 [1711.00491].

[115] S. Paban and R. Rosati, *Inflation in Multi-field Modified DBM Potentials*, *JCAP* **1809** (2018) 042 [1807.07654].

[116] T. Bjorkmo and M.C.D. Marsh, *Local, algebraic simplifications of Gaussian random fields*, 1805.03117.

[117] J.J. Blanco-Pillado, K. Sousa and M.A. Urkiola, *Slepian models for Gaussian Random Landscapes*, *JHEP* **05** (2020) 142 [1911.07618].

[118] L.F. Low, S. Hotchkiss and R. Easther, *The Distribution of Vacua in Random Landscape Potentials*, 2004.04429.

[119] P. Candelas, X.C. De La Ossa, P.S. Green and L. Parkes, *A Pair of Calabi-Yau manifolds as an exactly soluble superconformal theory*, *Nucl.Phys.* **B359** (1991) 21.

[120] S. Hosono, A. Klemm, S. Theisen and S.-T. Yau, *Mirror symmetry, mirror map and applications to complete intersection Calabi-Yau spaces*, *Nucl. Phys.* **B433** (1995) 501 [hep-th/9406055].

[121] D. Gallego, *On the Effective Description of Large Volume Compactifications*, *JHEP* **1106** (2011) 087 [1103.5469].

[122] A. Achucarro, S. Hardeman and K. Sousa, *F-term uplifting and the supersymmetric integration of heavy moduli*, *JHEP* **0811** (2008) 003 [0809.1441].

[123] K. Sousa and P. Ortiz, *Perturbative Stability along the Supersymmetric Directions of the Landscape*, *JCAP* **1502** (2015) 017 [1408.6521].

[124] A. Klemm and S. Theisen, *Considerations of one modulus Calabi-Yau compactifications: Picard-Fuchs equations, Kahler potentials and mirror maps*, *Nucl. Phys.* **B389** (1993) 153 [hep-th/9205041].

[125] C. Doran, B. Greene and S. Judes, *Families of quintic Calabi-Yau 3-folds with discrete symmetries*, *Commun.Math.Phys.* **280** (2008) 675 [hep-th/0701206].

[126] P. Candelas and C. Mishra, *Highly Symmetric Quintic Quotients*, *Fortsch. Phys.* **66** (2018) 1800017 [1709.01081].

[127] V. Braun, *The 24-Cell and Calabi-Yau Threefolds with Hodge Numbers (1,1)*, *JHEP* **05** (2012) 101 [1102.4880].

[128] V. Batyrev and M. Kreuzer, *Constructing new Calabi-Yau 3-folds and their mirrors via conifold transitions*, *Adv. Theor. Math. Phys.* **14** (2010) 879 [0802.3376].

[129] C.F. Doran and J.W. Morgan, *Mirror symmetry and integral variations of Hodge structure underlying one parameter families of Calabi-Yau threefolds*, in *Calabi-Yau varieties and mirror symmetry. Proceedings, Workshop, Mirror Symmetry 5, Banff, Canada, December 6-11, 2003*, pp. 517–537, 2005 [math/0505272].

[130] V. Braun, P. Candelas and X. de la Ossa, *Two One-Parameter Special Geometries*, 1512.08367.

[131] P. Candelas, X. de la Ossa, M. Elmi and D. Van Straten, *A One Parameter Family of Calabi-Yau Manifolds with Attractor Points of Rank Two*, 1912.06146.

[132] A. Joshi and A. Klemm, *Swampland Distance Conjecture for One-Parameter Calabi-Yau Threefolds*, *JHEP* **08** (2019) 086 [1903.00596].

[133] A. Font, *Periods and duality symmetries in Calabi-Yau compactifications*, *Nucl. Phys.* **B391** (1993) 358 [hep-th/9203084].

[134] F. Denef and M.R. Douglas, *Distributions of nonsupersymmetric flux vacua*, *JHEP* **0503** (2005) 061 [hep-th/0411183].

[135] D. Freedman and A. Van Proeyen, *Supergravity*, Cambridge University Press (2012).

[136] S. Gates, M.T. Grisaru, M. Rocek and W. Siegel, *Superspace Or One Thousand and One Lessons in Supersymmetry*, *Front.Phys.* **58** (1983) 1 [hep-th/0108200].

[137] R. D'Auria, S. Ferrara, M. Trigiante and S. Vaula, *N=1 reductions of N=2 supergravity in the presence of tensor multiplets*, *JHEP* **0503** (2005) 052 [hep-th/0502219].

[138] A. Achucarro, S. Hardeman and K. Sousa, *Consistent Decoupling of Heavy Scalars and Moduli in N=1 Supergravity*, *Phys.Rev.* **D78** (2008) 101901 [0806.4364].

[139] P. Candelas, X. De La Ossa, A. Font, S.H. Katz and D.R. Morrison, *Mirror symmetry for two parameter models. 1.*, *Nucl.Phys.* **B416** (1994) 481 [hep-th/9308083].

[140] P. Berglund, P. Candelas, X. De La Ossa, A. Font, T. Hubsch et al., *Periods for Calabi-Yau and Landau-Ginzburg vacua*, *Nucl.Phys.* **B419** (1994) 352 [hep-th/9308005].

[141] P. Candelas, A. Font, S.H. Katz and D.R. Morrison, *Mirror symmetry for two parameter models. 2.*, *Nucl.Phys.* **B429** (1994) 626 [hep-th/9403187].

[142] P. Candelas, X. de la Ossa and F. Rodriguez-Villegas, *Calabi-Yau manifolds over finite fields. 1.*, hep-th/0012233.

[143] E. Cremmer, C. Kounnas, A. Van Proeyen, J. Derendinger, S. Ferrara, B. de Wit et al., *Vector Multiplets Coupled to N=2 Supergravity: SuperHiggs Effect, Flat Potentials and Geometric Structure*, *Nucl. Phys. B* **250** (1985) 385.

[144] D. Farquet and C.A. Scrucca, *Scalar geometry and masses in Calabi-Yau string models*, *JHEP* **09** (2012) 025 [1205.5728].

[145] M.C.D. Marsh and K. Sousa, *Universal Properties of Type IIB and F-theory Flux Compactifications at Large Complex Structure*, *JHEP* **03** (2016) 064 [1512.08549].

[146] L. Covi, M. Gomez-Reino, C. Gross, J. Louis, G.A. Palma et al., *de Sitter vacua in no-scale supergravities and Calabi-Yau string models*, *JHEP* **0806** (2008) 057 [0804.1073].

[147] L. Covi, M. Gomez-Reino, C. Gross, G.A. Palma and C.A. Scrucca, *Constructing de Sitter vacua in no-scale string models without uplifting*, *JHEP* **0903** (2009) 146 [0812.3864].

[148] H. Abe, T. Higaki and T. Kobayashi, *Remark on integrating out heavy moduli in flux compactification*, *Phys. Rev. D* **74** (2006) 045012 [hep-th/0606095].

[149] D. Gallego and M. Serone, *An Effective Description of the Landscape. I.*, *JHEP* **0901** (2009) 056 [0812.0369].

[150] D. Gallego and M. Serone, *An Effective Description of the Landscape - II*, *JHEP* **0906** (2009) 057 [0904.2537].

[151] I. Bena, E. Dudas, M. Graña and S. Lust, *Uplifting Runaways*, *Fortsch. Phys.* **67** (2019) 1800100 [1809.06861].

[152] M. Demirtas, M. Kim, L. Mcallister and J. Moritz, *Vacua with Small Flux Superpotential*, *Phys. Rev. Lett.* **124** (2020) 211603 [1912.10047].

[153] M.C.D. Marsh, B. Vercnocke and T. Wrase, *Decoupling and de Sitter Vacua in Approximate No-Scale Supergravities*, *JHEP* **05** (2015) 081 [1411.6625].

[154] D. Gallego, M.C.D. Marsh, B. Vercnocke and T. Wrase, *A new class of de sitter vacua in type iib large volume compactifications*, *JHEP* **10** (2017) 193 [1707.01095].

[155] C. Brodie and M.C.D. Marsh, *The Spectra of Type IIB Flux Compactifications at Large Complex Structure*, 1509.06761.

[156] A. Sen, *Orientifold limit of F theory vacua*, *Phys. Rev.* **D55** (1997) R7345 [hep-th/9702165].

[157] A. Klemm, B. Lian, S.S. Roan and S.-T. Yau, *Calabi-Yau fourfolds for M theory and F theory compactifications*, *Nucl. Phys.* **B518** (1998) 515 [hep-th/9701023].

[158] D. Lust, P. Mayr, S. Reffert and S. Stieberger, *F-theory flux, destabilization of orientifolds and soft terms on D7-branes*, *Nucl. Phys. B* **732** (2006) 243 [hep-th/0501139].

[159] A. Collinucci, F. Denef and M. Esole, *D-brane Deconstructions in IIB Orientifolds*, *JHEP* **02** (2009) 005 [0805.1573].

[160] M. Alim, M. Hecht, H. Jockers, P. Mayr, A. Mertens and M. Soroush, *Hints for Off-Shell Mirror Symmetry in type II/F-theory Compactifications*, *Nucl. Phys. B* **841** (2010) 303 [0909.1842].

[161] Y. Honma and H. Otsuka, *On the Flux Vacua in F-theory Compactifications*, *Phys. Lett. B* **774** (2017) 225 [1706.09417].

[162] Y. Honma and H. Otsuka, *F-theory Flux Vacua and Attractor Equations*, *JHEP* **04** (2020) 001 [1910.10725].

[163] D. Bates, D. Brake and M. Niemerg, *Paramotopy: Parameter homotopies in parallel*, in *International Congress on Mathematical Software*, pp. 28–35, Springer, 2018.

[164] A.J. Sommese and C.W. Wampler, *Numerical algebraic geometry*, .

[165] A.J. Sommese and C.W. Wampler, *The Numerical Solution of Systems of Polynomials Arising in Engineering and Science*, World Scientific (2005).

[166] D. Martinez-Pedrera, D. Mehta, M. Rummel and A. Westphal, *Finding all flux vacua in an explicit example*, *JHEP* **06** (2013) 110 [1212.4530].

[167] Y.-H. He, D. Mehta, M. Niemerg, M. Rummel and A. Valeanu, *Exploring the Potential Energy Landscape Over a Large Parameter-Space*, *JHEP* **07** (2013) 050 [1301.0946].

[168] M. Kac, *On the average number of real roots of a random algebraic equation*, *Bull. Amer. Math. Soc.* **49** (1943) 314.

[169] S.O. Rice, *Mathematical analysis of random noise*, *Bell System Technical Journal* **23** (1944) 282.

[170] R.J. Adler and J.E. Taylor, *Random fields and geometry*, Springer Science & Business Media (2009).

[171] S. Ashok and M.R. Douglas, *Counting flux vacua*, *JHEP* **01** (2004) 060 [hep-th/0307049].

[172] J.P. Conlon and F. Quevedo, *On the explicit construction and statistics of Calabi-Yau flux vacua*, *JHEP* **10** (2004) 039 [hep-th/0409215].

[173] I. Broeckel, M. Cicoli, A. Maharana, K. Singh and K. Sinha, *Moduli Stabilisation and the Statistics of SUSY Breaking in the Landscape*, 2007.04327.

[174] A. Aazami and R. Easther, *Cosmology from random multifield potentials*, *JCAP* **0603** (2006) 013 [hep-th/0512050].

[175] D. Mehta, M. Niemerg and C. Sun, *Statistics of Stationary Points of Random Finite Polynomial Potentials*, *J. Stat. Mech.* **1509** (2015) P09012 [1504.02786].

[176] J. von Neuman and E. Wigner, *Uber merkwürdige diskrete Eigenwerte. Uber das Verhalten von Eigenwerten bei adiabatischen Prozessen*, *Physikalische Zeitschrift* **30** (1929) 467.

[177] D. Marsh, L. McAllister and T. Wrase, *The Wasteland of Random Supergravities*, *JHEP* **1203** (2012) 102 [1112.3034].

[178] T.C. Bachlechner, D. Marsh, L. McAllister and T. Wrase, *Supersymmetric Vacua in Random Supergravity*, *JHEP* **1301** (2013) 136 [1207.2763].

[179] A. Achucarro, P. Ortiz and K. Sousa, *A new class of de Sitter vacua in String Theory Compactifications*, *Phys. Rev.* **D94** (2016) 086012 [1510.01273].

[180] T. Guhr, A. Muller-Groeling and H.A. Weidenmuller, *Random matrix theories in quantum physics: Common concepts*, *Phys. Rept.* **299** (1998) 189 [cond-mat/9707301].

[181] J.P. Conlon, *The QCD axion and moduli stabilisation*, *JHEP* **05** (2006) 078 [hep-th/0602233].

[182] R. Kallosh, A.D. Linde, D.A. Linde and L. Susskind, *Gravity and global symmetries*, *Phys. Rev. D* **52** (1995) 912 [hep-th/9502069].

[183] T. Banks and N. Seiberg, *Symmetries and Strings in Field Theory and Gravity*, *Phys. Rev. D* **83** (2011) 084019 [1011.5120].

[184] A.P. Braun, N. Johansson, M. Larfors and N.-O. Walliser, *Restrictions on infinite sequences of type IIB vacua*, *JHEP* **10** (2011) 091 [1108.1394].

[185] U.H. Danielsson, N. Johansson and M. Larfors, *The World next door: Results in landscape topography*, *JHEP* **03** (2007) 080 [hep-th/0612222].

[186] D. Junghans, *Weakly Coupled de Sitter Vacua with Fluxes and the Swampland*, *JHEP* **03** (2019) 150 [1811.06990].

[187] T.W. Grimm, C. Li and I. Valenzuela, *Asymptotic Flux Compactifications and the Swampland*, 1910.09549.

[188] J.J. Blanco-Pillado, K. Sousa, M.A. Urkiola and J.M. Wachter, *Universal Class of Type-IIB Flux Vacua with Analytic Mass Spectrum*, *Phys. Rev. D* **103** (2021) 106006 [2011.13953].

[189] P. Mayr, *Phases of supersymmetric D-branes on Kahler manifolds and the McKay correspondence*, *JHEP* **01** (2001) 018 [hep-th/0010223].

[190] A. Achucarro and K. Sousa, *F-term uplifting and moduli stabilization consistent with Kahler invariance*, *JHEP* **0803** (2008) 002 [0712.3460].

[191] K. Sousa, *Consistent Supersymetric Decoupling in Cosmology*, Ph.D. thesis, Leiden U., 2012.

[192] I. Bena, J. Blåbäck, M. Graña and S. Lüst, *The Tadpole Problem*, 2010.10519.

[193] A.P. Braun, Y. Kimura and T. Watari, *The Noether-Lefschetz problem and gauge-group-resolved landscapes: F-theory on K3 × K3 as a test case*, *JHEP* **04** (2014) 050 [1401.5908].

[194] M. Demirtas, M. Kim, L. Mcallister and J. Moritz, *Conifold Vacua with Small Flux Superpotential*, 2009.03312.

[195] R. Álvarez-García, R. Blumenhagen, M. Brinkmann and L. Schlechter, *Small Flux Superpotentials for Type IIB Flux Vacua Close to a Conifold*, 2009.03325.

[196] C. Crinò, F. Quevedo and R. Valandro, *On de Sitter String Vacua from Anti-D3-Branes in the Large Volume Scenario*, 2010.15903.

[197] J.J. Blanco-Pillado, M.A. Urkiola and J.M. Wachter, *Racetrack Potentials and the de Sitter Swampland Conjectures*, *JHEP* **01** (2019) 187 [1811.05463].

[198] F. Denef, A. Hebecker and T. Wrase, *de Sitter swampland conjecture and the Higgs potential*, *Phys. Rev. D* **98** (2018) 086004 [1807.06581].

[199] K. Choi, D. Chway and C.S. Shin, *The dS swampland conjecture with the electroweak symmetry and QCD chiral symmetry breaking*, *JHEP* **11** (2018) 142 [1809.01475].

[200] H. Murayama, M. Yamazaki and T.T. Yanagida, *Do We Live in the Swampland?*, *JHEP* **12** (2018) 032 [1809.00478].

[201] M.P. Hertzberg, S. Kachru, W. Taylor and M. Tegmark, *Inflationary Constraints on Type IIA String Theory*, *JHEP* **12** (2007) 095 [0711.2512].

[202] D. Andriot, *New constraints on classical de Sitter: flirting with the swampland*, *Fortsch. Phys.* **67** (2019) 1800103 [1807.09698].

[203] D. Andriot, *On the de Sitter swampland criterion*, *Phys. Lett. B* **785** (2018) 570 [1806.10999].

[204] M. Cicoli, J.P. Conlon and F. Quevedo, *General Analysis of LARGE Volume Scenarios with String Loop Moduli Stabilisation*, *JHEP* **10** (2008) 105 [0805.1029].

[205] I. Bena, M. Graña, S. Kuperstein and S. Massai, *Giant Tachyons in the Landscape*, *JHEP* **02** (2015) 146 [1410.7776].

[206] J. Polchinski, *String theory (vols. 1,2)*, *Cambridge University Press* (1998) .

[207] J.P. Conlon, *The de Sitter swampland conjecture and supersymmetric AdS vacua*, *Int. J. Mod. Phys. A* **33** (2018) 1850178 [1808.05040].

[208] J. Blanco-Pillado, C. Burgess, J.M. Cline, C. Escoda, M. Gomez-Reino et al., *Inflating in a better racetrack*, *JHEP* **0609** (2006) 002 [hep-th/0603129].

[209] A. Hebecker and T. Wrase, *The Asymptotic dS Swampland Conjecture - a Simplified Derivation and a Potential Loophole*, *Fortsch. Phys.* **67** (2019) 1800097 [1810.08182].

[210] R. Kallosh and A.D. Linde, *Landscape, the scale of SUSY breaking, and inflation*, *JHEP* **0412** (2004) 004 [hep-th/0411011].

[211] J.J. Blanco-Pillado, R. Kallosh and A.D. Linde, *Supersymmetry and stability of flux vacua*, *JHEP* **0605** (2006) 053 [hep-th/0511042].

[212] M.R. Douglas, *Statistical analysis of the supersymmetry breaking scale*, hep-th/0405279.

[213] E.J. Copeland, A.R. Liddle, D.H. Lyth, E.D. Stewart and D. Wands, *False vacuum inflation with Einstein gravity*, *Phys. Rev. D* **49** (1994) 6410 [astro-ph/9401011].

[214] M. Badziak and M. Olechowski, *Volume modulus inflation and a low scale of SUSY breaking*, *JCAP* **07** (2008) 021 [0802.1014].

[215] L. Covi, M. Gomez-Reino, C. Gross, J. Louis, G.A. Palma et al., *Constraints on modular inflation in supergravity and string theory*, *JHEP* **0808** (2008) 055 [0805.3290].

[216] J. Blanco-Pillado, C. Burgess, J.M. Cline, C. Escoda, M. Gomez-Reino et al., *Racetrack inflation*, *JHEP* **0411** (2004) 063 [hep-th/0406230].

[217] R. Kallosh, A. Linde, B. Vercnocke and T. Wrase, *Analytic Classes of Metastable de Sitter Vacua*, *JHEP* **10** (2014) 011 [1406.4866].

[218] T.C. Bachlechner, *On Gaussian Random Supergravity*, *JHEP* **04** (2014) 054 [1401.6187].

[219] D. Slepian, *The one-sided barrier problem for gaussian noise*, *Bell System Technical Journal* **41** (1962) 463.

[220] R. Easther, A.H. Guth and A. Masoumi, *Counting Vacua in Random Landscapes*, 1612.05224.

[221] B. Greene, D. Kagan, A. Masoumi, D. Mehta, E.J. Weinberg and X. Xiao, *Tumbling through a landscape: Evidence of instabilities in high-dimensional moduli spaces*, *Phys. Rev.* **D88** (2013) 026005 [1303.4428].

[222] A. Aravind, D. Lorshbough and S. Paban, *Lower bound for the multifield bounce action*, *Phys. Rev.* **D89** (2014) 103535 [1401.1230].

[223] A. Aravind, B.S. DiNunno, D. Lorshbough and S. Paban, *Analyzing multifield tunneling with exact bounce solutions*, *Phys. Rev.* **D91** (2015) 025026 [1412.3160].

[224] M. Dine and S. Paban, *Tunneling in Theories with Many Fields*, *JHEP* **10** (2015) 088 [1506.06428].

[225] J.J. Blanco-Pillado, M. Dias, J. Frazer and K. Sousa, *Large Scale Power Suppression in a Multifield Landscape*, 1503.07579.

[226] G. Lindgren, *Stationary stochastic processes: theory and applications*, CRC Press (2012).

[227] G. Lindgren, *Local maxima of Gaussian Fields*, *G. Ark. Mat.* **10** (1972) .

[228] M. Bucher and T. Louis, *Filling in cosmic microwave background map missing data using constrained gaussian realizations*, *Monthly Notices of the Royal Astronomical Society* **424** (2012) 1694.

[229] A. Marcos-Caballero, E. Martínez-González and P. Vielva, *Local properties of the large-scale peaks of the cmb temperature*, *Journal of Cosmology and Astroparticle Physics* **2017** (2017) 023.

[230] J.M. Bardeen, J.R. Bond, N. Kaiser and A.S. Szalay, *The Statistics of Peaks of Gaussian Random Fields*, *Astrophys. J.* **304** (1986) 15.

[231] E. Bertschinger, *Path integral methods for primordial density perturbations. Sampling of constrained Gaussian random fields*, *Astrophys. J.* **323** (1987) L103.

[232] G. Ganon and Y. Hoffman, *Constrained realizations of Gaussian fields - Reconstruction of the large-scale structure*, *Astrophys. J.* **415** (1993) L5.

[233] P. Athron, C. Balázs, M. Bardsley, A. Fowlie, D. Harries and G. White, *BubbleProfiler: finding the field profile and action for cosmological phase transitions*, 1901.03714.

[234] J.R. Espinosa, *A Fresh Look at the Calculation of Tunneling Actions*, *JCAP* **1807** (2018) 036 [1805.03680].

[235] J.R. Espinosa and T. Konstandin, *A Fresh Look at the Calculation of Tunneling Actions in Multi-Field Potentials*, *JCAP* **1901** (2019) 051 [1811.09185].

[236] A.R. Brown, *Thin-wall approximation in vacuum decay: A lemma*, *Phys. Rev.* **D97** (2018) 105002 [1711.07712].

[237] I. Dasgupta, *Estimating vacuum tunneling rates*, *Phys. Lett.* **B394** (1997) 116 [hep-ph/9610403].

[238] D. Baumann, A. Dymarsky, I.R. Klebanov and L. McAllister, *Towards an Explicit Model of D-brane Inflation*, *JCAP* **0801** (2008) 024 [0706.0360].

[239] Planck collaboration, *Planck 2018 results. X. Constraints on inflation*, *Astron. Astrophys.* **641** (2020) A10 [1807.06211].

[240] M. Dias, J. Frazer and D. Seery, *Computing observables in curved multifield models of inflation—A guide (with code) to the transport method*, *JCAP* **1512** (2015) 030 [1502.03125].

[241] B. Freivogel, *Making predictions in the multiverse*, *Class. Quant. Grav.* **28** (2011) 204007 [1105.0244].

[242] M. Aronowich and R.J. Adler, *Extrema and Level Crossing of χ^2 Processes*, *Adv. Appl. Prob.* **18** (1986) 901.

[243] G. Lindgren, *Slepian models for χ^2-processes with dependent components with application to envelope upcrossings*, *J. Appl.Prob.* **26** (1989) 36.

[244] G. Lindgren and I. Rychlik, *Models and Regression Approximations in Crossing and Extreme Value Theory*, *Intern. Statist. Rev.* **59** (1991) 195.

[245] S. Weinberg, *Does Gravitation Resolve the Ambiguity Among Supersymmetry Vacua?*, *Phys. Rev. Lett.* **48** (1982) 1776.

[246] M. Cvetic, S. Griffies and S.-J. Rey, *Nonperturbative stability of supergravity and superstring vacua*, *Nucl. Phys. B* **389** (1993) 3 [hep-th/9206004].

[247] M. Cvetic, S. Griffies and S.-J. Rey, *Static domain walls in N=1 supergravity*, *Nucl. Phys. B* **381** (1992) 301 [hep-th/9201007].

[248] J.D. Brown and C. Teitelboim, *Dynamical Neutralization of the Cosmological Constant*, *Phys.Lett.* **B195** (1987) 177.

[249] J.D. Brown and C. Teitelboim, *Neutralization of the Cosmological Constant by Membrane Creation*, *Nucl. Phys. B* **297** (1988) 787.

[250] S.W. Hawking, *The Cosmological Constant Is Probably Zero*, *Phys. Lett. B* **134** (1984) 403.

[251] J.S. Schwinger, *On gauge invariance and vacuum polarization*, *Phys. Rev.* **82** (1951) 664.

[252] A. Vilenkin, *Creation of Universes from Nothing*, *Phys. Lett. B* **117** (1982) 25.

[253] A. Achucarro, J.P. Gauntlett, K. Itoh and P.K. Townsend, *World Volume Supersymmetry From Space-time Supersymmetry of the Four-dimensional Supermembrane*, *Nucl. Phys. B* **314** (1989) 129.

[254] I.A. Bandos and C. Meliveo, *Superfield equations for the interacting system of D=4 N=1 supermembrane and scalar multiplet*, *Nucl. Phys. B* **849** (2011) 1 [1011.1818].

[255] I.A. Bandos and C. Meliveo, *Supermembrane interaction with dynamical D=4 N=1 supergravity. Superfield Lagrangian description and spacetime equations of motion*, *JHEP* **08** (2012) 140 [1205.5885].

[256] S.J. Gates, Jr., *Super p-form gauge superfields*, *Nucl. Phys. B* **184** (1981) 381.

[257] P. Binetruy, F. Pillon, G. Girardi and R. Grimm, *The Three form multiplet in supergravity*, *Nucl. Phys. B* **477** (1996) 175 [hep-th/9603181].

[258] F. Farakos, S. Lanza, L. Martucci and D. Sorokin, *Three-forms in Supergravity and Flux Compactifications*, *Eur. Phys. J. C* **77** (2017) 602 [1706.09422].

[259] S. Lanza, *Exploring the Landscape of effective field theories*, Ph.D. thesis, Padua U., 2019. 1912.08935.

[260] I. Bandos, F. Farakos, S. Lanza, L. Martucci and D. Sorokin, *Three-forms, dualities and membranes in four-dimensional supergravity*, *JHEP* **07** (2018) 028 [1803.01405].

[261] L.E. Ibanez, M. Montero, A. Uranga and I. Valenzuela, *Relaxion Monodromy and the Weak Gravity Conjecture*, *JHEP* **04** (2016) 020 [1512.00025].

[262] J. Brown, W. Cottrell, G. Shiu and P. Soler, *Tunneling in Axion Monodromy*, *JHEP* **10** (2016) 025 [1607.00037].

[263] S. Lanza, F. Marchesano, L. Martucci and I. Valenzuela, *Swampland Conjectures for Strings and Membranes*, *JHEP* **02** (2021) 006 [2006.15154].

[264] D.J.H. Chung, L.L. Everett, G.L. Kane, S.F. King, J.D. Lykken and L.-T. Wang, *The Soft supersymmetry breaking Lagrangian: Theory and applications*, *Phys. Rept.* **407** (2005) 1 [hep-ph/0312378].

[265] J. Wess and J. Bagger, *Supersymmetry and supergravity*, *Princeton University Press* (1992) .

[266] J.R. Morris and D. Bazeia, *Supersymmetry breaking and Fermi balls*, *Phys. Rev. D* **54** (1996) 5217 [hep-ph/9607396].

[267] E. Dyer and K. Hinterbichler, *Boundary Terms, Variational Principles and Higher Derivative Modified Gravity*, *Phys. Rev. D* **79** (2009) 024028 [0809.4033].

[268] G. Gibbons and S. Hawking, *Action Integrals and Partition Functions in Quantum Gravity*, *Phys.Rev.* **D15** (1977) 2752.

[269] Y.-b. Kim, C.O. Lee, I.-b. Lee and J.-J. Lee, *Brane world of warp geometry: An Introductory review*, *J. Korean Astron. Soc.* **37** (2004) 1 [hep-th/0307023].

[270] A. Masoumi, S. Paban and E.J. Weinberg, *Tunneling from a Minkowski vacuum to an AdS vacuum: A new thin-wall regime*, *Phys. Rev. D* **94** (2016) 025023 [1603.07679].

[271] S. Banerjee, U. Danielsson, G. Dibitetto, S. Giri and M. Schillo, *Emergent de Sitter Cosmology from Decaying Anti–de Sitter Space*, *Phys. Rev. Lett.* **121** (2018) 261301 [1807.01570].

[272] S. Lanza, F. Marchesano, L. Martucci and D. Sorokin, *How many fluxes fit in an EFT?*, *JHEP* **10** (2019) 110 [1907.11256].

[273] J. Otto, A.G. Forbes and J. Verschelde, *Solving polynomial systems with phcpy*, *CoRR* **abs/1907.00096** (2019) [1907.00096].

[274] J. Gray, Y.-H. He, A. Ilderton and A. Lukas, *Stringvacua. a mathematica package for studying vacuum configurations in string phenomenology*, *Computer Physics Communications* **180** (2009) 107?119.

[275] D.J. Bates, J.D. Hauenstein, A.J. Sommese and C.W. Wampler, "Bertini: Software for numerical algebraic geometry." Available at bertini.nd.edu with permanent doi: dx.doi.org/10.7274/R0H41PB5.

[276] J. Klemelä, *Smoothing of Multivariate Data: Density Estimation and Visualization*, Wiley (2009).

[277] K.F. Riley, M.P. Hobson and S.J. Bence, *Mathematical methods for physics and engineering: a comprehensive guide*, Cambridge university press (2006).

[278] W.H. Press, S.A. Teukolsky, W.T. Vetterling and B.P. Flannery, *Numerical recipes 3rd edition: The art of scientific computing*, Cambridge university press (2007).

[279] I.L. Buchbinder and S.M. Kuzenko, *Ideas and methods of supersymmetry and supergravity or a walk through superspace*, Institute of Physics Publishing (1998).